Cold-Formed Steel Behavior:

Elastic Buckling Simplified Methods for Structural Members with Edge-Stiffened Holes and Purlin Distortional Buckling Strength Under Gravity Loading

Christopher N. Grey

Thesis submitted to the faculty of
Virginia Polytechnic Institute and State University
in partial fulfillment of the requirements for the degree of

MASTER OF SCIENCE
in
Civil Engineering

Cristopher D. Moen

Matthew R. Eatherton

William J. Wright

April 29, 2011
Blacksburg, Virginia

Cold-Formed Steel Behavior:

Elastic Buckling Simplified Methods for Structural Members with Edge-Stiffened Holes and Purlin Distortional Buckling Strength Under Gravity Loading

Christopher N. Grey

ABSTRACTS

Elastic Buckling Simplified Methods for Structural Members with Edge-Stiffened Holes

Presently, the current design methods available to engineers to predict the strength of cold-formed steel members with edge-stiffened holes remains largely unaddressed in the North American Specification for the Design of Cold-Formed Steel Structural Members (NAS). Research was conducted to explore and develop a further understanding of the effects of stiffened edge holes on the elastic buckling parameters for local, distortional, and global buckling. Elastic buckling parameter studies have been conducted on a suite of cold-formed members including recently developed DeltaSTUDs manufactured by Steelform Building Products, Inc. and a series of common Steel Stud Manufacturers Association (SSMA) members. Furthermore, a suite of simplified methods for determining elastic buckling parameters used to predict capacity with the Direct Strength Method (DSM) for members with edge stiffened holes were developed and validated. The elastic buckling studies are used to validate the simplified methods presented in this thesis. All simplified methods are further validated with thin shell finite element eigen-buckling parameter studies where the edge-stiffened holes are explicitly modeled.

Purlin Distortional Buckling Strength Under Gravity Loading

Laterally braced cold-formed steel beams generally fail due to local and/or distortional buckling in combination with yielding. For many members, distortional buckling is the dominant buckling mode and is addressed in the current North American Specification for the Design of Cold-formed Steel Structural Members. The current main code equation, AISI C3.1.4-10 for calculating the available distortional buckling stress was derived experimentally based on a series of four-point bending tests at John Hopkins University. Where this provides a good basis for determining capacity, in most loading conditions purlins are subjected to a downward uniform loading that provides additional resistance to distortional buckling in the top flange beyond the resistance of the steel roofing panel. This research describes an experimental study to explore and quantify the difference in distortional buckling flexural capacity of metal building Z-purlins treated as isolated components and Z-purlins loaded with a constant pressure applied to metal roof panels. A series of three different types of tests have been developed to quantify the system effect provided by the metal roof panels as well as downward pressure on distortional buckling. Results are also extended to validate the Direct Strength Method when predicting flexural capacity of purlins in a roof system.

ACHKNOWLEDGEMENTS

I would like to thank my committee chairman, Dr. Cristopher D. Moen for his guidance throughout my graduate studies. Also, I would like to thank Dr. William J. Wright and Dr. Matthew R. Eatherton for serving as my thesis committee members.

I wish to extend my gratitude to all of my fellow graduate students at the Structures and Materials Laboratory who provided assistance throughout my projects. A special thanks goes to the laboratory technicians, Dennis Huffman and Brett Farmer, for their daily assistance throughout my projects. My appreciation goes out to the Metal Building Manufacturers Association and Steelform Building Products Inc. for funding the projects.

Finally, I would like to thank my parents and family members, especially my mom and dad for believing in me and always supporting me in any way they could.

Table of Contents

LIST OF TABLES

LIST OF FIGURES

CHAPTER 1. INTRODUCTION

1.1 Cold-Formed Steel Structural Members

Today, there is an ever increasing effort to improve building construction efficiency, not only in speed and cost of construction, but in green building technology. In the steel manufacturing industry, there are two types of forming methods for structural steel sections: hot-rolled steel and cold-formed steel sections (more generally: thin-walled or light gage steel members). Hot-rolled steel sections are formed to their final set dimensions at elevated temperatures, whereas cold-formed structural members are manufactured from thin steel sheets at room temperature by either press braking or roll forming (Figure 1.1).

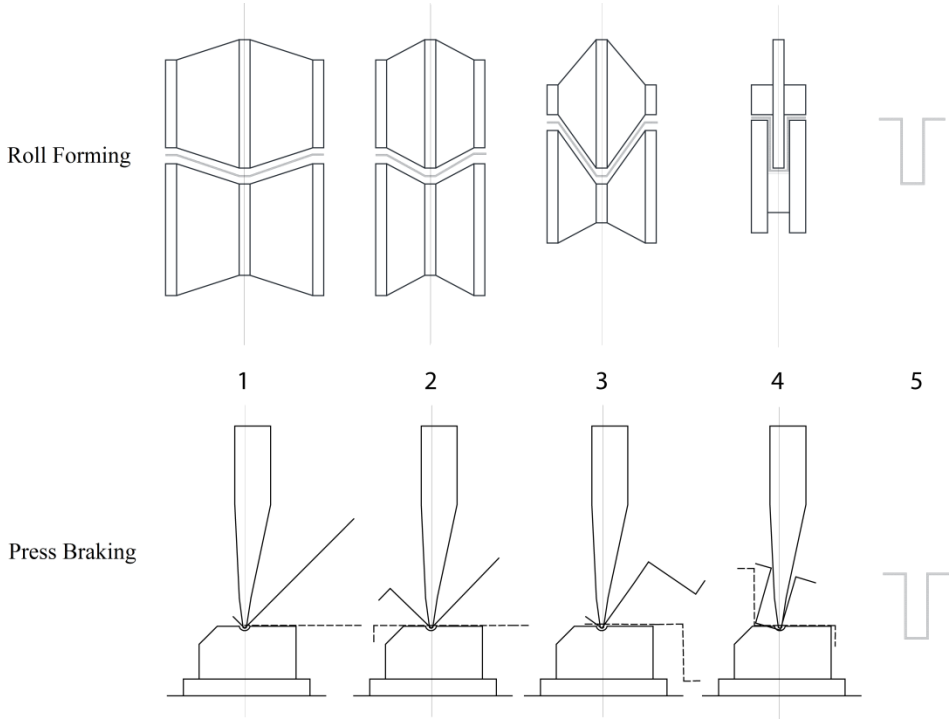

Figure 1.1 Forming methods for cold-formed steel members

Hot-rolled cross section dimensions are based on database of common sections (W, S, C, WT, HSS, etc) found in the American Institute of Steel Construction Manual (AISC 2006). In comparison, an unlimited number of section configurations are possible for cold-formed steel due to the ease of manufacturing. The section design for cold-formed members is extremely important, as the section is responsible for carrying the load rather than the strength of the steel such as in hot-rolled sections. This allows cold-formed structural members to be used in construction to achieve light, strong, and versatile building components, which can be mass produced and reduce labor costs on and off the jobsite. In addition, cold-formed steel members eliminate the use of formwork and delays due to weather are eliminated, and erection is fast compared to concrete and hot-rolled steel. Compared to its counterpart, hot-rolled steel, cold-formed steel can easily be shipped in mass quantities further reducing the costs of construction. Furthermore, with steel being the number one recycled product in North America, the push for green building is advanced by manufacturing cold-formed steel shapes from recycled steel (Steel Recycling Institute 2009).

1.2 **Elastic Buckling of Cold-Formed Steel Members**

The added versatility of cold-formed shapes comes with a penalty. Engineers usually design non-compact hot-rolled structural shapes for overall column buckling and lateral buckling stability. The dimensions of non-compact hot-rolled shapes are designed such that local buckling will not usually occur before the section yields. This is not the case with cold-formed shapes, where local buckling throughout the cross section must be considered. This is because cold-formed sections are made of thin sheet steel, which have width to thickness ratios ($b/t > 20$) that can cause buckling to occur well below the yield point of steel.

Since cold-formed cross sections are light and thin, buckling of section elements must be considered in addition to the typical global buckling one would calculate for a hot-rolled section. For most cold-formed sections, buckling can be broken down into three different modes: local, distortional, and global buckling (Ádány 2004). Each buckling mode is characterized by what portion of the cross section it affects and its respective half-wavelength. Half-wavelengths are the distance by which half a sinusoidal buckled wave is able to form, as shown in Figure 1.2. As a member is loaded, elements may buckle (local buckling); however, the member can still take additional load until global failure (i.e. post buckling strength). The AISI Direct Strength Method (AISI 2006) uses the elastic buckling parameters as well as a number of strength curves to predict the member capacity.

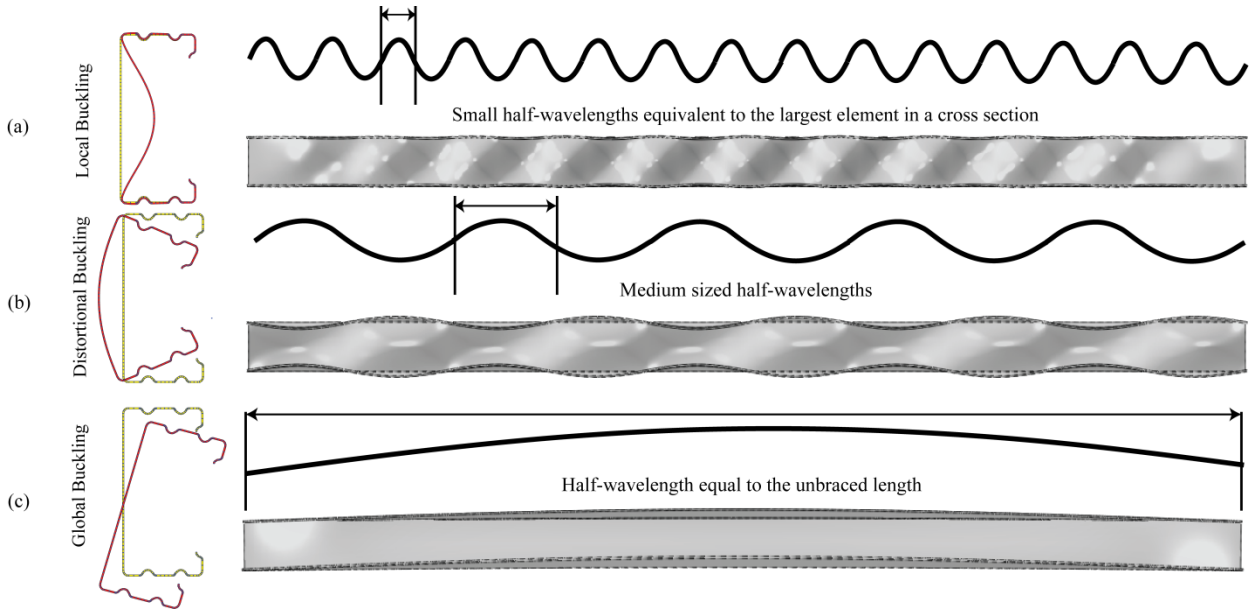

Figure 1.2 Half-wavelength definition (column loading shown)

Local buckling occurs when the individual elements, such as the web or flanges, rotate and distort around the folded edges of a section, as shown in Figure 1.2a. As local buckling involves buckling of individual elements within a cross section, it occurs at small half-wavelengths, and is a function of the largest plate dimension in the section as well as the loading.

This means that over the length of a member, there will be multiple local buckled half-waves based on the size of the cross section elements. Holes and flange/web stiffeners, as shown in the flanges of Figure 1.4, are often added to the section which forces local buckled half-waves to occur at smaller distances. This can result in an increase of local buckling strength.

Distortional buckling involves both rotation and translation at the fold lines in a section. Compared to local buckling, which only deforms individual elements, distortional buckling deforms the web in addition to rigidly translating the flanges around the fold lines as shown in Figure 1.2b. Due to the distortion and translation occurring in the entire cross section, distortional buckling half-wavelengths are longer than the typical local buckling half-wavelengths. Distortional buckling is a function of loading configuration, where in flexure, only one flange will distort compared to pure compression that deforms both flanges.

Global buckling modes are pure flexure, pure torsional, or flexural torsional. The global buckling half-wavelength is dependent on boundary conditions. For the simple pinned warping free condition, the global half-wavelength is defined over the entire length of the member. However, if the boundary conditions are warping fixed, the global half-wavelength is defined over a shorter unbraced length. Global buckling involves torsion and/or flexure of the entire cross section without any local distortion. In most cases, the cross section rotates and remains rigid; however, it is possible to have interaction between modes.

1.3 **Determination of Buckling Modes**

Three methods currently exist to determine local, distortional, and global buckling modes and their respective loads: Finite Element Method (FEM), Finite Strip Method (FSM), and Simplified Equations Method. While these methods are the most efficient and widely used, each method has its own set of limitations (Schafer and Ádány 2005). The first method uses a general purpose finite element program (ABAQUS in this thesis (ABAQUS 2010)) whereas the former two use a freely available open source program, CUFSM (Schafer and Ádány 2006). Each method varies in their limitations of predicting elastic buckling loads related to the addition of holes and boundary conditions.

The first method, FEM requires that a user generate a full 3-D model, then run an eigen-buckling analysis. An eigen-buckling analysis finds buckling loads (eigenvalues) that cause a structure to become unstable. Each eigenvalue has an associated buckled mode shape. FEM can account for any possible geometry, loading configuration, and boundary conditions; however, eigenbuckling results cannot automatically distinguish between buckling modes. The selection of modes is highly subjective, as they are manually selected from an increasing output of eigenvalues, each with an associated buckling mode. Starting at the lowest possible eigenvalue, the user visually inspects up to 100s of buckling modes until the most distinct buckling modes (shown in Figure 1.2 for local, distortional, and global buckling) are determined. In some instances, multiple modes interact (mix) together, and the most distinct mode is hard to determine. In this case, the user has to use his/her understanding of the features of each buckling mode judgment in determining the most relevant modes and critical loads. Although the fully modeled eigen-buckling analysis allows for the most accurate elastic buckling results, the eigen-

buckling analysis is computationally intensive, requiring multiple hours of computation for complex models with a large number of finite elements (Schafer and Ádány 2005).

The second method uses the semi-analytical finite strip method to break up a section into strips and treat each strip as a simply supported plate. FSM is used to determine elastic buckling properties for any open cross section without holes by generating an elastic buckling curve, as shown in Figure 1.3. The elastic buckling curve is a representation of the analysis of the cross-section at multiple lengths (specified by the user), analyzing as if one half-sine wave occurs over the desired length for local, distortional, and global. As it analyzes at every length, the elastic buckling curve, is actually composed of three individual curves, where the minimums are taken as the final curve. FSM tries to automate the elastic buckling determination process with the elastic buckling curve as it helps the user identify the modes easily (Schafer and Ádány 2005). For example the first minimum point identifies the local buckling mode, the second identifies the distortional buckling mode, and the global buckling load is taken at the unbraced length of the member.

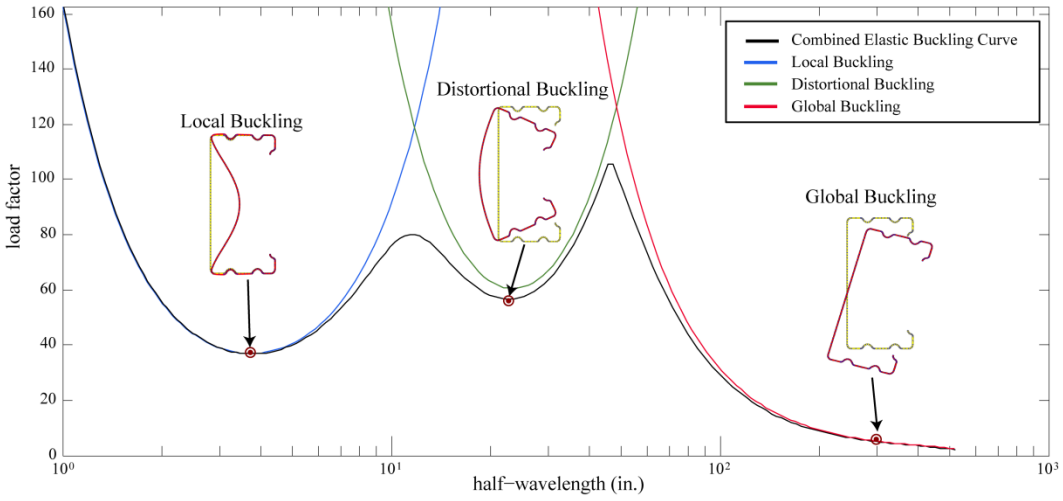

Figure 1.3 Typical finite strip (CUFSM) elastic buckling curve.

Simplified methods utilizing the finite strip method for practicing engineers exist for determining elastic buckling parameters for members with holes, which serve to eliminate the need for full eigen-buckling analysis (Moen and Schafer 2009). Using the finite strip method in conjunction with simplified methods gives the user the ability to analyze any open cross section. The simplified methods utilize weighted average section properties to account for the addition of holes, as shown in Figure 1.4a and edge-stiffened holes, as shown in Figure 1.4b along the length of a member. Determining section properties can readily be done using CUFSM. Simplified methods have been recently developed by Moen and Schafer (2009) and have been extended to edge-stiffened holes to predict local and global buckling parameters; however, the effects of hole edge-stiffeners on distortional buckling load is currently ignored. Elastic distortional buckling loads for edge-stiffened holes are currently determined based on the assumption that if a hole is introduced into an open cross-section, the rotational restraint provided by the element containing the hole is decreased, resulting in a lower critical distortional buckling load (Moen and Schafer 2009).

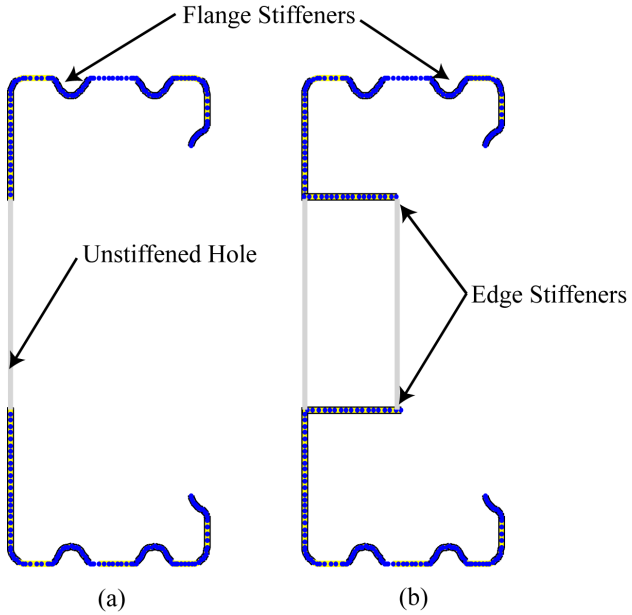

Figure 1.4 C-section with a) unstiffened hole and b) edge-stiffened hole

1.4 Previous Research – Structural Members with Edge-Stiffened Holes

Over the past several years, cold-formed steel members have been manufactured with web perforations without the effects on strength being addressed in the AISI Design Specification (AISI S100). A limited amount of research has been performed on studying the effects on elastic buckling parameters when holes are present in members. A limited amount of research exists on developing simplified methods for calculating elastic buckling parameters for members with unstiffened and edge-stiffened holes.

In 1999, the National Home Builder Association (NHBA) Research Center tested a total of 67 common joists with edge-stiffened holes to study the effects of holes on bending, shear, and web crippling failures. A total of 15 tests were performed for pure bending, 15 for pure shear, 16 for combined shear and bending, and 21 for web crippling (NHBA 1999). At that time, AISI had a design guide titled "Design Guide for Cold-Formed Steel Beams with Web Perforations" that provided design recommendations for beams with holes. The testing by the NHBA determined that the AISI design guide (AISI RG-9712) was conservative and that the presence of web openings with edge-stiffeners increased the ultimate shear, and combined shear and bending strengths in the joists studied (NHBA 1999).

Compression tests were performed by Moen and Schafer (2008) on 24 cold-formed steel columns with and without slotted web holes for varying column length and cross section dimensions (hole dimensions remained the same) to determine the effects on the buckling parameters. The experimental research demonstrated that the presence of holes considered in the study caused only a slight decrease in capacity. The holes which were located in the webs of the studs reduced the local buckling capacity of the web, causing the flanges to carry more load, which lead to a distortional type failure.

Moen and Schafer (2009a) developed simplified elastic buckling (local, distortional and global) equations to account for the presence of holes in columns and beams as an alternative to full finite element buckling analysis. Global buckling equations used "weighted average" section properties formulated using energy based stability solutions. Simplified equations for distortional buckling used the finite strip method to account for the loss in transverse rotational stiffness of the web due to a hole. The newly developed distortional buckling equations were validated for beams and columns by analyzing 222 specimens (78 columns and 144 beams) with varying boundary conditions and specimen geometry. The local buckling loads were determined using the finite strip method (CUFSM) with modifications to account for holes by analyzing the net section. Simplified equations for local buckling were also validated analyzing the same set of specimens as distortional buckling. All approximations were verified against finite element models with explicit holes included.

A new selection of members were being manufactured with hole edge stiffeners as shown in Figure 1.4b, and Yu (2007) studied the behavior and design of cold-formed C-section joists with edge-stiffened circular holes. Using finite element analyses, a total of 240 edge-stiffened C-section joists were studied, and new provisions were proposed to predict the flexural strength of the joists with optimized hole geometry. It was determined that as the hole diameters and hole edge-stiffener length got larger, the local web and distortional buckling loads did as well, due to the increase in rotational restraint. However, LTB loads decreased due to the decrease in the weak axis moment of inertia (Yu 2007).

Moen and Yu (2010) then extended and validated the previously developed simplified methods by Moen and Schafer (2009a) to members with circular holes with edge-stiffened holes over a range of hole height to web height ratios. Local and global buckling simplified methods

used the weighted average approach to account for the added edge-stiffeners around a hole; however, distortional buckling simplified methods only accounted for the loss in rotational stiffness from a hole. The addition of edge-stiffeners was shown to have a minimal effect on global buckling loads when compared to the same members in Moen and Schafer (2009a) with unstiffened holes. Local buckling was again prevented at a hole location forcing the half-waves to form between holes. A new distortional buckling mode was discovered where half-waves formed between holes at a similar load to columns without holes. Although the simplified methods were extended, a simplified method for distortional buckling that accounts for the addition of edge-stiffeners is still needed.

1.5 **Research Goals - Structural Members with Edge-Stiffened Holes**

The goal of the research presented in this thesis is to develop a further understanding of the effects of stiffened edge holes on the elastic buckling parameters for local, distortional, and global buckling. Holes can be found in most cold-formed steel structural components. For example, in low and midrise construction, closely-spaced edge-stiffened holes are placed in the webs of cold-formed steel columns and beams, allowing electrical, plumbing, and heating services to pass through walls and ceilings as shown in Figure 1.4. The presence of holes in a structural member often complicates the design process. For thin-walled structures, where elastic buckling and load-deformation response are directly related, edge-stiffened holes may promote unique elastic buckling modes with the potential to influence load-deformation response and collapse mechanisms at an ultimate limit state (Moen and Yu 2010).

Figure 1.5 Cold-formed steel framing with edge-stiffened holes

Currently, cold-formed steel members *with holes* can be designed with the American Iron and Steel Institute's Direct Strength Method (DSM) (AISI-S100), which utilizes the local, distortional, and global (Euler) elastic buckling properties along with weighted average section properties to predict ultimate strength. To decrease the effects of holes in columns and beams, edge-stiffeners are added to holes. The elastic buckling parameters can be determined from one of the three methods listed in Section 1.3.

Simplified methods utilizing the finite strip method for practicing engineers exist for determining elastic buckling parameters for members with holes that serve to eliminate the need for full eigen-buckling analysis (Moen and Schafer 2009a). The simplified methods have been extended to edge-stiffened holes to predict local and global buckling parameters; however, currently the effects of hole edge-stiffeners on distortional buckling load are ignored. Currently, elastic distortional buckling loads for edge-stiffened holes are determined based on the assumption that if a hole is introduced into an open cross-section, the rotational restraint provided by the element containing the hole is decreased resulting in a lower critical distortional buckling load (Moen and Schafer 2009a). This research serves to develop a simplified method

for determining the elastic distortional buckling load for columns and beams with edge-stiffened holes.

The simplified methods derived by Moen and Schafer (2009a) for unstiffened holes and validated for edge-stiffened holes by Moen and Yu (2010) were validated based on a series of Steel Stud Manufacturers Association (SSMA) members with simple edge-stiffened holes with varying hole height, hole length, and edge-stiffener lengths. The developed methods provide conservative engineering approximations for design but are only based on hole geometry found common to the cold-formed steel industry. As the cold-formed industry becomes more advanced and the manufacturing of complex shapes becomes easier, complex members such as in Figure 1.7 are manufactured that may cause the simplified methods to predict inaccurately and require validation to make sure they are still a viable option. The simplified methods will therefore be validated using common steel member dimensions, as well as the members in Figure 1.7 manufactured by Steelform, Inc.

(a) (b)

Figure 1.6 Thermally efficient Steelform Inc. structural edge-stiffened hole members. (a) LaBoube (2006) (b) Photo taken by author

Steelform Inc., the manufacturer and designer of the members in Figure 1.7, has designed and manufactured thermally efficient structural cold-formed studs (and beams) with complex edge-stiffened holes that require the elastic buckling parameters (local, distortional, and global) to be determined in order to commercialize their members for use in the construction industry. Finite element analysis with the holes explicitly modeled will be conducted to understand the effects of such complex geometry that includes the following: singly symmetric holes, opposing orientation of holes, multiple hole sizes, spacing of holes such that holes are not isolated from one another, varying edge-stiffener length and geometry around a hole, edge-stiffeners in both flange and web exist, and full section at ends of members that vary from 4 in. to 12 in.. The research aims to provide Steelform with elastic buckling parameters for their studs but also extend the already existing simplified methods as well as validate the developed distortional buckling method to complex studs of this nature. The research is conducted in two phases:

Phase 1 (Chapters 2 and 3)

1. Determine compressive elastic buckling parameters for Steelform DeltaSTUDS
2. Perform a torsional analysis to determine St Venant torsion constant, J and the warping torsion constant, C_w
3. Determine flexural elastic buckling parameters for Steelform DeltaSTUDS
4. Determine global elastic buckling modes for Steelform DeltaSTUDS
5. Take intermediate cross sections along length of Steelform DeltaSTUDS and calculate cross section properties to utilize for weighted average simplified methods.

Phase 2 (Chapters 4 and 5)

1. Develop simplified method for determining the influence of edge-stiffened holes on distortional buckling.
2. Validate all simplified methods using a selection of SSMA common studs and hole dimensions along with Steelform DELTSTUD members.
3. Extend simplified methods to Steelform DeltaSTUDS presented in Chapters 2 and 3.

1.6 **Previous Research – Purlin Distortional Buckling Strength**

A large amount of research has been completed prior on distortional buckling in standing seam roofing systems, which provide discrete bracing to the compression flange, and for distortional buckling in beams without any compression flange bracing (negative moment region). Most research dealing with metal building roof systems involved uplift conditions as that is usually the controlling factor (i.e. completely unbraced compression flange). Minimal research has been conducted on the effects of through-fastened panels on distortional buckling in gravity loading, and almost no research has been conducted on the effects of downward pressure on distortional buckling capacity. Experimental pressure box and four-point bending test results from tests of cold-formed Z- and C-section purlins used in roofing systems have been used to derive methods for determining distortional buckling capacity as reflected by the current North American Specification for Design of Cold-Formed Steel Structural members (AISI-S100 2007) and the Direct Strength Method (DSM). Included in this section is a summary of the relevant research pertaining to distortional buckling.

In 1990, Willis and Wallace (1990) studied the effects of fastener location on purlin capacity in through-fastened roof systems. They found that decking fastener location in Z-sections, had very little effect on flexural capacity. It was concluded that as downward load was applied, using concrete blocks, the bottom flange tended to roll underneath the top flange. This twisting was resisted by a contact compressive force between the deck and purlin, and as long as the flange was wide enough (2.5 in. minimum in their tests) to develop this force, no loss in capacity existed. As this testing did not directly pertain to distortional buckling, it was found that the current code at the time (AISI:Specification 1986) predicted unconservatively large

capacities for purlins with flange stiffener width to flange width ratios greater than 0.46, to the point where a reduction to flange buckling should be accounted for.

Schafer and Pekoz (1998a) further looked into the overall moment capacity of laterally braced cold-formed steel flexural members with edge-stiffened flanges and how the capacity could be affected by local or distortional buckling. At that point, the current code (AISI:Specification 1996) recognized the effects of local buckling but ignored distortional buckling. The 1996 AISI Specification tried to account for distortional buckling using the local buckling plate coefficient, k, which is dependent on boundary conditions and plate aspect ratios. The plate buckling coefficient was empirically derived based on a series of experimental tests by Desmond et al. (1981). However, much experimental work in the 1990s (by Willis and Wallace (1990), Schuster (1992) and Ellifritt (1997)) on laterally braced flexural members revealed that the strength prediction equations were still unconservative. Schafer and Pekoz suggested that even when the distortional buckling stress was higher than the local buckling stress (e.g when bracing exists), distortional buckling still had the ability to control the failure of the system.

A later paper by Schafer and Pekoz (1998b) studied the newly developed DSM prediction equations and compared it to the reduction factor for local-distortional interaction derived in Schafer and Pekoz (1998a). This paper also compared the results to the effective width approach. Experimental data based on 574 laterally braced flexural members (including channels, zees, hats, and trapezoidal sections) was analyzed. The results concluded that DSM provided the same overall average capacity prediction as the AISI Specification but at a much lower variation. However, for some sections, DSM was shown to be too conservative (Schafer and Pekoz 1998b).

Yu (2005) conducted local and distortional buckling four-point bending tests on a wide variety of industry standard laterally braced C and Z cold-formed steel beams. The first set of tests (local buckling tests) demonstrated that if additional restraint was provided by means of a through-fastened deck to the compression flange, the distortional buckling mode could be avoided. The second set of tests (distortional buckling tests) confirmed research by Schafer and Pekoz (1998a), which stated that the distortional buckling failures occurred even when local buckling was at a lower critical elastic buckling load. Comparing the experimental results with existing design specifications further confirmed that DSM, when compared with distortional buckling failure predictions was within 2% of the tested value on average.

Quantifying the additional rotational restraint provided by a through-fastened panel was also analyzed by use of a rotational spring in CUFSM (finite strip method) and ABAQUS (finite element method). Results concluded that the local buckling moment was unaffected by the additional restraint; however, the distortional buckling moment increased. A modified closed-form solution was proposed to determine the elastic distortional buckling moment of a section-panel system (Yu 2005) and was later added to the most current AISI: Specification (2007).

1.7 **Research Goals - Purlin Distortional Buckling Strength under Gravity Loading**

The most commonly produced cold-formed shapes are C- and Z-sections. Metal building wall and roofing systems are constructed with cold-formed Z-section since they are lightweight and can be easily erected and nested together. There are two types of conventional roofing systems: standing seam and through-fastened. The latter is composed of corrugated roofing panels that are attached directly to purlins by means of self-tapping screws. The main advantage of the through-fastened roofing system is that full lateral support is provided for the top compression flange of the purlins, whereas a standing seam roofing system only provides lateral

bracing at intermediate points. Determining the flexural capacity of cold-formed steel members in a roof system is complicated by the interaction between buckling modes(local, distortional, and global buckling) and material yielding (Yu and Schafer 2003). Research by Schafer and Yu (2004) stated that if additional rotational restraint was provided to the compression flange by means of a through-fastened metal deck, the distortional buckling mode could be avoided, and local buckling was triggered instead.

Two methods in the North American Specification (NAS) for Cold-Formed Steel currently exist for predicting the flexural capacity of stiffened compression flange members: the Main Specification in the NAS for the Design of Cold-Formed Steel Structural Members (AISI-S100 C3.1.4-10) and the Direct Strength Method (DSM) (DSM 2004). The NAS equation (AISI-S100 C3.1.4-10) for calculating the available distortional buckling capacity was derived based on a series of four-point bending tests at John Hopkins University (Schafer and Yu 2004). The DSM uses the finite strip method and considers that restrained bending exists when deck or sheathing restrains the section, allowing it to only deflect vertically. This can be compared to the unrestrained bending that occurs in Z-sections (deflection in both x and y directions) due to the rotation of the principal axes as denoted by x' and y' in Figure 1.8. In unrestrained bending, moment is applied through the principal axes causing stresses in the flanges contain both tensile and compressive stresses.

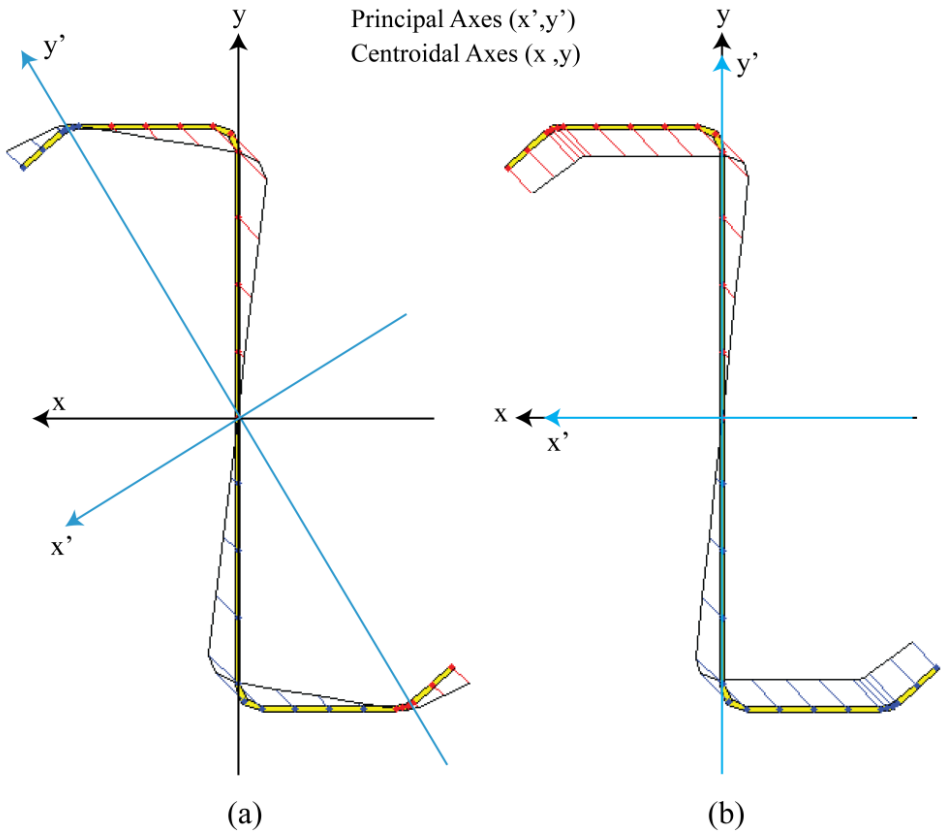

Figure 1.7 (a) Unrestrained versus (b) Restrained bending

In most loading conditions, purlins are subjected to downward uniform loading, such as a snow load. This downward uniform loading in theory could increase the rotational restraint provided to the compressive flange beyond the resistance of the through-fastened steel panel. To investigate this possible change in capacity, a MBMA fellowship project was undertaken where a series of gravity loading base tests were conducted in a custom built pressure box which isolated the effects of downward loading and quantifying the restraint provided to the purlin's compression flange in a through-fastened metal roof system.

CHAPTER 2. STEELFORM REPORT 1

2.1 Abstract

Steelform has requested research assistance from Virginia Tech to support the commercialization of a thermally efficient cold-formed steel structural stud. The members have stiffened holes with complex geometries that require finite element analysis to fully understand and explore their elastic buckling behavior. Steelform has asked Virginia Tech to calculate the elastic buckling parameters and torsional constants for two of their cold-formed steel structural studs with stiffened holes. These parameters will be utilized by others to predict member capacity. Virginia Tech will perform an elastic buckling analysis of two member types, the 1-5/8" x 3-5/8" and 1-5/8"x6" structural studs defined in Appendix A.

VIRGINIA POLYTECHNIC INSTITUTE AND STATE UNIVERSITY

The Charles E. Via, Jr. Department
of Civil and Environmental Engineering
Blacksburg, VA 24061

Structural Engineering and Materials

Structural Stud Elastic Buckling and Torsion Analysis

FINAL CONTRACT REPORT
CE/VPI-ST-10/01

Christopher N. Grey
Graduate Research Assistant

Dr. Cristopher D. Moen
Assistant Professor

for

Steelform Building Products, Inc.
60 Enterprise Road
Toronto, ON, M9W-1C9

2.2 Introduction

In this project, Virginia Tech performed an elastic buckling and torsional analysis of two cold-formed steel column types manufactured by Steelform Building Products, Inc., a 3.625 in. wide and a 6.000 in. wide structural stud, both with stiffened holes (see Appendix for details and dimensions). The studs are manufactured with a complex geometry that requires finite element analysis to accurately quantify structural behavior. The member properties summarized in this report will be utilized by others to predict column capacity with the American Iron and Steel Institute (AISI-S100) Direct Strength Method.

Structural studs with base metal thicknesses of 0.0346", 0.0451", 0.0566", and 0.0713" were analyzed for local, distortional, and global elastic buckling parameters along with St. Venants torsion constant, J, and the warping torsion constant, C_w. Nominal stud lengths of 80" and 88" (end gross sections varying from 4" to 12" respectively) were evaluated to quantify the influence of an unstiffened end section on local buckling. Also analyzed were the 3.625 in. and 6.000 studs without holes to verify the accuracy of the finite element analyses against finite strip results from the program CUFSM (Schafer and Ádány 2006).

2.3 Modeling Protocol

2.3.1 Structural Stud Notation

Structural stud dimension notation is described as follows:

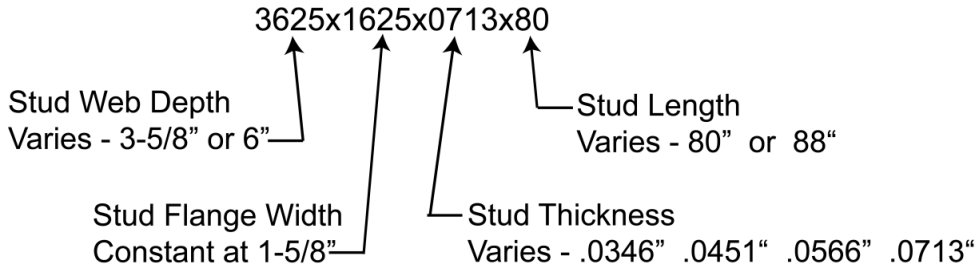

Figure 2.1 Structural stud nomenclature

2.3.2 Finite Element Meshing and Material Properties

Generating such unique geometry for finite element analysis required the use of the commercial 3-D modeling software Inventor by Autodesk (Autodesk 2010). Each column was drawn by hand in Inventor and then imported into the commercial finite element program ABAQUS (ABAQUS 2010). Once in ABAQUS, the model was meshed with S8R5 elements. The S8R5 element is an 8-node thin shell element that can accommodate geometries with complex radial surfaces. The modulus of elasticity, E, is assumed as 29500ksi and Poisson's ratio, ν, as 0.30 for all finite element models.

2.3.3 Loading and Boundary Conditions

The loading and boundary conditions employed in the eigen-buckling analyses are presented in Figure 2.2. Each column is compressed in ABAQUS with consistent nodal loads representing a uniform stress along the bearing edges. The column end nodes are restrained in 2 and 3 and the mid-length is restrained in 1. The loading and boundary conditions are consistent with finite strip analysis in CUFSM, which allows for a direct comparison and validation of ABAQUS results to CUFSM for columns without holes.

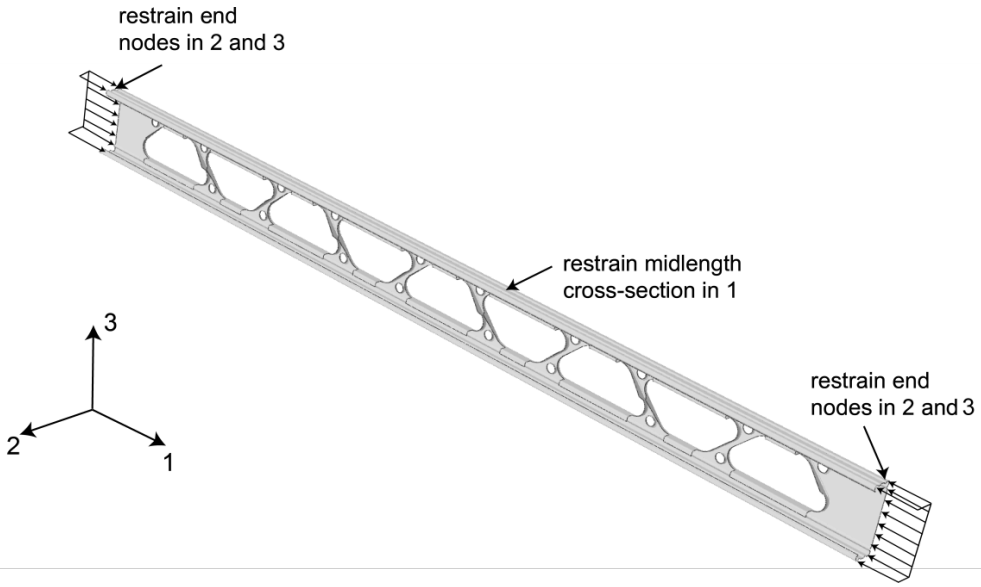

Figure 2.2 ABAQUS column boundary and loading conditions.

2.3.4 CUFSM Finite Strip Analysis

A finite strip analysis in CUFSM (Schafer and Ádány 2006) was performed for each column. Both gross section and net section (mid hole) finite strip models were considered. The local, distortional, and global buckling loads ($P_{cr\ell nh}$, P_{crd}, P_{cre}) and their respective half-wavelengths were determined from the gross section model. Figure 2.3 reveals the local and distortional modes for the gross cross section as they occur at distinct half wavelengths, as well as the global buckling mode at the physical member length, *L*. The net section finite strip model was used to predict the local buckling load at a hole, $P_{cr\ell h}$, as shown in Figure 2.4. The corners of the net cross-section were restrained in CUFSM to isolate local buckling from distortional buckling.

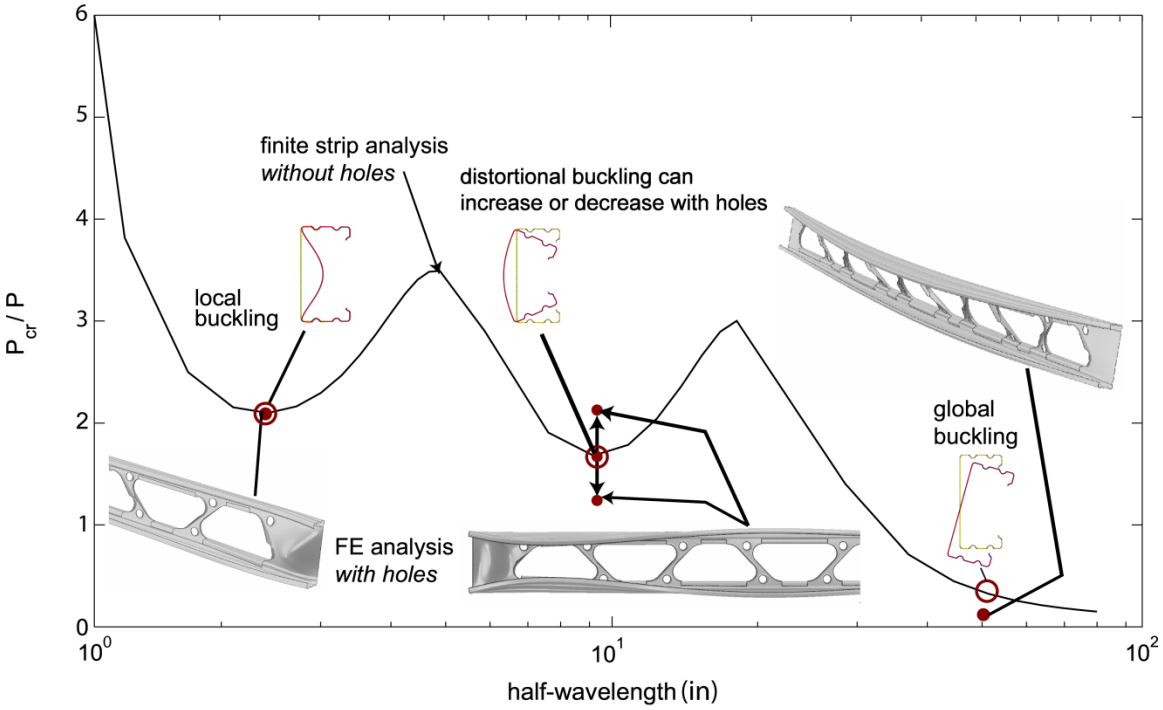

Figure 2.3 Elastic compression buckling curve for cold-formed section with the finite strip method.

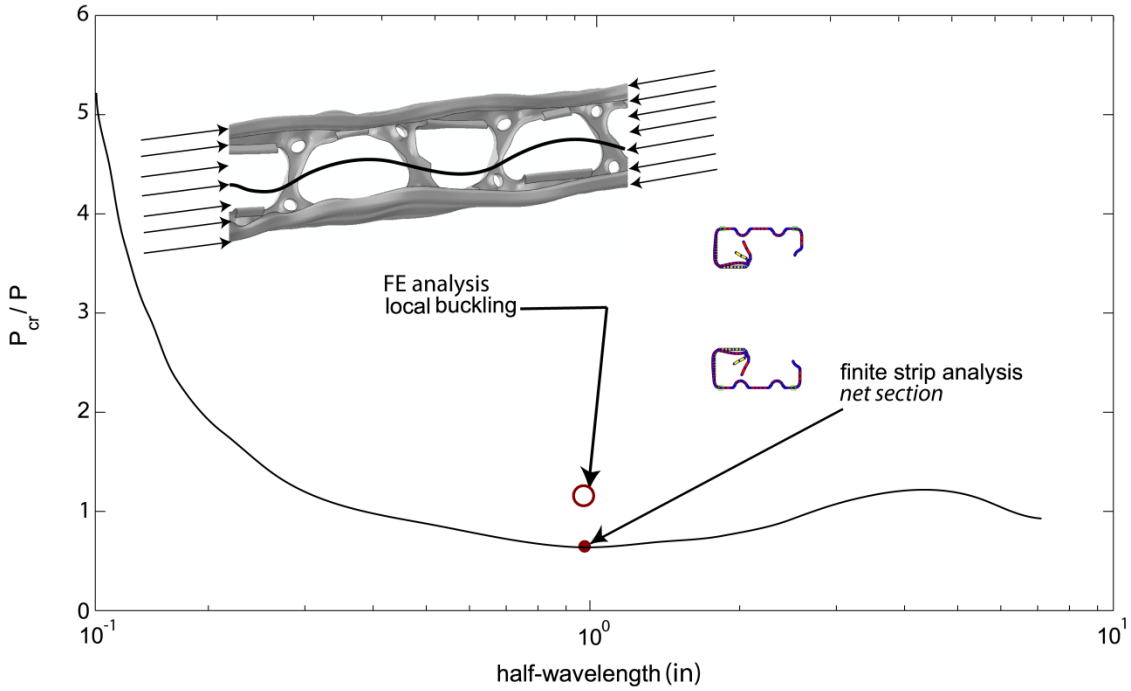

Figure 2.4 Elastic compression buckling curve for cold-formed net section with the finite strip method.

2.4 **Elastic Buckling Results**

Table 2.1 through Table 2.3 present the finite strip and finite element elastic buckling results. For all columns considered, $P_{cr\ell h} >> P_{cr\ell nh}$, demonstrating that the cross section at a hole is very stiff, and that local buckling will occur in the unstiffened portions of the cross-section near the ends of the column. The local buckling load without holes, $P_{cr\ell nh}$, from CUFSM (Table 2.1) is within 1% of the ABAQUS result (Table 2.2), confirming the accuracy of the S8R5 meshing scheme described in Section 2.3.2. (Note that P_{crd} and P_{cre} are also consistent between ABAQUS and CUFSM for columns without holes, further validating the modeling protocol.) The length of the unstiffened section at the end of a column (compare $P_{cr\ell nh}$ for L=80 in. to L=88 in. in Table 2.1) does not influence local buckling load.

The distortional buckling behavior is complicated by the presence of holes. New distortional "hole" modes are created at the ends of the column with buckling loads that can be higher or lower than a column without holes, and half-wavelengths that can be longer or shorter than a column without holes. The buckling loads for these "hole" modes are reported as P_{crd} in Table 2.3. The pure distortional buckling load (i.e. the mode consistent with CUFSM half-wavelengths) increases by as much as twice a member without holes, however it is hypothesized that the "hole" modes are more accurate predictors of capacity.

The presence of holes decreases the global (Euler) buckling load, P_{cre}, for all cases considered, with a maximum decrease of 28% occurring for the 6000x1625x0713 column. The lowest column buckling mode is flexural-torsional buckling for all 3.625 in. columns with holes except the 3625x1625x0713 as shown in Table 2.3. Note that the presence of holes causes the global buckling mode to switch from flexural-torsional buckling to weak axis flexure for this

column (compare Table 2.2 to Table 2.3). All 6.000 in. columns buckle in weak axis flexure. The global buckling load is penalized more in the 6.000 in. columns because the holes drive down the weak axis moment of inertia.

Table 2.1 CUFSM finite strip elastic buckling results.

Specimen	CUFSM gross section model							CUFSM net section	
	L=80 in.							section model	
	$P_{crℓnh}$ kips	$L_{crℓnh}$ in.	P_{crd} kips	L_{crd} in.	P_{cre} kips	J in^4	C_w in^6	$P_{crℓh}$ kips	$L_{crℓh}$ in.
3625x1625x0346	4.21	2.80	9.56	20.0	3.21	0.00012	0.294	69.13	1.00
3625x1625x0451	9.16	2.80	16.7	17.0	4.34	0.000263	0.373	127.6	1.00
3625x1625x0566	17.8	2.80	27.0	15.0	5.78	0.000516	0.452	228.2	1.00
3625x1625x0713	34.9	2.80	44.6	13.0	7.99	0.001020	0.548	404.9	1.00
6000x1625x0346	2.72	4.80	6.02	19.5	5.24	0.000157	0.863	58.05	1.00
6000x1625x0451	5.45	4.80	9.74	16.5	6.89	0.000347	1.08	127.7	1.00
6000x1625x0566	10.2	4.80	15.5	15.3	8.57	0.000686	1.32	241.2	1.00
6000x1625x0713	18.8	4.60	26.0	13.5	10.7	0.00136	1.61	476.4	1.00

Table 2.2 ABAQUS buckling results – columns without holes.

Specimen	ABAQUS model without holes							
	L=80 in.		L=88 in.		L=80 in.			
	$P_{crℓnh}$ kips	$L_{crℓ}$ in	$P_{crℓnh}$ kips	$L_{crℓ}$ in	P_{crd} kips	L_{crd} in	P_{cre} kips	
3625x1625x0346	4.10	2.77	4.14	2.77	9.55	20.0	3.23	FT
3625x1625x0451	8.92	2.77	8.92	2.77	16.8	16.0	4.39	FT
3625x1625x0566	17.4	2.85	17.5	2.85	27.4	16.1	5.83	FT
3625x1625x0713	34.2	2.85	34.2	2.85	44.9	13.3	8.07	FT
6000x1625x0346	2.65	4.73	2.65	4.72	5.34	20.0	5.23	WAF
6000x1625x0451	5.36	4.80	5.36	4.80	9.34	16.2	6.88	WAF
6000x1625x0566	9.89	4.80	9.89	4.80	15.6	16.1	8.55	WAF
6000x1625x0713	18.7	4.80	18.7	4.80	25.8	13.5	10.6	WAF

Note: "FT" stands for Flexural Torsional buckling mode
"WAF" stands for Weak Axis Flexure buckling mode

Table 2.3 ABAQUS buckling results – columns with holes.

Specimen	ABAQUS model with holes									
	L=80 in.		L=88 in.		L=80 in.				L=80 in.	
	$P_{crℓh}$ kips	$L_{crℓh}$ in	$P_{crℓh}$ kips	$L_{crℓh}$ in	P_{crd} kips	L_{crd} in	P_{cre} kips		J in^4	C_w in^6
3625x1625x0346	4.51	3.34	4.11	2.78	10.1	15.0	2.75	FT	0.000124	0.307
3625x1625x0451	9.78	3.45	8.96	2.82	14.3	12.3	3.75	FT	0.000268	0.384
3625x1625x0566	19.0	3.62	17.4	2.80	27.6	12.1	5.02	FT	0.000518	0.452
3625x1625x0713	37.0	3.79	34.3	2.85	37.0	10.9	6.61	WAF	0.00100	0.537
6000x1625x0346	3.64	4.50	2.69	4.72	7.1	16.5	4.10	WAF	0.000170	0.942
6000x1625x0451	7.50	4.64	5.44	4.76	14.8	15.5	5.45	WAF	0.000361	1.13
6000x1625x0566	13.8	4.65	9.95	4.76	17.7	15.4	6.44	WAF	0.000718	1.37
6000x1625x0713	25.8	4.70	18.7	4.83	25.8	11.6	7.68	WAF	0.00136	1.61

2.5 **Torsion Properties**

To determine the torsional constants J and and C_w, a torsional analysis was performed. The general equation for nonuniform torsion is defined as:

$$T = GJ\frac{d\beta}{dz} - EC_w\frac{d^3\beta}{dz^3}, \tag{2.1}$$

Where $d\beta/dz$ is the rate of twist along the stud, and G is the shear modulus. The St. Venant's torsion constant, J, was calculated by applying a unit twist, β_o, at the end of a stud about its center of twist (i.e. shear center) while maintaining the opposite column end fixed against twist, but warping free, i.e. $d^3\beta/dz^3=0$, as shown in Figure 2.5. Because the fixed end is warping free, it provides no warping resistance. The torsion, T, resulting from the imposed unit twist was read from ABAQUS, and then J (Table 2.3) was solved directly from Eq. 2.1 (AISI-S100).

The column boundary conditions were then modified so that the twist-fixed end was warping restrained ($d^3\beta/dz^3 \neq 0$). A unit twist was applied and C_w was solved for as a function of the gross $C_{w,g}$ (Moen and Schafer 2009) from either CUFSM or ABAQUS:

$$\frac{C_{w,FE}}{C_{w,g}} = \frac{T_0 - GJ_{FE}\frac{d\beta}{dz}}{T_{0,g} - GJ_g\frac{d\beta}{dz}}. \tag{2.2}$$

(Note that this procedure was validated by comparing J and C_w derived from an ABAQUS model without holes to the J and C_w calculated with CUFSM.)

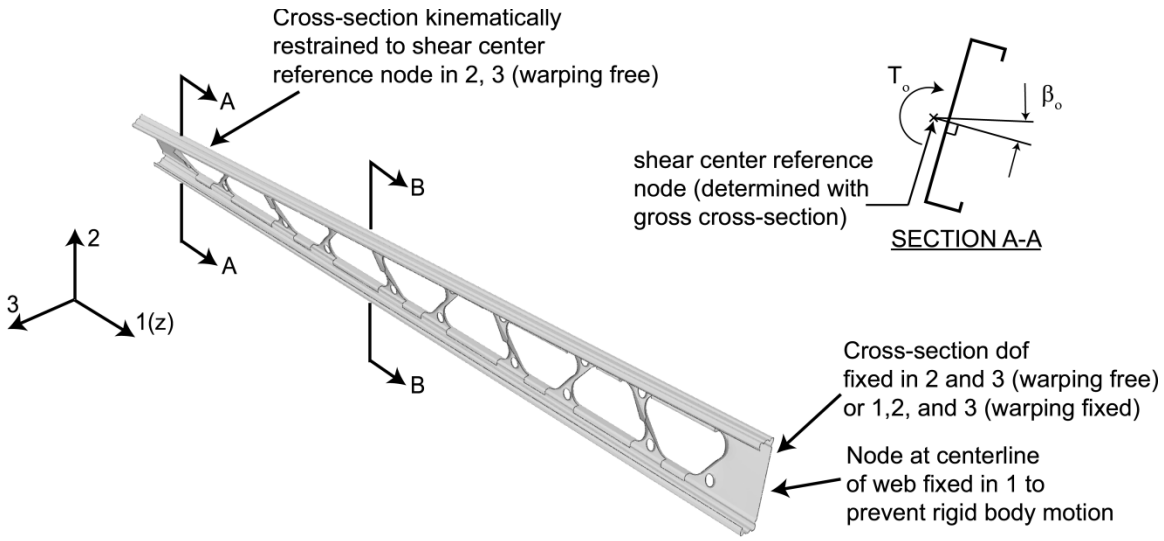

Figure 2.5 ABAQUS boundary conditions for the study of J and C_w including holes.

The torsional constants J and C_w are minimally affected by the presence of stiffened holes, and even increase in some cases (compare Table 2.1 to Table 2.3). The St. Venant torsional constant is a function of cross-section perimeter, and since stiffened holes are formed by punching through the cross-section, much of the removed hole material remains as part of the stiffener in the net section. The presence of stiffeners around the holes compensates for the loss in warping resistance by providing a path for the longitudinal warping stresses to travel around the hole, which is different behavior from unstiffened holes, where the longitudinal warping stresses (and resistance) terminates at a hole.

2.6 **Conclusions**

An elastic buckling and torsion analysis was performed for two different Steelform structural stud configurations. Local buckling was observed to be unaffected by the presence of holes, occurring in the gross cross-section near the ends of the column. The pure distortional buckling load increased when compared to the same columns without holes, however new distortional modes were initiated by the presence of holes that should be considered in design and evaluated with experiments. Global buckling loads decreased for all columns when compared to the same columns without holes. The largest decrease in global buckling load was observed for columns buckling in weak axis flexure because of the sharp reduction in weak axis moment of inertia resulting from the perforated web. The St. Venant and warping torsion resistance were minimally affected by the presence of stiffened holes and even increased in some cases.

CHAPTER 3. STEELFORM REPORT 2

3.1 **Abstract**

Steelform has requested research assistance from Virginia Tech to support the commercialization of an innovative cold-formed steel structural stud. The members have stiffened holes with complex geometries that require finite element analysis to fully understand and explore their elastic buckling behavior. Steelform has asked Virginia Tech to calculate the flexural and global elastic buckling parameters as well as determine cross-sectional properties at multiple instances for two member types, the 1-5/8 x 3-5/8 in. and 1-5/8 x 6 in. cold-formed steel structural studs with stiffened holes. These parameters will be utilized by others to predict member capacity.

VIRGINIA POLYTECHNIC INSTITUTE AND STATE UNIVERSITY

The Charles E. Via, Jr. Department
of Civil and Environmental Engineering
Blacksburg, VA 24061

Structural Engineering and Materials

Structural Stud Flexural Elastic Buckling and Global Columns Buckling Studies

FINAL CONTRACT REPORT
CE/VPI-ST-10/08

Christopher N. Grey
Graduate Research Assistant

Dr. Cristopher D. Moen
Assistant Professor

for

Steelform Building Products, Inc.
60 Enterprise Road
Toronto, ON, M9W-1C9

3.2 Introduction

In this project, Virginia Tech performed a flexural elastic buckling analysis of two cold-formed structural wind bearing studs manufactured by Steelform Building Products, Inc., a 3.625 in. wide and a 6.000 in. wide structural stud, both with stiffened holes (see Appendix A for details and dimensions). Global column buckling modes were also identified. The studs are manufactured with a complex geometry that requires specialized finite element analysis to accurately quantify structural behavior. The member properties summarized in this report will be utilized by others to predict capacity with the American Iron and Steel Institute (AISI-S100) Direct Strength Method.

Structural studs with base metal thicknesses of 0.0346 in., 0.0451 in., 0.0566 in., and 0.0713 in. were analyzed for local, distortional, and global flexural elastic buckling parameters. Nominal stud lengths of 80" and 88" (end gross sections varying from 4" to 12" respectively) were evaluated to quantify the influence of an unstiffened end section on local buckling. Also analyzed were the 3.625 in. and 6.000 in studs without holes to verify the accuracy of the finite element analyses against finite strip results from the program CUFSM (Schafer and Ádány 2006).

3.3 Modeling Protocol

3.3.1 Structural Stud Notation

Structural stud dimension notation is described as follows:

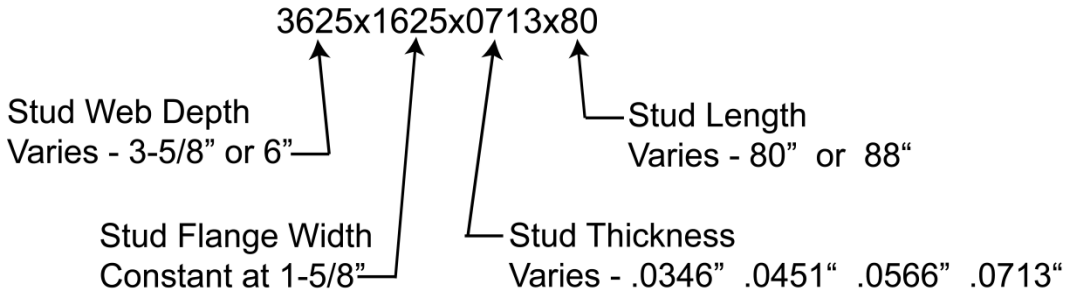

Figure 3.1 Structural stud nomenclature

3.3.2 Finite Element Meshing and Material Properties

Generating such unique geometry for finite element analysis required the use of the commercial 3D modeling software Inventor by Autodesk (Autodesk 2010). Each column was drawn by hand in Inventor and then imported into the commercial finite element program ABAQUS (ABAQUS 2010). Once in ABAQUS, the model was meshed with S8R5 elements. The S8R5 element is an 8-node thin shell element that can accommodate geometries with complex radial surfaces. The modulus of elasticity, E, is assumed as 29500 ksi and Poisson's ratio, ν, as 0.30 for all finite element models.

3.4 **Flexural Elastic Buckling**

3.4.1 Loading and Boundary Conditions

The loading and boundary conditions employed in the flexural eigen-buckling analyses are presented in Figure 3.2. Each stud is loaded in ABAQUS with consistent nodal loads representing a flexural stress along the bearing edges. Due to unsymmetrical hole geometry, the studs are loaded in both positive and negative bending to analyze the effects. (See Figure 3.2 for moment orientation) The column end nodes are restrained in 2 and 3 and the midlength is restrained in 1. The loading and boundary conditions are consistent with finite strip analysis in CUFSM, which allows for a direct comparison and validation of ABAQUS results to CUFSM for columns without holes.

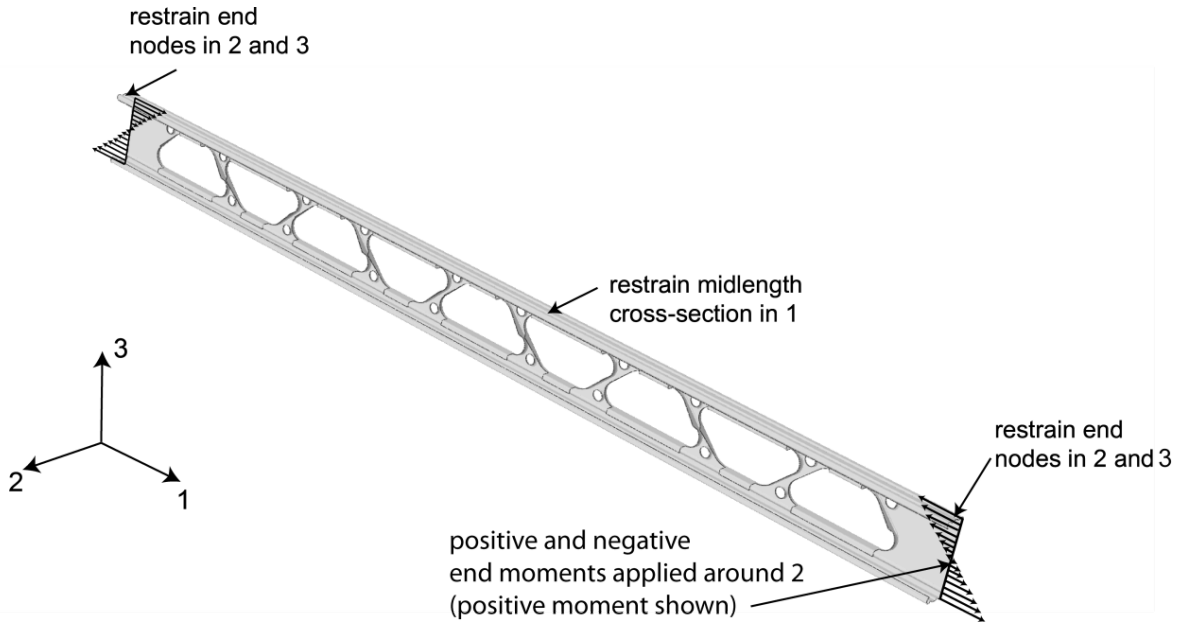

Figure 3.2 ABAQUS flexure boundary and loading conditions.

3.4.2 CUFSM Finite Strip Flexure Analysis

A finite strip analysis in CUFSM (Schafer and Ádány 2006) was performed for each stud. Both gross section and net section (mid hole) finite strip models were considered. The local, distortional, and global buckling moments ($M_{cr\ell nh}$, M_{crd}, M_{cre}) and their respective half-wavelengths were determined from the gross section model. Figure 3.3 reveals the local and distortional modes for the gross cross section as they occur at distinct half wavelengths, as well as the global buckling mode at the physical member length, L (in.). The same figure also shows how the finite element analysis on studs with holes compares. The net section finite strip model was used to predict the local buckling load at a hole, $M_{cr\ell h}$, as shown in Figure 3.4. The corners of the net cross-section were restrained in CUFSM to isolate local buckling from distortional buckling.

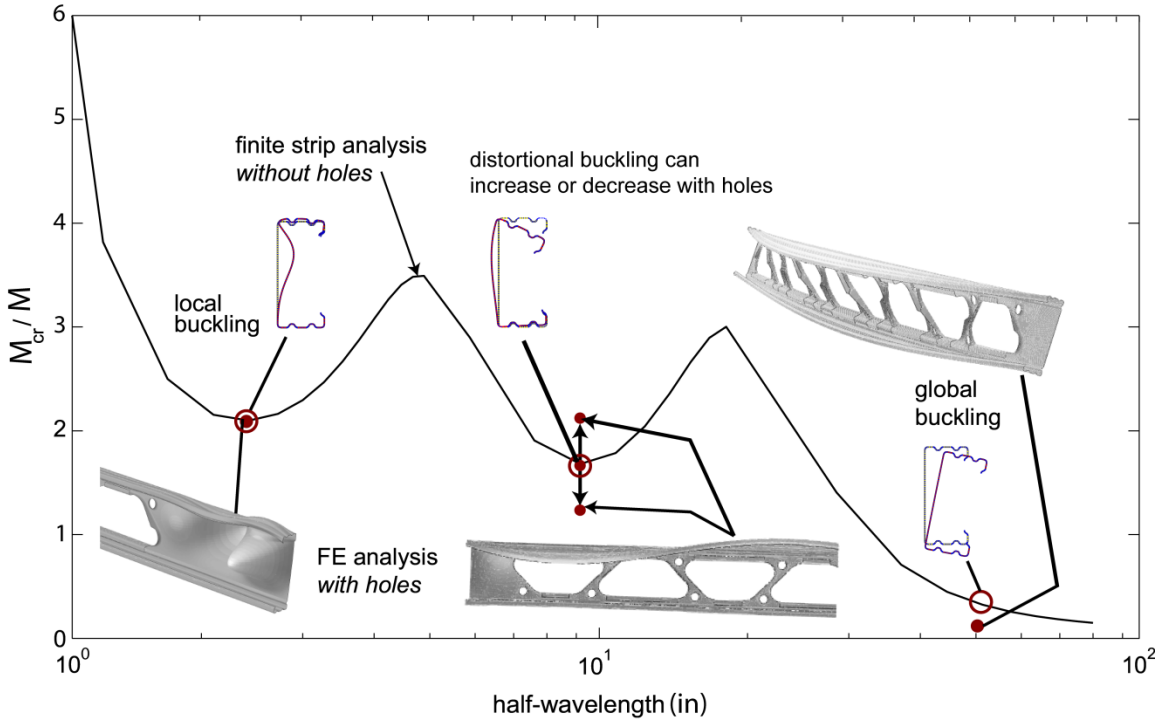

Figure 3.3 Flexural elastic buckling curve for cold-formed studs without holes using the finite strip method compared to finite element analysis of cold-formed studs with holes.

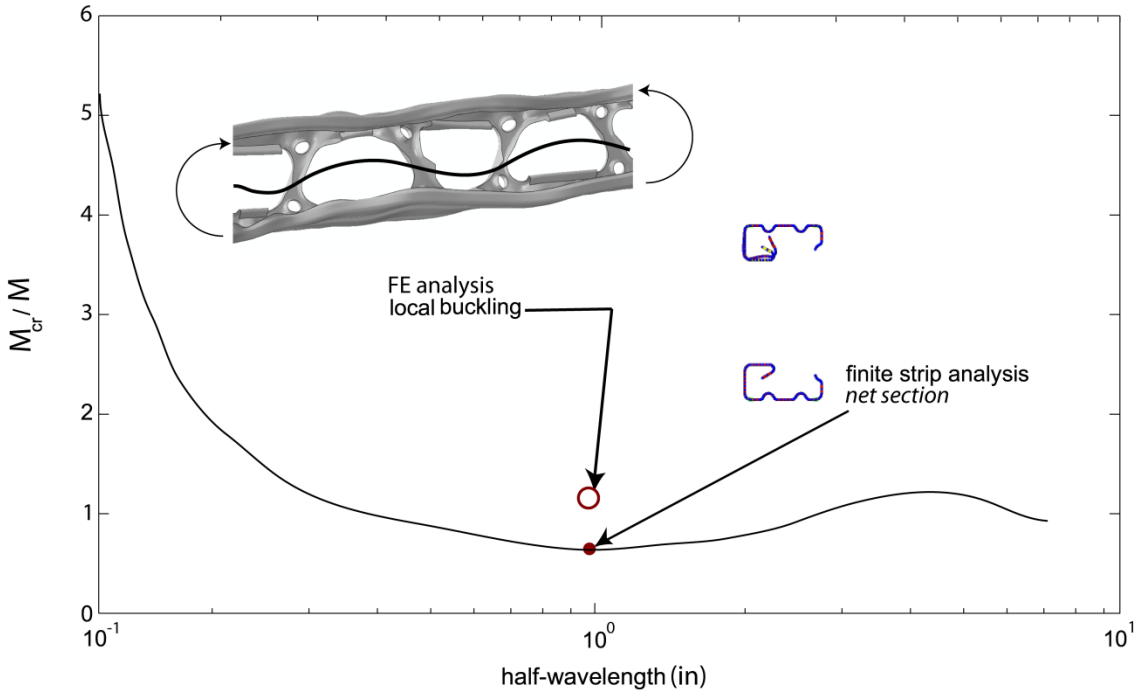

Figure 3.4 Flexural elastic buckling curve for cold-formed net section with the finite strip method compared to finite element analysis of cold-formed studs with holes.

3.4.3 Flexural Elastic Buckling Results

Tables 3.1, 3.2, 3.4, and 3.5 present the flexural elastic buckling results for each stud. Tables 3.3, 3.6, 3.7, 3.8, and 3.9 are comparison tables which accommodate interpretation.

3.4.3.1 Results - Studs without holes

Validation of the finite element properties used throughout the project is presented in Table 3.3. For all studs analyzed, the local buckling moment without holes, $M_{cr\ell nh}$, from CUFSM (Table 3.1) is within 2% of the ABAQUS result (Table 3.2), confirming the accuracy of the S8R5 meshing scheme described in Section 3.3.2. (Note that M_{crdnh} and M_{crenh} are also consistent between ABAQUS and CUFSM for columns without holes, further validating the modeling protocol.) Possible reasons for this 2% discrepancy is that ABAQUS takes into account multiple modes occurring at different half-wavelengths occurring at once which the finite strip method

(CUFSM) cannot. For this reason, local buckling with some influence from distortional buckling will occur at a lower load than the ideal local buckling mode shape. This is seen more in the thinner sections as distortional buckling loads predicted by CUFSM are within 10% of the local buckling loads versus the thicker sections in which up to a 50% difference exists.

Table 3.1 CUFSM finite strip elastic buckling results

Specimen	CUFSM gross section model					CUFSM net section	
	L=80 in.					section model	
	$M_{cr\ell nh}$ kipin	$L_{cr\ell nh}$ in.	M_{crdnh} kipin	L_{crdnh} in.	M_{crenh} kipin	$M_{cr\ell h}$ kipin	$L_{cr\ell h}$ in.
3625x1625x0346	26.94	2.00	19.62	17.9	8.21	133.8	1.00
3625x1625x0451	57.97	2.20	33.90	15.4	10.85	242.1	1.00
3625x1625x0566	102.1	3.00	54.66	13.6	13.78	434.4	1.00
3625x1625x0713	185.7	3.00	88.95	11.9	17.87	738.6	1.00
6000x1625x0346	30.66	4.40	28.13	19.3	14.83	187.0	1.00
6000x1625x0451	58.11	4.20	49.39	16.7	19.30	408.4	1.00
6000x1625x0566	104.5	4.00	80.72	14.8	24.04	777.4	1.00
6000x1625x0713	189.9	3.90	133.2	13.0	30.23	954.7	1.00

Table 3.2 ABAQUS buckling results – Studs without holes.

Specimen	ABAQUS model without holes						
	L=80 in.		L=88 in.		L=80 in.		
	$M_{cr\ell nh}$ kip in	$L_{cr\ell}$ in	$M_{cr\ell nh}$ kip in	$L_{cr\ell}$ in	M_{crdnh} kip in	L_{crdnh} in	M_{crenh} kip in
3625x1625x0346	26.80	2.02	26.80	2.03	20.06	20.0	8.27
3625x1625x0451	57.05	2.17	57.05	2.18	34.24	15.8	10.93
3625x1625x0566	104.1	3.60	104.3	3.00	55.23	13.3	13.96
3625x1625x0713	183.9	3.75	183.9	3.75	90.34	11.4	18.11
6000x1625x0346	30.12	4.43	30.12	4.27	28.40	20.0	14.87
6000x1625x0451	57.91	4.20	57.92	4.20	49.89	16.0	19.29
6000x1625x0566	102.6	4.05	102.6	3.97	81.90	16.0	23.94
6000x1625x0713	186.8	3.98	186.8	3.97	134.8	13.3	30.29

Table 3.3 ABAQUS validation with CUFSM - Positive bending

Specimen	ABAQUS validation with CUFSM - Positive bending								
	ABAQUS	CUFSM		ABAQUS	CUFSM		ABAQUS	CUFSM	
	$M_{cr\ell nh\ 80}$ kip in	$M_{cr\ell nh\ 80}$ kip in	% Difference	M_{crdnh} kip in	M_{crdnh} kip in	% Difference	M_{crenh} kip in	M_{crenh} kip in	% Difference
3625x1625x0346	26.80	26.94	0.5	20.06	19.62	-2.2	8.273	8.213	-0.7
3625x1625x0451	57.05	57.97	1.6	34.24	33.90	-1.0	10.93	10.85	-0.7
3625x1625x0566	104.1	102.1	-1.9	55.23	54.66	-1.0	13.96	13.78	-1.3
3625x1625x0713	183.9	185.7	1.0	90.34	88.95	-1.5	18.11	17.87	-1.3
6000x1625x0346	30.12	30.66	1.8	28.40	28.13	-1.0	14.87	14.83	-0.3
6000x1625x0451	57.91	58.11	0.3	49.89	49.39	-1.0	19.29	19.30	0.0
6000x1625x0566	102.6	104.5	1.9	81.90	80.72	-1.4	23.94	24.04	0.4
6000x1625x0713	186.8	189.9	1.7	134.8	133.2	-1.1	30.29	30.23	-0.2

3.4.4 Results - Studs with holes

For all studs except for the 3625x1625x0566 stud, $M_{cr\ell h} >> M_{cr\ell nh}$, demonstrating that the cross section at a hole is very stiff, and that local buckling will occur in the unstiffened portions of the cross-section near the ends of the column. The length of the unstiffened section at the end of a column (compare $M_{cr\ell nh}$ for L=80 in. to L=88 in. in Table 3.2 does not influence local buckling moment. This is because there is enough gross section still available for a local half-wavelength to form. However, the effect of positive and negative bending does affect the critical local buckling moment for the 80 in. long 6.000 in. studs as the thickness increases (Table 3.6). For example, the 6000x1625x0713x80 stud loaded in negative bending, the critical local buckling moment increases by 10.3% as the half-wavelength decreased by 12.3%. This decrease is shown in Figure 3.5 where in positive bending a 4.06 in. half wavelength forms compared to the 2.72 in. half wavelength that forms in negative bending. The nonsymmetrical holes decreases the unstiffened distance where a local half-wave can form as shown in Figure 3.5. This increase in buckling load does not occur in the 3.625 in studs the local buckling half-wavelength is short enough to fit within the unstiffened section. Also note that the critical local buckling load at the net section (mid hole) is approximately five times higher than the local buckling load at the gross section.

The distortional buckling moments are reported in Table 3.4 and Table 3.5 as M_{crdh} and compared in Table 3.7 and Table 3.8. Distortional buckling is minimally affected by the direction of loading (Table 3.6), however, for the 6000x1625x0713 stud, an additional distortional half wavelength is formed when loaded in positive bending versus negative bending (see Table 3.4 and Table 3.5). The presence of the stiffened holes shows an increase in distortional buckling load by as much as 13.4% in positive bending and by 11.3% in negative bending. In the thickest 3.625 in. studs, the distortional buckling capacity is decreased by 2.3% (Table 3.7 and Table 3.8). As was the case for the previous study on compression members, a pure distortional buckling mode was difficult to identify when holes were present. The presence of holes decreases the lateral-torsional buckling load, M_{cre}, for all cases considered, with a maximum decrease of 17.9% occurring for the 6000x1625x0713 stud in positive bending (Table 3.7).

Table 3.4 ABAQUS positive moment buckling results – Studs with holes.

Specimen	ABAQUS model with holes - Positive bending						
	L=80 in.		L=88 in.		L=80 in.		
	$M_{cr/h}$ kip in	$L_{cr/h}$ in	$M_{cr/h}$ kip in	$L_{cr/h}$ in	M_{crdh} kip in	L_{crdh} in	M_{creh} kip in
3625x1625x0346	27.74	2.23	26.85	2.04	21.45	16.0	6.94
3625x1625x0451	58.49	2.36	57.16	2.18	36.15	16.0	9.13
3625x1625x0566	103.0	3.90	104.6	2.97	56.43	13.3	11.58
3625x1625x0713	186.4	3.39	181.4	3.89	88.30	11.9	14.99
6000x1625x0346	32.18	4.40	30.40	4.26	32.18	20.0	12.42
6000x1625x0451	63.87	4.25	58.45	4.17	56.58	16.0	16.68
6000x1625x0566	101.1	4.12	102.5	3.92	90.21	16.0	20.22
6000x1625x0713	177.4	4.06	184.8	4.09	140.5	13.3	24.86

Table 3.5 ABAQUS negative moment buckling results – Studs with holes.

Specimen	ABAQUS model with holes - Negative bending						
	L=80 in.		L=88 in.		L=80 in.		
	$M_{cr\ell h}$ kip in	$L_{cr\ell h}$ in	$M_{cr\ell h}$ kip in	$L_{cr\ell h}$ in	M_{crdh} kip in	L_{crdh} in	M_{creh} kip in
3625x1625x0346	27.75	2.16	26.85	2.05	21.45	16.0	6.94
3625x1625x0451	58.51	2.43	57.16	2.24	36.14	16.0	9.13
3625x1625x0566	103.0	3.90	104.6	2.92	56.44	13.3	11.65
3625x1625x0713	186.4	3.41	181.4	4.05	88.26	11.9	15.01
6000x1625x0346	32.47	3.84	30.44	4.45	31.60	20.0	12.48
6000x1625x0451	65.52	3.72	58.54	4.08	54.91	16.0	16.32
6000x1625x0566	110.0	3.62	102.4	4.01	86.27	16.0	19.92
6000x1625x0713	195.7	3.56	185.1	4.08	138.3	16.0	25.02

Table 3.6 ABAQUS positive versus negative bending comparison – Studs with holes

Specimen	ABAQUS positive/negative bending comparison											
	L=80 in			L=88 in			L=80 in			L=80 in		
	$M_{cr\ell h}$ + kip in	$M_{cr\ell h}$ - kip in	% Difference	$M_{cr\ell h}$ + kip in	$M_{cr\ell h}$ - kip in	% Difference	M_{crdh} + kip in	M_{crdh} - kip in	% Difference	M_{creh} + kip in	M_{creh} - kip in	% Difference
3625x1625x0346	27.74	27.75	0.0	26.85	26.85	0.0	21.45	21.45	0.0	6.937	6.941	0.1
3625x1625x0451	58.49	58.51	0.0	57.16	57.16	0.0	36.15	36.14	0.0	9.126	9.133	0.1
3625x1625x0566	103.0	103.0	0.0	104.6	104.6	0.0	56.43	56.44	0.0	11.58	11.65	0.6
3625x1625x0713	186.4	186.4	0.0	181.4	181.4	0.0	88.30	88.26	0.0	14.99	15.01	0.1
6000x1625x0346	32.18	32.47	0.9	30.40	30.44	0.1	32.18	31.60	-1.8	12.42	12.48	0.5
6000x1625x0451	63.87	65.52	2.6	58.45	58.54	0.2	56.58	54.91	-3.0	16.68	16.32	-2.1
6000x1625x0566	101.1	110.0	8.8	102.5	102.4	-0.1	90.21	86.27	-4.4	20.22	19.92	-1.5
6000x1625x0713	177.4	195.7	10.3	184.8	185.1	0.2	140.5	138.3	-1.6	24.86	25.02	0.6

Table 3.7 ABAQUS influence of holes - Positive bending

Specimen	ABAQUS influence of holes - Positive Bending											
	Local Buckling 80 in.			Local Buckling 88 in.			Distortional Buckling 80 in			Global Buckling 80 in		
	$M_{cr\ell nh}$ kip in	$M_{cr\ell h}$ kip in	% Difference	$M_{cr\ell nh}$ kip in	$M_{cr\ell h}$ kip in	% Difference	M_{crdnh} kip in	M_{crdh} kip in	% Difference	M_{crenh} kip in	M_{creh} kip in	% Difference
3625x1625x0346	26.80	27.74	3.5	26.80	26.85	0.2	20.06	21.45	6.9	8.27	6.937	-16.1
3625x1625x0451	57.05	58.49	2.5	57.05	57.16	0.2	34.24	36.15	5.6	10.93	9.126	-16.5
3625x1625x0566	104.1	103.00	-1.0	104.3	104.6	0.2	55.23	56.43	2.2	13.96	11.58	-17.0
3625x1625x0713	183.9	186.43	1.4	183.9	181.4	-1.3	90.34	88.30	-2.3	18.11	14.99	-17.2
6000x1625x0346	30.12	32.18	6.8	30.12	30.40	0.9	28.40	32.18	13.3	14.87	12.42	-16.5
6000x1625x0451	57.91	63.87	10.3	57.92	58.45	0.9	49.89	56.58	13.4	19.29	16.68	-13.5
6000x1625x0566	102.6	101.11	-1.5	102.6	102.5	-0.1	81.90	90.21	10.1	23.94	20.22	-15.6
6000x1625x0713	186.8	177.36	-5.0	186.8	184.8	-1.1	134.8	140.5	4.3	30.29	24.86	-17.9

Table 3.8 ABAQUS influence of holes - Negative bending

Specimen	ABAQUS influence of holes - Negative Bending											
	Local Buckling 80 in.			Local Buckling 88 in.			Distortional Buckling 80 in			Global Buckling 80 in		
	$M_{cr\ell nh}$ kip in	$M_{cr\ell h}$ kip in	% Difference	$M_{cr\ell nh}$ kip in	$M_{cr\ell h}$ kip in	% Difference	M_{crdnh} kip in	M_{crdh} kip in	% Difference	M_{crenh} kip in	M_{creh} kip in	% Difference
3625x1625x0346	26.80	27.75	3.5	26.80	26.85	0.2	20.06	21.45	6.9	8.27	6.941	-16.1
3625x1625x0451	57.05	58.51	2.6	57.05	57.16	0.2	34.24	36.14	5.6	10.93	9.133	-16.4
3625x1625x0566	104.1	103.0	-1.0	104.3	104.6	0.2	55.23	56.44	2.2	13.96	11.65	-16.5
3625x1625x0713	183.9	186.4	1.3	183.9	181.4	-1.3	90.34	88.26	-2.3	18.11	15.01	-17.1
6000x1625x0346	30.12	32.47	7.8	30.12	30.44	1.1	28.40	31.60	11.3	14.87	12.48	-16.1
6000x1625x0451	57.91	65.52	13.1	57.92	58.54	1.1	49.89	54.91	10.1	19.29	16.32	-15.4
6000x1625x0566	102.6	110.0	7.2	102.6	102.4	-0.2	81.90	86.27	5.3	23.94	19.92	-16.8
6000x1625x0713	186.8	195.7	4.7	186.8	185.1	-0.9	134.8	138.3	2.6	30.29	25.02	-17.4

Table 3.9 CUFSM local buckling comparison at a hole versus gross section

CUFSM local buckling at a hole vs no hole			
Specimen	$M_{cr\ell nh}$ kip in	$M_{cr\ell h}$ kip in	% Difference
3625x1625x0346	26.94	133.81	396.7
3625x1625x0451	57.97	242.09	317.6
3625x1625x0566	102.11	434.41	325.4
3625x1625x0713	185.65	738.60	297.8
6000x1625x0346	30.66	187.01	509.9
6000x1625x0451	58.11	408.36	602.7
6000x1625x0566	104.54	777.40	643.6
6000x1625x0713	189.90	954.67	402.7

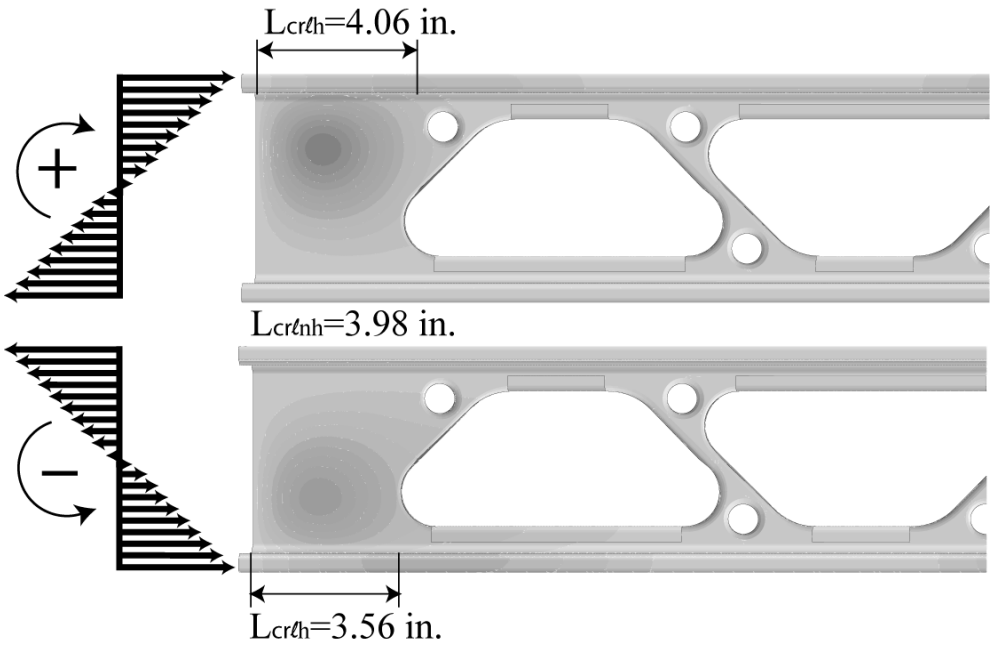

6000x1625x0713 local buckling half-wavelengths shown

Figure 3.5 Moment direction influence on local buckling half-wavelengths

3.5 **Global Column Elastic Buckling**

3.5.1 Loading and Boundary Conditions

The loading and boundary conditions employed in the column eigen-buckling analyses are presented in Table 3.6. Each column is compressed in ABAQUS with consistent nodal loads representing a uniform stress along the bearing edges. The column end nodes are restrained in 2 and 3 and the midlength is restrained in 1. The loading and boundary conditions are consistent with the classical differential theory equations that CUFSM is based on, which allows for a validation of ABAQUS results to CUFSM for columns without holes.

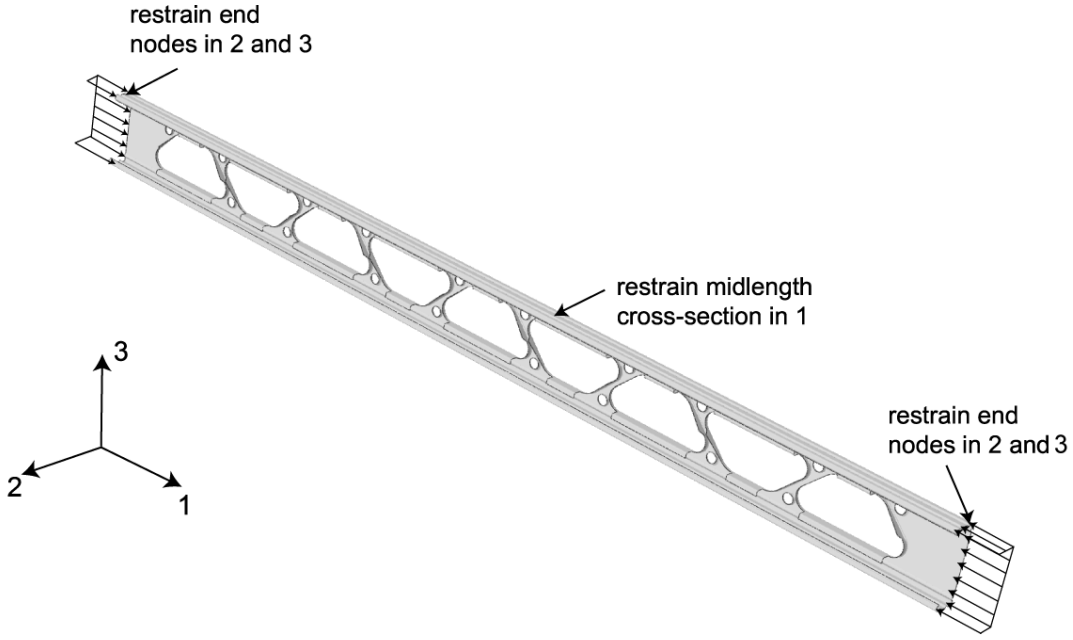

Figure 3.6 ABAQUS column boundary and loading conditions.

3.5.2 CUTWP/CUFSM Global Buckling Analysis

A classic global stability analysis using CUTWP (Sarawit 2006) was performed for each gross section stud. The higher order global buckling loads (P_{cre1}, P_{cre2}, P_{cre3}) were determined for the 80 in and 88 in stud lengths using CUTWP which solves the following classical cubic buckling analytical equation for columns:

$$\left(P_{cre,x}-P\right)\left(P_{cre,y}-P\right)\left(P_{cre,\emptyset}-P\right)-\left(P_{cre,y}-P\right)\frac{P^2{x_o}^2}{{r_o}^2}-\left(P_{cre,x}-P\right)\frac{P^2{y_o}^2}{{r_o}^2}=0. \qquad (3.1)$$

CUTWP solves for the analytical column stability solutions, however, CUFSM yields a more accurate solution when compared to the finite element analysis. Therefore, CUFSM was used in addition to determine the higher order global modes as shown in Figure 3.4.

In most cross sections, the finite strip method (CUFSM) and the classical global buckling theory (CUTWP) predict very similar global buckling loads. This holds true for sections that will buckle as a rigid cross section since that is what the analytical buckling equations assume. However, in some cases such as the 6 in. studs being analyzed, local plate buckling controls which causes the classical equations to diverge from the actual solution by as much as 25%. (Schafer 2008) This trend is described in detail in Section 4.3.1. As the section becomes thicker, the closer CUTWP is to predicting the actual buckling loads since plate buckling is less of a controlling factor in the thicker sections. The finite strip method is used to accurately predict the global buckling loads as it takes into account plate deformations and transverse bending which can be seen in Figure 3.8.

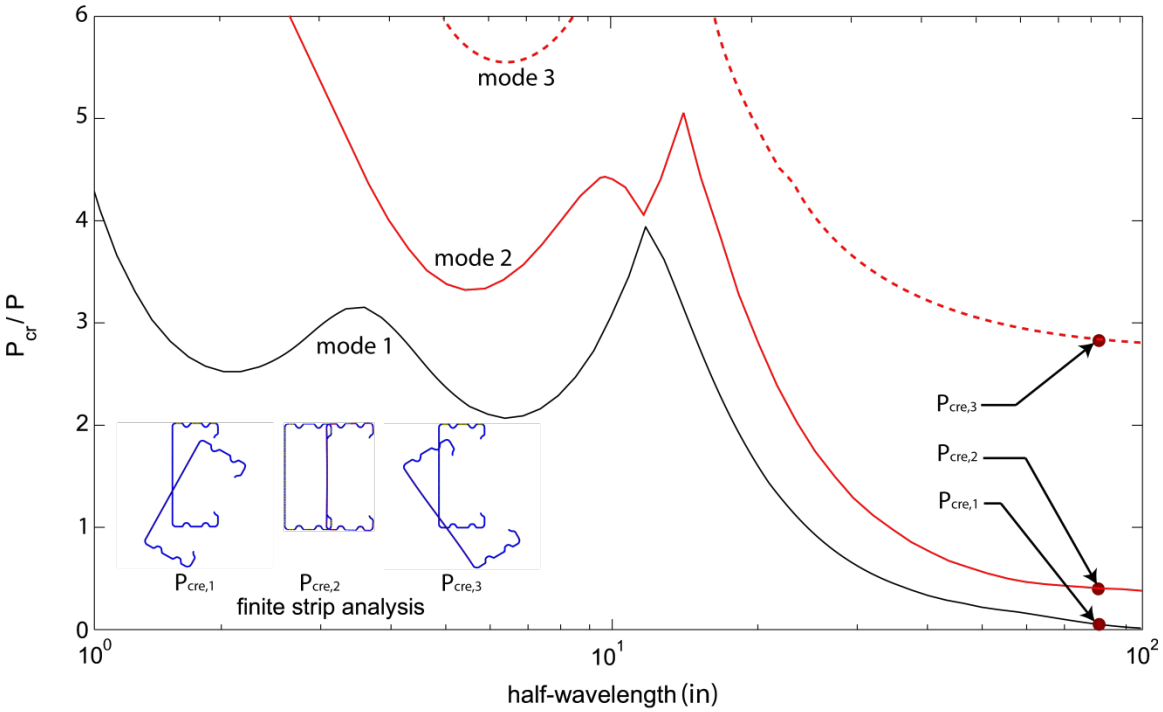

Figure 3.7 Elastic buckling mode curves for cold-formed gross section with the finite strip method.

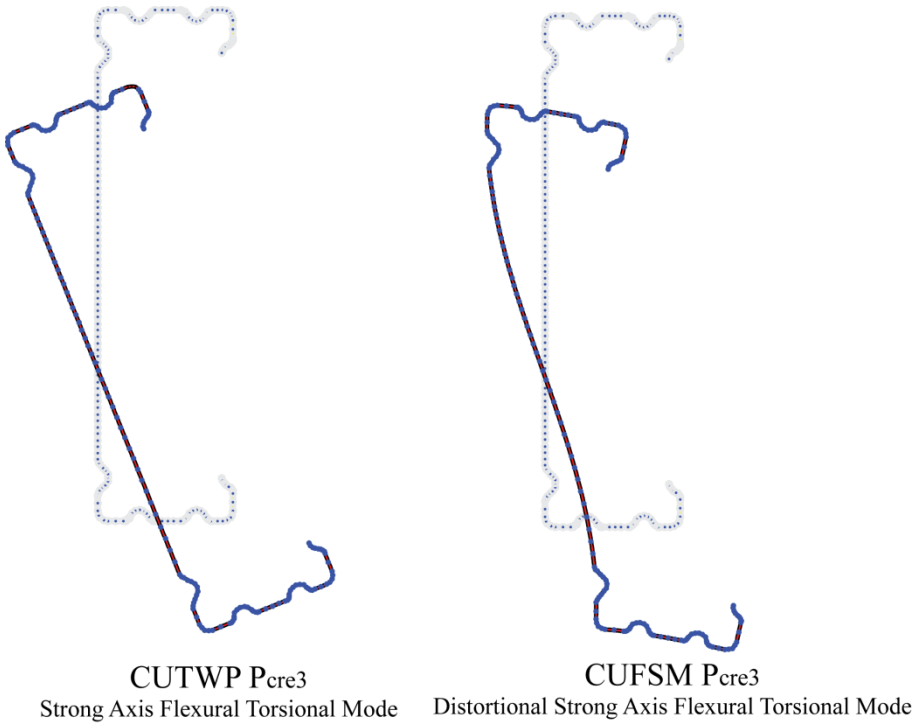

Figure 3.8 CUTWP/CUFSM Pcre3 global buckling mode comparison

3.5.3 Global Elastic Buckling Results

Tables 3.10, 3.11, and 3.14 present the global elastic buckling results for each stud. Tables 3.12, 3.13, 3.15, 3.16, and 3.17 are comparison tables which accommodate data interpretation.

3.5.3.1 Results – Studs without holes

Table 3.10 and Table 3.11 present the finite strip and finite element global elastic buckling results. The first three global modes are reported for both the 80 in. and 88 in. columns. Table 3.12 and Table 3.13 validate the finite element properties used throughout the project. For all studs analyzed, the local buckling moment without holes, $M_{cr\ell nh}$, from CUFSM (Table 3.10 and Table 3.11) is within 1.4% of the ABAQUS result (Table 3.12 and Table 3.13), confirming the accuracy of the S8R5 meshing scheme described in Section 3.3.2. CUTWP global buckling results are presented in Table 3.10 and Table 3.11 as well.

CUTWP accurately predicts all P_{cre1} and P_{cre2} global buckling loads when compared to CUFSM (Table 3.12 and Table 3.13), however, as discussed in Section 3.5.2, it does not accurately predict P_{cre3}. The first two % difference columns highlight the difference between ABAQUS and CUFSM (note that the buckling loads predicted by CUTWP and CUFSM are almost identical). The last column shows the % difference between CUTWP and Abaqus for the P_{cre3} buckling load. For the thinner sections, cross-sectional deformation accompanies global buckling and the loads predicted by CUTWP are higher by a maximum of 22.4% and 15.7% for the 6.000 in. 80 in. and 88 in. studs respectively. This new buckled shape is labeled as an asymmetric distortional strong-axis flexural torsional mode (Figure 3.8). Figure 3.8 compares the CUTWP global P_{cre3} buckling mode where the cross section has remained rigid to the actual critical buckled mode shape including cross-section deformation.

Table 3.10 CUTWP/CUFSM/ABAQUS gross section global buckling results – 80 in. studs without holes

Specimen	CUTWP model no holes L=80 in.						CUFSM model no holes L=80 in.						ABAQUS model no holes L=80 in.					
	Pcre1 kips	Bucking Mode	Pcre2 kips	Bucking Mode	Pcre3 kips	Bucking Mode	Pcre1 kips	Bucking Mode	Pcre2 kips	Bucking Mode	Pcre3 kips	Bucking Mode	P_{cre1} kips	Bucking Mode	P_{cre2} kips	Bucking Mode	P_{cre3} kips	Bucking Mode
3625x1625x0346	3.19	FT	4.77	WAF	49.4	FT	3.21	FT	4.74	WAF	47.1	FT	3.23	FT	4.76	WAF	46.7	FT
3625x1625x0451	4.34	FT	6.09	WAF	63.3	FT	4.34	FT	6.07	WAF	61.3	FT	4.39	FT	6.10	WAF	61.0	FT
3625x1625x0566	5.78	FT	7.46	WAF	78.2	FT	5.78	FT	7.43	WAF	75.4	FT	5.83	FT	7.49	WAF	76.0	FT
3625x1625x0713	8.00	FT	9.14	WAF	96.9	FT	7.99	FT	9.08	WAF	93.7	FT	8.07	FT	9.19	WAF	94.6	FT
6000x1625x0346	5.61	WAF	5.79	FT	109.2	FT	5.24	WAF	5.76	FT	84.6	DFT	5.23	WAF	5.77	FT	84.7	DFT
6000x1625x0451	7.16	WAF	7.64	FT	140.4	FT	6.89	WAF	7.62	FT	120.6	DFT	6.87	WAF	7.62	FT	120.4	DFT
6000x1625x0566	8.78	WAF	9.80	FT	173.5	FT	8.57	WAF	9.76	FT	155.4	DFT	8.55	WAF	9.83	FT	155.3	DFT
6000x1625x0713	10.74	WAF	12.86	FT	214.7	FT	10.70	WAF	12.93	FT	200.0	FT	10.58	WAF	12.88	FT	197.1	FT

Note: "FT" stands for Flexural Torsional buckling mode
"WAF" stands for Weak Axis Flexure buckling mode
"DFT" stands for Distortional Flexure Torsional buckling mode

Table 3.11 CUTWP/CUFSM/ABAQUS gross section global buckling results – 88 in. studs without holes

Specimen	CUTWP model no holes L=88 in.						CUFSM model no holes L=88 in.						ABAQUS model no holes L=88 in.					
	Pcre1 kips	Bucking Mode	Pcre2 kips	Bucking Mode	Pcre3 kips	Bucking Mode	Pcre1 kips	Bucking Mode	Pcre2 kips	Bucking Mode	Pcre3 kips	Bucking Mode	P_{cre1} kips	Bucking Mode	P_{cre2} kips	Bucking Mode	P_{cre3} kips	Bucking Mode
3625x1625x0346	2.68	FT	3.94	WAF	40.8	FT	2.70	FT	3.94	WAF	39.6	FT	2.70	FT	3.95	WAF	39.3	FT
3625x1625x0451	3.69	FT	5.03	WAF	52.4	FT	3.69	FT	5.03	WAF	51.4	FT	3.73	FT	5.05	WAF	51.1	FT
3625x1625x0566	4.97	FT	6.17	WAF	64.8	FT	4.97	FT	6.15	WAF	63.1	FT	5.01	FT	6.21	WAF	63.5	FT
3625x1625x0713	7.00	FT	7.55	WAF	80.5	FT	7.00	FT	7.51	WAF	78.4	FT	7.07	FT	7.62	WAF	79.1	FT
6000x1625x0346	4.64	WAF	4.83	FT	90.3	FT	4.43	WAF	4.82	FT	76.0	DFT	4.40	WAF	4.80	FT	76.1	DFT
6000x1625x0451	5.92	WAF	6.41	FT	116.1	FT	5.77	WAF	6.40	FT	104.3	DFT	5.76	WAF	6.41	FT	104.0	DFT
6000x1625x0566	7.25	WAF	8.28	FT	143.5	FT	7.11	WAF	8.25	FT	132.2	DFT	7.10	WAF	8.30	FT	132.1	DFT
6000x1625x0713	8.88	WAF	10.99	FT	177.5	FT	8.83	WAF	11.03	FT	168.7	FT	8.74	WAF	10.93	FT	166.3	FT

Table 3.12 ABAQUS validation from CUFSM - 80 in. stud

Specimen	ABAQUS validation with CUFSM - No holes 80 in. studs											
	CUTWP	CUFSM	ABAQUS		CUTWP	CUFSM	ABAQUS		CUTWP	CUFSM	ABAQUS		
	P_{cre1} kips	P_{cre1} kips	P_{cre1} kips	% Diff. CUFSM/ABAQUS	P_{cre2} kips	P_{cre2} kips	P_{cre2} kips	% Diff. CUFSM/ABAQUS	P_{cre3} kips	P_{cre3} kips	P_{cre3} kips	% Diff. CUFSM/ABAQUS	% Diff. CUTWP/ABAQUS
3625x1625x0346	3.19	3.21	3.23	0.5	4.77	4.74	4.76	0.3	49.4	47.1	46.7	-0.7	-5.3
3625x1625x0451	4.34	4.34	4.39	1.1	6.09	6.07	6.10	0.5	63.3	61.3	61.0	-0.5	-3.7
3625x1625x0566	5.78	5.78	5.83	0.9	7.46	7.43	7.49	0.9	78.2	75.4	76.0	0.7	-2.8
3625x1625x0713	8.00	7.99	8.07	1.0	9.14	9.08	9.19	1.3	96.9	93.7	94.6	1.0	-2.3
6000x1625x0346	5.61	5.24	5.23	-0.1	5.79	5.76	5.77	0.1	109.2	84.6	84.7	0.1	-22.4
6000x1625x0451	7.16	6.89	6.87	-0.2	7.64	7.62	7.62	0.0	140.4	120.6	120.4	-0.2	-14.3
6000x1625x0566	8.78	8.57	8.55	-0.2	9.80	9.76	9.83	0.7	173.5	155.4	155.3	-0.1	-10.5
6000x1625x0713	10.74	10.7	10.58	-1.2	12.86	12.9	12.9	-0.3	214.7	200.0	197.1	-1.4	-8.2

Table 3.13 ABAQUS validation from CUFSM - 88 in. stud

Specimen	ABAQUS validation with CUFSM - No holes 88 in. studs											
	CUTWP	CUFSM	ABAQUS		CUTWP	CUFSM	ABAQUS		CUTWP	CUFSM	ABAQUS		
	P_{cre1} kips	P_{cre1} kips	P_{cre1} kips	% Diff. CUFSM/ABAQUS	P_{cre2} kips	P_{cre2} kips	P_{cre2} kips	% Diff. CUFSM/ABAQUS	P_{cre3} kips	P_{cre3} kips	P_{cre3} kips	% Diff. CUFSM/ABAQUS	% Diff. CUTWP/ABAQUS
3625x1625x0346	2.68	2.70	2.70	0.2	3.94	3.94	3.95	0.2	40.8	39.6	39.3	-0.8	-3.7
3625x1625x0451	3.69	3.69	3.73	1.1	5.03	5.03	5.05	0.4	52.4	51.4	51.1	-0.6	-2.6
3625x1625x0566	4.97	4.97	5.01	0.7	6.17	6.15	6.21	1.0	64.8	63.1	63.5	0.7	-2.0
3625x1625x0713	7.00	7.00	7.07	1.1	7.55	7.51	7.62	1.4	80.5	78.4	79.1	0.9	-1.7
6000x1625x0346	4.64	4.43	4.40	-0.6	4.83	4.82	4.80	-0.4	90.3	76.0	76.1	0.1	-15.7
6000x1625x0451	5.92	5.77	5.76	-0.2	6.41	6.40	6.41	0.2	116.1	104.3	104.0	-0.3	-10.4
6000x1625x0566	7.25	7.11	7.10	-0.1	8.28	8.25	8.30	0.5	143.5	132.2	132.1	-0.1	-7.9
6000x1625x0713	8.88	8.8	8.74	-1.0	10.99	11.0	10.9	-0.9	177.5	168.7	166.3	-1.4	-6.3

3.5.3.2 Results – Studs with holes

Table 3.14 presents the finite element global elastic buckling results for studs with holes. The first three global modes are reported for both the 80 in. and 88 in. columns. The reduction in global buckling loads between the 80 in. and 88 in. columns is presented in Table 3.15. Table 3.16 and Table 3.17 present the influence of holes on the global buckling capacity and have been grouped according to their buckling mode for ease of comparison. For all columns considered, $P_{cre,nh\ 1\text{-}3} >> P_{cre,h\ 1\text{-}3}$ demonstrating that the global buckling load is reduced by the presence of the holes.

The presence of holes decreases the first global (Euler) buckling load, P_{cre1}, for all cases considered, with a maximum decrease of 24.5% occurring for the 6000x1625x0713x80 column (Table 3.16 and Table 3.17). The length of the unstiffened section at the end of a column (compare $P_{cre,h}$ for L=80 in. to L=88 in. in Table 3.15) decreases the global buckling loads with a maximum decrease of 19.7% for 6000x1625x0451 $P_{cre3,h}$. The lowest column buckling mode is flexural-torsional buckling for all 3.625 in. columns with holes except the 3625x1625x0713 shown in Table 3.15. Note that the presence of holes causes the global buckling mode to switch from flexural-torsional buckling to weak axis flexure for the 3625x1625x0713 column (compare Table 3.11 to Table 3.14).

All 6.000 in. columns exhibit weak axis flexural buckling as their lowest mode. The weak axis flexure buckling loads for all columns are penalized proportional to increasing thickness. With the presence of the holes, a maximum decrease of 28.4% at the thickest 3.625 in. section is predicted. (Table 3.16 and Table 3.17). However, the flexural–torsional buckling modes followed a different trend where the 3.625 in. columns decreased at a maximum of 15.9% whereas the 6.000 in. columns decreased at a maximum of 24.5%. The 6.000 in. columns are

penalized more since moment of inertia strong and weak axes are driven down by the presence of the holes when compared to the 3.625 in. columns.

The third critical global buckling mode is reduced by upwards of 48.7% due to the reduced section properties in both strong and weak axis moment of inertias at a hole. This third buckling mode (P_{cre3}) is a flexural-torsional mode which for a few of the 3.625 in. and 6.000 in. columns with no holes remains a flexural torsional mode with holes. However, most of the columns produce a unique asymmetric distortional strong axis flexural torsional buckled mode shape due local plate buckling as discussed in Section 4.2 and shown in Figure 3.8.

Table 3.14 ABAQUS global buckling results - studs with holes

Specimen	ABAQUS model with holes											
	L=80 in.						L=88 in.					
	Pcre1 kips	Bucking Mode	Pcre2 kips	Bucking Mode	Pcre3 kips	Bucking Mode	Pcre1 kips	Bucking Mode	Pcre2 kips	Bucking Mode	Pcre3 kips	Bucking Mode
3625x1625x0346	2.75	FT	3.48	WAF	35.6	FT	2.35	FT	2.89	WAF	30.7	FT
3625x1625x0451	3.75	FT	4.43	WAF	44.1	DFT	3.23	FT	3.68	WAF	41.1	DFT
3625x1625x0566	5.02	FT	5.42	WAF	51.6	DFT	4.39	FT	4.51	WAF	48.9	DFT
3625x1625x0713	6.61	WAF	6.93	FT	68.2	DFT	5.45	WAF	6.19	FT	61.8	DFT
6000x1625x0346	4.10	WAF	4.39	FT	51.6	FT	3.42	WAF	3.79	FT	41.8	DFT
6000x1625x0451	5.45	WAF	6.02	FT	66.4	FT	4.50	WAF	5.20	FT	53.3	DFT
6000x1625x0566	6.44	WAF	7.49	FT	80.4	FT	5.33	WAF	6.51	FT	67.7	DFT
6000x1625x0713	7.68	WAF	9.73	FT	107.7	FT	6.27	WAF	8.44	FT	97.0	DFT

Table 3.15 ABAQUS influence of end section 80 in. versus 88 in. studs with holes

Specimen	ABAQUS influence of end section 80 in. versus 88 in. studs with holes												
	80 in	88 in			80 in	88 in			80 in		88 in		
	P_{crehFT} kips	P_{crehFT} kips	Bucking Mode	% Diff.	$P_{crehWAF}$ kips	$P_{crehWAF}$ kips	Bucking Mode	% Diff.	$P_{crehFT2}$ kips	Bucking Mode	$P_{crehFT2}$ kips	Bucking Mode	% Diff.
3625x1625x0346	2.75	2.35	FT	-14.5	3.48	2.89	WAF	-16.9	35.6	FT	30.7	FT	-13.7
3625x1625x0451	3.75	3.23	FT	-13.7	4.43	3.68	WAF	-17.0	44.1	DFT	41.1	DFT	-6.6
3625x1625x0566	5.02	4.39	FT	-12.5	5.42	4.51	WAF	-16.8	51.6	DFT	48.9	DFT	-5.3
3625x1625x0713	6.93	6.19	FT	-10.7	6.61	5.45	WAF	-17.5	68.2	DFT	61.8	DFT	-9.3
6000x1625x0346	4.39	3.79	FT	-13.8	4.10	3.42	WAF	-16.5	51.6	FT	41.8	DFT	-18.9
6000x1625x0451	6.02	5.20	FT	-13.7	5.45	4.50	WAF	-17.4	66.4	FT	53.3	DFT	-19.7
6000x1625x0566	7.49	6.51	FT	-13.1	6.44	5.33	WAF	-17.2	80.4	FT	67.7	DFT	-15.8
6000x1625x0713	9.73	8.44	FT	-13.2	7.68	6.27	WAF	-18.2	107.7	FT	97.0	DFT	-10.0

Table 3.16 ABAQUS influence of holes - 80 in. stud

Specimen	ABAQUS influence of holes 80 in. studs											
	NO HOLE	HOLE			NO HOLE	HOLE			NO HOLE	HOLE		
	$P_{crenhFT}$ kips	P_{crehFT} kips	Bucking Mode	% Diff.	$P_{crenhWAF}$ kips	$P_{crehWAF}$ kips	Bucking Mode	% Diff.	$P_{crenhFT2}$ kips	Bucking Mode	$P_{crehFT2}$ kips	Bucking Mode	% Diff.
3625x1625x0346	3.23	2.75	FT	-14.9	4.76	3.48	WAF	-26.8	46.7	FT	35.6	FT	-23.8
3625x1625x0451	4.39	3.75	FT	-14.5	6.10	4.43	WAF	-27.4	61.0	FT	44.1	DFT	-27.8
3625x1625x0566	5.83	5.02	FT	-14.0	7.49	5.42	WAF	-27.6	76.0	FT	51.6	DFT	-32.1
3625x1625x0713	8.07	6.93	FT	-14.1	9.19	6.61	WAF	-28.1	94.6	FT	68.2	DFT	-28.0
6000x1625x0346	5.77	4.39	FT	-23.9	5.23	4.10	WAF	-21.7	84.7	DFT	51.6	FT	-39.1
6000x1625x0451	7.62	6.02	FT	-21.0	6.87	5.45	WAF	-20.7	120.4	DFT	66.4	FT	-44.9
6000x1625x0566	9.83	7.49	FT	-23.8	8.55	6.44	WAF	-24.6	155.3	DFT	80.4	FT	-48.2
6000x1625x0713	12.88	9.73	FT	-24.5	10.58	7.68	WAF	-27.4	197.1	FT	107.7	FT	-45.3

Table 3.17 ABAQUS influence of holes - 88 in. stud

Specimen	ABAQUS influence of holes 88 in. studs											
	NO HOLE	HOLE			NO HOLE	HOLE			NO HOLE	HOLE		
	$P_{crenhFT}$ kips	P_{crehFT} kips	Bucking Mode	% Diff.	$P_{crenhWAF}$ kips	$P_{crehWAF}$ kips	Bucking Mode	% Diff.	$P_{crenhFT2}$ kips	Bucking Mode	$P_{crehFT2}$ kips	Bucking Mode	% Diff.
3625x1625x0346	2.70	2.35	FT	-13.2	3.95	2.89	WAF	-26.7	39.3	FT	30.7	FT	-21.9
3625x1625x0451	3.73	3.23	FT	-13.3	5.05	3.68	WAF	-27.2	51.1	FT	41.1	DFT	-19.4
3625x1625x0566	5.01	4.39	FT	-12.3	6.21	4.51	WAF	-27.4	63.5	FT	48.9	DFT	-23.1
3625x1625x0713	7.07	6.19	FT	-12.4	7.62	5.45	WAF	-28.4	79.1	FT	61.8	DFT	-21.8
6000x1625x0346	4.80	3.79	FT	-21.1	4.40	3.42	WAF	-22.3	76.1	DFT	41.8	DFT	-45.0
6000x1625x0451	6.41	5.20	FT	-18.8	5.76	4.50	WAF	-21.8	104.0	DFT	53.3	DFT	-48.7
6000x1625x0566	8.30	6.51	FT	-21.6	7.10	5.33	WAF	-24.9	132.1	DFT	67.7	DFT	-48.7
6000x1625x0713	10.93	8.44	FT	-22.8	8.74	6.27	WAF	-28.2	166.3	FT	97.0	DFT	-41.7

3.6 **Intermediate Point Stud Properties**

Virginia Tech performed an analysis on each stud at intermediate points to quantify the effect of holes on member section properties. Custom MATLAB code captured node and element information from ABAQUS and then determined sectional properties using the CUFSM section property calculator. Figure 3.9 and Figure 3.10 provide the member sections considered. Table 3.18 presents the section properties results for each stud at each requested location.

3.7 **Section Descriptions**

The following intermediate sections are analyzed:

- A-A Section gross at ends
- B-B Section mid-length between two holes.
- C-C Section in beginning of large hole where no stiffeners exist
- D-D Section in large hole where one stiffener exists
- E-E Section mid-length of large hole with both stiffeners

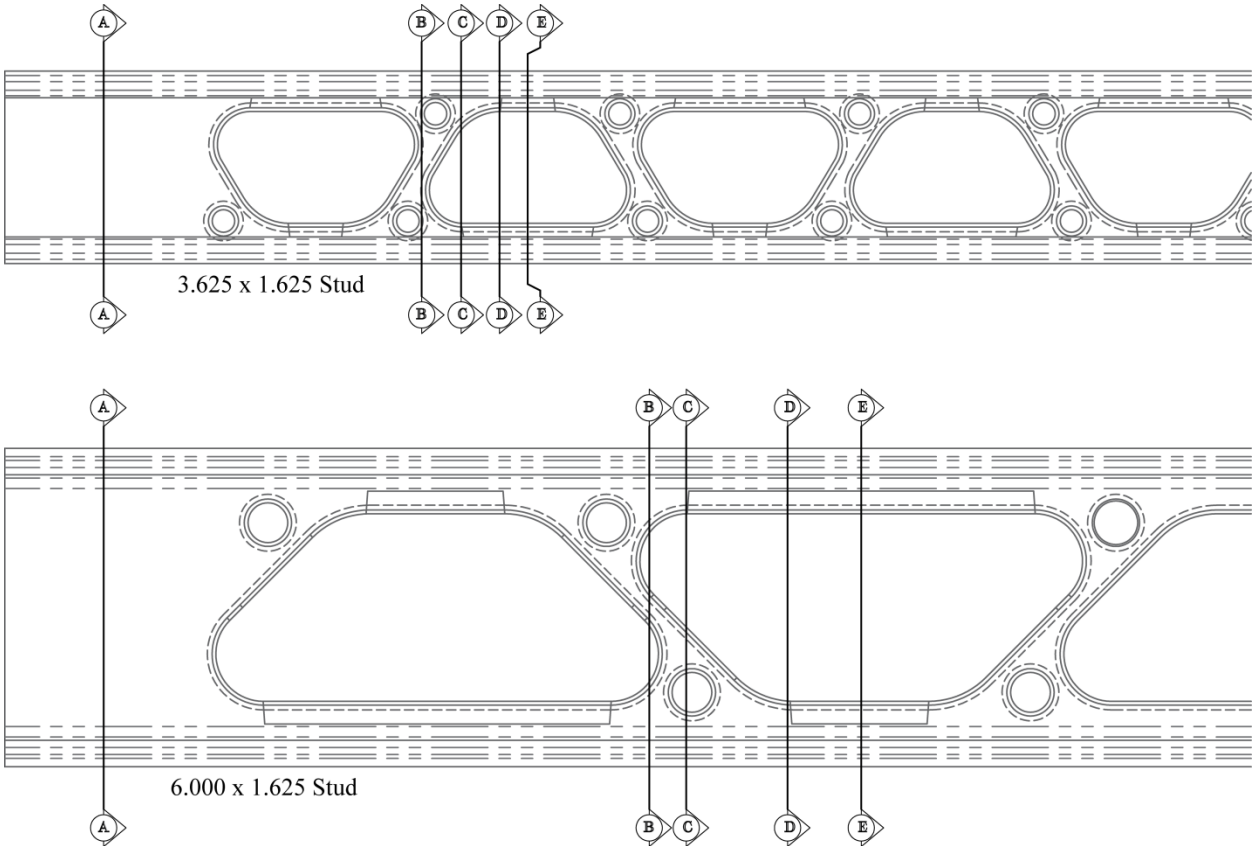

Figure 3.9 Point section locations

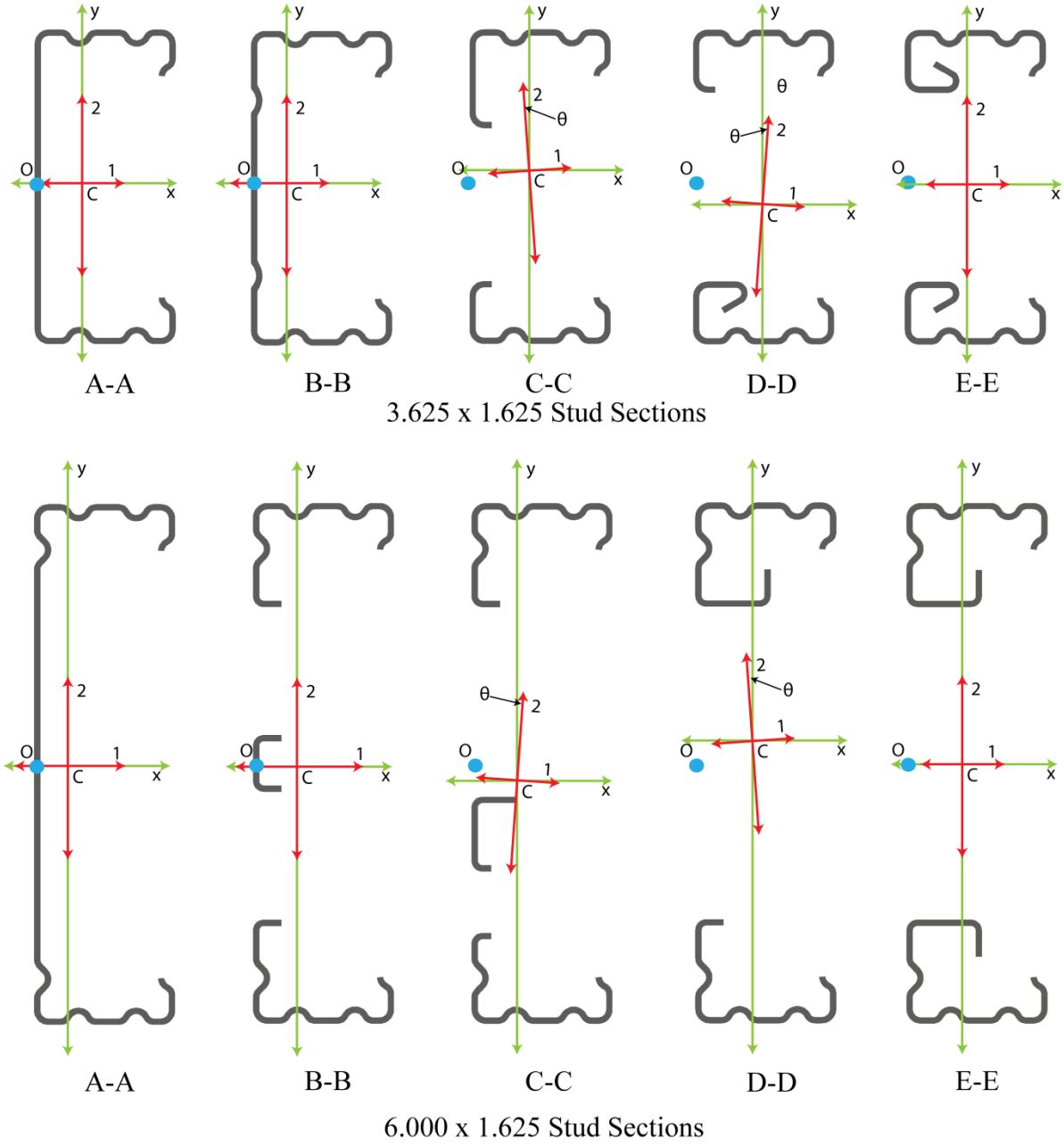

Figure 3.10 Cross sections at each taken section

3.7.1 Results

The following sectional properties are calculate:

- A Cross sectional area
- C_w Warping torsion constant
- J St. Venant's torsional constant
- I_{xx} Moment of inertia about the x direction
- I_{yy} Moment of Inertia about the y direction
- I_{xy} Product of moment of inertia Ix and Iy
- Θ Angle of principal axis rotation
- I_{11} Moment of inertia about principal axis 1
- I_{22} Moment of inertia about principal axis 2
- X_s, Y_s Shear center location
- X_c, Y_c Centroid location

Table 3.18 presents the intermediate cross section properties along each stud. Due to the geometry of the studs, sections such as C-C and D-D, the principal axis has rotated slightly by θ. Due to this rotation, the axes of rotational symmetry is not the same as in the gross section at the ends or at the net section and could be the contributing to the unique buckling modes found during the analysis. Table 3.19 presents the decrease or increase of section properties compared to the full gross section. In some cases, the cross section area is reduced by a maximum of 23.1% in section D-D for the 6.00 in. stud. With the reduction in cross sectional area, the weak axis moment of inertia, I_{yy}, decreases by a maximum of 26.5% in the same section D-D for the 6.000 in. stud. However, I_{xx}, the strong axis moment of inertia increases for all sections D-D and E-E with a maximum increase of 10.6%.

Table 3.18 Intermediate point stud properties

Intermediate cross sectional properties														
			Torsion Properties		Centroidal Properties			Principal Axes Properties			Shear Center Location		Centroid Location	
Specimen	Section	A (in^2)	Cw (in^6)	J (in^4)	Ixx (in^4)	Iyy (in^4)	Ixz (in^4)	θ (deg)	I11 (in^4)	I22 (in^4)	Xs (in)	Ys (in)	Xc (in)	Yc (in)
3625x1625x0346	A-A	0.2805	0.2947	0.0001119	0.5872	0.1055	0.0000	0.0000	0.5872	0.1055	-0.8098	0.0000	0.5515	0.0000
	B-B	0.2810	0.2946	0.0001121	0.5877	0.1054	0.0000	0.0015	0.5877	0.1054	-0.8060	0.0001	0.5513	0.0000
	C-C	0.2315	0.2874	0.0000924	0.5776	0.0846	-0.0078	0.9040	0.5777	0.0845	-0.8167	0.0335	0.6685	0.0306
	D-D	0.2419	0.2930	0.0000965	0.6007	0.0804	0.0078	-0.0863	0.6008	0.0803	-0.8138	-0.0481	0.6924	-0.1268
	E-E	0.2683	0.2953	0.0001071	0.6396	0.0823	0.0000	0.0008	0.6396	0.0823	-0.7860	0.0000	0.6673	-0.0002
3625x1625x0451	A-A	0.3648	0.3728	0.0002473	0.7610	0.1347	0.0000	0.0000	0.7610	0.1347	-0.8020	0.0000	0.5466	0.0000
	B-B	0.3654	0.3723	0.0002478	0.7616	0.1345	-0.0001	0.0062	0.7616	0.1345	-0.7965	0.0004	0.5469	0.0003
	C-C	0.2996	0.3643	0.0002031	0.7479	0.1077	-0.0097	0.8721	0.7480	0.1076	-0.8120	0.0425	0.6675	0.0336
	D-D	0.3147	0.3698	0.0002134	0.7799	0.1022	0.0100	-0.8419	0.7801	0.1020	-0.8058	-0.0464	0.6885	-0.1307
	E-E	0.3501	0.3735	0.0002374	0.8332	0.1045	0.0000	0.0000	0.8332	0.1045	-0.7773	0.0000	0.6640	0.0000
3625x1625x0566	A-A	0.4516	0.4497	0.0004823	0.9282	0.1644	0.0000	0.0000	0.9282	0.1644	-0.7957	0.0000	0.5407	0.0000
	B-B	0.4527	0.4484	0.0004834	0.9293	0.1638	-0.0001	0.0092	0.9293	0.1638	-0.7869	0.0008	0.5413	0.0004
	C-C	0.3659	0.4147	0.0003908	0.9068	0.1289	-0.0149	1.0946	0.9071	0.1286	-0.7978	0.0075	0.6589	0.0252
	D-D	0.3885	0.4375	0.0004149	0.9524	0.1237	0.0123	-0.8528	0.9525	0.1235	-0.8004	-0.0468	0.6860	-0.1355
	E-E	0.4335	0.4502	0.0004629	1.0210	0.1266	0.0000	0.0007	1.0210	0.1266	-0.7705	0.0000	0.6611	-0.0001
3625x1625x0713	A-A	0.5645	0.5426	0.0009566	1.1515	0.2007	0.0000	0.0000	1.1515	0.2007	-0.7846	0.0000	0.5327	0.0000
	B-B	0.5619	0.5183	0.0009522	1.1456	0.1958	-0.0054	0.3281	1.1457	0.1958	-0.7594	-0.0462	0.5266	-0.0102
	C-C	0.4542	0.5162	0.0007696	1.1239	0.1566	-0.0176	1.0441	1.1242	0.1563	-0.7908	-0.0186	0.6560	0.0286
	D-D	0.4822	0.5189	0.0008171	1.1767	0.1477	0.0086	-0.4793	1.1768	0.1476	-0.7764	-0.0902	0.6707	-0.1468
	E-E	0.5434	0.5742	0.0009208	1.2728	0.1532	-0.0001	0.0000	1.2728	0.1532	-0.7599	0.0000	0.6562	0.0000
6000x1625x0346	A-A	0.3685	0.8456	0.0001470	1.9539	0.1234	0.0000	0.0000	1.9539	0.1234	-0.6759	0.0000	0.4248	0.0000
	B-B	0.3228	0.8099	0.0001288	1.9155	0.1077	-0.0025	0.0793	1.9155	0.1077	-0.6867	-0.0311	0.5020	-0.0080
	C-C	0.2971	0.7064	0.0001186	1.8656	0.1009	0.0048	-0.1557	1.8656	0.1008	-0.7064	-0.0786	0.5463	-0.0583
	D-D	0.2924	0.7986	0.0001167	1.9741	0.0941	0.0037	-0.1138	1.9741	0.0941	-0.7039	0.0050	0.6160	0.1925
	E-E	0.3241	0.7897	0.0001293	2.0847	0.0942	-0.0022	0.0635	2.0847	0.0942	-0.6941	-0.0310	0.6187	-0.0081
6000x1625x0451	A-A	0.4788	1.0790	0.0003246	2.5292	0.1581	-0.0005	0.0124	2.5292	0.1581	-0.6699	0.0013	0.4208	0.0006
	B-B	0.4163	1.0445	0.0002822	2.4824	0.1382	0.0003	-0.0080	2.4824	0.1382	-0.6859	0.0006	0.5047	-0.0004
	C-C	0.3842	1.0086	0.0002605	2.4163	0.1295	0.0093	-0.2340	2.4164	0.1295	-0.7061	-0.0455	0.5480	-0.0493
	D-D	0.3760	1.0006	0.0002549	2.5411	0.1189	0.0016	-0.0377	2.5411	0.1189	-0.6947	-0.0234	0.6095	0.1855
	E-E	0.4162	1.0043	0.0002822	2.6918	0.1201	-0.0027	0.0606	2.6918	0.1201	-0.6887	-0.0295	0.6142	-0.0081
6000x1625x0566	A-A	0.5958	1.3084	0.0006362	3.1196	0.1930	0.0000	0.0000	3.1196	0.1930	-0.6623	0.0000	0.4153	0.0000
	B-B	0.5153	1.2680	0.0005502	3.0606	0.1684	0.0002	-0.0038	3.0606	0.1684	-0.6795	-0.0006	0.5013	-0.0008
	C-C	0.4738	1.2219	0.0005060	2.9725	0.1575	0.0106	-0.2157	2.9725	0.1574	-0.7007	-0.0443	0.5455	-0.0456
	D-D	0.4624	1.1899	0.0004938	3.1173	0.1430	-0.0031	0.0592	3.1173	0.1430	-0.6839	-0.0651	0.6016	0.1749
	E-E	0.5156	1.1955	0.0005506	3.3055	0.1447	-0.0083	0.1509	3.3055	0.1447	-0.6768	-0.0710	0.6056	-0.0176
6000x1625x0713	A-A	0.7452	1.5848	0.0012627	3.8644	0.2363	0.0000	0.0000	3.8644	0.2363	-0.6547	0.0000	0.4103	0.0000
	B-B	0.6366	1.5316	0.0010788	3.7811	0.2045	0.0001	-0.0019	3.7811	0.2045	-0.6734	-0.0006	0.5007	-0.0003
	C-C	0.5859	1.4739	0.0009929	3.6677	0.1910	0.0116	-0.1906	3.6677	0.1910	-0.6953	-0.0392	0.5450	-0.0415
	D-D	0.5733	1.4329	0.0009714	3.8508	0.1736	-0.0053	0.0826	3.8508	0.1736	-0.6765	-0.0723	0.5969	0.1721
	E-E	0.6376	1.4917	0.0010804	4.1138	0.1790	0.0000	0.0000	4.1138	0.1790	-0.6651	0.0000	0.6076	0.0000

Note: Strong axis is denoted by the x axis
Weak axis is denoted by the y axis

Table 3.19 Comparison of intermediate point stud properties to the gross full section

Specimen	Section	% Decreased intermediate cross sectional properties from gross section						
		A (in^2)	Cw (in^6)	J (in^4)	Ixx (in^4)	Iyy (in^4)	I11 (in^4)	I22 (in^4)
3625x1625x0346	A-A	0.0	0.0	0.0	0.0	0.0	0.0	0.0
	B-B	0.2	-0.1	0.2	0.1	-0.1	0.1	-0.1
	C-C	-17.5	-2.5	-17.5	-1.6	-19.7	-1.6	-19.9
	D-D	-13.8	-0.6	-13.8	2.3	-23.8	2.3	-23.9
	E-E	-4.3	0.2	-4.3	8.9	-22.0	8.9	-22.0
3625x1625x0451	A-A	0.0	0.0	0.0	0.0	0.0	0.0	0.0
	B-B	0.2	-0.1	0.2	0.1	-0.2	0.1	-0.2
	C-C	-17.9	-2.3	-17.9	-1.7	-20.0	-1.7	-20.2
	D-D	-13.7	-0.8	-13.7	2.5	-24.2	2.5	-24.3
	E-E	-4.0	0.2	-4.0	9.5	-22.4	9.5	-22.4
3625x1625x0566	A-A	0.0	0.0	0.0	0.0	0.0	0.0	0.0
	B-B	0.2	-0.3	0.2	0.1	-0.4	0.1	-0.4
	C-C	-19.0	-7.8	-19.0	-2.3	-21.6	-2.3	-21.8
	D-D	-14.0	-2.7	-14.0	2.6	-24.8	2.6	-24.9
	E-E	-4.0	0.1	-4.0	10.0	-23.0	10.0	-23.0
3625x1625x0713	A-A	0.0	0.0	0.0	0.0	0.0	0.0	0.0
	B-B	-0.5	-4.5	-0.5	-0.5	-2.5	-0.5	-2.5
	C-C	-19.5	-4.9	-19.5	-2.4	-22.0	-2.4	-22.1
	D-D	-14.6	-4.4	-14.6	2.2	-26.4	2.2	-26.5
	E-E	-3.7	5.8	-3.7	10.5	-23.7	10.5	-23.7
6000x1625x0346	A-A	0.0	0.0	0.0	0.0	0.0	0.0	0.0
	B-B	-12.4	-4.2	-12.4	-2.0	-12.7	-2.0	-12.7
	C-C	-19.4	-16.5	-19.4	-4.5	-18.3	-4.5	-18.3
	D-D	-20.6	-5.6	-20.6	1.0	-23.8	1.0	-23.8
	E-E	-12.0	-6.6	-12.0	6.7	-23.6	6.7	-23.7
6000x1625x0451	A-A	0.0	0.0	0.0	0.0	0.0	0.0	0.0
	B-B	-13.1	-3.2	-13.1	-1.9	-12.6	-1.9	-12.6
	C-C	-19.8	-6.5	-19.8	-4.5	-18.1	-4.5	-18.1
	D-D	-21.5	-7.3	-21.5	0.5	-24.8	0.5	-24.8
	E-E	-13.1	-6.9	-13.1	6.4	-24.0	6.4	-24.0
6000x1625x0566	A-A	0.0	0.0	0.0	0.0	0.0	0.0	0.0
	B-B	-13.5	-3.1	-13.5	-1.9	-12.8	-1.9	-12.8
	C-C	-20.5	-6.6	-20.5	-4.7	-18.4	-4.7	-18.4
	D-D	-22.4	-9.1	-22.4	-0.1	-25.9	-0.1	-25.9
	E-E	-13.4	-8.6	-13.4	6.0	-25.0	6.0	-25.0
6000x1625x0713	A-A	0.0	0.0	0.0	0.0	0.0	0.0	0.0
	B-B	-14.6	-3.4	-14.6	-2.2	-13.4	-2.2	-13.4
	C-C	-21.4	-7.0	-21.4	-5.1	-19.1	-5.1	-19.2
	D-D	-23.1	-9.6	-23.1	-0.4	-26.5	-0.4	-26.5
	E-E	-14.4	-5.9	-14.4	6.5	-24.2	6.5	-24.2

Note: Negative number represents a decrease
Positive number represents an increase

3.8 **Conclusions**

Elastic column and flexural buckling analyses were performed for two different Steelform structural stud configurations. Elastic global buckling analysis revealed that global buckling loads decreased for all columns when compared to the same columns without holes. Due to the presence of the holes and cross-sectional instabilities, the 3625x1625x0713 stud's lowest buckling mode changed from flexural-torsional buckling to weak axis bending. New global modes were discovered in most studs where asymmetric distortional buckling mixed with flexural-torsional buckling.

Elastic flexural buckling analysis revealed that local buckling was unaffected by the presence of holes, occurring in the gross cross-section near the ends of the column. And with the studs orientated with negative bending, the local buckling load increased. Distortional buckling was observed to also be unaffected by the presence of holes, although difficulties were encountered when attempting to identify a pure distortional mode. Global buckling loads decreased for all columns with holes when compared to the same columns without holes.

CHAPTER 4. SSRC CONFERENCE PAPER

Proceedings of the
Annual Stability Conference
Structural Stability Research Council
Pittsburgh, Pennsylvania, May 10-14, 2011

Elastic Buckling Simplified Methods for Cold-Formed Columns and Beams with Edge-Stiffened Holes

Grey, C.N.[1], Moen, C.D.[2]

4.1 Abstract

This paper presents a suite of prediction methods for approximating the elastic buckling properties of cold-formed steel columns and beams with edge-stiffened holes. The simplified methods supplement recently developed elastic buckling prediction procedures supporting the extension of the American Iron and Steel Institute's Direct Strength Method to members with holes. Weighted average section properties are used with classical column stability equations to predict flexural and flexural-torsional buckling loads and beam lateral-torsional buckling moments including the influence of edge-stiffened holes. Cross-sectional instability of lipped C-sections including stiffened holes is evaluated with eigen-buckling analysis and the finite strip method. Critical elastic distortional buckling is shown to be minimally affected by the presence of stiffened holes when edge stiffener dimensions around web holes are sized to replace bending stiffness lost by the removal of web material at a hole. Finite strip analysis of the net section at a stiffened hole is performed to evaluate local buckling. The simplified methods are validated with thin shell finite element eigen-buckling parameter studies where the edge-stiffened holes are explicitly modeled.

[1] Graduate Research Assistant, Virginia Tech (cgrey@vt.edu)
[2] Assistant Professor, Virginia Tech (cmoen@vt.edu)

4.2 Introduction

Elastic buckling and load-deformation response are intimately related for thin-walled cold-formed steel structural members with or without holes. For members with unstiffened holes, local buckling half-waves can form at a hole or between holes (Moen and Schafer 2009a; Moen and Schafer 2009b). Experiments have demonstrated that distortional buckling deformations in columns and joists increase with the presence of unstiffened web holes (Moen and Schafer 2008; Schudlich et al. 2011). Nonlinear finite element modeling results provide evidence that cold-formed steel column global buckling capacity decreases when large holes are present and that the controlling global buckling mode can switch from weak axis flexure to flexural-torsional buckling (Moen 2008; Moen and Schafer 2011). Edge stiffeners may prevent unstiffened strip local buckling in the compressed regions above or below a hole (Yu 2007) and can cause distortional buckling to occur between holes (Moen and Yu 2010) as shown in Figure 4.1c.

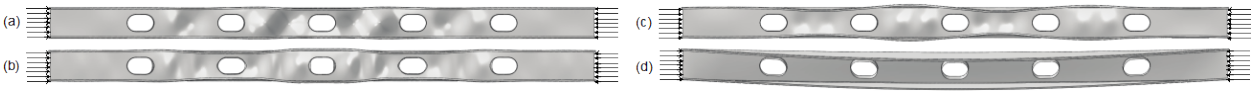

Figure 4.1 Lipped C-section column elastic buckling with stiffened holes - (a) local buckling between holes, (b) distortional buckling at a hole, (c) distortional buckling between holes, and (d) global (flexural-torsional) buckling

Currently, cold-formed steel members *without holes* can be designed with the American Iron and Steel Institute's Direct Strength Method (DSM) (AISI-S100 2007), which utilizes the local, distortional, and global (Euler) elastic buckling properties to predict ultimate strength. The elastic buckling properties for members without holes can be determined from an elastic buckling curve generated with the semi-analytical finite strip method. However, discontinuities caused by holes cannot be explicitly modeled with the finite strip method, and therefore, simplified methods for use in design are needed.

This paper presents procedures for approximating the change in the elastic buckling load (or moment) of cold-formed steel columns and beams due to the presence of edge-stiffened holes. Similar procedures were recently validated for cold-formed steel members with unstiffened holes (Moen and Schafer 2009a). The stiffened hole simplified methods for predicting global buckling, distortional buckling, and local buckling are evaluated with finite element eigen-buckling parameter studies on industry standard Structural Stud Manufacturers Association (SSMA) cold-formed steel members (Table 4.1, Figure 4.2). The selected cross-sections were part of an experimental program evaluating the flexural capacity of cold-formed steel joists with edge-stiffened holes sponsored by the National Association of Home Builders (Elhajj 1999).

Table 4.1 SSMA structural stud and stiffened hole dimensions

SSMA Designation	Thickness (in.)	Web Size (in.)	Flange Width (in.)	Stud Length (in.)	Hole Depth (in.)	Hole Length (in.)	Hole Spacing (in.)	Inside Corner Radius (in.)	Hole Stiffener Length (in.)	Hole Radius (in.)
	t	H	B	L	h_{hole}	L_{hole}	S	R	Q_{hole}	R_{hole}
800S162-43	0.0451	8	1.625	144	4.25	7	24	0.0712	0.688	2.21
800S162-54	0.0566	8	1.625	144	4.25	7	24	0.0849	0.688	2.21
1000S162-54	0.0566	10	1.625	240	6.25	9	24	0.0849	0.688	3.21
1200S162-54	0.0566	12	1.625	240	6.25	9	24	0.0849	0.688	3.21
1200S162-68	0.0713	12	1.625	240	6.25	9	24	0.1069	0.688	3.21

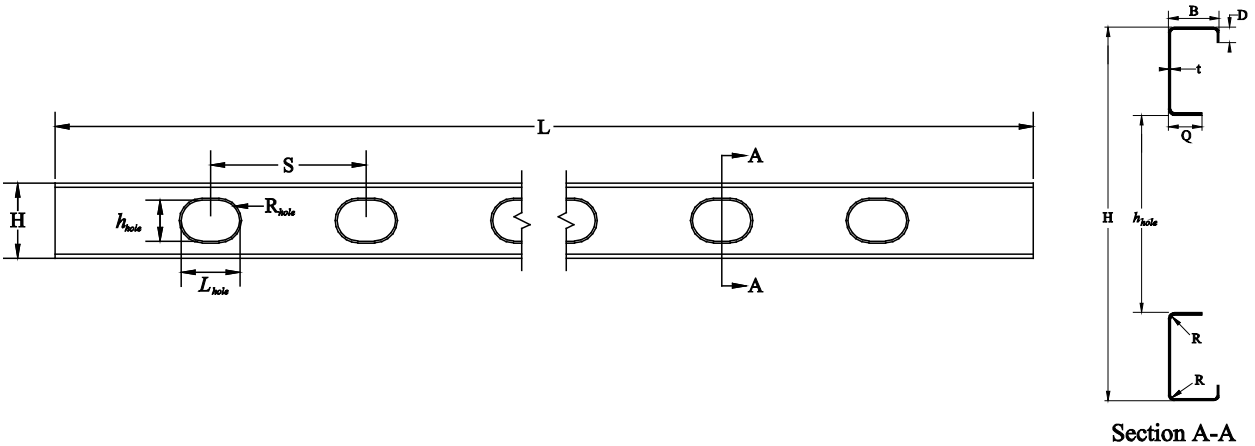

Figure 4.2 Structural stud dimension nomenclature

4.3 Global buckling of cold-formed steel columns and beams with edge-stiffened holes

The nominal global axial capacity, P_n, of a cold-formed steel column is defined by its global slenderness, $\lambda_c = (P_y/P_{cre})^{0.5}$. If the global elastic buckling load, P_{cre}, decreases due to the presence of holes, then λ_c increases, and the column (with holes) is predicted to have less capacity (Moen and Schafer 2011). A similar design approach is employed for laterally unbraced cold-formed steel beams with holes, except the nominal flexural strength, M_n, is predicted with the global slenderness of the beam, $\lambda_b = (M_y/M_{cre})^{0.5}$, where M_y is the yield moment for the beam and M_{cre} is calculated including the presence of holes. Simplified methods for predicting P_{cre} and M_{cre} for columns and beams with unstiffened holes have recently been developed (Moen and Schafer 2009a,b). These methods are extended to structural members with edge-stiffened holes in the following sections.

4.3.1 Global flexural buckling

4.3.1.1 Weak axis flexure prediction equations

A Rayleigh–Ritz energy solution is employed in this section as an approximate equation for the critical elastic global flexural (Euler) buckling load, P_{cre}, of a uniaxially loaded simply-supported column with holes (Moen and Schafer 2009a). This approximate method is motivated by existing analytical solutions for the elastic buckling of a column with a variable cross-section (Timoshenko 1908; Falk 1956; Timoshenko 1961). For the common case when holes are spaced symmetrically about the longitudinal midline of the column, P_{cre} is determined as follows:

$$P_{cre} = \frac{\pi^2 E}{L^2}\left(\frac{I_g L_g + I_{net} L_{net}}{L}\right). \tag{4.1}$$

The Euler buckling load, P_{cre}, is proportional to the weighted average of the gross cross section moment of inertia, I_g, and the net section moment of inertia at a hole, I_{net}. The portion of

column without holes has length L_g, and the length of column with holes is L_{net}, so that $L=L_g+L_{net}$. The validity of this "weighted average" approximate method for P_{cre} is explored next for flexural buckling of cold-formed steel columns with evenly spaced edge-stiffened holes.

4.3.1.2 Verification for flexural buckling of columns with edge-stiffened holes

Thin shell finite element eigen-buckling analysis in ABAQUS (ABAQUS 2010) was employed to evaluate the ''weighted average'' approximation of Eq. 4.1 for the global flexural critical elastic buckling load of a column with evenly spaced edge-stiffened holes. This example considers weak-axis flexural buckling of the industry standard cold-formed steel SSMA stud columns listed in Table 4.1 with oval-shaped web holes (SSMA 2001). The length of the column, L, varies from 144 in. to 240 in.; the hole spacing, S, is 24 in.; the hole depth, h_{hole}, varies between 4.25 in. and 6.25 in.; the hole width, L_{hole}, varies between 7 in. and 9 in.; and the hole stiffener length, Q, is 0.688 in. The compression members are loaded with consistent nodal loads simulating a uniform stress at the member ends. The end boundary conditions are pinned-warping free as shown in Figure 4.3. The modulus of elasticity, E, is 29500 ksi and Poisson's ratio, ν, is 0.30.

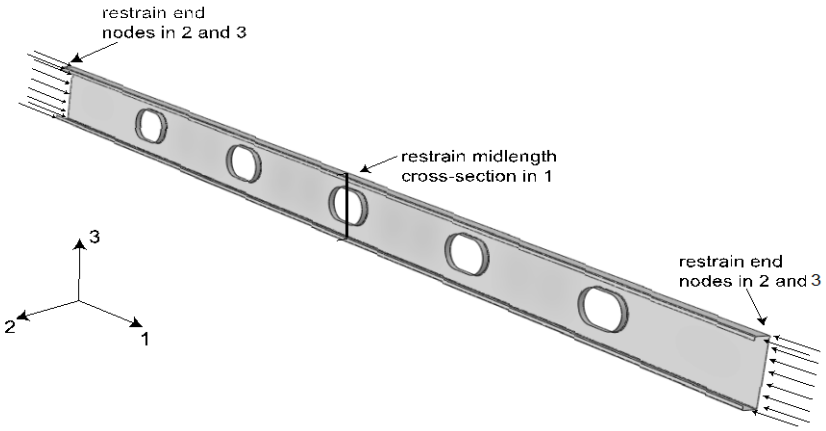

Figure 4.3 ABAQUS column boundary and loading conditions

The presence of stiffened holes reduces the critical elastic global buckling load by a maximum of 13% for the 1000S162-54 column (see $P_{cre,ABAQUS\ with\ holes}/P_{cre,\ ABAQUS\ no\ holes}$ in Table 4.2). The ‘‘weighted average’’ approximate method of Eq. 4.1, denoted as $P_{cre,avg}$ in Table 4.2, is shown to be a viable and slightly unconservative predictor of the weak-axis flexural buckling load across the range of column and hole dimensions considered in this study, with $P_{cre,ABAQUS\ with\ holes}/P_{cre,avg}$ ranging from 0.94 to 0.97.

Table 4.2 Influence of edge-stiffened holes on column global buckling

Buckling Mode	Comparison		SSMA Section					ABAQUS-to-predicted statistics	
			800S162-43	800S162-54	1000S162-54	1200S162-54	1200S162-68		
			L=144 in	L=144 in	L=240 in	L=240 in	L=240 in	Mean	COV
Column weak-axis flexural buckling	$P_{cre,CLASSICAL\ no\ holes}$ [b]	(kip)	2.24	2.73	1.03	1.07	1.29		
	$P_{cre,ABAQUS\ no\ holes}$	(kip)	2.23	2.72	1.03	1.07	1.30		
	$P_{cre,ABAQUS\ with\ holes}$	(kip)	2.04	2.49	0.90	0.98	1.18		
	$P_{cre,avg}$	(kip)	2.14	2.61	0.96	1.02	1.22		
	$P_{cre,ABAQUS\ no\ holes}/P_{cre,CLASSICAL\ no\ holes}$		0.99	1.00	1.00	1.00	1.01	1.00	0.01
	$P_{cre,ABAQUS\ with\ holes}/P_{cre,ABAQUS\ no\ holes}$		0.92	0.91	0.87	0.91	0.91	0.90	0.02
	$P_{cre,ABAQUS\ with\ holes}/P_{cre,avg}$ [a]		0.95	0.95	0.94	0.96	0.97	0.95	0.01
Column flexural-torsional buckling	$P_{cre,CLASSICAL\ no\ holes}$ [b]	(kip)	3.33	4.41	2.21	2.29	3.25		
	$P_{cre,ABAQUS\ no\ holes}$	(kip)	3.29	4.35	2.19	2.28	3.24		
	$P_{cre,ABAQUS\ with\ holes}$	(kip)	2.96	3.92	1.74	1.87	2.66		
	$P_{cre,avg}$	(kip)	2.92	3.92	1.76	1.92	2.69		
	$P_{cre,ABAQUS\ no\ holes}/P_{cre,CLASSICAL\ no\ holes}$		0.99	0.99	0.99	0.99	1.00	0.99	0.00
	$P_{cre,ABAQUS\ with\ holes}/P_{cre,ABAQUS\ no\ holes}$		0.90	0.90	0.80	0.82	0.82	0.85	0.06
	$P_{cre,ABAQUS\ with\ holes}/P_{cre,avg}$		1.01	1.00	0.99	0.98	0.99	0.99	0.01

[a] The weak axis flexure buckling load with holes predicted by ABAQUS is 5-7% lower than the flexural buckling load predicted by the weighted average approach.

[b] The classical Euler buckling solution for a column without a hole is $P_{cre,CLASSICAL\ nohole}$.

4.3.2 Global flexural-torsional buckling

4.3.2.1 Flexural-torsional prediction equations

For singly-symmetric sections subjected to flexural-torsional buckling, the elastic flexural-torsional buckling load, P_{cre}, including the influence of holes, can be calculated with the “weighted average” approach and the following equation motivated by AISI-S100-07:

$$P_{cre} = \frac{A_g}{2\beta}\left[(\sigma_{ex} + \sigma_t) - \sqrt{(\sigma_{ex} + \sigma_t)^2 - 4\beta\sigma_{ex}\sigma_t}\right], \tag{4.2}$$

where

$$\beta = 1 - \left(\frac{x_{o,avg}}{r_{o,avg}}\right)^2, \quad \sigma_{ex} = \frac{\pi^2 E I_{x,avg}}{A_g \left(K_x L_x\right)^2}, \quad \sigma_t = \frac{1}{A_g r_{o,avg}^2}\left[GJ_{avg} + \frac{\pi^2 E C_{w,net}}{\left(K_t L_t\right)^2}\right]. \tag{4.3}$$

The radius of gyration about the shear center is defined as $r_{o,avg}=(r_{x,avg}^2 + r_{y,avg}^2 + x_{o,avg}^2)^{0.5}$, where the "weighted average" x distance from the shear center to the centroid of the cross-section is $x_{o,avg}$

$$x_{o,avg} = \frac{x_{o,g} L_g + x_{o,net} L_{net}}{L}. \tag{4.4}$$

The column buckling load, P_{cre}, is also a function of the radii of gyration of a cross section about the centroidal axes, i.e., $r_{x,avg} = (I_{x,avg} / A_{avg})^{0.5}$ and $r_{y,avg} = (I_{y,avg}/A_{avg})^{0.5}$, where $I_{x,avg}$, $I_{y,avg}$, and A_{avg} are calculated using a similar form of Eq. 4.4. (Note that the gross cross-sectional area, A_g, in Eq. 4.3 and Eq. 4.4 converts the uniform compressive stress at the ends of the column to a force and should not be confused with A_{avg}).

The St. Venant torsional constant, J_{avg}, including the influence of holes, can be calculated with weighted average approach with a similar form of Eq. 4.4. However, the warping torsion constant, C_w, does not follow the weighted average approximation, as the presence of holes prevents warping resistance from developing (Moen and Schafer 2009a). A viable approximation for warping stiffness at the net section is $C_{w,net}$ (see Eq. 4.3). Note that all net section properties, e.g., $I_{x,net}$, $I_{y,net}$, A_{net}, $x_{o,net}$, $y_{o,net}$, J_{net}, and $C_{w,net}$, can readily be calculated with the built-in section property calculations in the freely available open source program CUFSM (Schafer and Ádány 2006) by setting the element thicknesses to zero at the hole (Moen and Schafer 2010a). The validity of the weighted average approach for flexural-torsional buckling is evaluated in the following sections.

4.3.2.2 Evaluation of torsional property approximations

A procedure for calculating torsional properties of a thin-walled structural member with holes is described in Moen and Schafer (2009b). An imposed torsional rotation (twist) is applied at the member end in a finite element model with either warping free or warping fixed boundary conditions. The torsion created by the imposed twist is read from the finite element model and input into the classical differential equation for nonuniform torsion to obtain J and C_w for the member, including the influence of holes. The torsional properties for the SSMA member dimensions in Table 4.1 are calculated with this procedure ($J_{ABAQUS\ with\ holes}$ and $C_{w,\ ABAQUS\ with\ holes}$ in Table 4.3) to evaluate the viability of the weighted average J_{avg} and net section $C_{w,net}$ approximations in Eq. 4.4.

The results in Table 4.3 demonstrate that the weighted average approach is a viable, conservative predictor of the St. Venant torsional constant for the SSMA members with stiffened holes considered in this study, with the weighted average predicting a maximum of 13% lower than that predicted by the semi-analytical approach (compare $J_{ABAQUS\ with\ holes}$ to J_{avg} in Table 4.3). It is hypothesized that J_{avg} underpredicts the actual torsional resistance because the weighted average approach assumes the stiffened holes are rectangular, whereas the actual holes are oval and taper to the gross cross-section. The net section warping torsion constant, $C_{w,net}$, is consistent with that predicted by the semi-analytical approach (compare $C_{w\ ABAQUS\ with\ holes}$ to $C_{w,net}$ in Table 4.3). The addition of edge-stiffened holes has a minimal effect on J and C_w for the members evaluated in this study (compare $J_{,ABAQUS\ with\ holes}$ to $J_{,ABAQUS\ no\ holes}$ and $C_{,w\ ABAQUS\ with\ holes}$ to $C_{,w\ ABAQUS\ no\ holes}$ in Table 4.3).

Table 4.3 Influence of edge-stiffened holes on torsion properties

Buckling Mode	Comparison		SSMA Section					ABAQUS-to-predicted statistics	
			800S162-43	800S162-54	1000S162-54	1200S162-54	1200S162-68		
			L=144 in	L=144 in	L=240 in	L=240 in	L=240 in	Mean	COV
St Venant's torsion constant, J	$J_{,g}$ [a]	($in.^4$)	0.000364	0.000715	0.000836	0.000957	0.001899		
	$J_{,ABAQUS\ no\ holes}$	($in.^4$)	0.000364	0.000714	0.000835	0.000957	0.001896		
	$J_{,ABAQUS\ with\ holes}$	($in.^4$)	0.000367	0.000730	0.000831	0.000942	0.001878		
	$J_{,avg}$	($in.^4$)	0.000342	0.000670	0.000733	0.000854	0.001692		
	$J_{,ABAQUS\ no\ holes}/J_{,g}$		1.00	1.00	1.00	1.00	1.00	1.00	0.00
	$J_{,ABAQUS\ with\ holes}/J_{,g}$		1.01	1.02	0.99	0.98	0.99	1.00	0.02
	$J_{,ABAQUS\ with\ holes}/J_{,avg}$		1.08	1.09	1.13	1.10	1.11	1.10	0.02
Warping torsion constant, C_w	$C_{w,g}$ [a]	($in.^6$)	1.99	2.41	4.00	6.05	7.24		
	$C_{w,ABAQUS\ no\ holes}$	($in.^6$)	1.99	2.41	4.00	6.05	7.24		
	$C_{w,ABAQUS\ with\ holes}$	($in.^6$)	2.01	2.47	3.98	5.95	7.17		
	$C_{w,net}$	($in.^6$)	1.91	2.30	3.67	5.77	6.88		
	$C_{w,ABAQUS\ no\ holes}/C_{w,g}$		1.00	1.00	1.00	1.00	1.00	1.00	0.00
	$C_{w,ABAQUS\ with\ holes}/C_{w,g}$		1.01	1.02	1.00	0.98	0.99	1.00	0.02
	$C_{w,ABAQUS\ with\ holes}/C_{w,net}$		1.06	1.07	1.09	1.03	1.04	1.06	0.02

[a] $J_{,g}$ and $C_{w,g}$ are calculated for the gross cross-section with the CUFSM section property calculator

4.3.2.3 Verification for flexural-torsional buckling of a column with edge-stiffened holes

The second elastic global mode of all SSMA columns analyzed is flexural-torsional buckling. Table 4.2 shows that the flexural-torsional mode is more sensitive to hole size than the weak-axis flexural mode (compare $P_{cre,ABAQUS\ with\ holes}/P_{cre,ABAQUS\ no\ holes}$ in Table 4.2). The flexure-torsional buckling loads of the SSMA columns with edge-stiffened holes from ABAQUS are within 2% of the flexural buckling loads predicted by the weighted average approach (compare $P_{cre,ABAQUS\ with\ holes}/P_{cre,avg}$ in Table 4.2).

4.3.3 Lateral-torsional buckling

4.3.3.1 Lateral-torsional buckling prediction equation

The "weighted average" method developed for columns with holes is extended to beams with edge-stiffened holes in this section. The classical lateral-torsional stability equation for a simply-supported beam with holes loaded with a constant moment along its length can be represented as:

$$M_{cre} = \frac{\pi}{L}\sqrt{EI_{y,avg}\left(GJ_{avg} + EC_{w,net}\frac{\pi^2}{L^2}\right)}. \quad (4.5)$$

The approximate method for beams with edge-stiffened holes is implemented by replacing I_y and J with $I_{y,avg}$ and J_{avg} (see form of Eq. 4.4) and by calculating $C_{w,net}$ assuming the cross-section thickness is zero over the hole as discussed in Section 4.3.2.1.

4.3.3.2 Verification for lateral-torsional bucking of a beam with edge-stiffened holes

The cold-formed steel SSMA members evaluated in the previous sections as columns are now evaluated as beams with uniform moments. The beam ends are modeled as pinned warping-free and the cross-section at the longitudinal midline is warping-fixed as shown in Figure 4.3. The critial elastic lateral-torsional buckling moment, M_{cre}, decreases with the presence of edge-stiffened holes by a maximum of 8% as shown in Table 4.4. The "weighted average" prediction method is demonstrated to be an accurate predictor of M_{cre} when compared to the ABAQUS eigen-buckling results (see $M_{cre,ABAQUS\ with\ holes}/M_{cre,avg}$ in Table 4.4).

Table 4.4 Influence of edge-stiffened holes on beam global buckling

Buckling Mode	Comparison		SSMA Section					ABAQUS-to-predicted statistics	
			800S162-43	800S162-54	1000S162-54	1200S162-54	1200S162-68		
			L=144 in	L=144 in	L=240 in	L=240 in	L=240 in	Mean	COV
Beam lateral-torsional buckling	$M_{cre,CLASSICAL\ no\ holes}$ [a]	(kip-in.)	8.48	10.72	5.54	6.66	8.65		
	$M_{cre,ABAQUS\ no\ holes}$	(kip-in.)	8.52	10.77	5.58	6.69	8.74		
	$M_{cre,ABAQUS\ with\ holes}$	(kip -in.)	8.09	10.23	5.11	6.33	8.27		
	$M_{cre,avg}$	(kip -in.)	8.22	10.36	5.17	6.36	8.20		
	$M_{cre,ABAQUS\ no\ holes}/M_{cre,CLASSICAL\ no\ holes}$ [a]		1.00	1.01	1.01	1.00	1.01	1.01	0.00
	$M_{cre,ABAQUS\ with\ holes}/M_{cre,ABAQUS\ no\ holes}$		0.95	0.95	0.92	0.95	0.95	0.94	0.01
	$M_{cre,ABAQUS\ with\ holes}/M_{cre,avg}$		0.98	0.99	0.99	1.00	1.01	0.99	0.01

[a] The critical lateral-torsional buckling moment for a beam without holes is denoted as $M_{cre,CLASSICAL\ no\ holes}$

4.4 Distortional buckling of cold-formed steel columns and beams with edge-stiffened holes

Distortional buckling is recognized as a design limit state for cold-formed steel columns and beams with open cross-sections separate from that of global or local-global buckling interaction (Lau and Hancock 1987; AISI-S100 2007). Rotational restraint of the web to the flange is interrupted in open-cross sections when unstiffened holes are present, reducing the critical elastic distortional buckling load (Moen and Schafer 2009a). A recent study demonstrated that the addition of edge stiffeners to holes may compensate for the loss in web bending stiffness at a web hole, causing distortional buckling to occur between holes (Moen and Yu 2010) in the same way that local buckling can occur at a hole or between holes (Moen and Schafer 2009b). This idea is implemented in the next section with a simplified approach for predicting the distortional buckling load including the effect of stiffened holes.

4.4.1 Distortional buckling prediction for columns with holes

The distortional critical elastic buckling load, P_{crd}, is calculated for a cold-formed steel column with holes as:

$$P_{crd} = \min(P_{crdnh}, P_{crdh}), \tag{4.6}$$

where P_{crdnh} is the distortional buckling load for a buckled half-wave without a hole, which may be calculated by finite strip or hand methods (AISI-S100 2007). The buckling load for a distortional buckling half-wave including a hole, P_{crdh}, can be calculated for unstiffened holes by simulating the effect of the hole with a reduced web thickness in a finite strip analysis, as detailed in Moen and Schafer (2010a). A similar finite strip approach for calculating P_{crdh} of cold-formed steel columns with edge-stiffened holes is derived in the next section.

4.4.2 Effective web stiffness considering edge-stiffened holes

A web with an edge-stiffened hole will have a reduction in bending stiffness from the removal of hole material and an increase in web bending stiffness from the presence of the edge stiffeners around the hole. The reduced transverse rotational stiffness of a web with an unstiffened hole over a distortional buckling half-wavelength, L_{crd}, was approximated in Moen and Schafer (2009a) as:

$$K_{\theta,hole} = \left(1 - \frac{L_{hole}}{L_{crd}}\right) K_{\theta} \tag{4.7}$$

where K_{θ} is the cumulative web stiffness without a hole over L_{crd} for a column with an open cross-section (Schafer 2002):

$$K_{\theta} = \left(\frac{Et^3}{6H(1-\nu^2)}\right) L_{crd} \tag{4.8}$$

For a stiffened holes, the two parallel transverse hole edge stiffeners can be thought of as beams spanning h_{hole}, each adding rotational restraint $K_{\theta,stiffener}$ to the web over L_{crd} , i.e.,

$$K_{\theta,stiffener} = \frac{2EI_{stiffener}}{h_{hole}} \left(\frac{h_{hole}}{H}\right)^n \left(\frac{L_{hole}}{L_{crd}}\right)^m, \quad I_{stiffener} = \frac{1}{12} t Q^3. \tag{4.9}$$

The rotational restraint $K_{\theta,stiffener}$ is formulated assuming concentrated moments at each end. The $(h_{hole}/H)^n$ multiplier in Eq. 4.9 is included because a stiffener will be less effective at restraining the flanges when h_{hole} is small relative to the web width H. The $(L_{hole}/ L_{crd})^m$ multiplier expresses the influence of the two parallel stiffeners along the length of the hole on web rotational restraint. When L_{hole} is small relative to the distortional half-wavelength L_{crd}, the stiffeners along h_{hole} are assumed to be less effective at restraining the compressed flanges. (It should be noted that Eq. 4.9 is a mechanics-based "educated guess" that produces a simple

equation conducive to design. A preliminary validation of Eq. 4.9 is provided in the next section, with further validation planned in the near future for other cross-sections and hole dimensions.)

An equivalent cumulative web rotational stiffness, $K_{\theta,r}$, can be written including the loss of web material and the presence of edge stiffeners as

$$K_{\theta,r} = \left(\frac{E t_r^3}{6H(1-\nu^2)} \right) L_{crd} = K_{\theta hole} + 2K_{\theta,stiffener} . \tag{4.10}$$

Substituting Eq. 4.7 and Eq. 4.9 into Eq. 4.10 and solving for the effective web thickness, t_r, results in

$$t_r = \left[\left(1 - \frac{L_{hole}}{L_{crd}} \right) t^3 + \frac{2tQ^3 H}{h_{hole}} \left(\frac{1-\nu^2}{L_{crd}} \right) \left(\frac{h_{hole}}{H} \right)^n \left(\frac{L_{hole}}{L_{crd}} \right)^m \right]^{1/3} . \tag{4.11}$$

The exponents n=1 and m=3 produce the most accurate predictions for P_{crdh} considering the columns in this study (see the following validation section) . Therefore, the effect of a stiffened hole on the critical elastic distortional buckling load can thus be approximated by changing the cross-section web thickness to t_r in a finite strip analysis. The procedure for calculating P_{crdh} is the same as that outlined in Moen and Schafer (2010a). First, the distortional buckling half-wavelength, L_{crd}, is obtained from a finite strip analysis of the gross cross-section. The effective thickness, t_r, is then implemented in a second finite strip analysis performed just at L_{crd}, which produces P_{crdh}.

4.4.3 Distortional buckling prediction for beams with holes

The distortional critical elastic buckling moment, M_{crd}, is calculated for a cold-formed steel beam with holes as:

$$M_{crd} = \min(M_{crdnh}, M_{crdh}), \tag{4.12}$$

where M_{crdnh} is the distortional buckling load of a half-wave without a hole, which may be calculated by finite strip or hand methods (AISI-S100 2007). The buckling load for a distortional buckling half-wave including a hole, M_{crdh}, can be calculated for unstiffened holes by simulating the effect of the hole by reducing the web thickness in a finite strip analysis, as detailed in Moen and Schafer (2010b). The exponents n=1 and m=1 are recommended in Eq. 4.11, and the same finite strip analysis discussed in Section 4.4.2 is used to approximate M_{crdh} for cold-formed beams with edge-stiffened holes. The viability of this approach is confirmed in the next section with thin shell finite element eigen-buckling parameter studies.

4.4.4 Verification for distortional bucking of members with edge-stiffened holes

The critical elastic distortional buckling loads (moments) for the cold-formed steel SSMA member dimensions in Table 4.1 at a stiffened hole and away from a stiffened holes are approximated with finite strip methods in this section i.e., $P_{crdnh,simp}$, $P_{crdh,simp}$ for columns and $M_{crdnh,simp}$, $M_{crdh,simp}$ for beams. The same distortional buckling modes (at a hole and between holes) were identified in thin shell finite element eigen-buckling analyses ($P_{crdnh,ABAQUS}$, $P_{crdh,ABAQUS}$ for columns and $M_{crdnh,ABAQUS}$, $M_{crdh,ABAQUS}$) for comparison (Figure 4.1). The modeled FE boundary conditions are described in Figure 4.3. Note that $P_{crdnh,simp}$ and $M_{crdnh,simp}$ were calculated with the gross cross-section in CUFSM, and $P_{crdh,simp}$ and $M_{crdh,simp}$ were calculated with a reduced web thickness (Eq. 4.11) in CUFSM.

For both columns and beams with stiffened holes considered in this study, the simplified method is on average an accurate predictor of P_{crd} (ABAQUS-to-predicted mean of 1.01 for columns in Table 5, 1.07 for beams in Table 4.6), however the coefficient of variation (COV) of the ABAQUS-to-predicted buckling loads is high, especially for columns (0.14 for columns, 0.09 for beams). In some cases the finite strip distortional buckling prediction is lower than the ABAQUS results ($P_{crd,\ ABAQUS}/P_{crd,simp}$=0.86 for the 1000S162-54 column in Table 4.5). Both the ABAQUS results and the simplified method predict that distortional buckling occurs between stiffened holes (P_{crdnh}, M_{crdnh}) in all cases. In other words, the hole stiffeners with Q=0.688 in. provide enough rotational restraint to the compressed flanges to compensate for the loss in web material at the hole, resulting in distortional buckling between holes. Unfortunately this prediction trend cannot be confirmed based on the NAHB tests conducted for these members because the experimental report does not describe specimen failure modes in detail.

The finite strip simplified method for predicting P_{crdh} and M_{crdh} using the modified web thickness in Eq. 4.11 and n=1, m=3 for columns, n=1, m=1 for beams, is on average an accurate predictor when compared to the ABAQUS results (ABAQUS-to-predicted mean is 1.06 for columns in Table 4.5, 1.07 for beams for Table 4.6). The ABAQUS-to-prediction COV is high however, and in some cases the prediction is unconservative ($P_{crdh,ABAQUS}/P_{crdh,simp}$=0.91 for the 800S162-54 column in Table 4.5, $M_{crdh,ABAQUS}/M_{crdh,simp}$=0.93 for the 800S162-43 beam in Table 4.6).

Table 4.5 Influence of edge-stiffened holes on column distortional buckling

SSMA Section	$P_{crdnh,simp}$ (kip)	L_{crd} (in.)	t_r (in.)	$P_{crdh,simp}$ (kip)	$P_{crd,simp}$ (kip)	$P_{crdnh,ABAQUS}$ (kip)	$L_{crdnh,ABAQUS}$ (in.)	$P_{crdh,ABAQUS}$ (kip)	$L_{crdh,ABAQUS}$ (in.)	$P_{crd,ABAQUS}$ (kip)	$P_{crdh,ABAQUS}/P_{crdh,simp}$	$P_{crd,ABAQUS}/P_{crd,simp}$
800S162-43	4.44	19.43	0.053	5.31	4.44	3.90	26.00	6.73	25.00	3.90	1.27	0.88
800S162-54	7.16	16.07	0.062	9.20	7.16	7.42	25.25	8.35	24.00	7.42	0.91	1.04
1000S162-54	4.98	20.12	0.061	6.17	4.98	4.29	24.75	5.31	24.50	4.29	0.86	0.86
1200S162-54	3.39	20.03	0.059	4.26	3.39	3.66	24.75	4.77	26.00	3.66	1.12	1.08
1200S162-68	5.85	16.58	0.069	8.08	5.85	6.96	24.75	9.26	26.25	6.96	1.15	1.19
						ABAQUS-to-predicted statistics				Mean	1.06	1.01
										COV	0.16	0.14

Table 4.6 Influence of edge-stiffened holes on beam distortional buckling

SSMA Section	$M_{crdnh,simp}$ (kip-in.)	L_{crd} (in.)	t_r (in.)	$M_{crdh,simp}$ (kip-in.)	$M_{crd,simp}$ (kip-in.)	$M_{crdnh,ABAQUS}$ (kip-in.)	$L_{crdnh,ABAQUS}$ (in.)	$M_{crdh,ABAQUS}$ (kip-in.)	$L_{crdh,ABAQUS}$ (in.)	$M_{crd,ABAQUS}$ (kip-in.)	$M_{crdh,ABAQUS}/M_{crdh,simp}$	$M_{crd,ABAQUS}/M_{crd,simp}$
800S162-43	43.88	15.72	0.055	55.69	43.88	43.51	15.75	52.03	23.75	43.51	0.93	0.99
800S162-54	71.82	12.94	0.063	85.30	71.82	72.15	12.90	83.44	19.75	72.15	0.98	1.00
1000S162-54	68.40	16.67	0.062	76.41	68.40	73.90	15.60	99.14	27.50	73.90	1.30	1.08
1200S162-54	59.36	16.60	0.060	66.59	59.36	70.48	18.25	75.34	24.75	70.48	1.13	1.19
1200S162-68	97.82	11.11	0.068	111.25	97.82	107.65	12.20	111.14	21.50	107.65	1.00	1.10
						ABAQUS-to-predicted statistics				Mean	1.07	1.07
										COV	0.14	0.07

4.5 Local buckling of cold-formed steel columns and beams with edge-stiffened holes

4.5.1 Local buckling prediction equations

The local critical elastic buckling load, $P_{cr\ell}$, is calculated for a cold-formed steel column with holes as:

$$P_{cr\ell,simplified} = \min(P_{cr\ell nh}, P_{cr\ell h}), \tag{4.13}$$

where $P_{cr\ell nh}$ is the local buckling load of the gross section, ignoring the hole, which may be calculated by finite strip or hand methods (AISI-S100 2007). The buckling load including the hole, $P_{cr\ell h}$, may be calculated by a finite strip analysis of the net cross-section (e.g., in CUFSM) as shown in Figure 4.4 and examining only those buckling half-wavelengths shorter than the length of the hole. (It should be noted that in previous publications by the second author it was recommended to restrain the cross-section corners in a finite strip analysis of the net section. Recent experiments by Schudlich et al. (2011) have determined that an Euler type buckling

failure of the unstiffened strip and compressed flange is a possible local buckling failure mode when hole depth is large relative to web height. This local buckling mode can be readily identified with a net section finite strip model if the corners are unrestrained in CUFSM.)

Figure 4.4 Local buckling at a stiffened hole in CUFSM

Once the net cross section is input into CUFSM, an eigen-buckling analysis is performed (zero thickness line can remain or it may be removed), and an elastic buckling curve is generated (Moen and Schafer 2009b). The half-wavelength corresponding to the minimum buckling load is $L_{cr\ell h}$. When $L_{hole} < L_{cr\ell h}$, $P_{cr\ell h}$ is equal to the buckling load at the length of the hole. If $L_{hole} \geq L_{cr\ell h}$, $P_{cr\ell h}$ is the minimum on the buckling curve. Use of the net cross-section for buckling half-wavelengths greater than L_{hole} is conservative and fails to reflect the stiffness contributions of the gross section in a finite strip analysis.

4.5.2 Verification for local bucking of members with edge-stiffened holes

The elastic local buckling properties of the SSMA members summarized in Table 4.1 are predicted with the finite strip approach discussed in the previous section and compared to ABAQUS thin shell finite element eigen-buckling analysis. The finite element model boundary conditions are summarized in Figure 4.3, and both a uniaxially loaded column and a beam with a constant moment are considered. For both columns and beams, local buckling is predicted to occur between holes, i.e., $P_{cr\ell h} >> P_{cr\ell nh}$ and $M_{cr\ell h} >> M_{cr\ell nh}$ (Table 4.7, Table 4.8).

Table 4.7 Influence of edge-stiffened holes on column local buckling

SSMA Section	$P_{cr\ell nh,simp}$ (kip)	$L_{cr\ell nh}$ (in.)	$P_{cr\ell h,simp}$ (kip)	$L_{cr\ell h}$ (in.)	$P_{cr\ell,simp}$ (kip)	$P_{cr\ell,ABAQUS}$ (kip)	$P_{cr\ell,ABAQUS}/P_{cr\ell,simp}$
800S162-43	2.68	6.14	32.3	1.70	2.68	2.70	1.01
800S162-54	5.24	6.10	63.4	1.70	5.24	5.26	1.01
1000S162-54	3.88	7.68	63.4	1.70	3.88	3.90	1.00
1200S162-54	3.00	11.18	37.2	2.30	3.00	3.05	1.01
1200S162-68	5.62	13.41	74.4	2.30	5.62	5.74	1.02
			ABAQUS-to-predicted statistics			Mean	1.01
						COV	0.01

Table 4.8 Influence of edge-stiffened holes on beam local buckling

SSMA Section	$M_{cr\ell nh,simp}$ (kip)	$L_{cr\ell nh}$ (in.)	$M_{cr\ell h,simp}$ (kip)	$L_{cr\ell h}$ (in.)	$M_{cr\ell,simp}$ (kip)	$M_{cr\ell,ABAQUS}$ (kip)	$M_{cr\ell,ABAQUS}/M_{cr\ell,simp}$
800S162-43	32.0	4.22	140.0	1.60	32.0	32.1	1.00
800S162-54	62.4	4.19	274.1	1.60	62.4	62.6	1.00
1000S162-54	55.9	5.28	333.8	1.60	55.9	56.2	1.00
1200S162-54	51.1	6.36	212.7	2.20	51.1	51.3	1.00
1200S162-68	96.7	6.48	424.6	2.20	96.7	96.9	1.00
			ABAQUS-to-predicted statistics			Mean	1.00
						COV	0.00

4.6 **Conclusions**

Recently developed elastic buckling simplified prediction methods for thin-walled cold-formed steel members with holes are also viable for members with edge-stiffened holes. Global buckling loads (moments) of lipped C-section columns and beams with edge-stiffened holes were accurately predicted by inputting weighted average cross section properties into classically derived engineering expressions for flexural and torsional buckling. An effective web thickness equation was derived and validated for distortional buckling of C-section members with edge-stiffened holes. A finite strip analysis can be performed to simulate the removal of web material and the increase in flange rotational restraint provided by edge stiffeners in the web over a distortional buckling half-wave. For local buckling, finite strip based simplified methods, including a local buckling analysis of the net cross-section, accurately predicted that the edge stiffeners minimized buckling at a hole, causing buckled half-waves to form between the holes.

Acknowledgements

The authors wish to thank Tom Trestain for his willingness over the past year to thoughtfully discuss and critique the topics and ideas presented in this paper.

CHAPTER 5. STEELFORM SIMPLIFIED METHODS EVALUATION

5.1 Abstract

This supplemental section presents a validation to the suite of prediction methods for approximating the elastic buckling properties of cold-formed steel columns and beams with edge-stiffened holes presented in Chapter 4. Validation is given by using these prediction methods to predict elastic buckling properties for the complex edge-stiffened structural studs manufactured by Steelform, Inc. Weighted average section properties are used with classical column stability equations to predict flexural and flexural-torsional buckling loads and beam lateral-torsional buckling moments including the influence of edge-stiffened holes. Cross-sectional instability of lipped C-sections including stiffened holes is evaluated with eigen-buckling analysis and the finite strip method. Critical elastic distortional buckling is shown to be minimally affected by the presence of stiffened holes when edge stiffener dimensions around web holes are sized to replace bending stiffness lost by the removal of web material at a hole. Finite strip analysis of the net section at a stiffened hole is performed to evaluate local buckling. The simplified methods are validated with thin shell finite element eigen-buckling parameter studies where the edge-stiffened holes are explicitly modeled.

5.2 **Introduction**

This section extends validation to the simplified procedures outlined in Chapter 4 for approximating the change in the elastic buckling load (or moment) of cold-formed steel columns and beams due to the presence of complex edge-stiffened holes. The stiffened hole simplified methods for predicting global buckling, distortional buckling, and local buckling are evaluated with finite element eigen-buckling parameter studies on the Steelform cold-formed structural steel members analyzed in Chapters 2 and 3 of this thesis (Table 5.1,Figure 5.1). This will be a more rigorous test for the Chapter 4 prediction methods as the Steelform structural members include complex geometry that includes the following: singly symmetric holes , hole orientation changes, hole sizes vary along stud, spacing of holes is such that holes are not isolated from one another, varying edge-stiffener length and geometry around a hole, and edge-stiffeners in both flange and web and flange lip exist.

Table 5.1 Steelform structural stud and stiffened hole dimensions

SSMA Designation	Thickness	Web Size	Flange Width	Flange Stiffener	Stud Length	End Length	Hole Depth	Hole Length	Hole Spacing	Inside Corner Radius	Hole Stiffener Length	Hole Radii
	(in.)	(in.)	(in.)	(in.)	(in.)	(in.)	(in.)	(in.)	(in.)	(in.)	(in.)	(in.)
	t	H	B	D	L	L_{end}	h_{hole}	L_{hole1} / L_{hole2} / L_{hole3}	S	R	Q_{hole1} / Q_{hole2} / Q_{hole3}	R_{hole1} / R_{hole2}
3625x1625-33	0.0346	3.625	1.625	0.500	80	4	2.125	1.041 / 2.484 / 3.734	4	0.094	0.255 / 0.500 / 0.627	0.625 / 1.000
3625x1625-43	0.0451	3.625	1.625	0.500	80	4	2.125	1.041 / 2.484 / 3.735	4	0.094	0.255 / 0.500 / 0.627	0.625 / 1.000
3625x1625-54	0.0566	3.625	1.625	0.500	80	4	2.125	1.041 / 2.484 / 3.736	4	0.094	0.255 / 0.500 / 0.627	0.625 / 1.000
3625x1625-68	0.0713	3.625	1.625	0.500	80	4	2.125	1.041 / 2.484 / 3.737	4	0.094	0.255 / 0.500 / 0.627	0.625 / 1.000
6000x1625-33	0.0346	6.000	1.625	0.500	80	8	3.500	2.550 / 6.568 / 8.318	8	0.094	0.325 / 0.584 / 0.868	0.875 / 1.500
6000x1625-43	0.0451	6.000	1.625	0.500	80	8	3.500	2.550 / 6.568 / 8.319	8	0.094	0.325 / 0.584 / 0.868	0.875 / 1.500
6000x1625-54	0.0566	6.000	1.625	0.500	80	8	3.500	2.550 / 6.568 / 8.320	8	0.094	0.325 / 0.584 / 0.868	0.875 / 1.500
6000x1625-68	0.0713	6.000	1.625	0.500	80	8	3.500	2.550 / 6.568 / 8.321	8	0.094	0.325 / 0.584 / 0.868	0.875 / 1.500

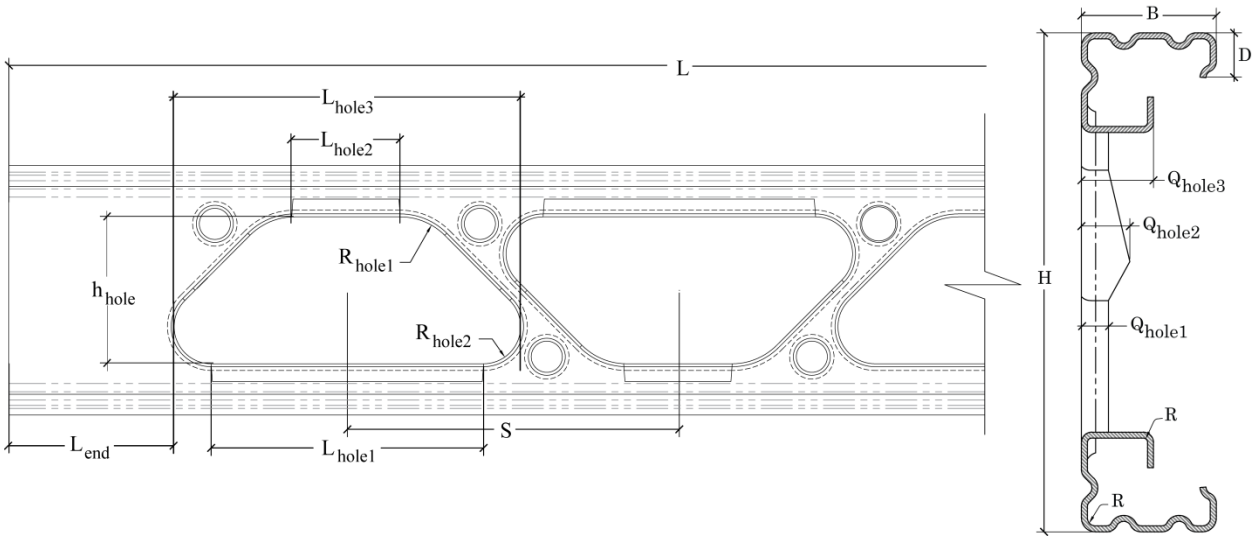

Figure 5.1 Structural stud dimension nomenclature

5.3 **Analysis assumptions for elastic buckling validation of Steelform columns**

Due to the complex web geometry of the Steelform structural members, certain geometric simplifications must be made in order to utilize the simplified method equations presented in Chapter 4. For global buckling, members are analyzed as if there is one hole over the entire center section of the member. To determine which section properties should be chosen when a complex section exists, the buckling analysis is performed multiple times varying the method by which the cross section properties were taken as shown in Table 5.2. The first method, utilizes the worst case section properties. For example, the strong axis moment of inertia, I_{yy}, is taken at section C-C (See section definitions in Chapter 3 Figure 3.9) and the weak axis moment of inertia, I_{xx}, is taken at section D-D (Figure 3.9). The second method uses the cross section with the worst percentage of controlling properties. For example, in Table 5.2, the 3.625” studs use section C-C properties whereas the 6.000” members use section D-D properties. The use of only the mid-hole section properties is also analyzed (Method 3, Section E-E).

Table 5.2 Variations of section property methods – Global Buckling

Method	Method Description	Steelform Section	Section Designation: Area	Torsion Properties		Centroidal Properties		Shear Center
			A (in^2)	C_w (in^6)	J (in^4)	I_{yy} (in^4)	I_{xx} (in^4)	X_o (in)
Method 1	Worst Section Properties	3.625"	C-C	C-C	C-C	C-C	D-D	D-D
		6.000"	D-D	D-D	D-D	C-C	D-D	D-D
Method 2	Worst Case Section Properties	3.625"	C-C	C-C	C-C	C-C	C-C	C-C
		6.000"	D-D	D-D	D-D	D-D	D-D	D-D
Method 3	Mid Hole Section Properties	3.625"	E-E	E-E	E-E	E-E	E-E	E-E
		6.000"	E-E	E-E	E-E	E-E	E-E	E-E

Note: X-X refers to Section X-X in Figure 3.9

Whereas the simplified methods assume sections properties over the entire length of the hole section as in Figure 5.2a, the simplified distortional buckling equations require a definite hole spacing or else the prediction equations produce unrealistic effective thicknesses. See Equation 4.11 where increasing L_{hole} increases the effective web thickness greatly overestimating capacity. Therefore, a hole length, L_{hole}, equal to L_{hole1} (See Figure 5.1 for nomenclature) is assumed. Figure 5.2b shows the assumed hole geometry for this analysis. The edge-stiffener is also taken conservatively as Q_{hole1} (See Figure 5.1 for nomenclature) for distortional buckling calculations.

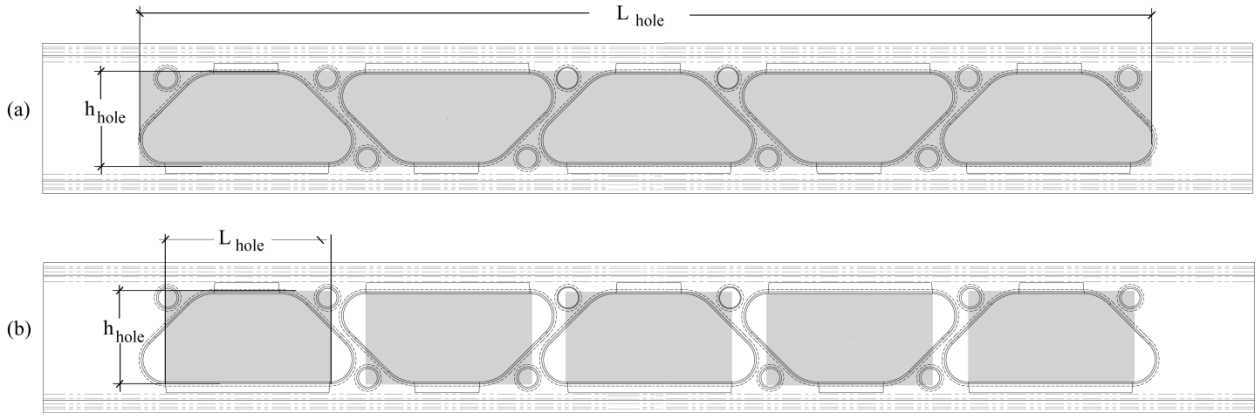

Figure 5.2 Structural stud hole dimension assumptions (shaded area denotes hole location)
(a) Global buckling assumptions (b) Distortional buckling assumptions

5.4 Global Buckling

5.4.1 Comparison between methods for global buckling of columns and beams with edge-stiffened holes

Table 5.3 compares all three methods and their ability to predict the global buckling loads accurately (See Appendix A.4 for further details). Using the worst possible section properties (Method 1) overall is most accurate predictor of all three methods with an average mean-of-means of 0.99. Picking the worst case properties no matter what section they are in makes sense as some of the sections provide greater stiffness to the section when it does not actually exist. By assuming the hole runs the entire center section of the member (Figure 5.2a), picking a stiffer section would produce very unconservative values just as was confirmed using only the mid-hole properties (Method 3). This increased stiffness (greater strong axis moment of inertia) does not actually contribute to the increased global properties as the large stiffeners at mid-hole are not engaged since the force cannot make its way to them. If definite holes, such as in Figure 5.2b were assumed, other section properties might be able to be used. Future research could be performed to confirm this hypothesis. Furthermore, by using mid-hole properties, an engineer may not be able to pick up that a controlling buckling may change, such as the 3625-68 stud did in compression switching from controlling in flexural-torsional to controlling weak-axis bending when holes are added.

Table 5.3 Method comparison for global buckling on columns and beams

Buckling Mode	Method	Comparison	Steelform Section								ABAQUS-to-predicted statistics	
			3625-33	3625-43	3625-54	3625-68	6000-33	6000-43	6000-54	6000-68		
			L=80 in	L=80 in	L=80 in	L=80 in	L=80 in	L=80 in	L=80 in	L=80 in	Mean	COV
Column weak-axis flexural buckling	Method 1		0.92	0.92	0.93	0.94	0.94	0.98	0.96	0.95	**0.94**	**0.02**
	Method 2	$P_{cre,ABAQUS\ with\ holes}/P_{cre,avg}$	0.88	0.88	0.89	0.90	0.94	0.98	0.96	0.95	0.92	0.04
	Method 3		0.82	0.82	0.83	0.83	0.89	0.93	0.91	0.88	0.86	0.05
Column flexural-torsional buckling	Method 1		1.02	1.04	1.11	1.09	1.01	1.05	1.05	1.06	1.05	**0.03**
	Method 2	$P_{cre,ABAQUS\ with\ holes}/P_{cre,avg}$	1.01	1.03	1.10	1.09	1.08	1.01	1.00	1.01	**1.04**	0.04
	Method 3		0.91	0.92	0.92	1.04	0.97	1.01	1.00	0.98	0.97	0.05
Beam lateral-torsional buckling	Method 1		0.94	0.95	0.99	0.99	0.97	1.02	1.01	1.00	**0.98**	**0.03**
	Method 2	$M_{cre,ABAQUS\ with\ holes}/M_{cre,avg}$	0.92	0.93	0.97	0.97	0.97	1.02	1.01	1.00	0.97	0.04
	Method 3		0.88	0.88	0.88	0.87	0.95	0.99	0.97	0.94	0.92	0.05

ABAQUS-to-predicted statistics		Method 1	Method 2	Method 3
	Mean-of-Means	0.99	0.98	0.92
	Mean-of-COV	0.03	0.04	0.05

ABAQUS results are systematically 7% lower than the Euler buckling solutions due to the assumption of rigid cross section in the classical buckling equations (Moen 2008). Because of this, the mean for $P_{cre,ABAQUS\ with\ holes}/P_{cre,avg}$ should be compared to 0.93 instead of 1.0 for weak-axis flexure in Table 5.3. If this is accounted for, using the worst possible section properties (Method 1) is proven to be conservative for all members considered except for 3625-33 and 3625-43 which are unconservative by 1% as shown in Figure 5.3. Figure 5.3 and Figure 5.4 present the prediction to ABAQUS results for global buckling of the considered columns and beams. See Appendix A.4.1 for individual iterations of each prediction method.

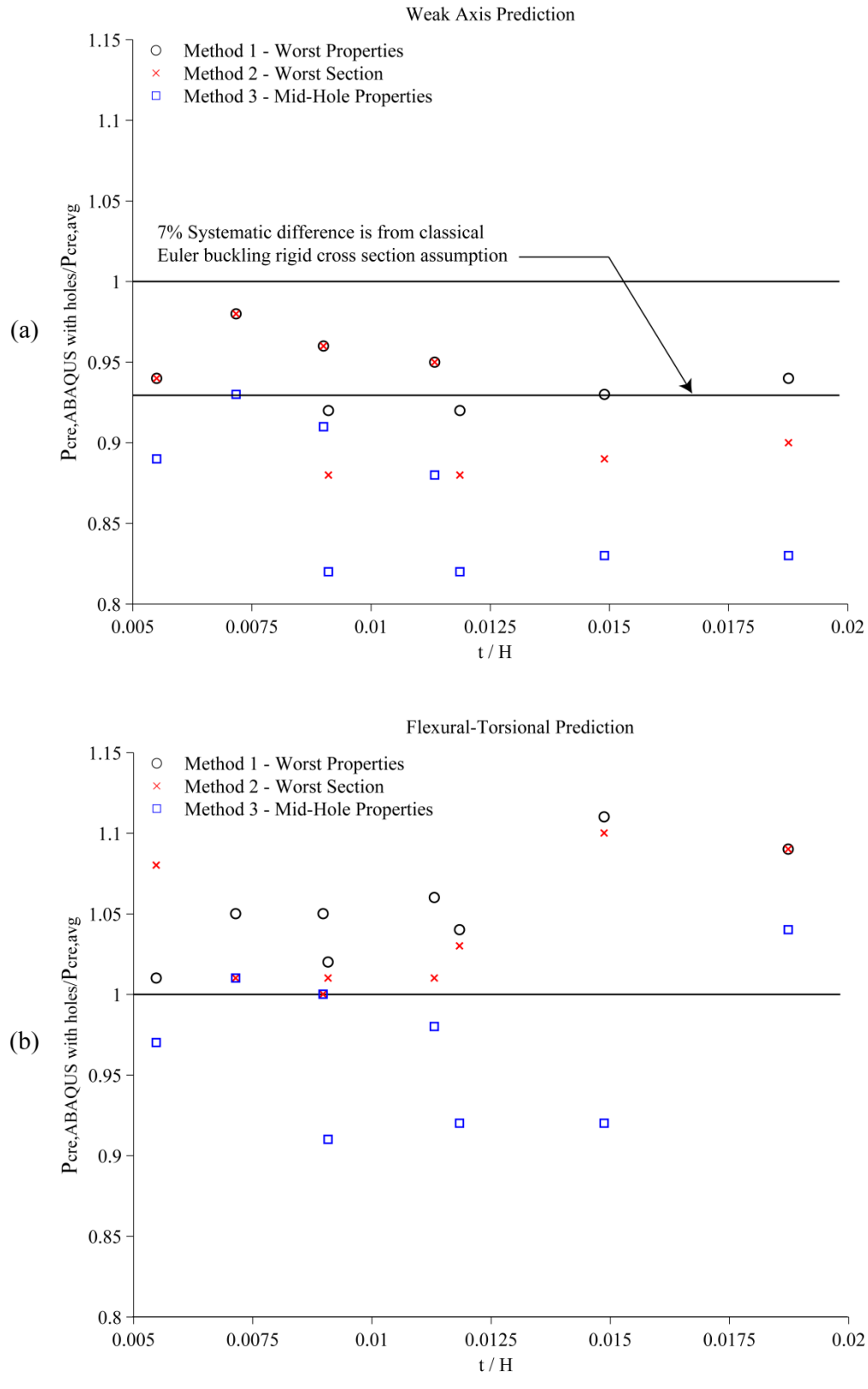

Figure 5.3 (a) Column weak-axis flexural (b) flexural-torsional buckling predictions

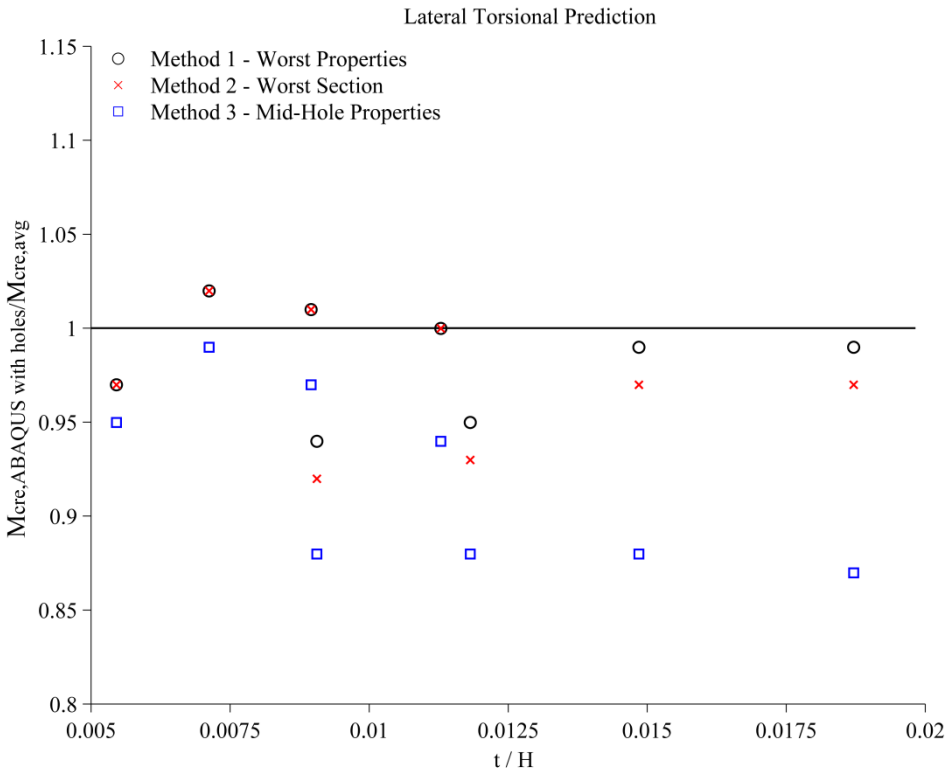

Figure 5.4 Beam lateral-torsional buckling predictions

5.5 Distortional Buckling

5.5.1 Evaluation for distortional bucking of members with edge-stiffened holes

The critical elastic distortional buckling loads (moments) for the Steelform cold-formed steel member dimensions in Table 5.1 at a stiffened hole and away from a stiffened holes are approximated with finite strip methods in this section i.e., $P_{crdnh,simp}$, $P_{crdh,simp}$ for columns and $M_{crdnh,simp}$, $M_{crdh,simp}$ for beams. Note that $P_{crdnh,simp}$ and $M_{crdnh,simp}$ were calculated with the gross cross-section in CUFSM, and $P_{crdh,simp}$ and $M_{crdh,simp}$ were calculated with a reduced web thickness (Eq. 4.11) in CUFSM using the assumed hole dimensions in Figure 5.2b. Unlike the SSMA studs, which allowed enough gross section length to accommodate distortional half-wavelengths between holes, it is hypothesized that the Steelform members considered in this

study will not allow this to occur as there is no distinct gross section between holes. In addition, the end gross sections only measure 4.0 in. which is too small to allow a distortional half-wavelength to form. To consider and catch all possible distortional modes, two different modes are taken from the ABAQUS eigen-buckling analysis. The first, a distortional buckling mode as shown in Figure 5.5b with half-waves occurring the full length. The second, a not so distinct distortional mode that occurs at the ends of the members that mixes with local buckling as well as engaging the holes is shown in Figure 5.5c. It should be noted that this end mode only exists in members in pure compression. The flexure distortional mode is presented in Figure 5.5d.

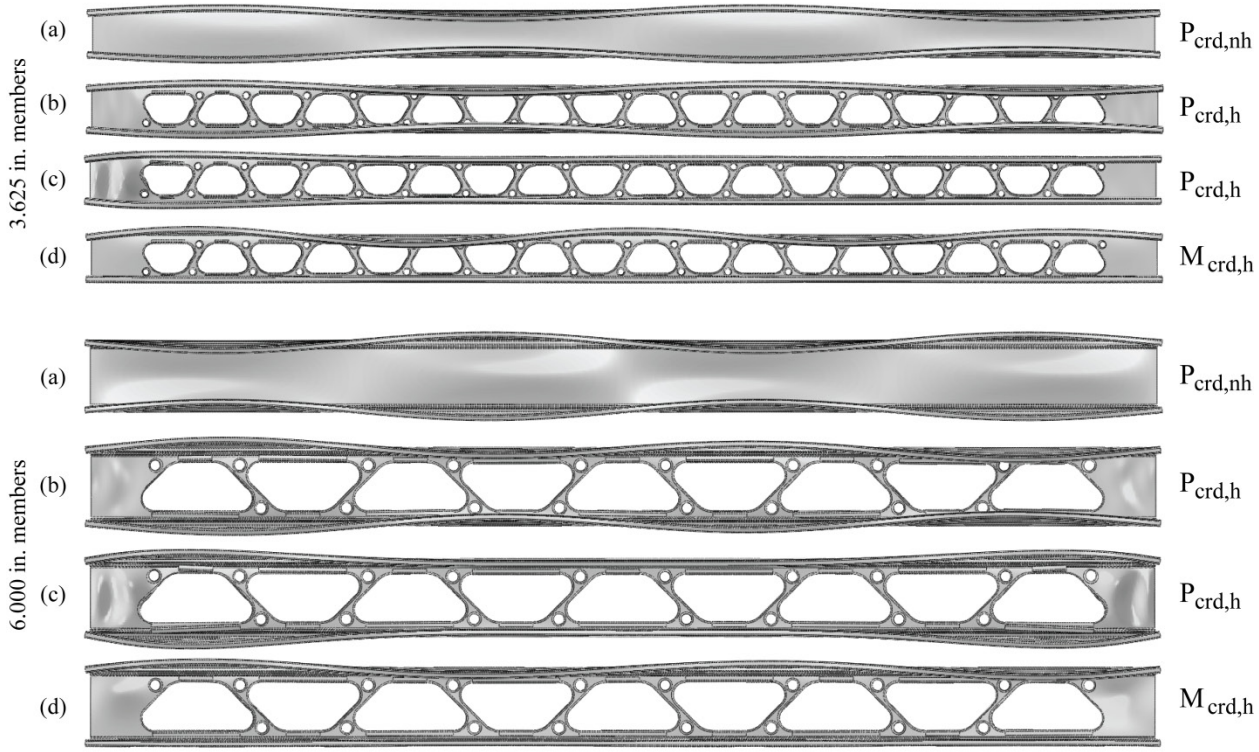

Figure 5.5 Distortional modes considered
a) Typical distortional mode for a column without holes b) Most distinct distortional mode for column with holes c) End distortional mode for column with holes d) Distortional mode for beam with holes

Three methods were looked at to determine which works best for predicting the distortional buckling loads for the Steelform members with complex edge-stiffened holes considered in this study. This validation and method variation will hopefully allow these simplified methods to be extended to other complex members that exist. The three methods are presented in Table 5.4.

Table 5.4 Method comparison for distortional buckling equations

Method	Method Description	Steelform Section	Hole Length	Edge-Stiffener Length
			L_{hole} (in)	Q (in)
Method 1	Conservative edge-stiffener length Hole length equal to longest horizontal leg	3.625" 6.000"	2.484 6.568	0.255 0.325
Method 2	Weighted average edge-stiffener length Hole length equal to longest horizontal leg	3.625" 6.000"	2.484 6.568	0.400 0.600
Method 3	Conservative edge-stiffener length Hole length equal edge-to-edge hole width	3.625" 6.000"	3.734 8.318	0.255 0.325
Method 4	Weighted average of only vertical edge-stiffener Hole length equal to longest horizontal leg	3.625" 6.000"	2.484 6.568	0.333 0.389

5.5.2 Comparison between methods for distortional buckling of members with edge-stiffened holes

Presented in Table 5.5 are the results for the various methods and their ability to determine the distortional buckling hole load, $P_{crdh,simp}$,accurately. Method 2 (Weighted average edge-stiffener and hole length equal to the longest leg) is the most accurate for predicting $P_{crdh,simp}$ with a mean prediction of 1.07 and a COV of 0.15. Method 3 (Conservative edge-stiffener length and hole length equal to outer bounds of hole), produces the most conservative results with all members with a mean of 1.28 but a relatively high COV of 0.22. This method is the most conservative due to the assumed increasing length of hole, L_{hole} , which decreases the rotational stiffness provided by the web.

The most accurate method for determining $P_{crdh,simp}$ (Method 2) is the most unconservative prediction method for $M_{crdh,simp}$ by a 51% maximum for the 6.000in. members. It is concluded that using the weighted average stiffener length is contributing too much rotational stiffness to the web. This is also confirmed when Method 2 is compared to Method 1, where the only change is the stiffener length. In Eq. 4-11, the stiffener length is a scalar therefore a slight change in that value could cause a large change in contributing stiffness. Method 1 predicts distortional buckling moments at a mean of 1.03 and a low COV of 0.05.

It should be noted that according the prediction method outlined in Chapter 4 for predicting distortional buckling loads, that the minimum of $P_{crdh,simp}$ and $P_{crdnh,simp}$ (or $M_{crdh,simp}$ and $M_{crdnh,simp}$) should be taken. In most cases, distortional buckling strength increased when edge-stiffened holes are present in the web. Presented in Table 5.6 is the accuracy of the overall prediction method which shows that no matter what method is chosen, conservative buckling loads are produced except for the 3625-43 and 3625-68 columns (unconservative by maximum of 9%). Table 5.5 and Table 5.6 as well as Figure 5.6 and Figure 5.7 show that Method 1 is overall the most accurate method using the most conservative stiffener length, Q_{hole1}, and a hole length equal to L_{hole} in Figure 5.1.

One assumption made in the method outlined in Chapter 4 is that the distortional buckling half-wavelength remains the same between a member with holes and without holes. Preliminary column testing at the Thomas Murray Structures Lab at Virginia Tech revealed that the distortional half-wavelength predicted (using the no hole half-wavelength) did not occur in testing with the Steelform Inc. studs with edge-stiffened holes. Instead, one large distortional buckling half wave length formed over the entire hole section. It is suggested that full finite

element analysis is still needed to determine the effects of edge-stiffened holes on distortional buckling.

Table 5.5 Comparison of methods for predicting distortional buckling hole loads

Method	Comparison	Steelform Section								ABAQUS-to-predicted statistics	
		3625-33	3625-43	3625-54	3625-68	6000-33	6000-43	6000-54	6000-68		
		L=80 in	L=80 in	L=80 in	L=80 in	L=80 in	L=80 in	L=80 in	L=80 in	Mean	COV
Method 1	$P_{crdend,ABAQUS}/P_{crdh,simp}$	1.13	0.93	1.11	0.92	1.51	1.84	1.37	1.24	1.26	0.25
Method 2		1.13	0.93	1.11	0.91	1.17	1.38	1.04	0.92	1.07	0.15
Method 3		1.17	0.97	1.16	0.97	1.50	1.82	1.38	1.26	1.28	0.22
Method 4		1.13	0.93	1.11	0.92	1.45	1.75	1.31	1.18	1.22	0.23
Method 1	$M_{crdh,ABAQUS}/M_{crdh,simp}$	1.07	1.07	1.05	1.03	0.92	1.01	1.06	1.07	1.03	0.05
Method 2		0.92	0.94	0.94	0.91	0.49	0.54	0.58	0.59	0.74	0.28
Method 3		1.06	1.07	1.06	1.05	0.88	0.98	1.04	1.07	1.03	0.06
Method 4		0.99	1.00	1.00	0.98	0.78	0.86	0.91	0.93	0.93	0.09

Table 5.6 Comparison of methods for predicting distortional buckling load of a member with holes

Method	Comparison	Steelform Section								ABAQUS-to-predicted statistics	
		3625-33	3625-43	3625-54	3625-68	6000-33	6000-43	6000-54	6000-68		
		L=80 in	L=80 in	L=80 in	L=80 in	L=80 in	L=80 in	L=80 in	L=80 in	Mean	COV
Method 1	$P_{crd,ABAQUS}/P_{crd,simp}$	1.13	0.93	1.11	0.92	1.51	1.84	1.37	1.24	1.26	0.25
Method 2		1.13	0.93	1.11	0.91	1.18	1.52	1.14	0.99	1.11	0.17
Method 3		1.17	0.97	1.16	0.97	1.50	1.82	1.38	1.26	1.28	0.22
Method 4		1.13	0.93	1.11	0.92	1.45	1.75	1.31	1.18	1.22	0.23
Method 1	$M_{crd,ABAQUS}/M_{crd,simp}$	1.09	1.07	1.05	1.03	1.14	1.15	1.12	1.07	1.09	0.04
Method 2		1.09	1.07	1.03	0.99	1.14	1.15	1.12	1.05	1.08	0.05
Method 3		1.09	1.07	1.06	1.05	1.14	1.15	1.12	1.07	1.09	0.03
Method 4		1.09	1.07	1.03	0.99	1.14	1.15	1.12	1.05	1.08	0.05

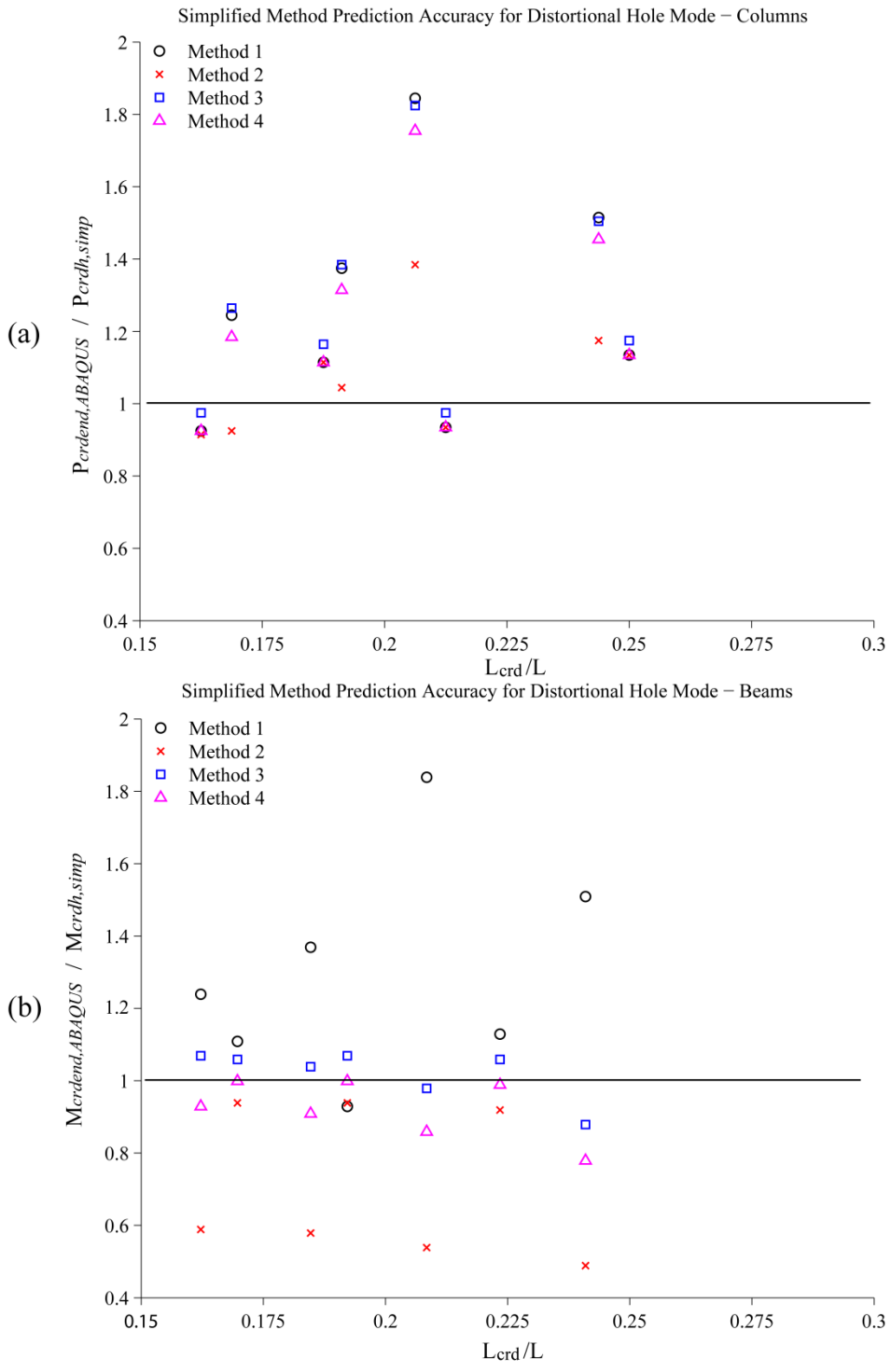

Figure 5.6 Accuracy of simplified method for predicting distortional hole loads (Table 5.5) (Figure 5.5 b/c). (a) Columns (b) Beams of members with edge-stiffened holes

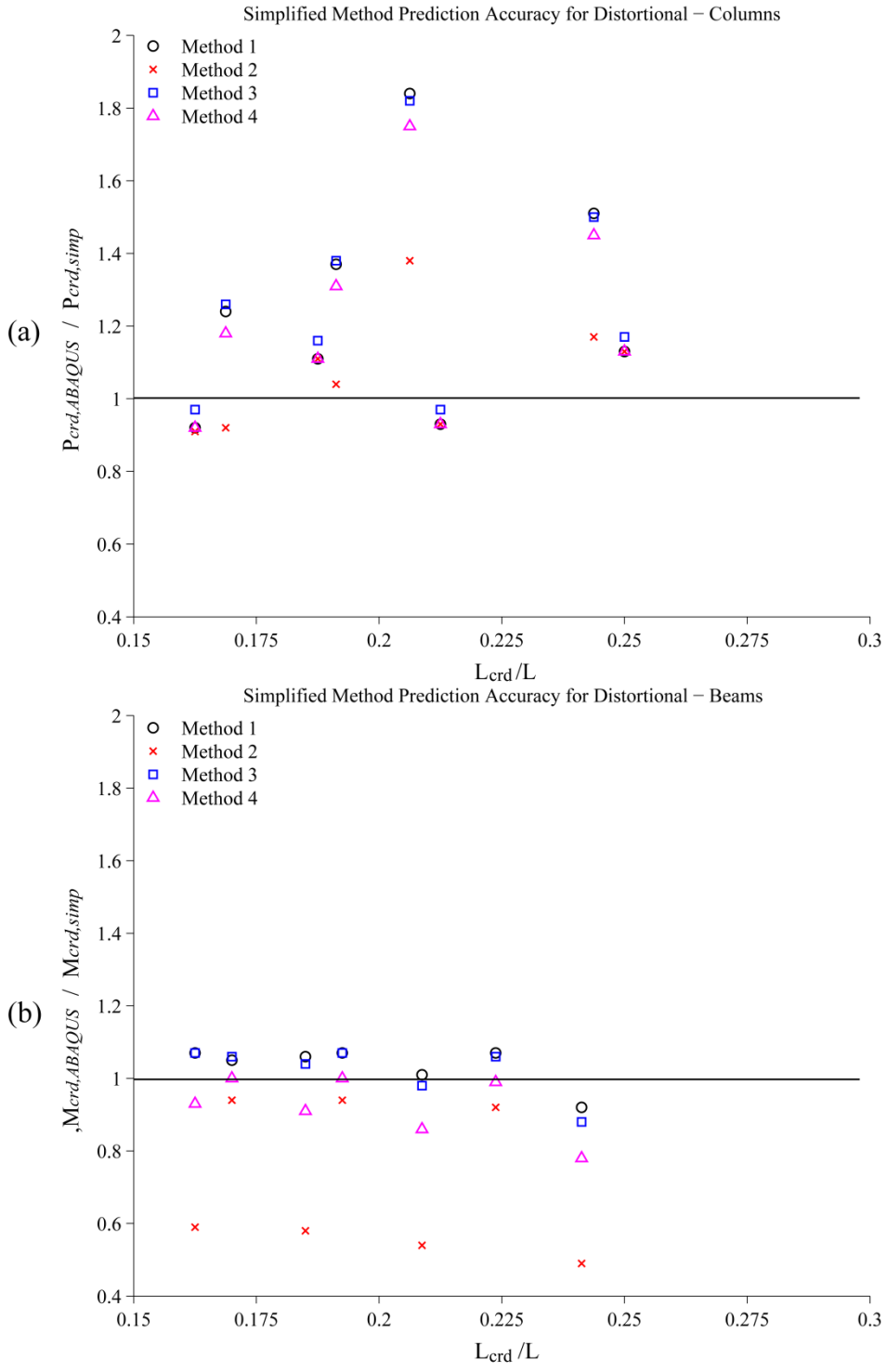

Figure 5.7 Accuracy of simplified method overall for predicting distortional buckling of a (a) Column or (b)Beam with edge-stiffened holes (Table 5.6)

5.6 **Local Buckling**

5.6.1 Verification for local bucking of members with edge-stiffened holes

The elastic local buckling properties of the Steelform members summarized in Table 5.1 are predicted with the finite strip approach discussed in the Chapter 4 and compared to ABAQUS thin shell finite element eigen-buckling analysis. The finite element model boundary conditions, uniaxially loaded column and a beam with a constant moment are considered. For both columns and beams, local buckling is predicted to occur between holes, i.e., $P_{cr\ell h} >> P_{cr\ell nh}$ and $M_{cr\ell h} >> M_{cr\ell nh}$ (Table 5.7). A slight increase in the predicted local buckling load occurs due to location of the holes. For example, the local buckling half-wavelength for the gross section for the 3625-54 stud is 2.80 in., however, the total gross section is 4 in. on each end. This means that two half-wavelengths are forced to form which increases the overall local buckling load. The hole geometry is also slightly different which contributes to this increase. Whereas, the 3.625 in. members have a terminal point that is close to being square, the 6.000in. members holes are more trapezoidal. The influence of the end hole geometry boosts local buckling more in compression than in flexure (Compare $P_{crl,ABAQUS\ with\ holes}$ / $P_{crl,simplified}$ mean values in Table 5.7). In compression, the local buckling half-wave that can form can only form up to the start of a hole. Therefore, for the 3.625 in. studs, which have a half-wavelength of 2.80in. and have 4 in. to form, however the 6.000 in. studs have a halfwavelength of 4.80 in. and still only have 4 in. to form. This boost could be accounted for by using CUFSM and moving to the uninterrupted length on the x-axis to get the modified local buckling load.

Table 5.7 Influence of edge-stiffened holes on local buckling

Loading Type	Comparison		Steelform Section								ABAQUS-to-predicted statistics	
			3625-33	3625-43	3625-54	3625-68	6000-33	6000-43	6000-54	6000-68	Mean	COV
Columns	$P_{cr\ell,nh}$	(kip)	4.21	9.16	17.80	34.90	2.72	5.45	10.20	18.80		
	$P_{cr\ell,h}$	(kip)	69.13	127.58	228.22	404.93	58.05	127.69	241.18	476.39		
	$P_{cr\ell,ABAQUS\ with\ holes}$	(kip)	4.51	9.78	19.00	37.00	3.64	7.50	13.80	25.80		
	$P_{cr\ell,simplified}$	(kip)	4.21	9.16	17.80	34.90	2.72	5.45	10.20	18.80		
	$P_{cr\ell,ABAQUS\ with\ holes}$ / $P_{cr\ell,simplified}$		1.07	1.07	1.07	1.06	1.34	1.38	1.35	1.37	1.21	0.13
Beams	$M_{cr\ell,nh}$	(kip in.)	26.94	57.97	102.11	185.65	30.66	58.11	104.54	189.90		
	$M_{cr\ell,h}$	(kip in.)	133.81	242.09	434.41	738.60	187.01	408.36	777.40	954.67		
	$M_{cr\ell,ABAQUS\ with\ holes}$ - Positive	(kip in.)	27.74	58.49	103.00	186.43	32.18	63.87	101.11	177.36		
	$M_{cr\ell,ABAQUS\ with\ holes}$ - Negative	(kip in.)	27.75	58.51	103.00	186.35	32.47	65.52	109.99	195.66		
	$M_{cr\ell,simplified}$	(kip in.)	26.94	57.97	102.11	185.65	30.66	58.11	104.54	189.90		
	$M_{cr\ell,ABAQUS\ with\ holes}$/ $M_{cr\ell,simplified}$	Positive	1.03	1.01	1.01	1.00	1.05	1.10	0.97	0.93	1.01	0.05
	$M_{cr\ell,ABAQUS\ with\ holes}$/ $M_{cr\ell,simplified}$	Negative	1.03	1.01	1.01	1.00	1.06	1.13	1.05	1.03	1.04	0.04

5.7 **Conclusions**

The developed elastic buckling simplified prediction methods for local and global buckling of thin-walled cold-formed steel members with holes are also viable for members with even the most complex edge-stiffened holes such as the Steelform members presented in this section. However, the recently developed effective thickness equation (Chapter 4) to determine the distortional buckling loads breaks down when complicated stiffeners and hole geometry are present. It is recommended that full finite element eigen-buckling analyses is still required to determine the distortional buckling loads. Global buckling loads (moment of the Steelform C-section columns and beams with edge-stiffened holes were predicted at a lower accuracy than the SSMA studs presented in Chapter 4 by inputting weighted average cross section properties into classically derived engineering expressions for flexural and torsional buckling. This lower accuracy is caused by the simplifying geometric assumptions made in order to find weighted average properties which would be too cumbersome to accurately find. For local buckling, finite strip based simplified methods, including a local buckling analysis of the net cross-section, accurately predicted that the edge stiffeners minimized buckling at a hole, causing buckled half-waves to form in the gross sections of the members.

CHAPTER 6. MBMA DISTORTIONAL BUCKLING STUDY

Twentieth International Specialty Conference on Cold-Formed Steel Structures
St. Louis, Missouri, USA, November 2012

Distortional Buckling Capacity of Z-Purlins Under Gravity Loading

Christopher N. Grey[1], Cristopher D. Moen [2]

6.1 Abstract

Laterally braced cold-formed steel beams generally fail due to local and/or distortional buckling in combination with yielding. For many members, distortional buckling is the dominant buckling mode and is addressed in the current North American Specification for the Design of Cold-formed Steel Structural Members. The current main code equation, AISI C3.1.4-10 for calculating the available distortional buckling stress was derived experimentally based on a series of four-point bending tests at John Hopkins University. Where this provides a good basis for determining capacity, in most loading conditions purlins are subjected to a downward uniform loading that provides additional resistance to distortional buckling in the top flange beyond the resistance of the steel roofing panel. This paper describes an experimental study to explore and quantify the difference in distortional buckling flexural capacity of metal building Z-purlins treated as isolated components and Z-purlins loaded with a constant pressure applied to metal roof panels. A series of three different types of tests have been developed to quantify the system effect provided by the metal roof panels as well as downward pressure on distortional buckling. This paper covers the setup of the distortional buckling tests, test results, and possible modifications to the current design methods. Results are also extended to validate the Direct Strength Method when predicting flexural capacity of purlins in a roof system.

[1] Graduate Research Assistant, Virginia Tech, Blacksburg, VA, 24061, USA. (cgrey@vt.edu)
[2] Assistant Professor, Virginia Tech, Blacksburg, VA, 24061, USA. (cmoen@vt.edu)

6.2 Introduction

Through-fastened metal building roof systems are constructed with corrugated roofing panels attached to cold-formed steel Zee or Cee purlins with self tapping screws. The purlin compression flange is assumed fully braced by the through-fastened roof. Purlin flexural capacity predictions are calculated with the AISI Direct Strength Method (DSM) (AISI-S100 2007) employing the local and distortional elastic buckling parameters from a finite strip analysis (Schafer and Adany 2006) and the flexural yield strength. Recent research has demonstrated that rotational restraint provided to the compression flange by means of a through-fastened metal deck can boost distortional buckling capacity (Schafer and Yu 2006, Schafer, B.W., Sangree,R.H., Guan Y. (2008)). These experiments were conducted with four point bending, however a uniform pressure loading is a more realistic loading condition, e.g., a snow loading. It has been hypothesized that downward pressure improves distortional buckling capacity by preventing the upward half-waves from forming. The goal of the research described herein is to evaluate the viability of this hypothesis.

6.3 Experimental Program

6.3.1 Rationale for cross-section selection and test setup

A Zee cross-section was chosen with a predicted distortional buckling capacity lower than local and local-global buckling interaction limit states as shown in Figure 6.1. The selected cross section is a 8.5 in. web height, 2.5 in. flange, and 0.079 in. thickness Zee section with nominal dimensions summarized in Figure 6.2. Mid-span bracing is provided to prevent lateral torsional buckling for tests where the panel in not attached. Bracing locations were determined by increasing the midspan unbraced distance to a point where at least 3 distortional buckling half-waves (measured from elastic buckling curve in Figure 6.1) could form but still adequately

prevent lateral-torsional buckling (Figure 6.3). An initial DSM unrestrained (assumes panel prevents lateral-torsional buckling) capacity calculation assuming an initial yield stress of 70 ksi was further performed on a nominal section to confirm bracing was at an adequate spacing restraining global buckling. The lateral-torsional buckling load would also be higher due to the conservative effective length factors assumptions. As bracing does not provide full torsional restraint the flanges are free to warp, however, they are restrained by the rest of the purlin beyond mid-span. Therefore, K_t, could be reduced to less than 1.0 however, it is conservatively assumed to equal 1.0 simulating warping free conditions. The effective bending length factor, K_b, is also conservatively taken as 1.0 as biaxial bending exists (unrestrained) and bracing only providing partial restraint against the other purlin.

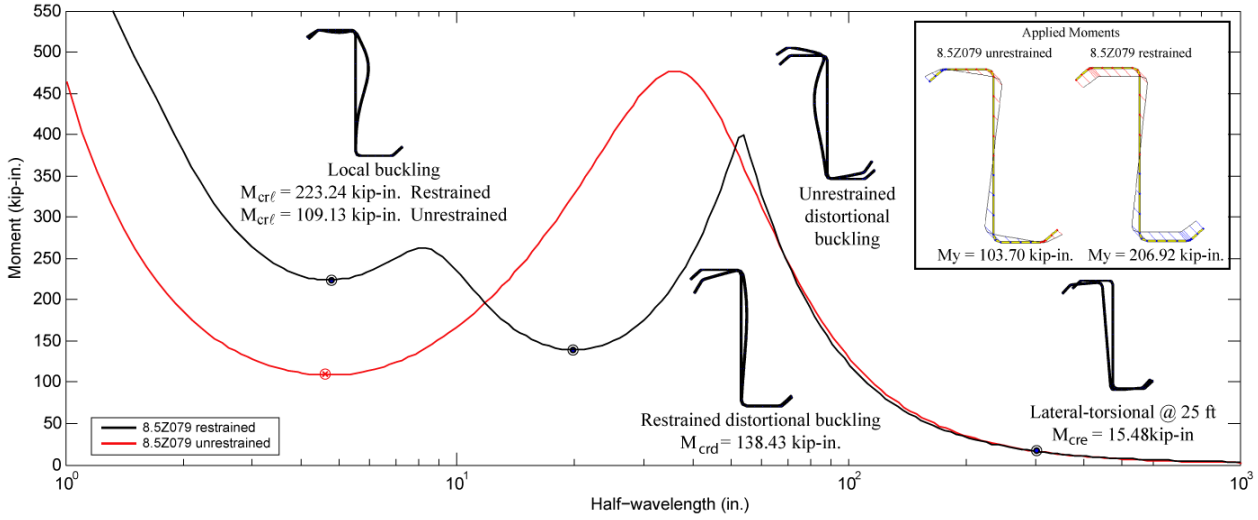

Figure 6.1 Cold-formed steel beam Z-section elastic buckling modes

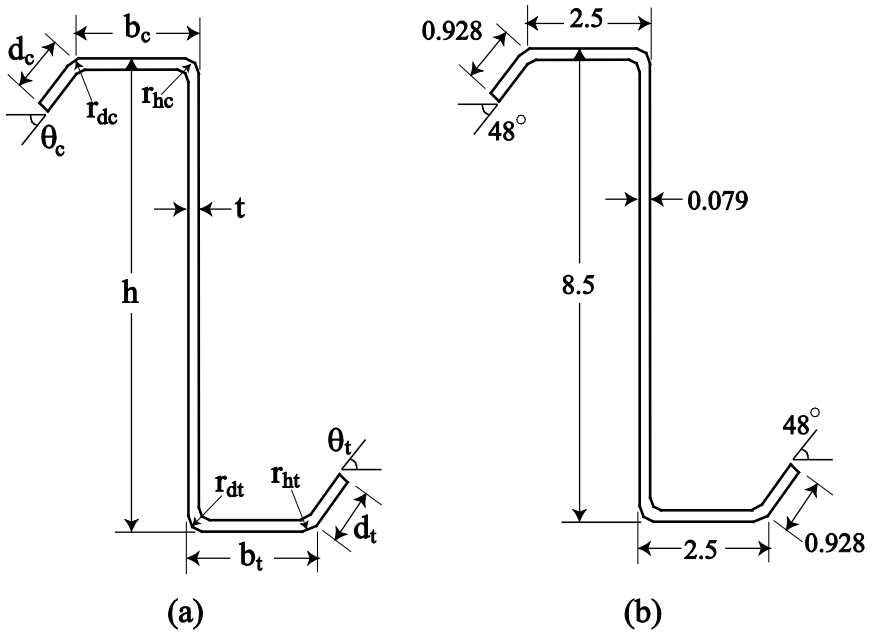

Figure 6.2 (a) Cross-section dimension notation and (b) nominal dimensions (in.)

Table 6.1 Nominal capacity prediction

	Elastic Buckling Properties				Direct Strength Method						
	Yield	Unrestrained Bending			Global	Local		Distortional		Nominal	
Section	$M_{y,u}$ (kip-in.)	$M_{crl,u}$ (kip-in.)	$M_{crd,u}$ (kip-in.)	$M_{cre,u}$ (kip-in.)	M_{ne} (kip-in.)	λ_ℓ	$M_{n\ell}$ (kip-in.)	λ_d	M_{nd} (kip-in.)	$M_{n,DSM}$ (kip-in.)	Controlling Mode
8.5Z079	103.7	109.13	109.13	194.61	98.17	0.95	86.40	0.97	82.37	82.37	(distortional controls)

Table 6.2 Measured cross-section dimensions

Test Label	Purlin Label	h (in)	b_c (in)	$b_{c\,(flat)}$ (in)	d_c (in)	$d_{c(flat)}$ (in)	θ_c (deg)	r_{hc} (in)	r_{dc} (in)	b_t (in)	$b_{t(flat)}$ (in)	d_t (in)	$d_{t(flat)}$ (in)	θ_t (deg)	r_{ht} (in)	r_{dt} (in)	t (in)	f_y (ksi)
UB-P-1-24E25W	24	8.371	2.424	1.956	0.821	0.683	53	0.254	0.385	2.644	1.955	0.902	0.648	56	0.321	0.543	0.081	72.56
	25	8.391	2.518	1.876	0.856	0.674	47	0.279	0.513	2.590	1.884	0.955	0.764	53	0.453	0.366	0.081	72.61
UB-P-2-22E23W	22	8.373	2.389	2.069	0.808	0.704	52	0.271	0.535	2.490	1.999	0.822	0.496	53	0.241	0.447	0.080	72.25
	23	8.403	2.240	2.044	0.808	0.624	47	0.291	0.467	2.325	2.046	0.937	0.708	53	0.232	0.489	0.081	72.13
UB-P-3-12E13W	12	8.224	2.238	2.008	0.768	0.648	45	0.175	0.303	2.617	2.027	0.833	0.499	55	0.284	0.587	0.082	71.83
	13	8.196	2.574	2.084	0.928	0.705	53	0.288	0.447	2.495	2.129	0.764	0.625	45	0.205	0.338	0.079	71.68
4PB-P-1-16E14W	16	8.221	2.518	1.913	0.813	0.619	47	0.338	0.504	2.558	2.136	0.841	0.701	53	0.197	0.486	0.080	72.21
	14	8.214	2.424	2.018	0.816	0.667	55	0.254	0.373	2.544	2.087	0.836	0.603	46	0.194	0.453	0.080	71.97
4PB-P-2-19E11W	19	8.185	2.629	2.124	0.955	0.703	52	0.255	0.597	2.316	1.923	0.816	0.637	46	0.143	0.420	0.081	71.61
	11	8.241	2.588	2.122	0.980	0.782	52	0.219	0.426	2.499	2.058	0.770	0.594	47	0.218	0.445	0.080	72.25
4PB-P-3-21E7W	21	8.295	2.540	2.187	0.879	0.607	53	0.270	0.550	2.550	2.084	0.794	0.529	45	0.234	0.540	0.081	72.40
	7	8.237	2.329	2.001	0.783	0.596	54	0.246	0.678	2.359	1.996	0.840	0.672	44	0.243	0.522	0.081	72.38
4PB-NP-1-15E8W	15	8.254	2.444	1.987	0.787	0.633	46	0.268	0.378	2.568	2.111	0.709	0.520	53	0.184	0.415	0.081	71.83
	8	8.324	2.599	2.050	0.933	0.707	53	0.293	0.473	2.454	2.000	0.881	0.758	47	0.233	0.375	0.080	73.00
4PB-NP-2-10E9W	10	8.201	2.458	1.985	0.836	0.669	50	0.184	0.409	2.553	2.153	0.910	0.726	53	0.217	0.484	0.079	71.67
	9	8.216	2.622	2.063	0.963	0.686	53	0.274	0.592	2.446	2.063	0.747	0.582	46	0.138	0.405	0.080	72.18
4PB-NP-3-17E18W	17	8.267	2.386	1.846	0.789	0.585	44	0.267	0.632	2.675	2.070	1.029	0.819	52	0.283	0.502	0.087	74.46
	18	8.250	2.535	2.072	0.808	0.567	55	0.313	0.581	2.388	1.964	0.713	0.546	47	0.313	0.527	0.088	73.60
4PB-NP-4-32E20W	32	8.304	2.452	2.085	1.061	0.869	51	0.170	0.522	2.426	1.917	0.876	0.687	48	0.318	0.457	0.080	75.89
	20	8.215	2.483	2.136	0.765	0.634	52	0.293	0.608	2.415	2.001	0.895	0.549	45	0.176	0.498	0.080	71.54

Note: Typical test label is xx-x-x-xxxx.
For example, test 4PB-NP-2-8E15W means Four-point Bending No Panel Test 2
with the paired specimens 8.5Z079-24 on the east side and 8.5Z079-25 on the west side

6.3.2 Test setup

Each test specimen is constructed with 2 parallel simply supported (pin-roller) Zee purlins spaced at 5 ft on center to center of web. The purlins are oriented in opposing directions to equilibrate the tendency of the purlin to roll laterally about its weak principal axis when the paneling is attached. Corrugated roofing panel (t=0.018 in.) spans between purlins with a 1 ft overhang (measured from center of the web) and is attached to the purlins with 2 ½ in. self-tapping screws spacing at 12 in. on center. Connectivity between purlins is achieved with hot-rolled tube sections, 2 x 5 x 5 x 0.375 in. welded to a 6 x 6 x 0.375 in. plate bolted to the webs at the support and at the third points as shown in Figure 6.3. Bracing provides full web restraint at the supports and loading locations.

Figure 6.3 Bracing provided for lateral-torsional buckling prevention

The three testing scenarios designed to quantify the influence of downward pressure are presented in Figure 6.5. The first testing scenario (Figure 6.5a, UB-P) follows the standard base test method for purlins supporting standing seam roof systems, AISI S908-08(AISI-TS (2007)) which simulates uniform bending from a downward pressure. The through-fastened roof system is sealed in the box with plastic, and air is pulled from the box with a series of vacuum pumps. Load (negative pressure) is increased by closing multiple outflow valves at a controlled rate.

The second test configuration (Figure 6.5b, 4PB-P) uses a loading frame (Figure 6.4) inside the pressure chamber to apply four-point bending to the purlins (panel included). The box is sealed with plastic and a negative pressure is applied. The loading frame transforms the pressure loading into four-point bending. Load cells are placed at the loading points as shown in Figure 6.4. The four point-bending test is performed inside the box to ensure that the boundary conditions are consistent between test types. Comparing the four point bending tests to the downward pressure tests described previously isolates the influence of downward gravity pressure on system capacity.

The third test type (4PB-NP) also uses the loading frame to apply four-point bending with a negative pressure, except for these specimens, the through-fastened panel has been removed. This test configuration isolates the contribution of the panel to distortional buckling capacity.

Figure 6.4 Loading frame and load cells

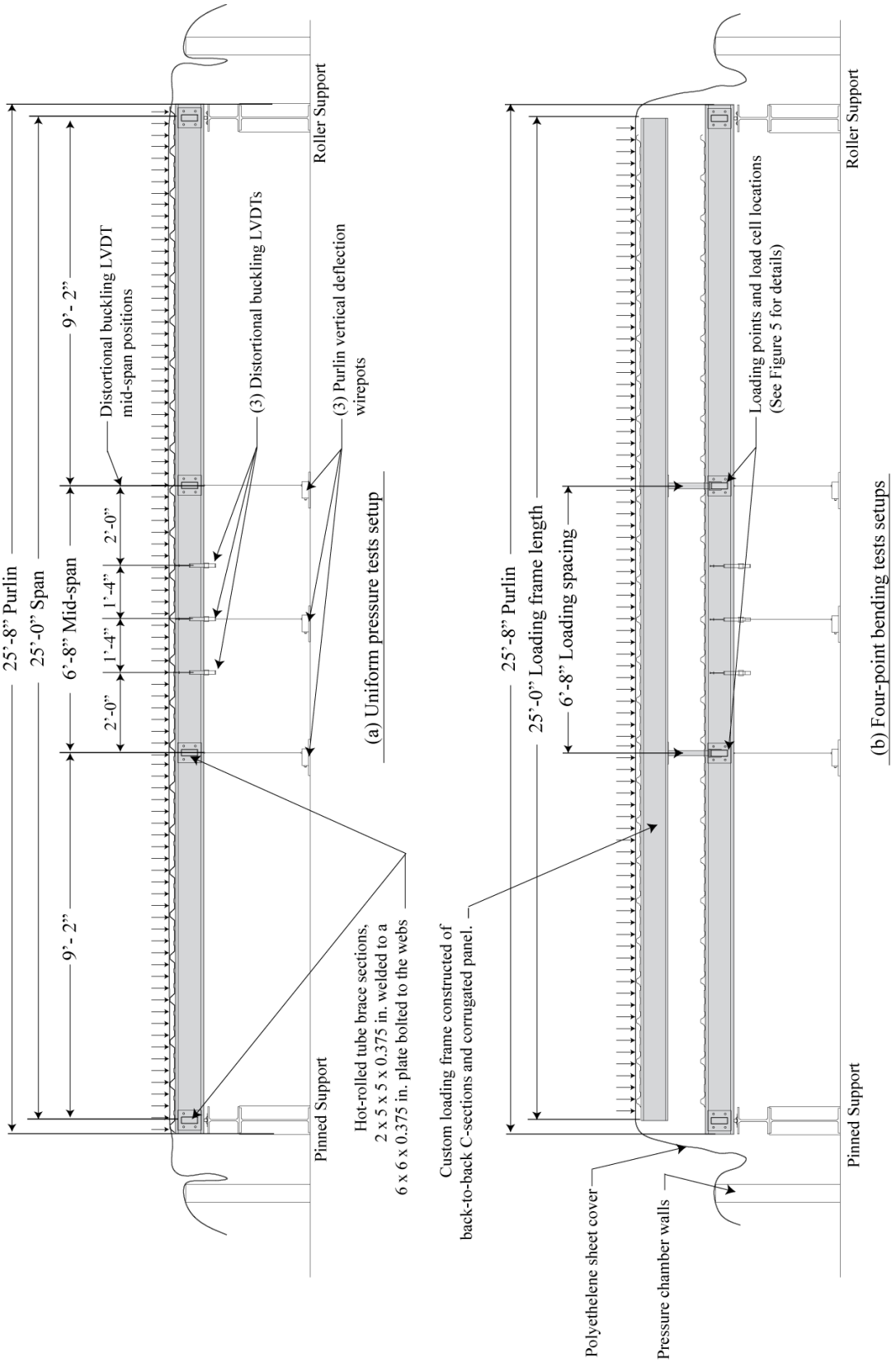

Figure 6.5 Elevation views of test setups

6.3.2.1 Instrumentation

All data acquisition is managed using a National Instruments(NI) PXI-1052 Data Acquisition system managed by NI Labview graphical environment software. Labview provides a graphical interface which allows the user to monitor all instrumentation on one screen as the test is being conducted. All instrumentation is calibrated using NI Automation and Measurement software.

Pressure transducers with a range of 0-2160 psf accurate to +/-0.1 psf are positioned at each end of the box to ensure loading is consistent throughout the box. Wire pot displacement transducers with a range of +/-5 in. and accuracy of +/-0.01 in. are used to record vertical purlin deflection at mid-span and load (brace) points. To detect the formation of distortional buckling half-wavelengths, linear variable differential transducers (LVDTs) with a range of +/-3 in. and an accuracy of +/-0.001 in., are placed at midspan at three locations dimensioned in Figure 6.5 and shown in Figure 6.6. The information from these transducers is valuable and necessary as it will indicate the magnitude of distortional buckling if occurring as well as half-wavelength directionality. The first test, UB-P-1 does not have any distortional buckling data as it was used to determine positioning of the LVDTs at the half-wavelength maximums. To ensure equal loading is applied to the purlin system during the 4PB-P and 4PB-NP tests, a load cell with a range of 0-10 kip and accuracy of +/-.001 kip is positioned at each load point.

Figure 6.6 Distortional buckling LVDTs

All calibration is conducted by finding a correlation between a known variable and the output voltage from the instrumentation. The pressure transducers are calibrated using a water manometer and determining a linear relationship between the voltage output from a resulting a specific height of water in the manometer. The wire pots and LVDTs are calibrated by recording the output voltage at multiple positions in the range of the displacement transducers. The load cells are calibrated by varying known weights and recording the voltage output.

6.3.3 Specimen measurements

The cross-section dimensions were measured at the mid-length of each purlin and are summarized in Table 6.2. Each purlin was clamped down over two sawhorses. A 6.0 in. contour gauge shown in Figure 6.7 is a tool composed of steel pins that can replicate shapes. The steel pins were lined up perpendicular to the flanges and compressed which creates a duplicate of the shape on the opposing side. The outlined shape is then traced onto engineering paper at which

point all dimensions were determined using a digital caliper accurate to +/- 0.001 in.. Radii, flange widths, lip lengths, and angles were measured using this method.

Figure 6.7 Specimen measuring - contour gauge

6.3.4 Material properties

Tensile coupon tests were performed on all specimens using ASTM A370-05, (ASTM 2005). Three tensile coupons were taken from a 1 ft. untested section at the end of each specimen; one coupon from the compression flange, tension flange, and web. Sharp yielding stress results are reported as the average of the 3 coupons in Table 6.2, with an average across all specimens of 72.5 ksi.

6.4 Elastic Buckling and DSM Strength Prediction

The critical elastic restrained and unrestrained buckling moments for local (M_{crl}), distortional (M_{crd}), and global (M_{cre}) were obtained with a finite strip analysis and measured specimen cross-section dimensions in CUFSM (Schafer and Ádány 2006) presented in Table 6.3. Note that the finite strip method predicts no distinctive distortional buckling mode as there is modal interaction with local buckling. This is due to the stiffener lip being in tension which

braces the flange and $M_{crl,u}$ and $M_{crd,u}$ are taken to be the same. Presented are all elastic buckling parameters for the measured cross-section properties in Table 6.2 along with yield moments using CUFSM. The global buckling moment is reported as M_{cre} and is taken at an unbraced length equal to the midspan as discussed previously.

Table 6.3 Elastic buckling results

		Finite Strip Method (CUFSM)							
Test Label	Purlin Label	Yield Moment		Restrained Bending			Unrestrained Bending		
		$M_{y,r}$ (kip-in.)	$M_{y,u}$ (kip-in.)	$M_{crl,r}$ (kip-in.)	$M_{crd,r}$ (kip-in.)	$M_{cre,r}$ (kip-in.)	$M_{crl,u}$ (kip-in.)	$M_{crd,u}$ (kip-in.)	$M_{cre,u}$ (kip-in.)
UB-P-1-24E25W	24	211.79	106.59	228.22	167.60	168.83	118.93	118.93	172.96
	25	211.70	106.77	230.29	156.08	170.50	118.24	118.24	174.88
UB-P-2-22E23W	22	206.93	104.44	238.37	160.86	205.96	107.50	107.50	214.55
	23	215.80	106.83	232.40	146.99	184.13	117.33	117.33	190.91
UB-P-3-12E13W	12	203.25	102.56	229.31	146.37	147.54	123.68	123.68	151.04
	13	200.72	100.03	228.60	156.60	192.31	105.78	105.78	200.82
4PB-P-1-16E14W	16	204.70	101.17	224.50	143.48	168.44	116.26	116.26	174.47
	14	203.66	100.54	226.51	161.63	168.03	111.38	111.38	173.95
4PB-P-2-19E11W	19	199.06	101.57	254.29	163.23	216.01	110.67	110.67	229.08
	11	206.29	102.42	236.90	164.30	199.98	109.95	109.95	208.23
4PB-P-3-21E7W	21	213.09	105.81	246.23	154.93	212.36	113.23	113.23	223.09
	7	210.48	104.69	243.46	165.49	198.52	115.62	115.62	206.74
4PB-NP-1-15E8W	15	203.95	101.25	230.17	142.63	160.05	114.47	114.47	166.10
	8	211.70	105.89	234.20	162.36	197.15	110.60	110.60	205.21
4PB-NP-2-10E9W	10	199.22	99.53	208.72	149.14	155.68	113.82	113.82	159.13
	9	202.24	102.14	242.21	161.89	207.35	107.81	107.81	217.68
4PB-NP-3-17E18W	17	228.22	115.27	276.08	167.71	172.41	152.75	152.75	177.34
	18	229.76	114.17	314.38	191.29	217.09	145.17	145.17	229.51
4PB-NP-4-32E20W	32	219.01	109.26	240.04	172.71	215.63	110.99	110.99	222.88
	20	200.86	101.31	244.02	153.28	213.86	107.45	107.45	226.15

The predicted nominal purlin capacities are presented in Table 6.4. Capacities for tests UB-P and 4PB-P assume restrained bending and 4PB-NP tests assume unrestrained bending for predicting capacities. Distortional buckling controls the strength in most members, however, the local-global buckling mode is very close to the distortional load and sometimes controls even though the local buckling load is much higher. This is due to the local slenderness ratio, λ_ℓ,which is close to the limit of 0.776 (See Table 6.4, e.g. purlin 19 with λ_ℓ=.0.80) causing the

section to not be influenced by local buckling, rather its strength is driven down by global buckling.

Table 6.4 DSM strength predictions

Test Group	Purlin Label	Direct Strength Method Predictions							
		Global	Local		Distortional		Nominal	Controlling Mode	$M_{DSM,sys}$ (kip-in.)
		M_{ne} (kip-in.)	λ_ℓ	$M_{n\ell}$ (kip-in.)	λ_d	M_{nd} (kip-in.)	$M_{n,DSM}$ (kip-in.)		
UB-P Tests	24	153.32	0.82	148.15	1.12	151.53	148.15	(local-global)	147.44
	25-F^D	154.09	0.82	149.08	1.16	147.44	147.44	(distortional)	
	22-F	165.76	0.83	158.43	1.13	147.06	147.06	(distortional)	145.77
	23^D	161.72	0.83	154.54	1.21	145.77	145.77	(distortional)	
	12-F^D	139.41	0.78	138.98	1.18	140.28	138.98	(local-global)	138.98
	13	158.36	0.83	151.55	1.13	142.84	142.84	(distortional)	
4PB-P Tests	16-F^D	150.66	0.82	145.63	1.19	139.81	139.81	(distortional)	139.81
	14	150.11	0.81	145.67	1.12	145.88	145.67	(local-global)	
	19-F^D	164.56	0.80	160.89	1.10	144.35	144.35	(distortional)	144.35
	11	163.53	0.83	156.67	1.12	147.95	147.95	(distortional)	
	21-F^D	170.77	0.83	163.36	1.17	147.61	147.61	(distortional)	147.61
	7	164.99	0.82	158.99	1.13	150.22	150.22	(distortional)	
4PB-NP Tests	15-F^D	93.45	0.90	84.86	0.94	82.47	82.47	(distortional)	82.47
	8	100.79	0.95	88.32	0.98	83.89	83.89	(distortional)	
	10-F	91.38	0.90	83.43	0.94	81.40	81.40	(distortional)	81.22
	9^D	98.70	0.96	86.36	0.97	81.22	81.22	(distortional)	
	17-F	104.95	0.83	100.69	0.87	99.09	99.09	(distortional)	96.80
	18^D	109.33	0.87	101.88	0.89	96.80	96.80	(distortional)	
	32	104.87	0.97	90.81	0.99	85.70	85.70	(distortional)	80.70
	20-F^D	98.56	0.96	86.18	0.97	80.70	80.70	(distortional)	

Notes: 1. Purlin Label XX-F^D
D denotes the controlling specimen according to DSM
F denotes the specimen that controlled in testing

6.5 **Test Results**

The predicted capacity is presented using the Direct Strength Method (DSM), M_{DSM} in Table 6.5. The final predicted capacities for the purlin systems are notated as $M_{DSM,sys}$ which are the capacity of the controlling purlin. The capacities for UB-P and 4PB-P tests are predicted using restrained properties contrary to the 4PB-NP tests which assumed unrestrained bending.

All load (moment)-displacement system responses of all tests are presented in Figure 6.8. There is variation in the 4PB-NP tests as they are highly affected by cross section properties and imperfections as there is no additional restraint or composite action with a panel present which

could counteract some of the imperfections in the beam by providing bracing to the compression flange. Tests 4PB-NP-3 and 4PB-NP-4 had purlins in each test (Purlins 17,18, and 32) with a higher yield stress and thickness compared to the other tests (Reference Table 6.2 for section properties). This caused the system stiffness to increase as depicted by plot (c) in Figure 6.8. Also note that tests 4PB-P (Figure 6.8b) and 4PB-NP (Figure 6.8c) plots do not start at zero moment as the weight of the loading frame (shown in Figure 6.5) induces a preload moment of 22 kip-in. into the purlins.

Table 6.5 Test results

Test Group	Purlin Label	DSM Strength Predictions			Comparison		DSM Predicted-to-Tested Statistics	
		$M^{n,DSM}$ (kip-in.)	Controlling Mode	$M_{DSM,sys}$ (kip-in.)	M_{TEST} (kip-in.)	$M_{TEST}/M_{DSM,sys}$	Mean	COV
UB-P Tests	24	148.15	(local-global)	147.44	125.62	0.85	0.88	0.05
	25-F^{D}	147.44	(distortional)					
	22-F	147.06	(distortional)	145.77	124.71	0.86		
	23^{D}	145.77	(distortional)					
	12-F^{D}	138.98	(local-global)	138.98	129.72	0.93		
	13	142.84	(distortional)					
4PB-P Tests	16-F^{D}	139.81	(distortional)	139.81	148.70	1.06	1.03	0.04
	14	145.67	(local-global)					
	19-F^{D}	144.35	(distortional)	144.35	150.02	1.04		
	11	147.95	(distortional)					
	21-F^{D}	147.61	(distortional)	147.61	146.12	0.99		
	7	150.22	(distortional)					
4PB-NP Tests	15-F^{D}	82.47	(distortional)	82.47	94.59	1.15	1.23	0.07
	8	83.89	(distortional)					
	10-F	81.40	(distortional)	81.22	95.42	1.17		
	9^{D}	81.22	(distortional)					
	17-F	99.09	(distortional)	96.80	119.77	1.24		
	18^{D}	96.80	(distortional)					
	32	85.70	(distortional)	80.70	109.17	1.35		
	20-F^{D}	80.70	(distortional)					

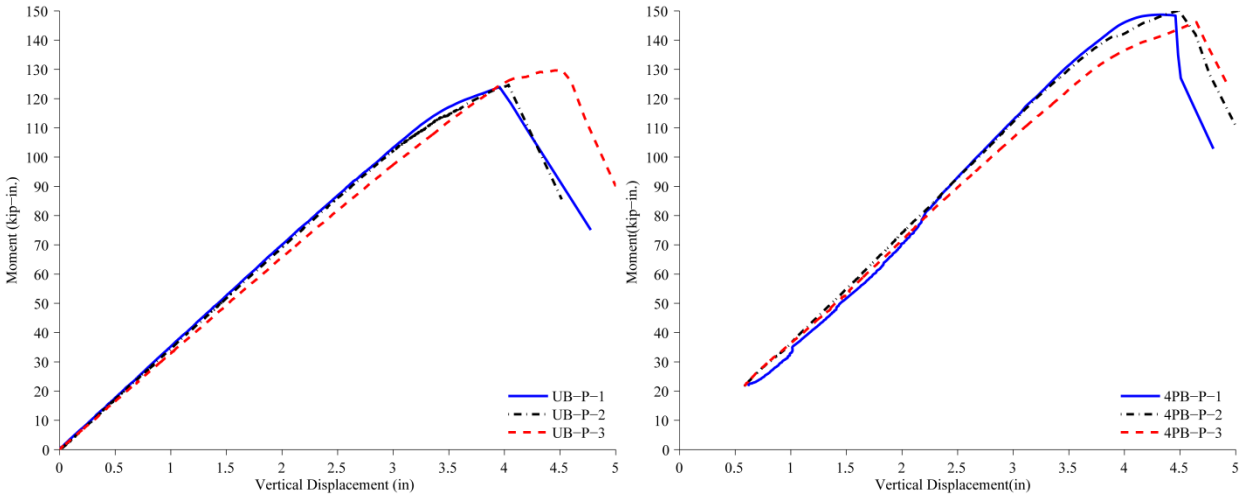

(a) (b)

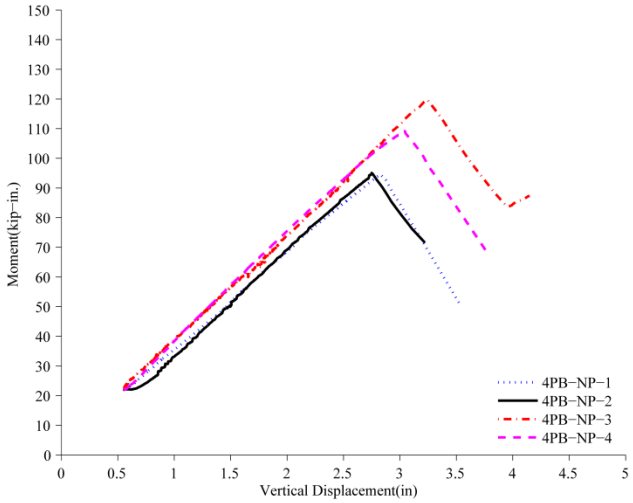

(c)

Figure 6.8 Force - displacement responses
(a) UB-P Tests (b) 4PB-P Tests (c) 4PB-NP Tests

6.6 Test Comparisons

6.6.1 Distortional Buckling

Figure 6.9 through Figure 6.11 present the distortional buckling results for the tests in this investigation. The failure mode changes between tests UB-P / 4PB-P and the 4PB-NP test. Whenever there was a panel present, distortional buckling and lateral-torsional buckling were not the governing failure modes and local buckling controlled (**Figure 6.9**). The elastic global buckling moment is lower than the local moment when restrained (Compare $M_{crl,r}$ and $M_{cre,r}$ in Table 6.2) and the capacity driven down by a combination of local-global interaction. However, when unrestrained (4PB-NP tests), the section is now controlled by primarily distortional buckling as the global buckling moment is higher than the restrained case (Figure 6.10). It is also assumed distortional will control regardless for all Z-sections due to reduced post-buckling strength in distortional beam failures (Schafer and Peköz 1999).

Measured distortional buckling data is presented in Figure 6.11. Some systems failed off center caused by either uneven loading or imperfections in the purlins which causes distortional halfwaves to occur unevenly. The direction of the distortional half-waves should be noted as well. In the UB-P tests, the midspan half-wave at maximum moment always formed downward whereas the 4PB-P and 4PB-NP tests, the waves formed waves in both directions. Figure 6.11 presents the growth of distortional halfwaves as loading increases. Only loading up to 80% of the failure moment is shown in Figure 6.11 as compression flange local buckling was picked up by the distortional lvdts on tests UB-P and 4PB-P. It is shown that a panel does provide some rotational restraint to the compression flange. Comparing flange displacements (distortional buckling) at 80% of the failure load for 4PB-NP to 4PB-P tests in Figure 6.11 confirms that the panel reduces distortional buckling up to 50%. Distortional buckling is reduced up to 75% until

right before failure (80%Mmax) when downward pressure exists with a panel (Compare UB-P to 4PB-P flange displacements in Figure 6.11). Comparing UB-P to the other tests, it can be concluded downward pressure restrains distortional buckling up to until failure and forces the system to fail in an alternate failure mode.

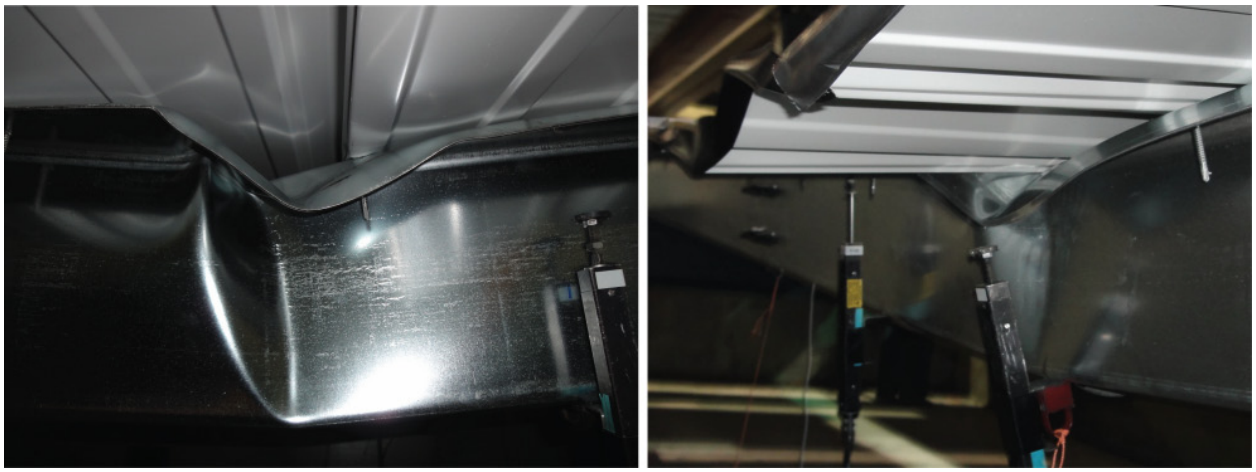

Figure 6.9 Failure Mode UB-P and UB-P Tests

Figure 6.10 Failure Mode 4PB-NP Tests

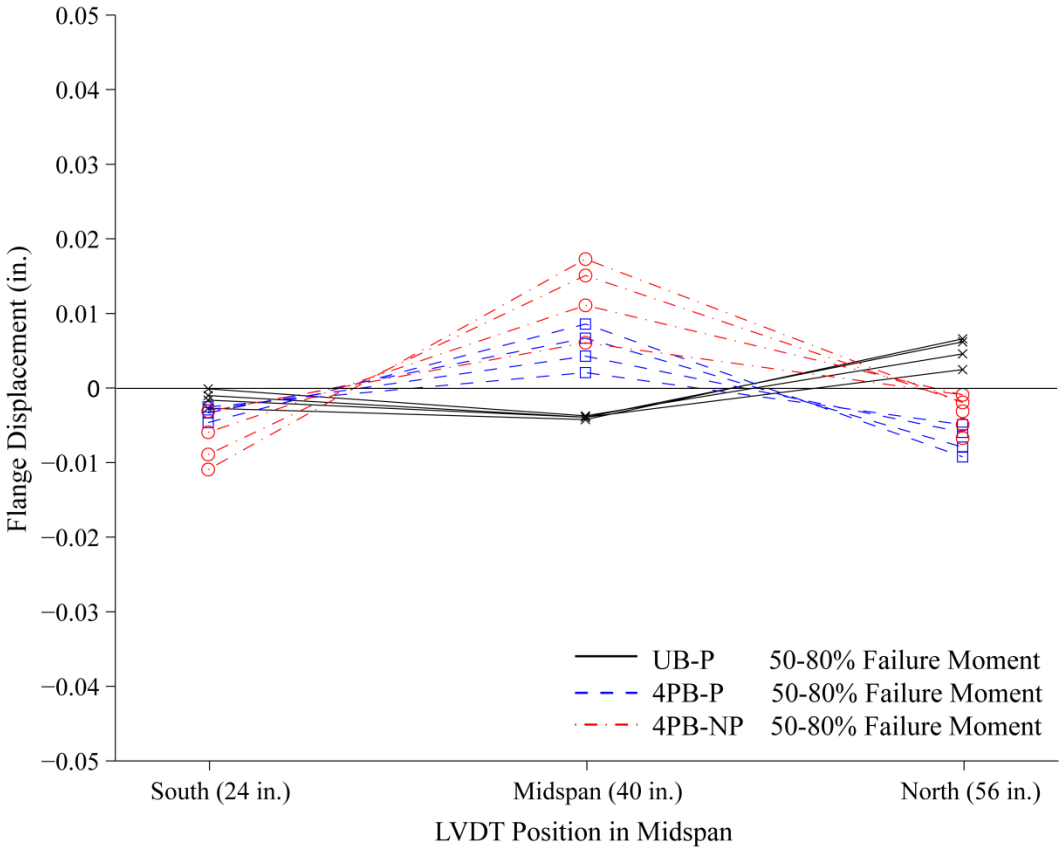

Figure 6.11 Typical distortional displacement responses comparison

6.6.2 Moment Capacity

The capacity of test 4PB-NP-3 should not be directly compared with other 4PB-NP tests due to its higher capacity resulting from an abnormally high yield stress compared to the other 4PB-NP tests. Figure 6.12 provides a comparison between all three test types in regards to their moment capacity. There is on average a 30% increase in capacity when a panel is added to the system (Compare 4PB-NP to 4PB-NP tests in Figure 6.12 or M_{TEST} values in Table 6.5). This also confirms that restrained bending can be assumed in the prediction methods to determine elastic buckling parameters. Comparing tests 4PB-P to UB-P in Table 6.5, it is shown that when

uniform pressure exists, overall moment capacity decreases by an average 12%. It is hypothesized that increased bending in the flange occurs due to the loading conditions. Since the pressure loads the entire flange instead of just over the web as in four-point bending tests, moment develops around the web-flange junction creating a deformation (imperfection) as shown in Figure 6.13. With this deformation present, the effective moment of inertia would be decreased causing moment capacity of the purlin to decrease as well. It is also possible this case would not exist in real systems as the panel is continuous transverse to the purlins therefore providing additional rotational restraint as shown in Schafer, Sangree, and Guan (2008).

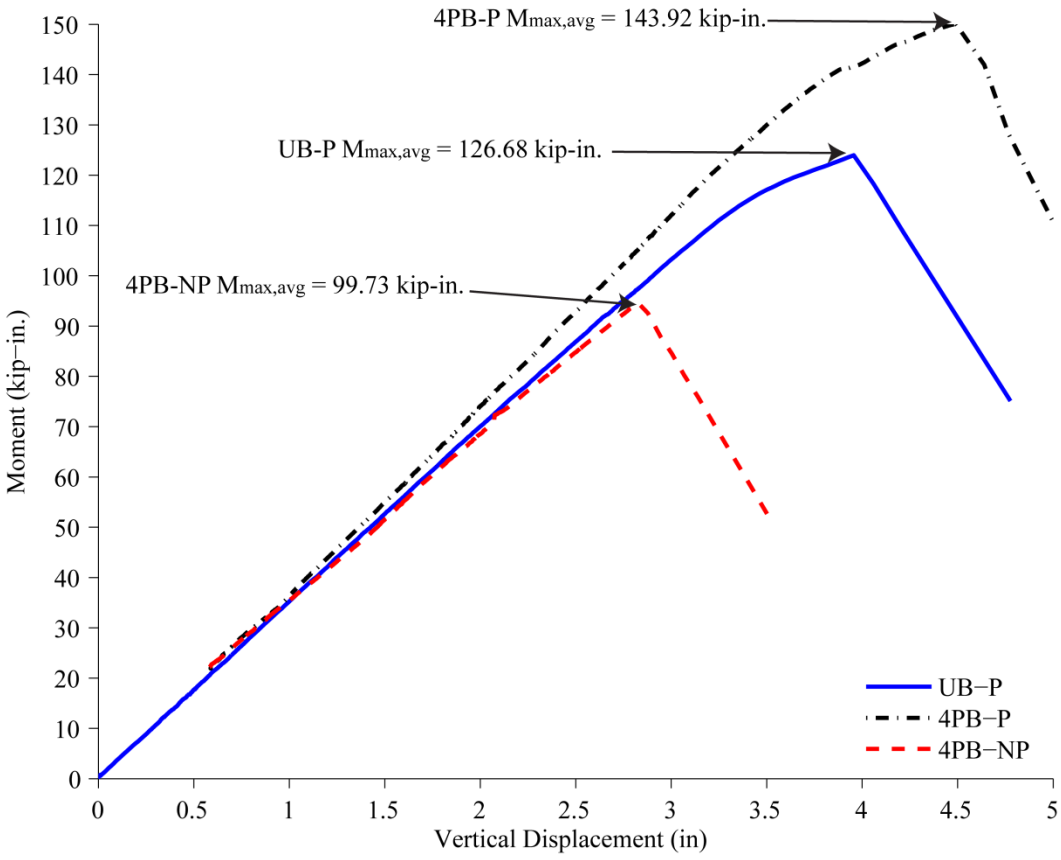

Figure 6.12 Force-displacement responses – All Groups

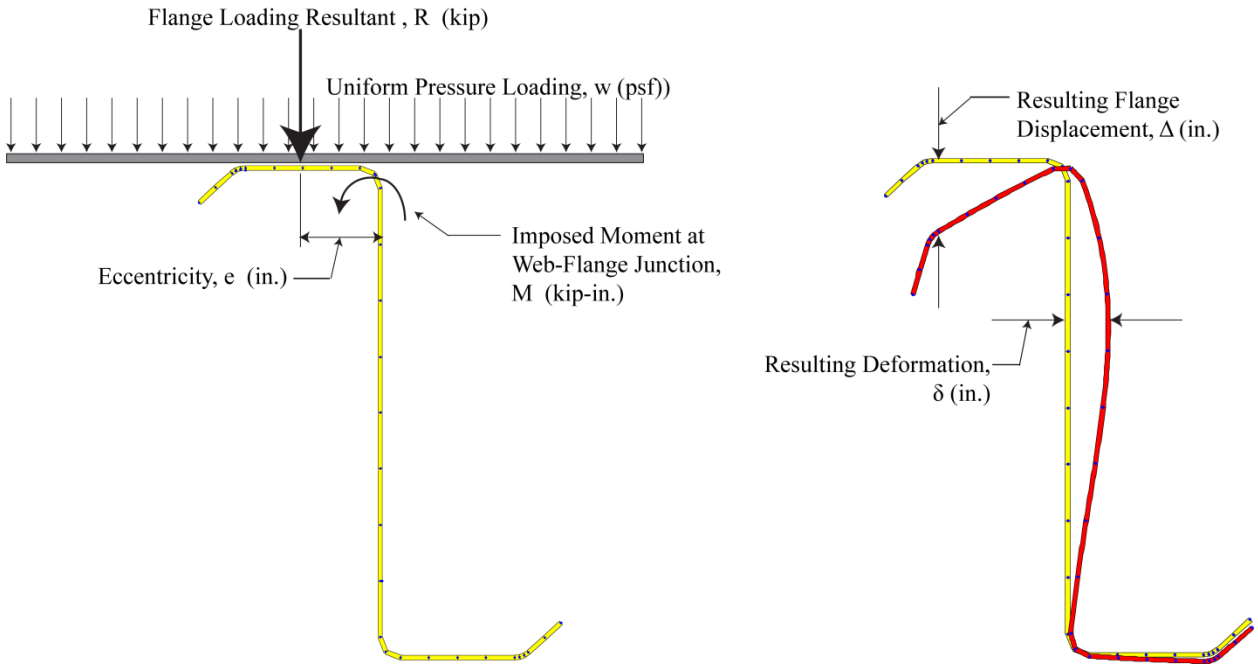

Figure 6.13 Imposed imperfection from uniform gravity loading

6.6.3 Design Methods

All predicted capacities by DSM are presented in Table 6.5. Comparing DSM predictions to the tested capacities shows DSM is conservative by on average 3% for the 4PB-P tests. The 4PB-NP tests are predicted very conservatively by a maximum of 35%. This conservativeness could be due to the loading conditions in the four-point bending tests. The four-point bending tests in this investigation are conducting by loading the system braces to transmit the load to the purlins. Compared to the typical four-point bending tests which load directly over the web, the purlins in these tests are loaded at the centroid and shear center, providing a more stable loading condition. All uniform bending capacities are over predicted by both design methods by a maximum of 15% due to induced web deformation, δ caused by eccentrically loading the flanges as shown in Figure 6.13.

6.7 **Conclusions**

Distortional buckling of cold-formed steel purlins with compression flange bracing subjected to downward pressure in a metal building roof system is significantly reduced. A series of distortional buckling pressure box tests have been conducted and have shown that distortional buckling displacements can be restrained up to 75% of the distortional buckling. Including the rotational stiffness provided by a restraining element (e.g. brace, panel, and sheathing), k_ϕ in CUFSM would predict the distortional buckling moment at a greater accuracy. Although, distortional buckling is restrained, an overall decrease in system capacity occurred in the downward pressure tests. It is hypothesized the decrease in capacity due to downward pressure is due to the setup conditions (e.g. panel overhang) which induces additional forces into the purlins that would not me present if the panel were continuous. As this investigation is based on a small number of tests, future research is needed to determine if this reduction in capacity exists.

6.8 **Future Work**

Additional testing and finite modeling research is recommended to determine if the decreased moment capacity is isolated to testing in this investigation or occurs in a multi-purlin roof system by either supporting the overhung panel or setting up a multi span system for testing. Nonlinear finite modeling also is required to determine the effects of applied forces on flange and web displacements.

CHAPTER 7. CONCLUSIONS

7.1 Elastic Buckling Simplified Methods for Members with Edge-Stiffened Holes

The objective of this research was to investigate buckling behavior of cold-formed columns and beams with edge-stiffened holes. Currently, cold-formed steel members *without holes* can be designed with the American Iron and Steel Institute's Direct Strength Method (DSM) (AISI-S100 2007), which utilizes the local, distortional, and global (Euler) elastic buckling properties to predict ultimate strength. The elastic buckling properties for members without holes can be determined from an elastic buckling curve generated with the semi-analytical finite strip method. However, discontinuities caused by holes cannot be explicitly modeled with the finite strip method, and therefore, simplified methods for use in design are needed. Recently developed elastic buckling simplified methods for cold-formed steel members with holes are viable for members with edge-stiffened holes.

7.1.1 SSMA member validation

For the SSMA members considered, all global buckling loads (moments) of the lipped C-sections with edge-stiffened holes decreased due to the presence of holes. Weak-axis flexural decreased due to the large decrease in weak-axis moment of inertia. Flexural-torsional buckling loads was shown to be more sensitive to hole size than the weak-axis flexural mode. All global buckling modes were accurately predicted by inputting weighted average cross section properties into derived engineering expressions for weak axis flexure, flexural-torsional, and lateral-torsional buckling.

Local buckling is unaffected by the presence of holes has local buckling half-waves were able to form between holes. Finite strip simplified methods were also extended to local buckling

including an analysis of the net cross-section accurately predicting that the edge stiffeners minimize buckling at a hole forcing the half-waves to form between holes.

Distortional buckling was found to be minimally effected by the presence of edge-stiffened holes in the SSMA members considered. It was determined that the hole stiffeners length considered provided enough rotational restraint to the compression flanges to compensate for the loss in web material at the hole, resulting in distortional buckling between holes. Using mechanics, an effective web thickness equation was derived and validated for distortional buckling of the considered SSMA members with edge-stiffened holes. A finite strip analysis can be performed to simulate the removal of web material and the increase in flange rotational restraint provided by the edge stiffeners in the web over a distortional buckling half-wavelength. The assumption that the distortional buckling half-wavelength remained constant between a member with and without holes held true for the SSMA members considered.

7.1.2 Steelform DeltaSTUD member validation

For the Steelform, Inc. DeltaSTUD members considered, local and global buckling loads (moments) of the lipped C-sections with edge-stiffened holes were accurately predicted. Global buckling loads decreased for all columns and beams considered compared to the same members without holes. In some cases, the governing global buckling mode changed to weak axis flexure from flexural-torsional buckling when holes were present. This was due to the large decrease in global buckling load observed for columns buckling in weak axis flexure because of the sharp reduction in weak axis moment of inertia from the perforated web. The St. Venant and warping torsion resistance were minimally affected by the presence of stiffened holes and even increased in some cases. Furthermore, a new global buckling mode was discovered due to the addition of

complex hole-edge-stiffeners and notated as asymmetric distortional buckling mixed with flexural-torsional buckling.

Finding weighted average cross-section properties for the Steelform members with edge-stiffened holes is complicated by constantly changing geometry along the length. As presented in Chapter 3, some cross-sections along the member are stiffer than the full no hole cross-section. Assuming a hole runs the entire center section of the member and using the worst cross-section properties provides a conservative mean of determining the global buckling loads. If the mid-hole cross-section was taken as in the SSMA members, the simplified methods produce an unconservative buckling load. In addition, the large stiffeners which attribute to the increased stiffness cannot contribute to the global properties as they are not engaged by the applied force (i.e there is no way for the force in the member to get to the large horizontal stiffeners).

Elastic buckling analysis revealed that local buckling is unaffected by the presence of holes, occurring in the gross cross-section near the ends of the column. It was determined that local buckling can be controlled by moving the holes closer to the ends of the members. By decreasing the overall gross cross-section that can accept a local half-wave, the local buckling is boosted greatly compared to the same members with out holes. Finite strip simplified methods were also extended to local buckling using an analysis of the net cross-section. This method accurately predicted that the edge stiffeners minimize buckling at a hole forcing the half-waves to form at the full cross-section at the ends of the Steelform DeltaSTUDS.

Distortional buckling was observed to be unaffected by the presence of holes, although difficulties were encountered when attempting to identify a pure distortional buckling mode. Preliminary testing not presented in this thesis demonstrated that even the distortional buckling

modes predicted by finite element software may not occur when actually loaded for complex members. The newly developed effective thickness distortional buckling equation is in the early stages of development, but provided a conservative distortional buckling load for most members. Future research is needed to study the effects of complex edge-stiffened holes on distortional buckling. Modification to the effective thickness equation is needed to account for any possible change in distortional buckling half-wavelength in members with complex edge-stiffened holes (e.g. Steelform DELTAStuds).

7.2 Purlin Distortional Buckling Strength under Gravity Loading

The objective of this research was to investigate experimentally to explore and quantify the difference in distortional buckling flexural capacity of metal building Z-purlins treated as isolated components and Z-purlins loaded with a constant pressure applied to metal roof panels. A series of three different types of tests have been conducted to quantify the system effect provided by the metal roof panels as well as downward pressure on distortional buckling. The AISI distortional buckling stress equation C3.1.4-10 has determined to be a conservative predictor of the distortional buckling moment. As downward pressure restrains about 75% of the distortional buckling, including the rotational stiffness provided by a restraining element (e.g. brace, panel, and sheathing), k_ϕ would predict the distortional buckling moment at a greater accuracy. However, the conducted tests have shown that a reduction in capacity exists due to downward pressure. It is hypothesized that increased flange and web deformations decrease moment capacity. It is also hypothesized that this condition may not exist in real loading conditions. Due to the specialized setup conditions and small number of tests, future research is needed to determine if a reduction in capacity actually occurs.

REFERENCES

ABAQUS (2010). ABAQUS/Standard Version 6.9-2. Providence (RI), Dessault Systèmes: ABAQUS V.6.9-2 Finite Element Program.

Ádány, S (2004). "Buckling Mode Classification of Members with Open Thin-Walled Cross-Sections by Using the Finite Strip Method, Research Report", Johns Hopkins University.

AISI:Specification (1986). Specification for the design of cold-formed steel structural members. (1986). American Iron and Steel Institute (AISI), 1st Printing, W. P. Reyman Associates, Inc., New York, N.Y.

AISI:Specification (1996). American Iron and Steel Institute (1996). AISI Specification for the Design of Cold-Formed Steel Structural Members. American Iron and Steel Institute. Washington, D.C.

AISI-S100 (2007). North American Specification for the Design of Cold-Formed Steel Structural Members. Washington, D.C., American Iron and Steel Institute.

AISI-TS (2007). "S908-08 Base Test Method for Purlins Supporting a Standing Seam Roof System", Test Standards for Use with the North American Cold-Formed Steel Specification. Washington, D.C., American Iron and Steel Institute.

ASTM(2005) "A370-05, Standard Test Methods and Definitions for Mechanical Testing of Steel Products", American Society for Testing and Materials. Pennsylvania.

DSM (2004). "Appendix 1 of the North American Specification for the Design of Cold-Formed Steel Structural Members", American Iron and Steel Institute. Washington, DC, USA.

DSM (2006) American Iron and Steel Institute (2006), Direct Strength Method (DSM) Design Guide, Design Guide CF06-1, Washington, DC, June 2006

ASTM(2009) " E8-09, Standard test methods for tension testing of metallic material", American Society for Testing and Materials. Pennsylvania.

Elhajj, P. E. (1999). "Innovative Residential Floor Construction: Structural Evaluation of Steel Joists with Pre-Formed Web Openings." Upper Marlboro, MD, NAHB Research Center, Inc.

Ellifritt, D., Glover, B., Hren, 1. (1997) "Distortional Buckling of Channels and Zees Not Attached to Sheathing." Report for the American Iron and Steel Institute.

Falk, S. (1956). "Die Knickformeln fuer den Stab mit n Teilstuecken konstanter Biegesteifigkeit (Buckling formulas for members with n segments of constant bending resistance)." *Ingenieur—Archiv,* 24(2), 85-91.

Lau, S. C. W. and G. J. Hancock (1987). "Distortional buckling formulas for channel columns." *ASCE Journal of Structural Engineering,* 113(5), 1063-1078.

Moen, C.D. (2008). "Direct Strength Design for Cold-Formed Steel Members with Perforations," Ph.D. Thesis, Johns Hopkins University, Baltimore.

Moen, C.D., and Schafer, B.W. (2008). "Experiments on cold-formed steel columns with holes." *Thin-Walled Structures*, 46, 1164-1182.

Moen, C. D. and B. W. Schafer (2009a). "Elastic buckling of cold-formed steel columns and beams with holes." *Engineering Structures,* 31(12), 2812-2824.

Moen, C.D., and Schafer, B.W. (2009b). "Elastic buckling of thin plates with holes in compression or bending." *Thin-Walled Structures*, 47(12), 1597-1607.

Moen, C.D., and Yu, C. (2010). "Elastic buckling of thin-walled structural components with stiffened holes." *51th AIAA/ASME/ASCE/AHS/ASC Structures, Structural Dynamics and Materials Conference*, April 12, 2005 - April 15, 2010, Orlando, FL.

Moen, C. D. and B. W. Schafer (2010a). "Extending Direct Strength Design to Cold-Formed Steel Columns with Holes." *Twentieth International Specialty Conference on Cold-Formed Steel Structures*, St. Louis, Missouri, USA.

Moen, C.D., and Schafer, B.W. (2010b). "Extending Direct Strength Design to Cold-formed Beams with Holes." *20th International Specialty Conference on Cold-Formed Steel Structures*, St. Louis, MO.

Moen, C.D., and Schafer, B.W. (2011). "Direct Strength Method for the Design of Cold-Formed Steel Columns with Holes." *ASCE Journal of Structural Engineering (accepted)*.

Schafer, B.W., and Pekoz, T., (1998a), "Laterally Braced Cold-Formed Steel Flexural Members with Edge Stiffened Flanges," Proceedings of the Fourteenth International Specialty Conference on Cold-Formed Steel Structures, St. Louis, MO., October 15-16.

Schafer, B.W., and Pekoz, T., (1998b), "Direct Strength Prediction of Cold-Formed Steel Members using Numerical Elastic Buckling Solutions," Proceedings of the Fourteenth International Specialty Conference on Cold-Formed Steel Structures, St. Louis, MO., October 15-16.

Schafer, B.W., and T. Pekoz (1999), "Laterally Braced Cold-Formed Steel Flexural Members with Edge Stiffened Flanges." Journal of Structural Engineering. ASCE, Vol. 125 No. 2, February 1999

Schafer, B. W. (2002). "Local, distortional, and Euler buckling of thin-walled columns." *Journal of Structural Engineering,* 128(3), 289-299.

Schafer, B. W. and S. Ádàny (2005). " Understanding and Classifying Local, Distortional, and Global Buckling in Open Thin-Walled Members." *Structural Stability Research Council Annual Conference*, Montreal, Canada

Schafer, B. W. and S. Ádàny (2006). "Buckling analysis of cold-formed steel members using CUFSM: conventional and constrained finite strip methods." *Eighteenth International Specialty Conference on Cold-Formed Steel Structures*, Orlando, FL.

Schafer, B.W., Sangree, R.H., Guan Y. (2008) "Rotational Restraint of Distortional Buckling in Cold-Formed Steel Framing Systems." Fifth International Conference on Thin-Walled Structures Brisbane, Australia, 2008

Schudlich, A., von der Heyden, A., and Moen, C.D. (2011) "Distortional Buckling of Cold-Formed Steel Joists with Unstiffened Holes." *Sixth International Conference on Thin-Walled Structures*, Timisoara, Romania.

Schuster. R.M. (1992). "Testing of Perforated C-Stud Sections in Bending." Report for the Canadian Sheet Steel Building Institute, University ofWaterIoo, Waterloo Ontario.

SSMA (2001). Product Technical Information, ICBO ER-4943P, Steel Stud Manufacturers Association.

Steel Construction Manual (13th ed.). American Institute of Steel Construction. 2006. ISBN 156424055X

Timoshenko, S. P. (1908). Buckling of Bars with Variable Cross-Section. Kiev, Bull. Polytech. Inst.

Timoshenko, S. P., Gere, J. M. (1961). Theory of Elastic Stability. New York, McGraw-Hill.

Willis, C.T., and Wallace, B., (1990), "Behavior of Cold-Formed Steel Purlins Under Gravity Loading," Journal of Structural Engineering, ASCE, Vol. 116, No. 8, pp. 2061-2069.

Yu, C., Schafer, B.W. (2003). "Local buckling Test on Cold-Formed Steel Beams", Journal of Structural Engineering, ASCE 129 (12) 1596-1606.

Yu, C., Schafer, B.W. (2004). "Distortional Buckling Tests on Cold-Formed Steel Beams", Proceedings of the 17th International Specialty Conference on Cold-Formed Steel Structures, Orlando, FL, USA.

Yu, C. (2005). "Distortional Buckling of Cold-formed Steel Members in Bending." Ph.D Thesis, Johns Hopkins University, Baltimore, MD, 2005

Yu, C. (2007). "Behavior and design of cold-formed steel joists with edge stiffened perforations." *2007 Annual Stability Conference*, April 18, 2007 - April 21, 2007. Structural Stability Research Council, New Orleans, LA, United states, 2007, 239-258.

APPENDIX A - STEELFORM

APPENDIX A.1 Steelform Cross Section Details

Below are details used for 3-D modeling of the Steelform Inc. DeltaSTUD Geometry.

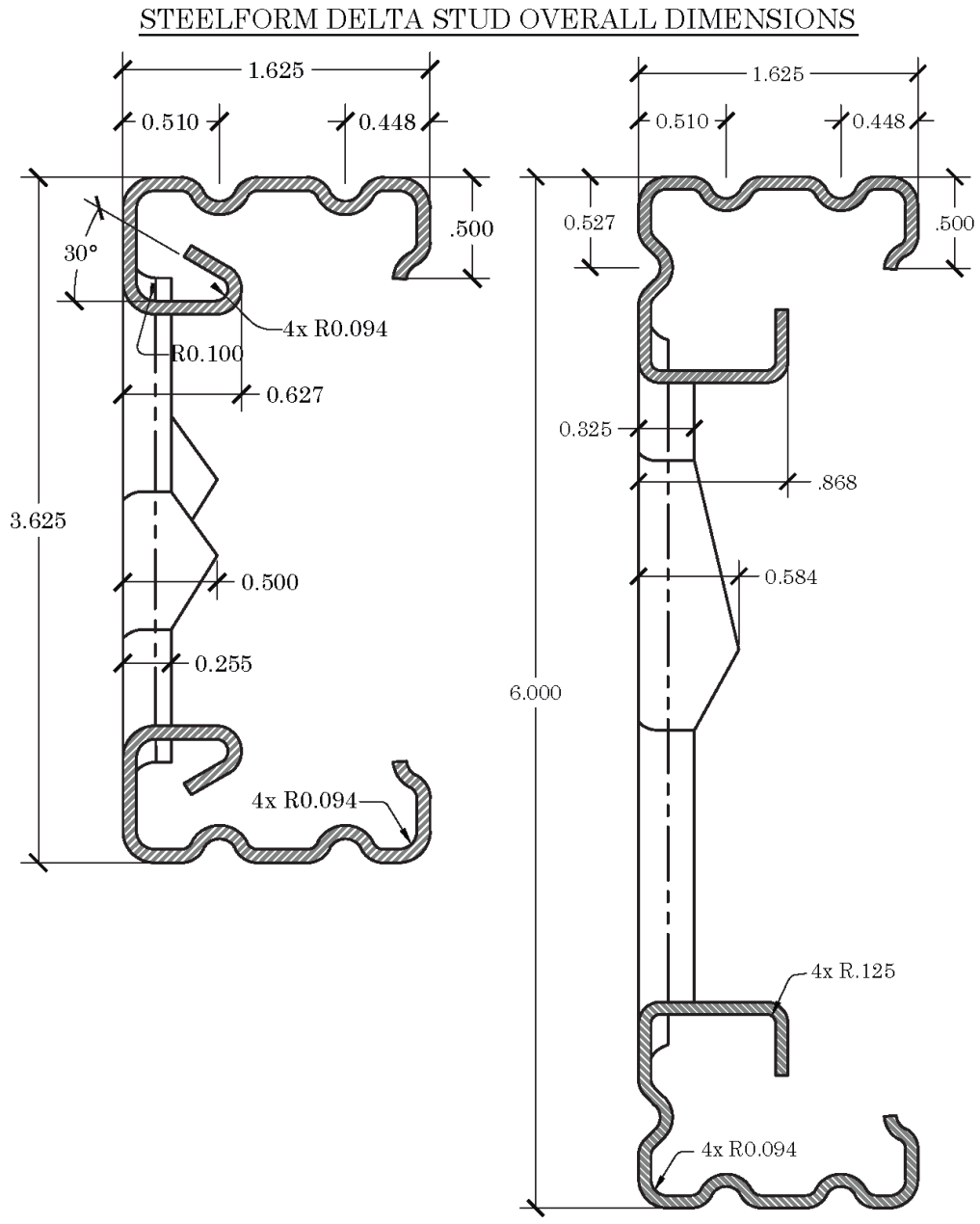

Figure A.1 Steelform cross section dimensions (Cut shown at mid-hole, Section E-E)

STEELFORM DELTA STUD STIFFENER DIMENSIONS

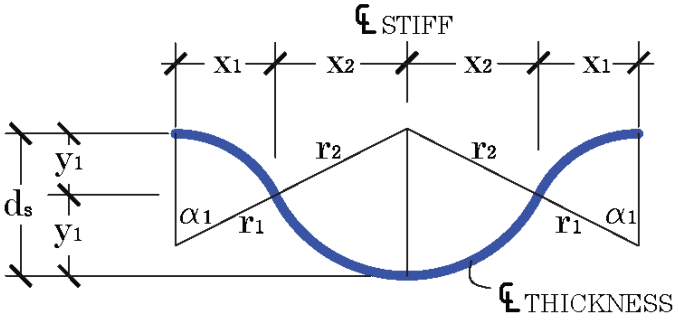

DELTA STUD FLANGE STIFFENER DIMENSIONS

d_s = .125"

r_1 = .063" + T/2

r_2 = .094" + T/2

$y_1 = r_1 (1 - \cos(\alpha_1))$

$y_2 = r_2 (1 - \cos(\alpha_1))$

$\alpha_1 = \cos^{-1}[1 - d_s/(r_1 + r_2)]$

$x_1 = r_1 \sin(\alpha_1)$

$x_2 = r_2 \sin(\alpha_1)$

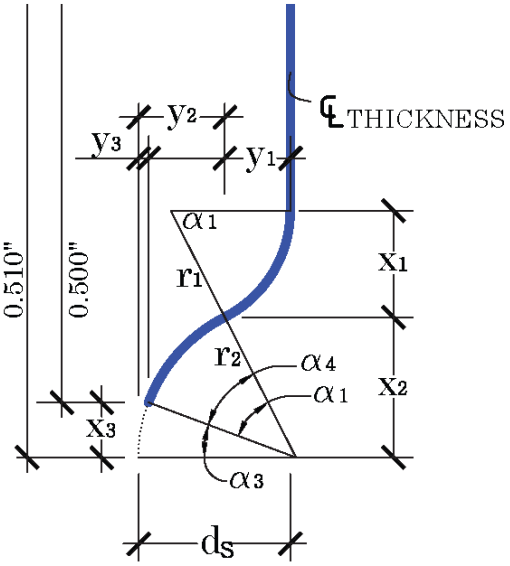

DELTA STUD FLANGE LIP STIFFENER

DIMENSIONS d_s, r_1, r_2, x_1, x_2, y_1, y_2, x_1, α_1
ARE THE SAME AS IN FLANGE STIFFENER

$x_3 = 0.510" - 0.500" = .01$

$\alpha_3 = \sin^{-1}[x_3/r_2]$

$\alpha_4 = \alpha_1 - \alpha_3$

$y_3 = r_2 (1 - \cos(\alpha_3))$

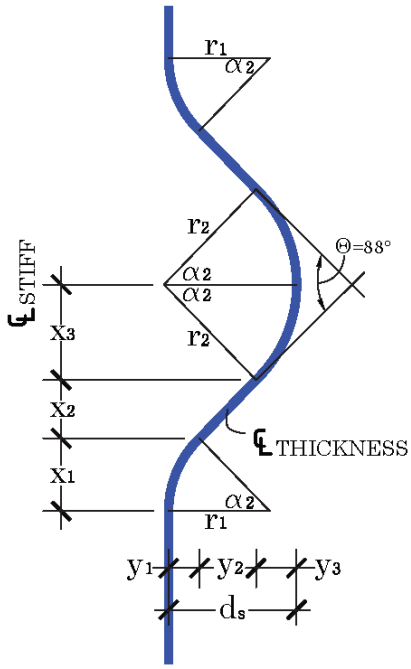

DELTA STUD WEB STIFFENER DIMENSIONS

d_s = .125"

r_1 = .063" + T/2

r_2 = .094" + T/2

α_2 = 90 - Θ/2

$y_1 = r_1 (1 - \cos(\alpha_2))$

$y_3 = r_2 (1 - \cos(\alpha_2))$

$y_2 = d_s - y_1 - y_3$

$x_1 = r_1 \sin(\alpha_2)$

$x_2 = y_2 \tan(\Theta/2)$

$x_3 = r_2 \sin(\alpha_2)$

Figure A.2 Steelform cross section stiffener dimensions

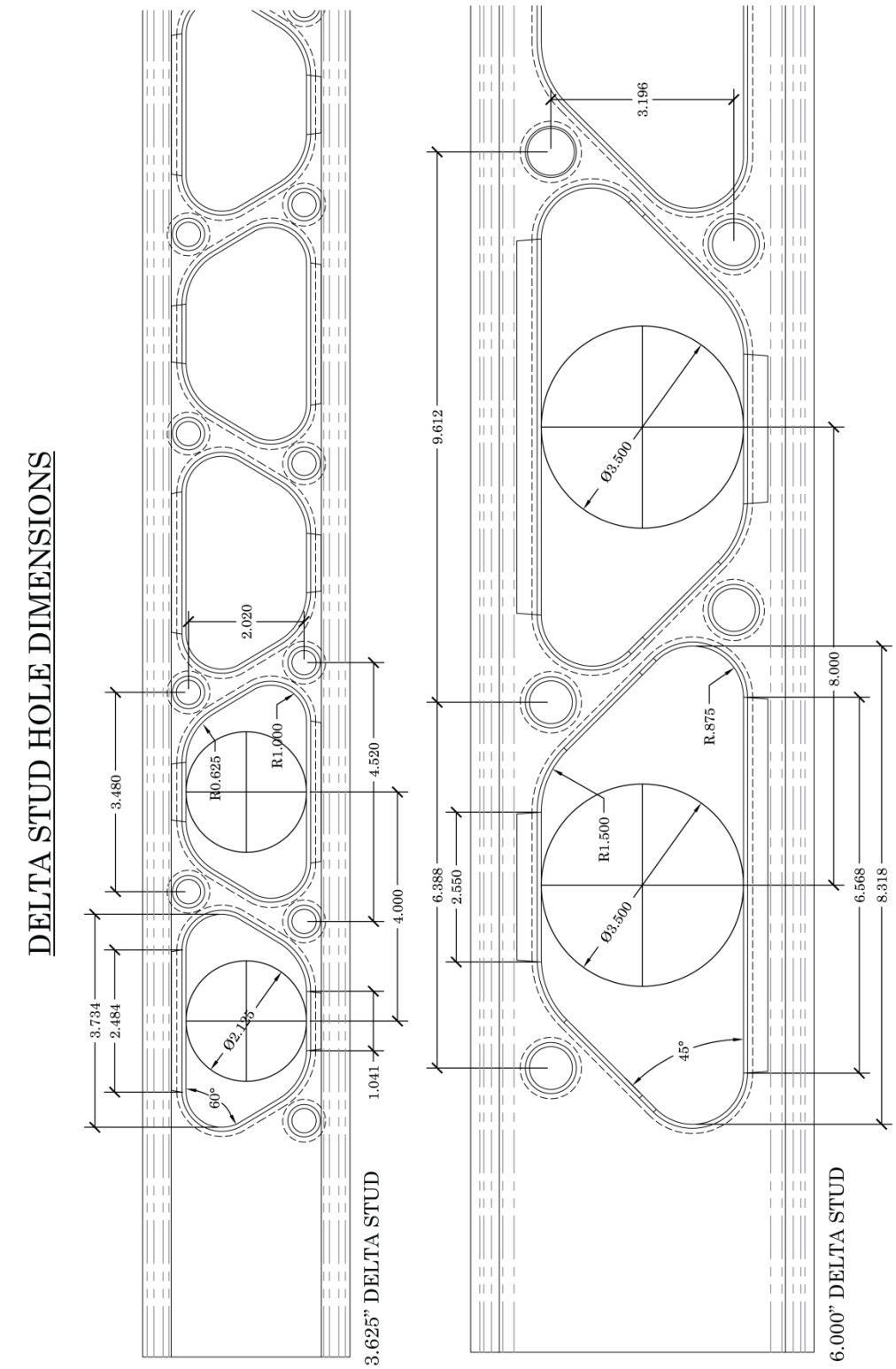

Figure A.3 Steelform web geometry details

APPENDIX A.2 3-D Modeling Process

The 3-D models in this thesis were generated using Autodesk Inventor and Autodesk AutoCAD. Cross sections and web geometry was created in AutoCAD and then imported and modified in Inventor. The 3-D models are generated as a surface rather than a solid and are drawn to the center line thickness of each member. The models are then exported to .IGES format and imported into ABAQUS for mesh generation. The following Appendix outlines step-by-step process by which the models were generated.

STEP 1 - Autodesk AutoCAD cross section / hole geometry creation

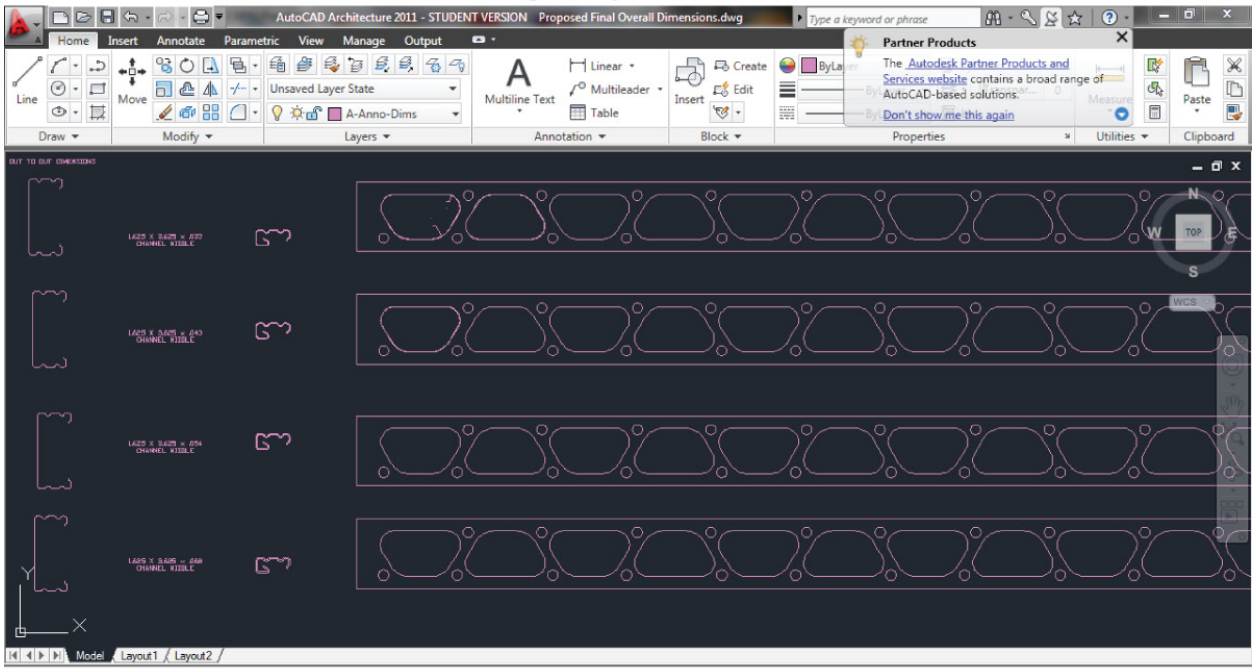

STEP 2 - Create new Part.IPT file and import AutoCAD .DWG file into Autodesk Inventor

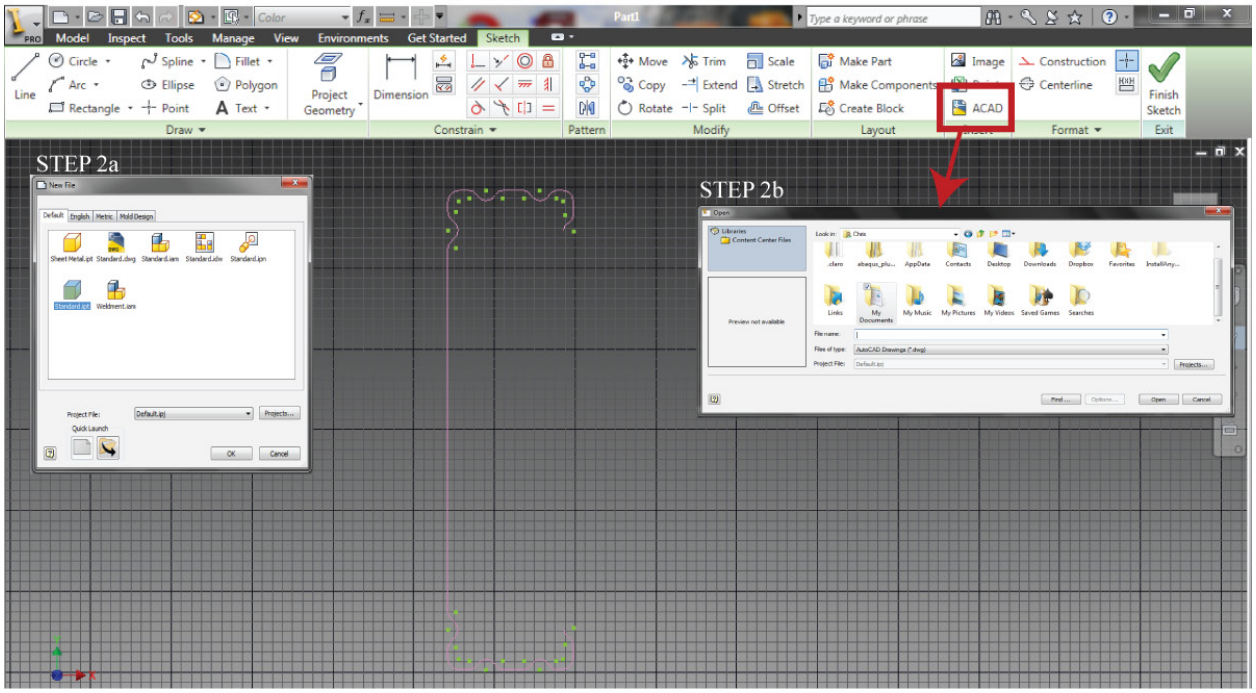

STEP 3 - Extrude imported cross section to desired length

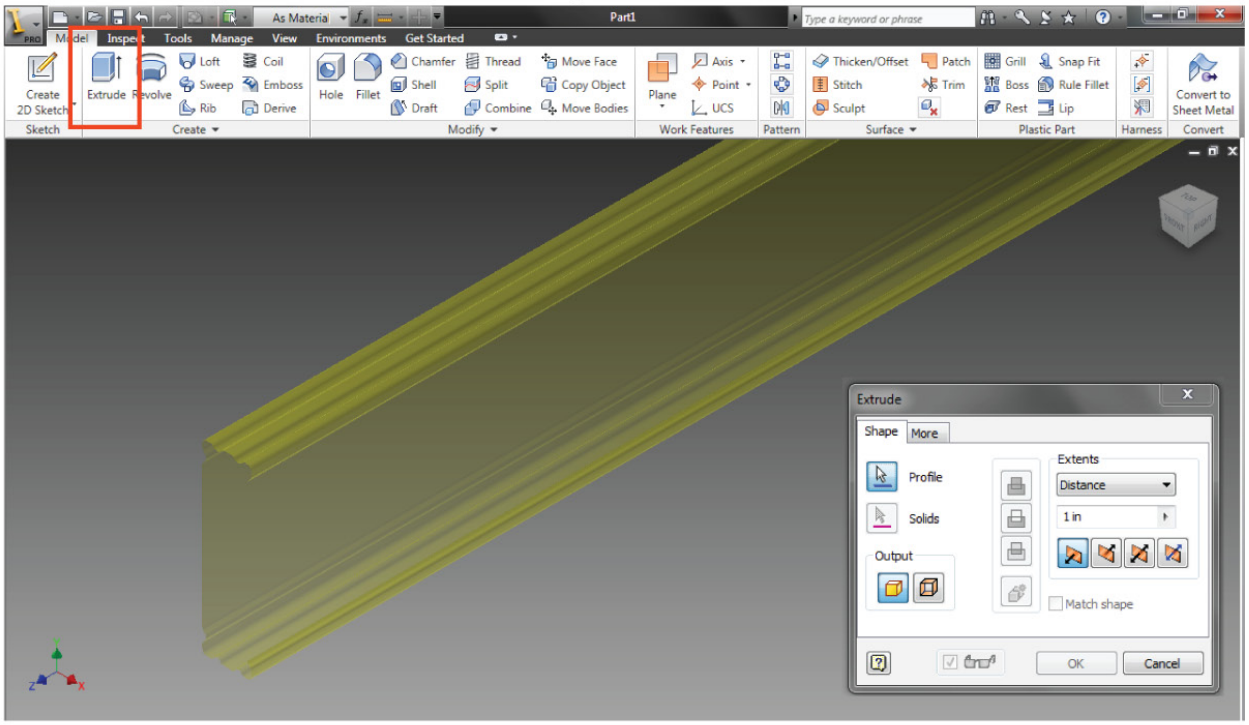

STEP 4 - Create 2D-sketch on web plane

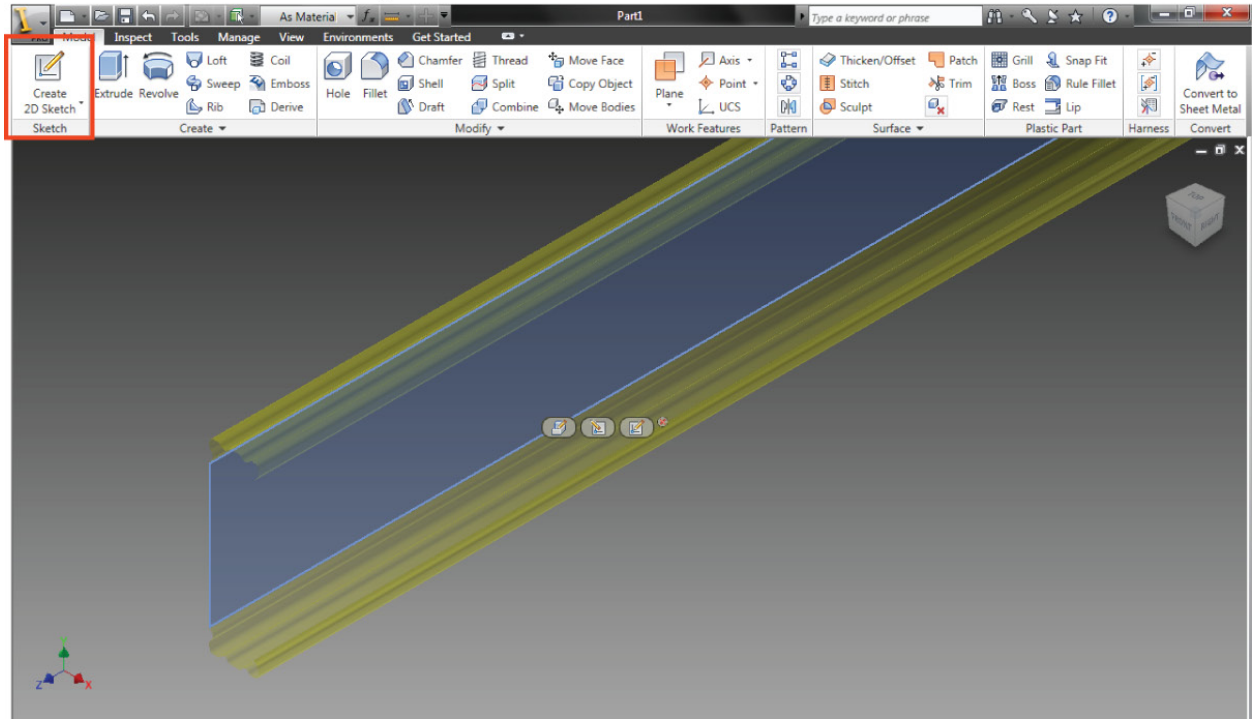

STEP 5 - Import AutoCAD .DWG file onto Autodesk Inventor extruded section plane

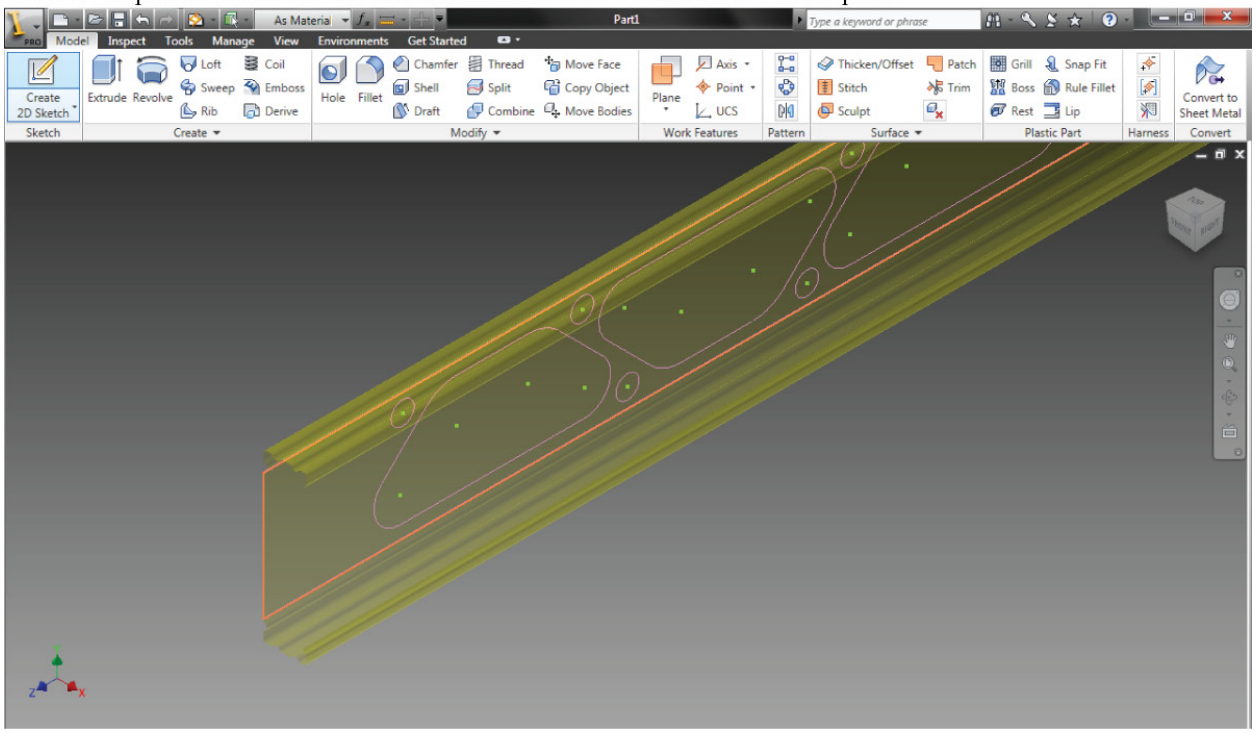

STEP 6 - Delete extruded section web plane

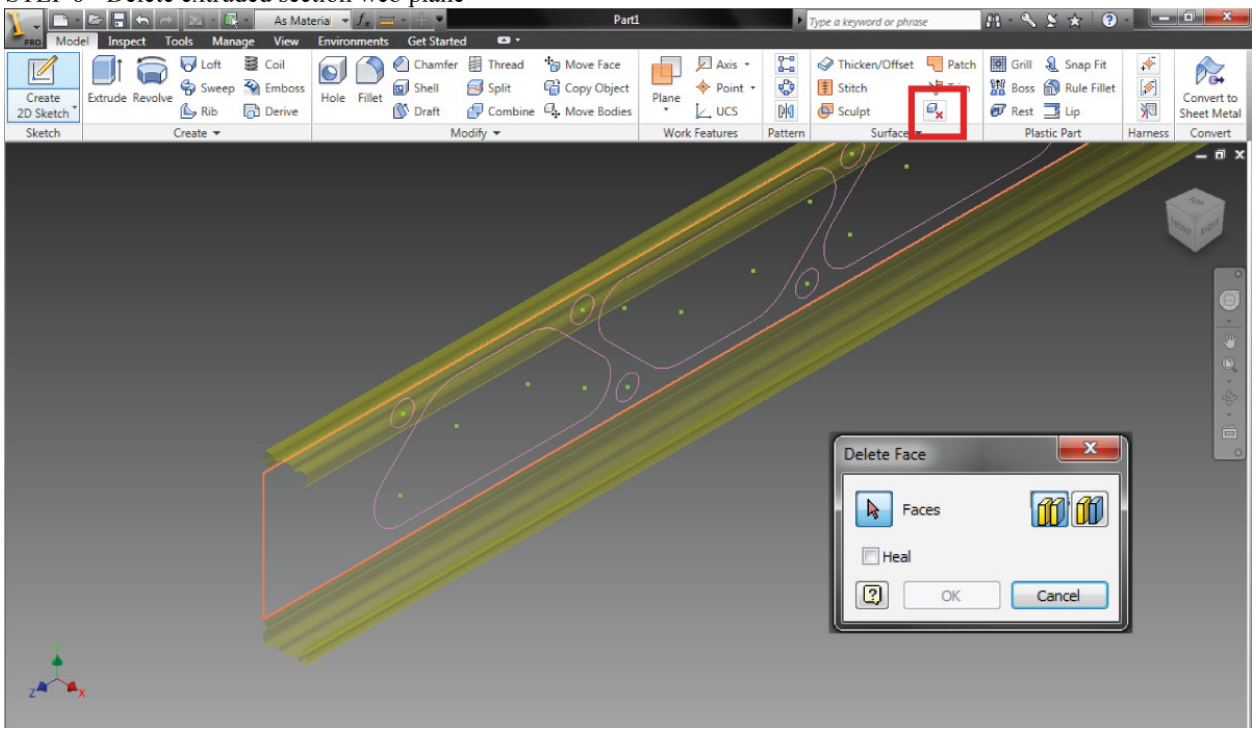

STEP 7 - Recreate web plane selecting imported web geometry as a constraint

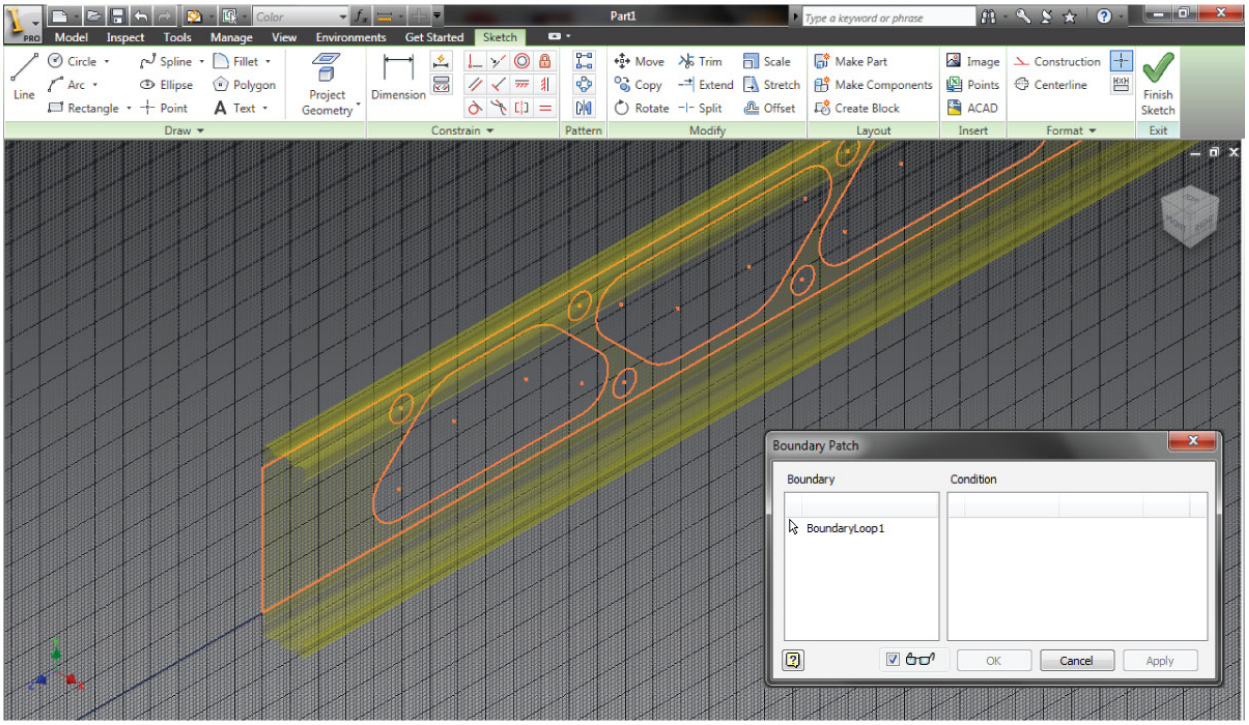

STEP 8 - Create 2D-Sketch on newly created web plane

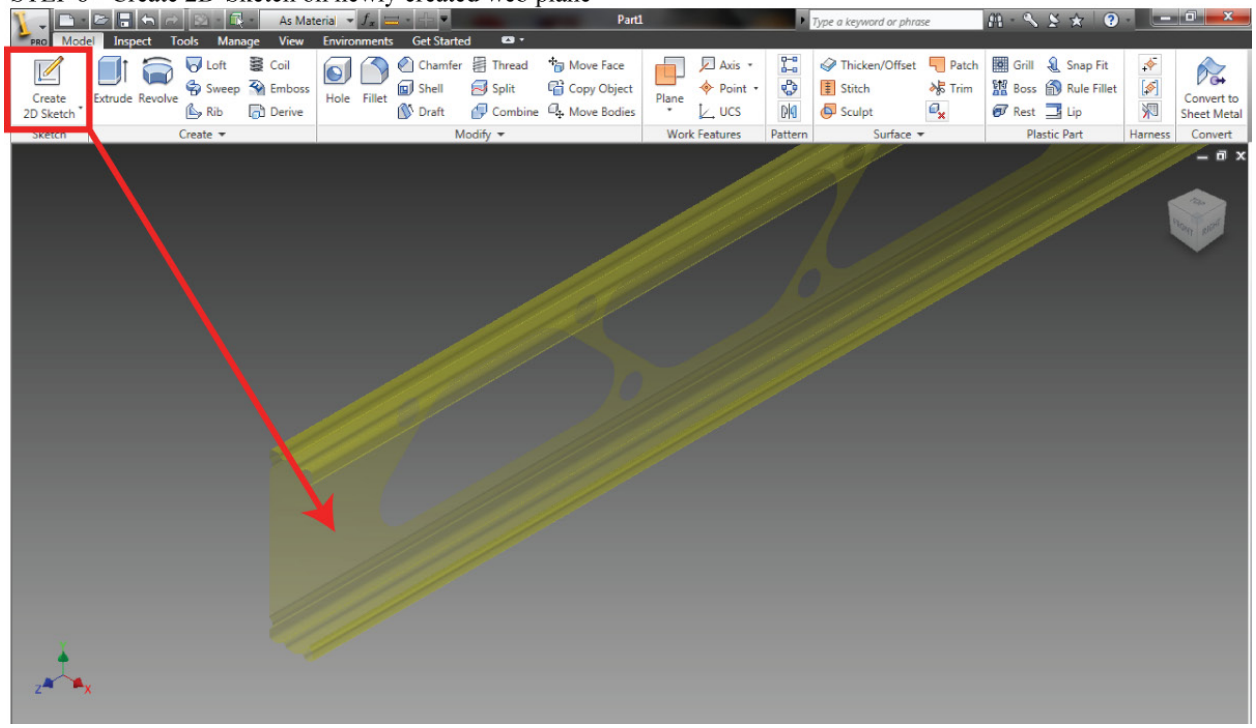

STEP 8 - Extrude holes to desired edge stiffener length

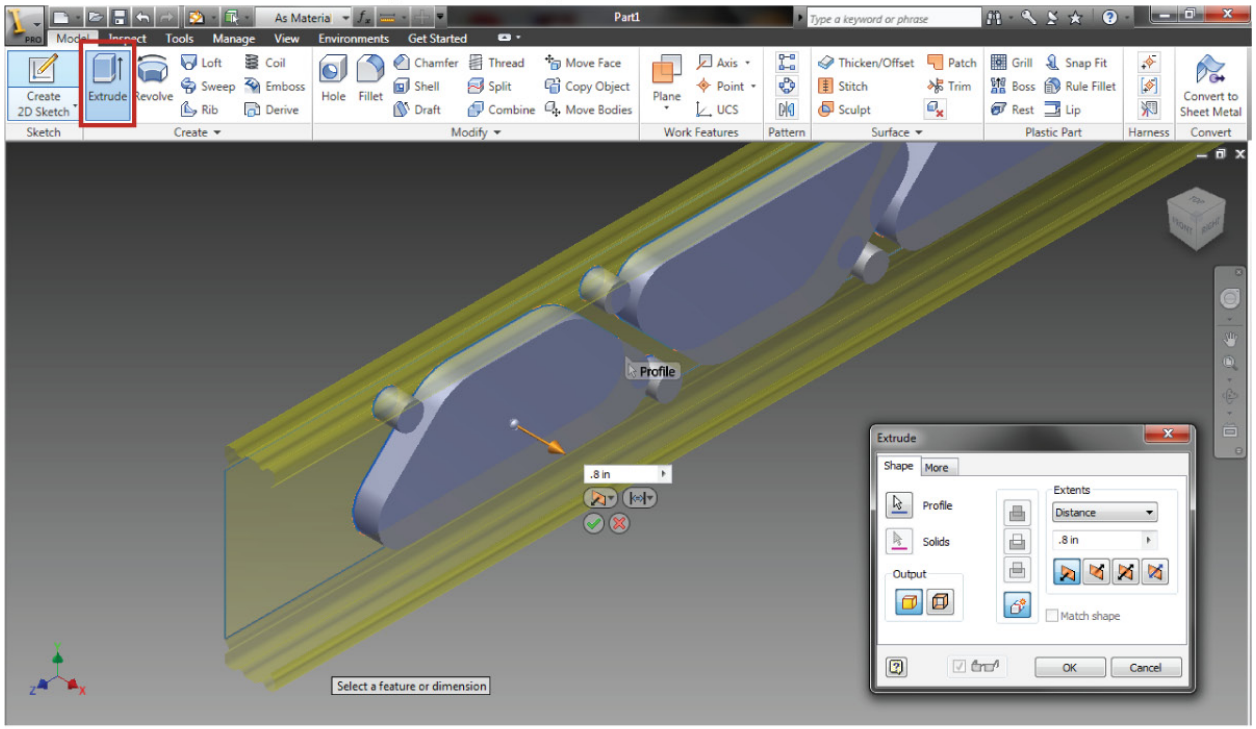

STEP 9 - Select first set of hole surfaces to delete

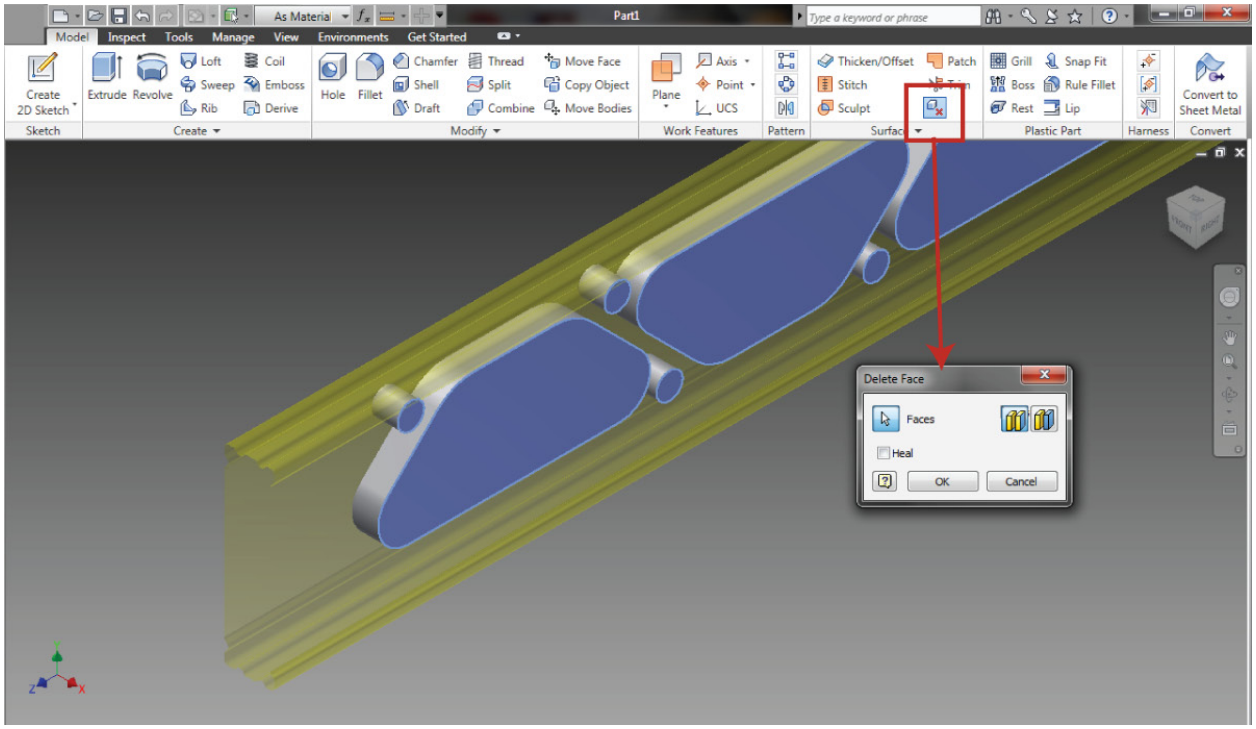

STEP 10 - Delete lower set of hole faces

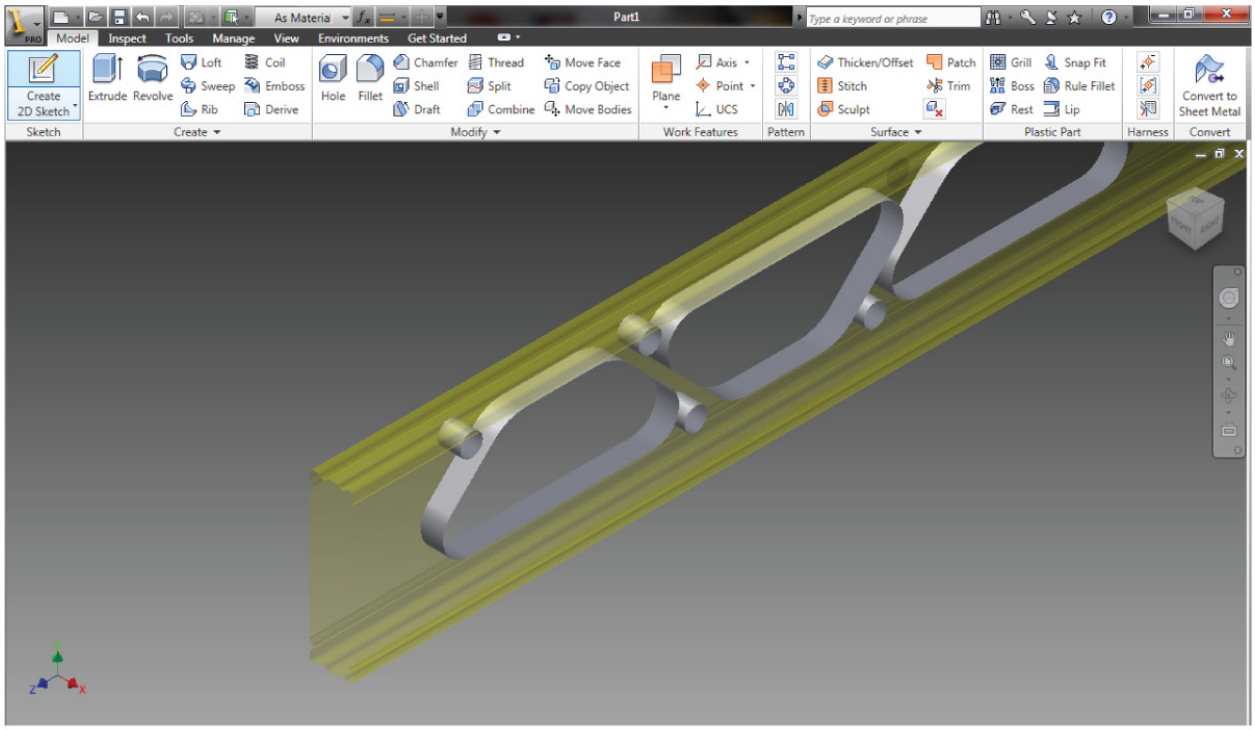

STEP 11 - Stitch newly extruded hole to original stud to make one continuous surface

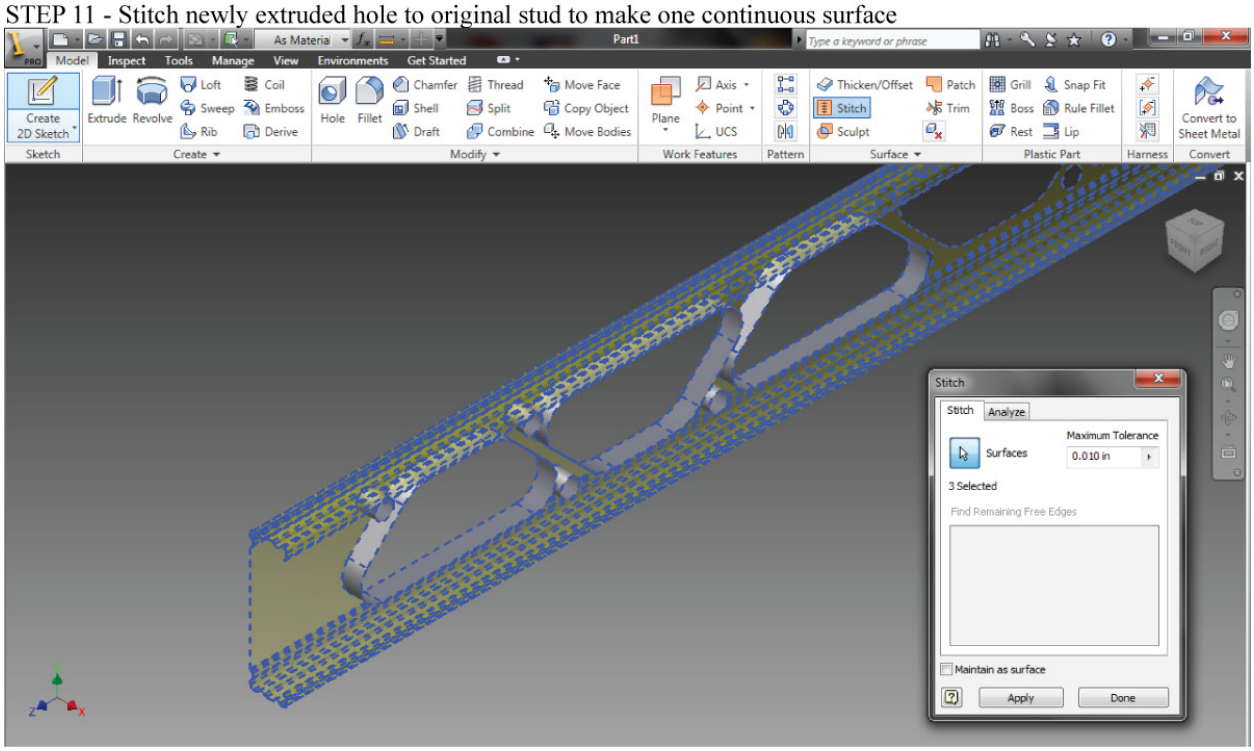

STEP 12 - Finish fully stitching model together

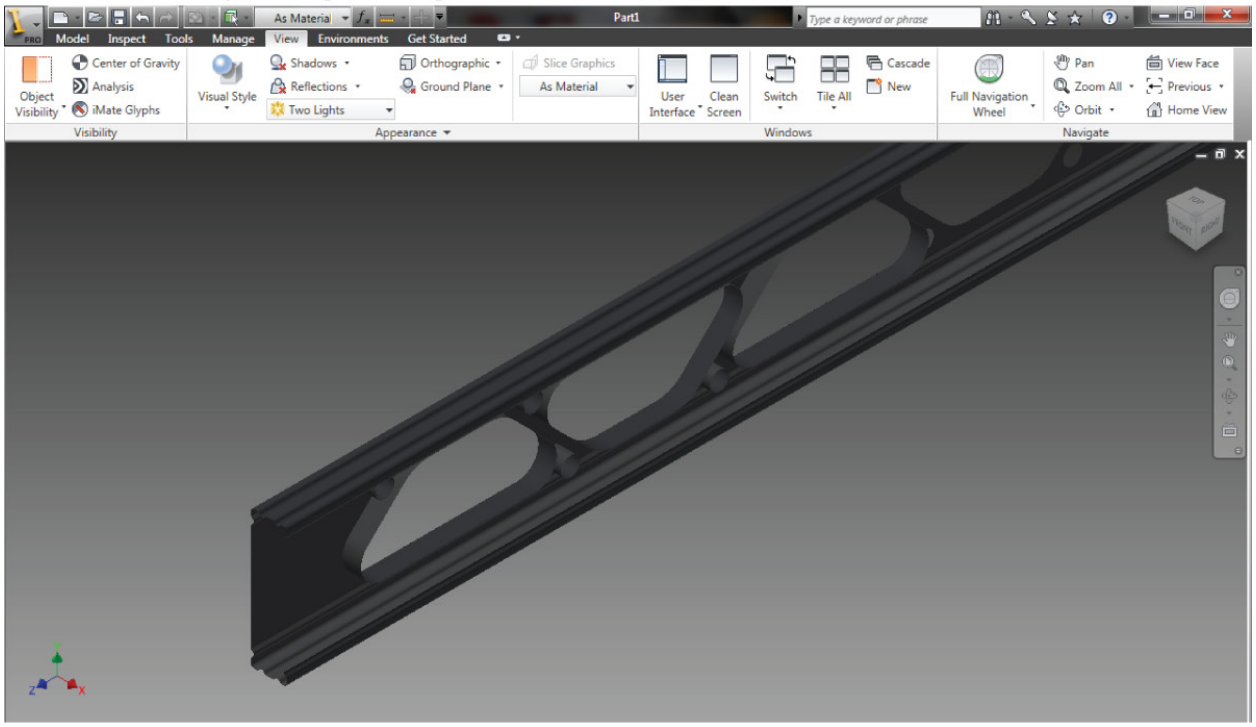

STEP 13 - Select using loop feature all hole edges on web to fillet corners

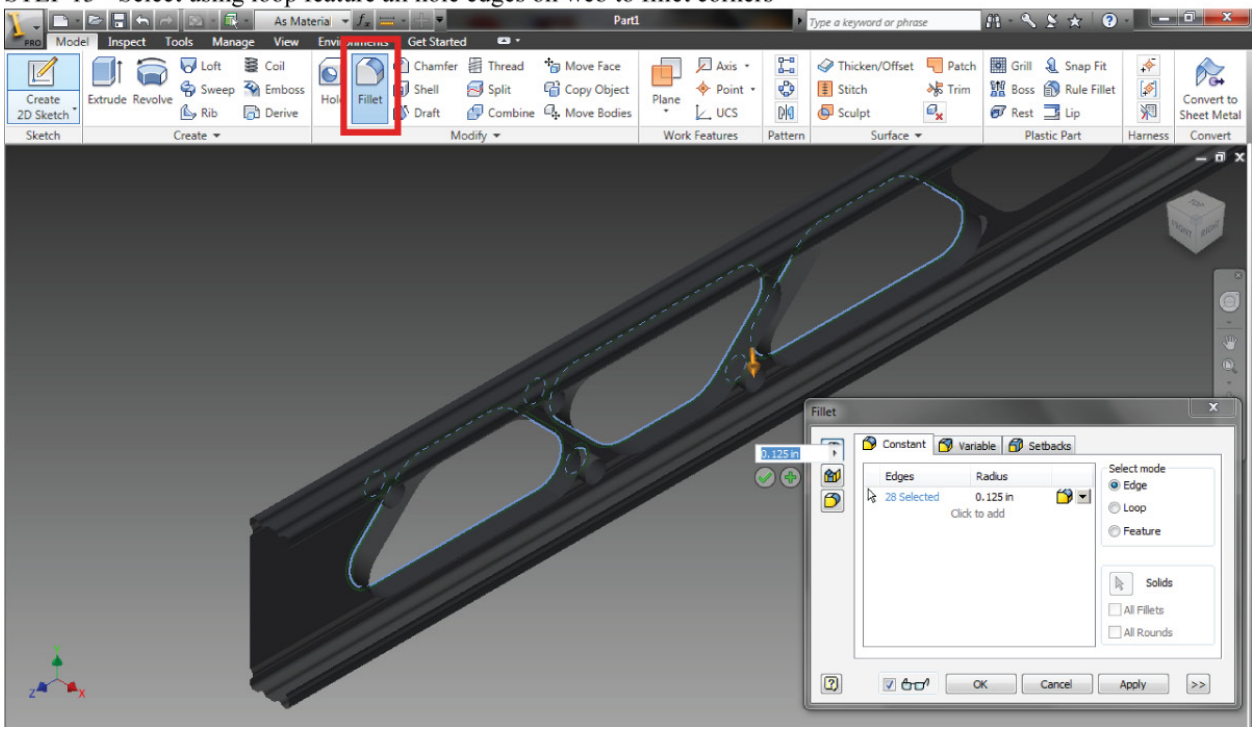

STEP 14 - Create a 2D-sketch on the extruded edge-stiffer

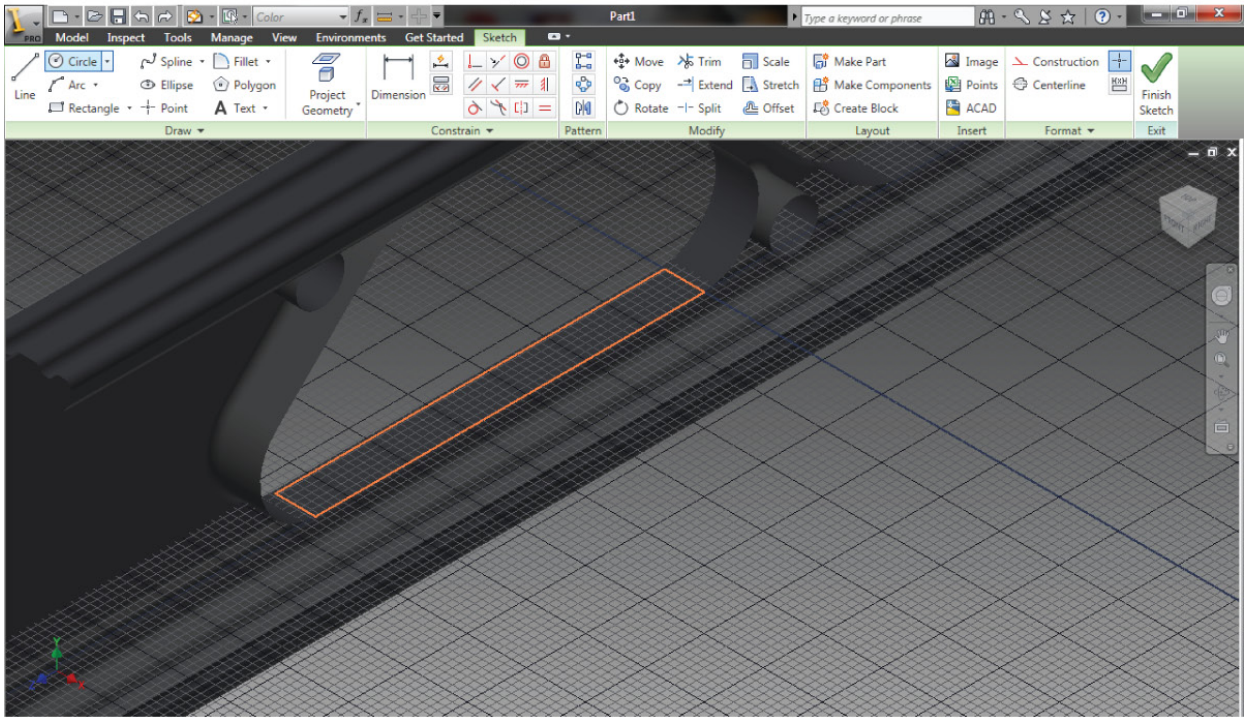

STEP 15 - Construct using line tools the extruded stiffener

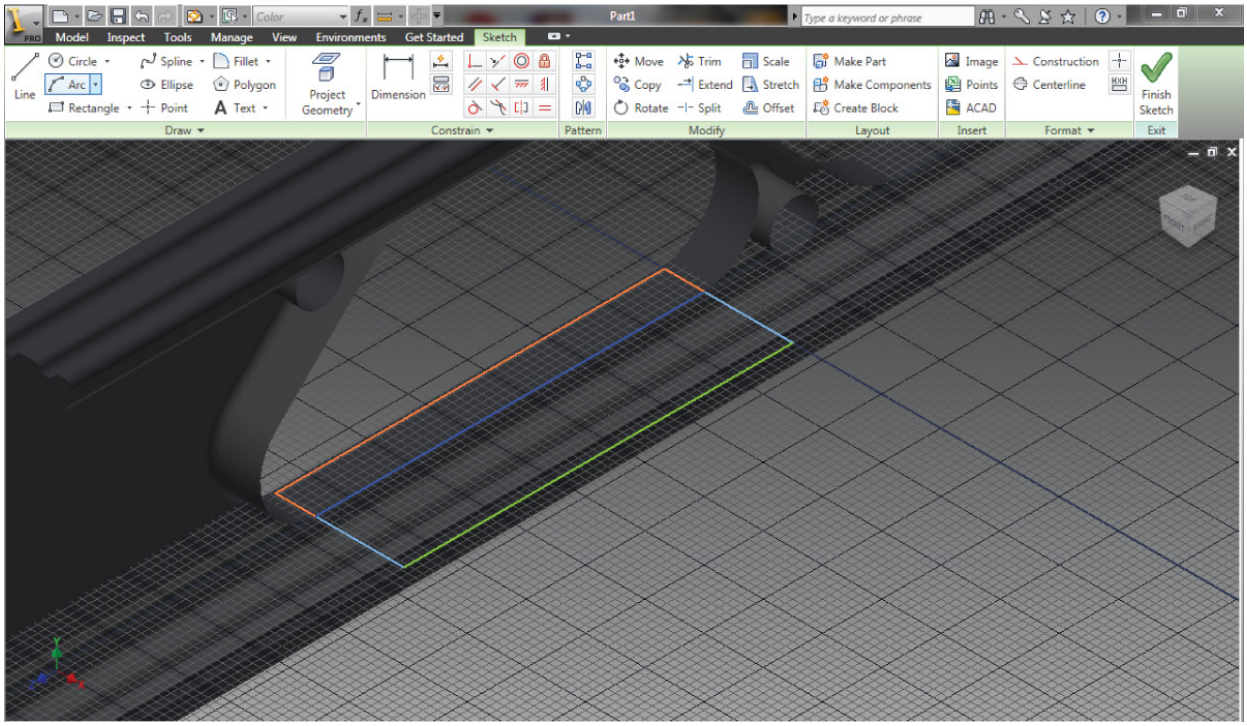

STEP 16 - Create plane using patch tool on the newly created sketch in Step 16

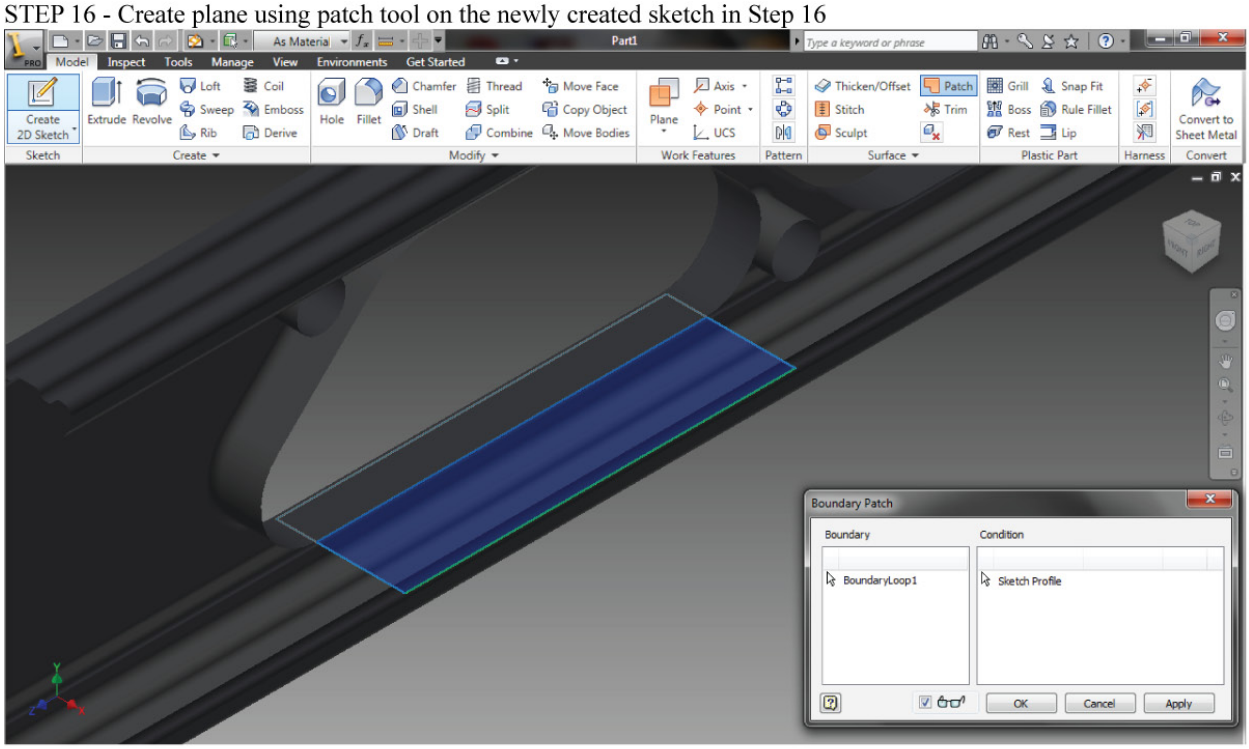

STEP 17 - Stitch the new plan to the rest of the part

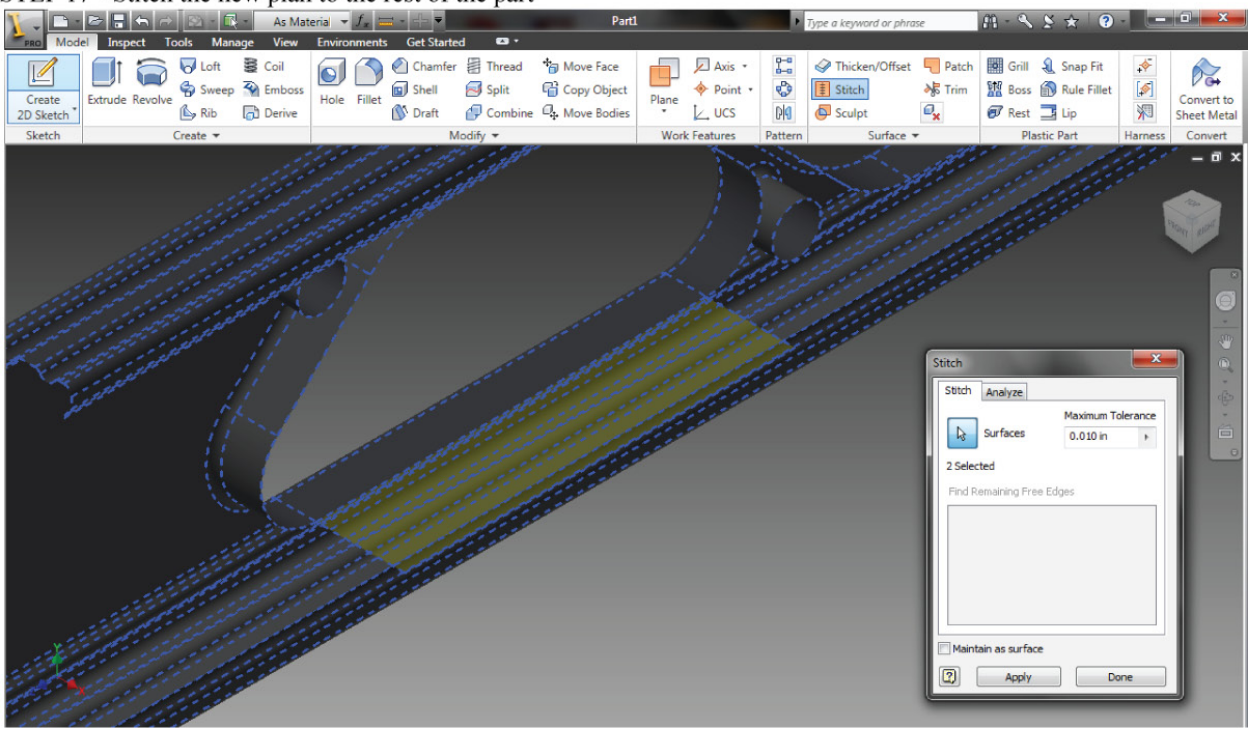

STEP 18 - Create a 3-D sketch and using the line tools create the return stiffener

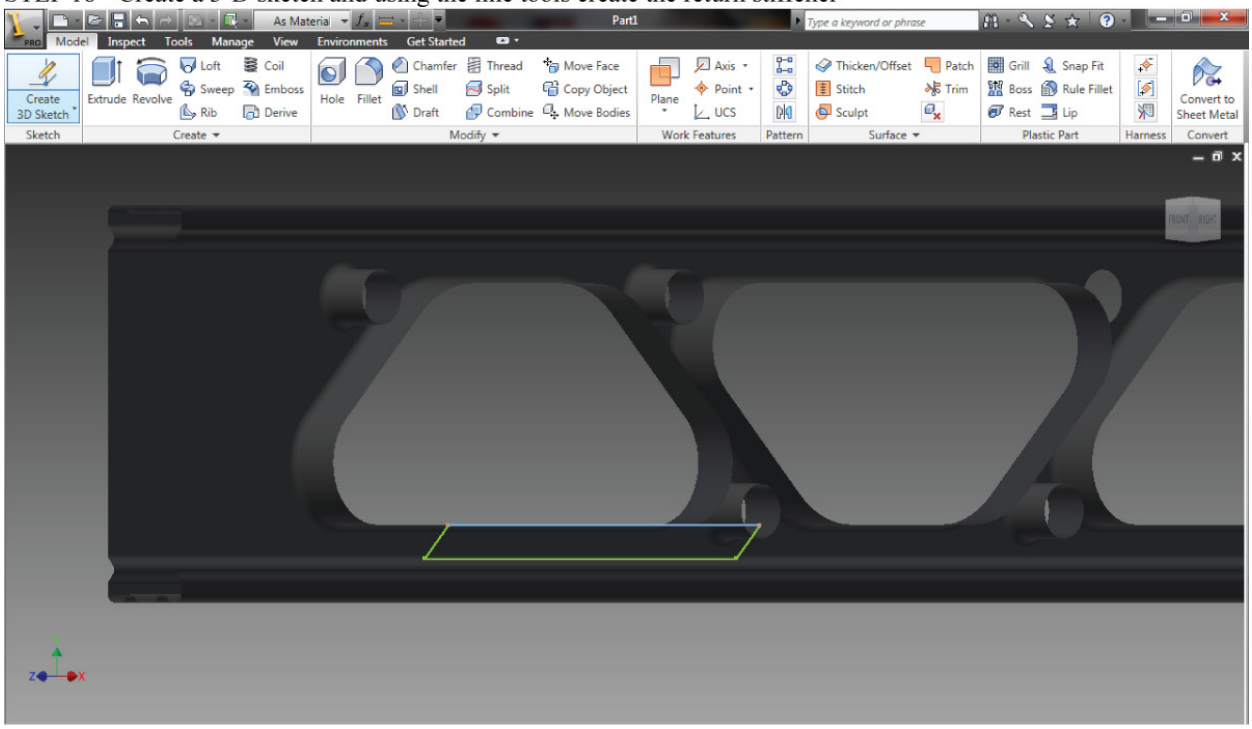

STEP 19 - Create a plane on the finished sketch and stitch it to the rest of the part as in previous steps

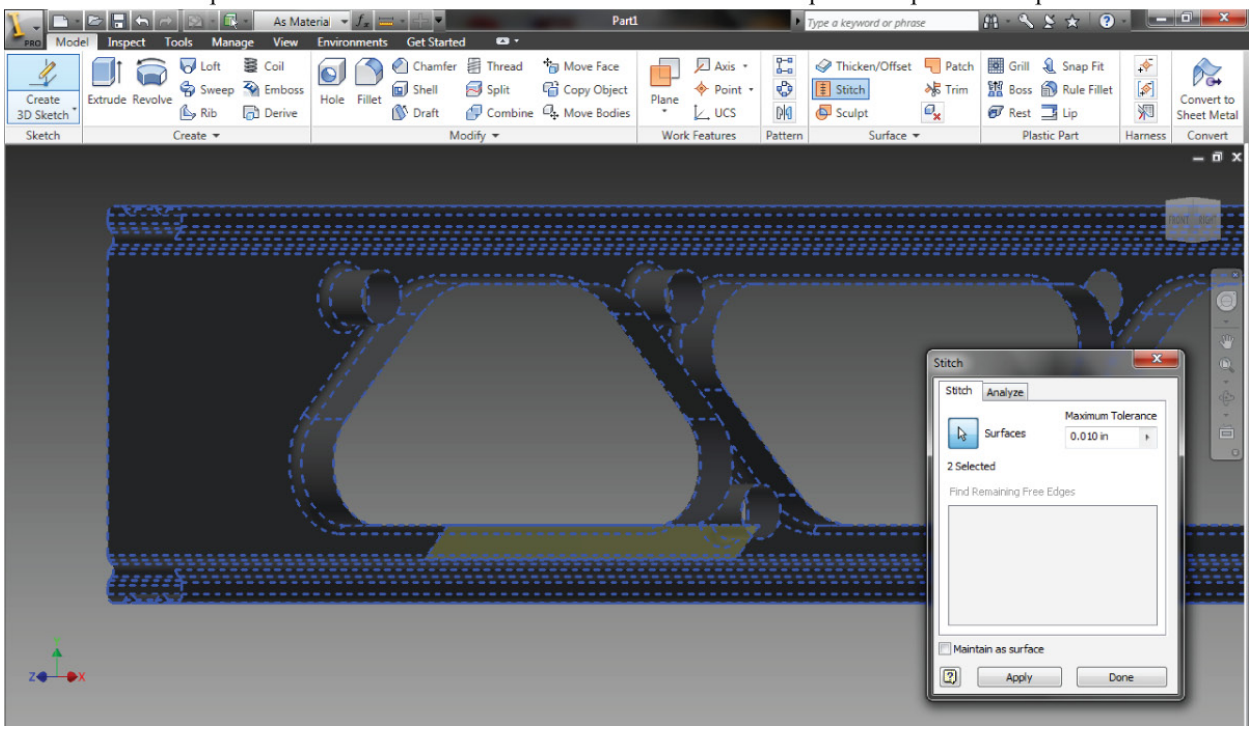

STEP 20 - Fillet return edge using fillet tool

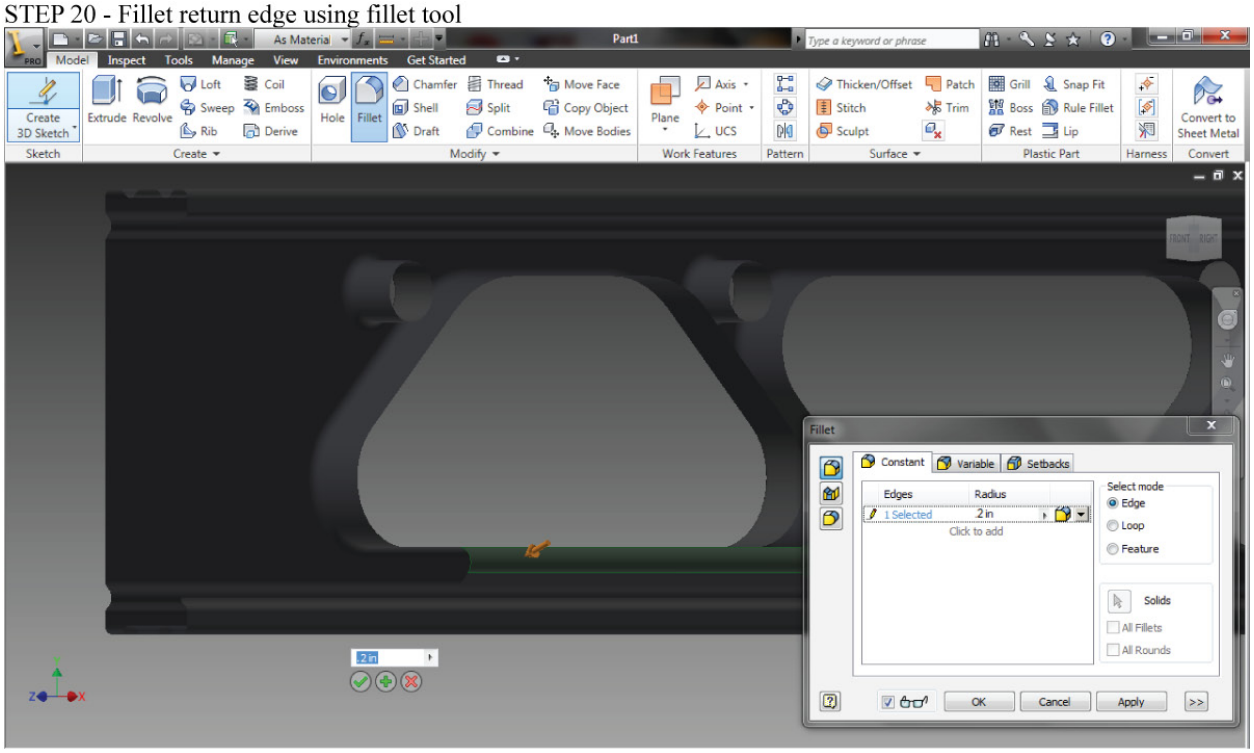

STEP 21 - Export final model to .IGS CAD format

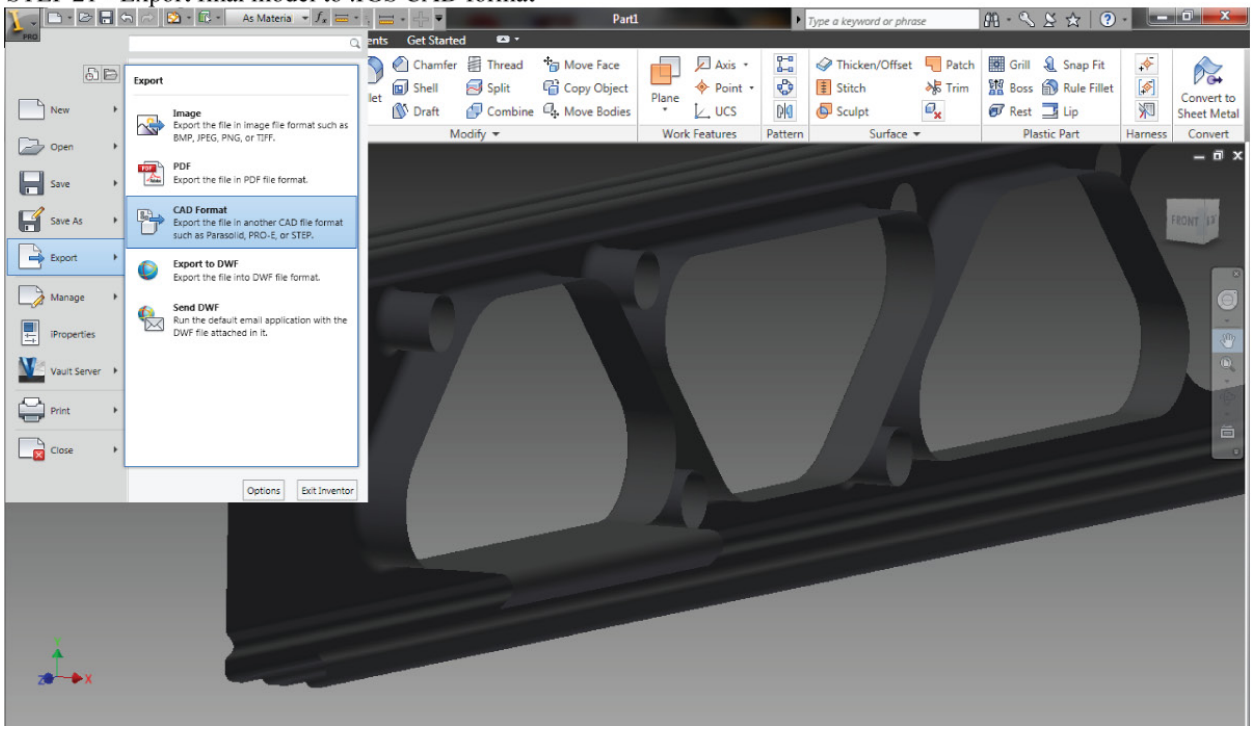

APPENDIX A.3 Matlab/Abaqus Input File Generator

The finite element models in this thesis were generated with a custom MATLAB program which assembles an ABAQUS elastic buckling input files for any externally created 3-D S8R5 meshed geometry. The members in this thesis were modeled in Autodesk INVENTOR and then imported into ABAQUS where they were meshed in S8R5 elements and exported to a node and element list in text file format. The user has the ability to apply boundary conditions, compression, different types of loading, and specify the material properties. The program was used throughout this research to generate groups of ABAQUS input files for elastic buckling.

```
clear all
close all
%The following code was originally by Dr. Cris Moen using S9R5 elements
%Has since been modified for this project for use of S8R5 thin-shell elements
%This example code generates an elastic buckling ABAQUS input file
%from a 3-D meshed geometry node and element list.

%SETS PATH FOLDER TO WHERE ALL SUPPORTING FUNCTIONS ARE--------------------
sourceloc=['C:\Users\Chris\Desktop\Moen Research\'];
addpath([sourceloc '\jhab\functions\filewriting\'])
addpath([sourceloc '\jhab\functions\holes\'])
addpath([sourceloc '\jhab\functions\'])
addpath([sourceloc '\jhab\templates\'])
addpath([sourceloc '\'])

%DEFINE JOBNAME------------------------------------------------------------
jobname={'6000x1625x0713x80'}

%READS IN MESHED GEOMETRY-------------------------------------------------
%reads in meshed nodes
fid=fopen('6000X1625X0713x80nodes.txt', 'r')
FEnode=fscanf(fid,'%g, %g, %g, %g', [4 inf]);
FEnode=FEnode';
fclose(fid)

%reads in meshed elements
fid=fopen('6000X1625X0713x80elements.txt', 'r')
FEelem=fscanf(fid,'%g, %g, %g, %g, %g, %g, %g, %g, %g', [9 inf]);
FEelem=FEelem';
fclose(fid)

%SETS ELEMENT TYPE---------------------------------------------------------
eltype='S8R5';

%3-D MODEL DETAILS ---------------------------------------------------------
%Shell Thickness
t=0.0713;
%Member Length
L=-min(FEnode(:,4));
%Flange Width (for locating 1 warping dof to prevent rigid body motion)
b=1.625;

%SHIFTS MODEL TO SET ORIGIN AT MID HEIGHT OF WEB--------------------------
%Shift nodes in Z direction (delta can vary)
delta=0;
FEnode(:,4)=FEnode(:,4)-delta;

%Shift nodes in X direction
maxx=min(FEnode(:,2));
FEnode(:,2)=FEnode(:,2)-maxx;

%Sifht nodes in Y direction
maxy=max(FEnode(:,3));
miny=min(FEnode(:,3));
Q=maxy-(6.0-0.0713)/2
```

```
FEnode(:,3)=FEnode(:,3)-Q;

%Rounds Node Coordinates
FEnode(:,2:4)=round(FEnode(:,2:4)*1000)/1000;

%Imperfection types, not used for elastic buckling analysis
imptypes=[0];
for i=1:1
    for j=1:length(imptypes)

        %NUMBER OF SECTION POINTS THROUGH THE THICKNESS--------------------
        sectionpoints=5;

        %ADD ADDITIONAL NODES----------------------------------------------
        nodeadd=[];

        %MATERIAL PROPERTIES-----------------------------------------------
        %steel
        matprops(AISI-S100).name='MAT100';
        matprops(AISI-S100).elastic=[29500 0.3];
        matprops(AISI-S100).plastic=[];

        %IMPERFECTIONS-----------------------------------------------------
        %*****IMPERFECTIONS*****
        %type=0   no imperfections
        %type=1   use mode shapes from ABAQUS results file
        %type=2   input from file
        %type 3   impose CUFSM shapes as imperfections

        %imperfections.member   =1 column
        %imperfections.member   =2 beam

        imperfections.type=0;
        imperfections.filename=[];
        imperfections.step=[];
        imperfections.mode=[]
        imperfections.member=[]
        imperfection.magnitude=[]
        imperfections.plumb=[];
        imperfections.wavelength=[];

        %DEFINE HOLES------------------------------------------------------
        %Add holes to your member.
        %hole.type=1  circular
        %hole.type=2  rectangular
        %hole.type=3  slotted w\radial ends
        %hole.dimension=['width or length (ABAQUS x direction)' 'height or
         diameter']
        %hole.location=['CUFSM cross section node (must be odd!)'
        'longitudinal location' 'shift hole in direction of height']
        %hole.thickness = thickness of finite elements making up hole,
         usually the same as the rest of the member
        hole=[];

        %MEMBER END LOADINGS-----------------------------------------------
```

```
  %Loading notation is similar to CUFSM.  Apply P for compression, M
for moment, or a combination of both.  Compression at both ends of
column are shown here.  Loads are applied as consistent nodal loads in
ABAQUS.
  end1load.P=-1;
  end1load.Mxx=0;
  end1load.Mzz=0;
  end1load.M11=0;
  end1load.M22=0;

  end2load.P=1;
  end2load.Mxx=0;
  end2load.Mzz=0;
  end2load.M11=0;
  end2load.M22=0;
  %Define STARTNODE coordinates
  %(Requires the imput of the cross section node that you want the
    numbering to start at)

  %FINDS CROSS SECTION NODES AT Z=0----------------------------------
  %Finds all nodes and creates node and element connectively list
  %that can be imported into CUFSM
  nodesetinfo={'XSECTION' [-1000 1000 0]  [-1000 1000 0] [0 0 0] 0;
      'STARTNODE' [1.428 1.430 0] [-2.465 -2.463 0] [0 0 0] 0};
  [nodeset]=nodesetcalc(nodesetinfo,FEnode);
  nodeset2=nodeset
  nodeset=nodeset{1};
  nodeinit=nodeset2{2};
  newnodelist(AISI-S100)=nodeinit;
  FEnodetemp=FEnode;
  for k=1:length(nodeset)
      x1=FEnodetemp(nodeinit,2);
      y1=FEnodetemp(nodeinit,3);
      x2=FEnodetemp(nodeset,2);
      y2=FEnodetemp(nodeset,3);
      dist=sqrt((y2-y1).^2+(x2-x1).^2);
      [c d]=sort(dist);
      newnodelist(k+1)=nodeset(d(2));
      FEnodetemp(newnodelist(k),2:3)=1000000+k;
      nodeinit=newnodelist(k+1);
  end

  nodeset1=newnodelist(1:length(newnodelist)-1)';
  node=[(1:length(nodeset1))' FEnode(nodeset1,2) FEnode(nodeset1,3)
         ones(length(nodeset1),5)];
  elem=[(1:length(nodeset1)-1)' (1:length(nodeset1)-1)'
        (2:length(nodeset1))' ones(length(nodeset1)-1,1).*t
         ones(length(nodeset1)-1,1).*100];
  node1=node;
  elem1=elem;
  figure(AISI-S100)
  for p=1:length(node)

      hold on
      plot(node1(p,2),node1(p,3),'.-')
      text(node1(p,2),node1(p,3),num2str(p))
```

```
end
clear nodesetinfo
clear nodeset
clear nodeinit
clear newnodelist
clear FEnodetemp
clear dist
clear node
clear elem

%FINDS CROSS SECTION NODES AT Z=L----------------------------------
nodesetinfo={'XSECTION' [-1000 1000 0]  [-1000 1000 0] [-L -L 0] 0;
    'STARTNODE' [1.428 1.430 0] [-2.465 -2.463 0] [-L -L 0] 0};

[nodeset]=nodesetcalc(nodesetinfo,FEnode);
nodeset2=nodeset
nodeset=nodeset{1};
nodeinit=nodeset2{2};
newnodelist(AISI-S100)=nodeinit;
FEnodetemp=FEnode;
for k=1:length(nodeset)
    x1=FEnodetemp(nodeinit,2);
    y1=FEnodetemp(nodeinit,3);
    x2=FEnodetemp(nodeset,2);
    y2=FEnodetemp(nodeset,3);
    dist=sqrt((y2-y1).^2+(x2-x1).^2);
    [c d]=sort(dist);
    newnodelist(k+1)=nodeset(d(2));
    FEnodetemp(newnodelist(k),2:3)=1000000+k;
    nodeinit=newnodelist(k+1);
end

nodeset2=newnodelist(1:length(newnodelist)-1)';
node=[(1:length(nodeset2))' FEnode(nodeset2,2) FEnode(nodeset2,3)
       ones(length(nodeset2),5)];
elem=[(1:length(nodeset2)-1)' (1:length(nodeset2)-1)'
      (2:length(nodeset2))' ones(length(nodeset2)-1,1).*t
       ones(length(nodeset2)-1,1).*100];
node2=node;
elem2=elem;
%
figure(2)
for p=1:length(node2)
    hold on
    plot(node2(p,2),node2(p,3),'.-')
    text(node2(p,2),node2(p,3),num2str(p))
end

%set equal to zero, not needed
nL=0
FEsection_increment=0

%ADDS THICKNESS TO ELEMENT GROUP-----------------------------------
FEelem=[FEelem t.*ones(length(FEelem),1)  1.*ones(length(FEelem),1)]
```

```
        %CALCULATE CONSISTENT NODAL LOADS ON MEMBER ENDS-------------------
          unsymm=0
          [end1cload, end2cload, A,Ixx]
          =consist_endloads(node1,elem1,node2,elem2,end1load,end2load,unsymm,
           nL, FEsection_increment, nodeset1,nodeset2);

          %ABAQUS NODE SETS-----------------------------------------------------
          %Define these node sets to apply boundary conditions in ABAQUS
          nodesetinfo={'ENDXZERO' [-1000 1000 0]  [-1000 1000 0] [0 0 0] 0;
           'ENDXL' [-1000 1000 0]  [-1000 1000 0] [-L -L 0] 0;
           'WARP' [b/2-0.04 b/2+0.04 0]  [max(FEnode(:,3)) max(FEnode(:,3)) 0]
                  [-L/2 -L/2 0] 0};

          %DEFINE SPRINGS-------------------------------------------------------
          springs=[]

          %DEFINE CONTACT SURFACES, NODE SURFACES, KINEMATIC CONSTRAINTS-----
          surface.type={}
          surface.type=[]
          surface.local=[]
          surface.coord=[]

          %SET UP WARPING FIXED BOUNDARY CONDITIONS-------------------------
          surface.coupling={};
          surface.interaction=[]
          surface.contact=[]
          surface.areadist=[]

          %DEFINE ANALYSIS STEP-------------------------------------------------
          step(AISI-S100).stepinfo={'STEP 1,' 'perturbation' []};
          step(AISI-S100).solutiontype='Buckle, EIGENSOLVER=LANCZOS';
          %DEFINES NUMBER OF BUCKLING MODES TO SEARCH FOR AND RANGE----------
          step(AISI-S100).solutionsteps={'150, , ,'};
          step(AISI-S100).solutioncontrols={ };
          %DEFINES BOUNDARY CONDITIONS 1,2,3 ARE DOFS-----------------------
          step(AISI-S100).boundarycon={'ENDXZERO' 1 2;
              'ENDXL' 1 2;
              'WARP' 3 3}
          step(AISI-S100).coupling=[]
          %DEFINES LOADING TO NODESETS--------------------------------------
          step(AISI-S100).loads={'*Cload' nodeset1 3 -end1cload(:,2);
              '*Cload' nodeset2 3 -end2cload(:,2)}
          %DEFINES OUTPUT REQUESTED-----------------------------------------
          step(AISI-S100).outrequest={'*Output, field, variable=PRESELECT'};
          nele=length(FEelem(:,1))

          %WRITE ABAQUS INP FILE
          jhabnl(L, node, elem, nele, end1load, end2load, hole, nodesetinfo,
                 surface, nodeadd, step,
          jobname{i},matprops,imperfections,springs,sectionpoints, FEnode,
                    FEelem, eltype)
      end
  end
```

APPENDIX A.4 Chapter 5 Supplement-Elastic Buckling Method Validations

The following Appendix provides the validation tables and work for each simplified variation method outlines in Chapter 5. Please note that Appendix A.4 is considered to be Chapter 6.

A.4.1 Verification for global buckling of columns with edge-stiffened holes

A.4.1.1 Verification for weak-axis flexural buckling of columns with edge-stiffened holes - Method 1

The presence of stiffened holes reduces the critical elastic global buckling load by a maximum of 28% for the 3625-54 and 3625-68 columns (see $P_{cre,ABAQUS\ with\ holes}/P_{cre,\ ABAQUS\ no\ holes}$ in Table A.4.1). The ''weighted average'' approximate method of Eq. 4.1 using worst possible section properties, denoted as $P_{cre,avg}$ in Table A.4.1, is shown to be a viable predictor of the weak-axis flexural buckling load across the range of Steelform members considered in this study, with $P_{cre,ABAQUS\ with\ holes}/P_{cre,avg}$ ranging from 0.92 to 0.98. This method is the best of all three methods looked at in this study. ABAQUS results are systematically 7% lower than the Euler buckling solutions due to the assumption of rigid cross section in the classical buckling equations. Because of this, the mean for $P_{cre,ABAQUS\ with\ holes}/P_{cre,avg}$ should be compared to 0.93 instead of 1.0. If this is accounted for, Method 1 is proven to be conservative for all members considered except for 3625-33 and 3625-43 which are unconservative by 1%.

Table A.4.1 Influence of edge-stiffened holes on column global buckling – Method 1

Buckling Mode	Comparison		Steelform Section								ABAQUS-to-predicted statistics	
			3625-33 L=80 in	3625-43 L=80 in	3625-54 L=80 in	3625-68 L=80 in	6000-33 L=80 in	6000-43 L=80 in	6000-54 L=80 in	6000-68 L=80 in	Mean	COV
Column weak-axis flexural buckling	$P_{cre,CLASSICAL\ no\ holes}$ [a]	(kip)	4.83	6.17	7.53	9.19	5.57	7.14	8.71	10.66		
	$P_{cre,ABAQUS\ no\ holes}$	(kip)	4.76	6.10	7.49	9.19	5.23	6.87	8.55	10.58		
	$P_{cre,ABAQUS\ with\ holes}$	(kip)	3.48	4.43	5.42	6.61	4.10	5.45	6.44	7.68		
	$P_{cre,avg}$	(kip)	3.80	4.83	5.85	7.01	4.38	5.54	6.68	8.12		
	$P_{cre,ABAQUS\ no\ holes}/P_{cre,CLASSICAL\ no\ holes}$		0.98	0.99	1.00	1.00	0.94	0.96	0.98	0.99	0.98	0.02
	$P_{cre,ABAQUS\ with\ holes}/P_{cre,ABAQUS\ no\ holes}$		0.73	0.73	0.72	0.72	0.78	0.79	0.75	0.73	0.74	0.04
	$P_{cre,ABAQUS\ with\ holes}/P_{cre,avg}$		0.92	0.92	0.93	0.94	0.94	0.98	0.96	0.95	0.94	0.02
Column flexural-torsional buckling	$P_{cre,CLASSICAL\ no\ holes}$ [a]	(kip)	3.35	4.52	6.15	8.61	5.59	7.42	9.55	12.61		
	$P_{cre,ABAQUS\ no\ holes}$	(kip)	3.23	4.39	5.83	8.07	5.77	7.62	9.83	12.88		
	$P_{cre,ABAQUS\ with\ holes}$	(kip)	2.75	3.75	5.02	6.93	4.39	6.02	7.49	9.73		
	$P_{cre,avg}$	(kip)	2.68	3.62	4.51	6.37	4.37	5.73	7.14	9.20		
	$P_{cre,ABAQUS\ no\ holes}/P_{cre,CLASSICAL\ no\ holes}$		0.96	0.97	0.95	0.94	1.03	1.03	1.03	1.02	0.99	0.04
	$P_{cre,ABAQUS\ with\ holes}/P_{cre,ABAQUS\ no\ holes}$		0.85	0.85	0.86	0.86	0.76	0.86	0.76	0.75	0.82	0.06
	$P_{cre,ABAQUS\ with\ holes}/P_{cre,avg}$		1.02	1.04	1.11	1.09	1.01	1.05	1.05	1.06	1.05	0.03

[a] The classical Euler buckling solution for a column without a hole is $P_{cre,CLASSICAL\ nohole}$.

A.4.1.2 Verification for weak-axis flexural buckling of columns with edge-stiffened holes - Method 2

The ‘‘weighted average’’ approximate method of Eq. 4.1 using worst case section properties, denoted as $P_{cre,avg}$ in Table A.4.1, is shown to be a viable but slightly unconservative predictor of the weak-axis flexural buckling load across the range of Steelform members considered in this study, with $P_{cre,ABAQUS\ with\ holes}/P_{cre,avg}$ ranging from 0.88 to 0.98. Again, compare the means to .93 instead of 1.0.

Table A.4.2 Influence of edge-stiffened holes on column global buckling – Method 2

Buckling Mode	Comparison		Steelform Section								ABAQUS-to-predicted statistics	
			3625-33	3625-43	3625-54	3625-68	6000-33	6000-43	6000-54	6000-68		
			L=80 in	L=80 in	L=80 in	L=80 in	L=80 in	L=80 in	L=80 in	L=80 in	Mean	COV
Column weak-axis flexural buckling	$P_{cre,CLASSICAL\ no\ holes}$ [a]	(kip)	4.83	6.17	7.53	9.19	5.57	7.14	8.71	10.66		
	$P_{cre,ABAQUS\ no\ holes}$	(kip)	4.76	6.10	7.49	9.19	5.23	6.87	8.55	10.58		
	$P_{cre,ABAQUS\ with\ holes}$	(kip)	3.48	4.43	5.42	6.61	4.10	5.45	6.44	7.68		
	$P_{cre,avg}$	(kip)	3.97	5.06	6.07	7.38	4.38	5.54	6.68	8.12		
	$P_{cre,ABAQUS\ no\ holes}/P_{cre,CLASSICAL\ no\ holes}$		0.98	0.99	1.00	1.00	0.94	0.96	0.98	0.99	0.98	0.02
	$P_{cre,ABAQUS\ with\ holes}/P_{cre,ABAQUS\ no\ holes}$		0.73	0.73	0.72	0.72	0.78	0.79	0.75	0.73	0.74	0.04
	$P_{cre,ABAQUS\ with\ holes}/P_{cre,avg}$		0.88	0.88	0.89	0.90	0.94	0.98	0.96	0.95	0.92	0.04
Column flexural-torsional buckling	$P_{cre,CLASSICAL\ no\ holes}$ [a]	(kip)	3.35	4.52	6.15	8.61	5.59	7.42	9.55	12.61		
	$P_{cre,ABAQUS\ no\ holes}$	(kip)	3.23	4.39	5.83	8.07	5.77	7.62	9.83	12.88		
	$P_{cre,ABAQUS\ with\ holes}$	(kip)	2.75	3.75	5.02	6.93	4.39	6.02	7.49	9.73		
	$P_{cre,avg}$	(kip)	2.71	3.64	4.58	6.35	4.08	5.94	7.51	9.65		
	$P_{cre,ABAQUS\ no\ holes}/P_{cre,CLASSICAL\ no\ holes}$		0.96	0.97	0.95	0.94	1.03	1.03	1.03	1.02	0.99	0.04
	$P_{cre,ABAQUS\ with\ holes}/P_{cre,ABAQUS\ no\ holes}$		0.85	0.85	0.86	0.86	0.76	0.86	0.76	0.75	0.82	0.06
	$P_{cre,ABAQUS\ with\ holes}/P_{cre,avg}$		1.01	1.03	1.10	1.09	1.08	1.01	1.00	1.01	1.04	0.04

[a] The classical Euler buckling solution for a column without a hole is $P_{cre,CLASSICAL\ nohole}$.

A.4.1.3 Verification for weak-axis flexural buckling of columns with edge-stiffened holes - Method 3

The ‘‘weighted average’’ approximate method of Eq. 4.1 using mid-hole section properties, denoted as $P_{cre,avg}$ in Table A.4.3, is shown to be an unconservative predictor of the weak-axis flexural buckling load across the range of Steelform members considered in this study, with $P_{cre,ABAQUS\ with\ holes}/P_{cre,avg}$ ranging from 0.88 to 0.93. However, this method produced very unconservative buckling loads by on average 14%. This is because at mid-hole exists a very large stiffener that increases the weak axis moment of inertia which drives the weak axis buckling load upward closer to the no hole loads. Although it drives up the strong axis moment of inertia, the large mid-hole stiffener isn't actually contributing to the flexural stiffness of the member since it is discontinuous. There is no way for the applied force to engage the stiffener.

Table A.4.3 Influence of edge-stiffened holes on column global buckling – Method 3

Buckling Mode	Comparison		Steelform Section								ABAQUS-to-predicted statistics	
			3625-33 L=80 in	3625-43 L=80 in	3625-54 L=80 in	3625-68 L=80 in	6000-33 L=80 in	6000-43 L=80 in	6000-54 L=80 in	6000-68 L=80 in	Mean	COV
Column weak-axis flexural buckling	$P_{cre,CLASSICAL\ no\ holes}$ [a]	(kip)	4.83	6.17	7.53	9.19	5.57	7.14	8.71	10.66		
	$P_{cre,ABAQUS\ no\ holes}$	(kip)	4.76	6.10	7.49	9.19	5.23	6.87	8.55	10.58		
	$P_{cre,ABAQUS\ with\ holes}$	(kip)	3.48	4.43	5.42	6.61	4.10	5.45	6.44	7.68		
	$P_{cre,avg}$	(kip)	4.24	5.39	6.56	7.97	4.60	5.87	7.11	8.76		
	$P_{cre,ABAQUS\ no\ holes}/P_{cre,CLASSICAL\ no\ holes}$		0.98	0.99	1.00	1.00	0.94	0.96	0.98	0.99	0.98	0.02
	$P_{cre,ABAQUS\ with\ holes}/P_{cre,ABAQUS\ no\ holes}$		0.73	0.73	0.72	0.72	0.78	0.79	0.75	0.73	0.74	0.04
	$P_{cre,ABAQUS\ with\ holes}/P_{cre,avg}$		0.82	0.82	0.83	0.83	0.89	0.93	0.91	0.88	0.86	0.05
Column flexural-torsional buckling	$P_{cre,CLASSICAL\ no\ holes}$ [a]	(kip)	3.35	4.52	6.15	8.61	5.59	7.42	9.55	12.61		
	$P_{cre,ABAQUS\ no\ holes}$	(kip)	3.23	4.39	5.83	8.07	5.77	7.62	9.83	12.88		
	$P_{cre,ABAQUS\ with\ holes}$	(kip)	2.75	3.75	5.02	6.93	4.39	6.02	7.49	9.73		
	$P_{cre,avg}$	(kip)	3.02	4.07	5.42	6.64	4.55	5.96	7.51	9.97		
	$P_{cre,ABAQUS\ no\ holes}/P_{cre,CLASSICAL\ no\ holes}$		0.96	0.97	0.95	0.94	1.03	1.03	1.03	1.02	0.99	0.04
	$P_{cre,ABAQUS\ with\ holes}/P_{cre,ABAQUS\ no\ holes}$		0.85	0.85	0.86	0.86	0.76	0.86	0.76	0.75	0.82	0.06
	$P_{cre,ABAQUS\ with\ holes}/P_{cre,avg}$		0.91	0.92	0.92	1.04	0.97	1.01	1.00	0.98	0.97	0.05

[a] The classical Euler buckling solution for a column without a hole is $P_{cre,CLASSICAL\ nohole}$.

A.4.2 Verification for torsional properties of members with edge-stiffened holes

A.4.2.1 Evaluation of torsional property approximations

The torsional properties for the Steelform member dimensions in Table 5.1 are calculated with the procedure outlined in Chapter 2 Section 5.2. to evaluate the viability of the weighted average J_{avg} and net section $C_{w,net}$ approximations in Eq. 4.4.

A.4.2.2 Verification of torsional property approximations – Methods 1 and 2

Methods 1 and 2 use the same sections for the torsion and warping constants analyzed in this section therefore they are combined into one section. Section C-C properties are taken for the 3.625" members and Section D-D properties are taken for the 6.000" members as shown in Table 5.2 The results in Table A.4.4 demonstrate that the weighted average approach for methods 1 and 2 underpredicts the St. Venant torsional constant by a maximum of 41% compared to that predicted by the finite element approach (compare $J_{ABAQUS\ with\ holes}$ to J_{avg} in Table A.4.4). The weighted average approach also underpredicts the deeper member's torsional constant by a maximum of 10% more than the smaller members. It is hypothesized that J_{avg} under predicts the actual torsional resistance because the weighted average approach assumes the most conservative cross section, whereas the actual complex edge-stiffeners provide more torsional stiffness than calculated using the St. Venants equation. Also note that $J_{ABAQUS\ with\ holes}$ is greater than $J_{ABAQUS\ no\ holes}$ in Table A.4.4 which insinuates that the basic torsional constant equations may not work for such a complex shape and there may be some underlying factors contributing to an increase in torsional stiffness for members considered in this study. At this point in time, there is no such study that looks at the possibility of the St. Venant's equation breaking down in certain conditions.

The net section warping torsion constant, $C_{w,net}$, under predicts C_w by a maximum of 15% for the 6000-33 member when compared to the semi-analytical approach (compare $C_{w\ ABAQUS\ with\ holes}$ to $C_{w,net}$ in Table A.4.4). The addition of edge-stiffened holes has a large effect on J and C_w for the members evaluated in this study (compare $J_{,ABAQUS\ with\ holes}$ to $J_{,ABAQUS\ no\ holes}$ and $C_{,w\ ABAQUS\ with\ holes}$ to $C_{,w\ ABAQUS\ no\ holes}$ in Table A.4.4).

Table A.4.4 Influence of edge-stiffened holes on torsion properties – Methods 1 and 2

Buckling Mode	Comparison		Steelform Section								ABAQUS-to-predicted statistics	
			3625-33 L=80 in	3625-43 L=80 in	3625-54 L=80 in	3625-68 L=80 in	6000-33 L=80 in	6000-43 L=80 in	6000-54 L=80 in	6000-68 L=80 in	Mean	COV
St Venant's torsion constant, J	$J_{,g}$ [a]	($in.^4$)	0.000120	0.000259	0.000516	0.001018	0.000156	0.000347	0.000682	0.001361		
	$J_{,ABAQUS\ no\ holes}$	($in.^4$)	0.000119	0.000262	0.000516	0.001024	0.000156	0.000346	0.000680	0.001354		
	$J_{,ABAQUS\ with\ holes}$	($in.^4$)	0.000124	0.000268	0.000518	0.001003	0.000170	0.000361	0.000718	0.001356		
	$J_{,avg}$	($in.^4$)	0.000095	0.000209	0.000403	0.000795	0.000121	0.000264	0.000513	0.001010		
	$J_{,ABAQUS\ no\ holes}/J_{,g}$		1.00	1.01	1.00	1.01	1.00	1.00	1.00	1.00	1.00	0.01
	$J_{,ABAQUS\ with\ holes}/J_{,g}$		1.04	1.03	1.00	0.99	1.09	1.04	1.05	1.00	1.03	0.03
	$J_{,ABAQUS}/J_{,avg}$		1.30	1.28	1.28	1.26	1.41	1.37	1.40	1.34	1.33	0.04
Warping torsion constant, C_w	$C_{w,g}$ [a]	($in.^6$)	0.29	0.37	0.45	0.54	0.85	1.08	1.31	1.58		
	$C_{w,ABAQUS\ no\ holes}$	($in.^6$)	0.30	0.38	0.45	0.55	0.86	1.08	1.32	1.61		
	$C_{w,ABAQUS\ with\ holes}$	($in.^6$)	0.31	0.38	0.45	0.54	0.94	1.13	1.39	1.61		
	$C_{w,net}$	($in.^6$)	0.29	0.36	0.41	0.52	0.80	1.00	1.19	1.43		
	$C_{w,ABAQUS\ no\ holes}/C_{w,g}$		1.01	1.01	1.01	1.01	1.02	1.00	1.01	1.02	1.01	0.01
	$C_{w,ABAQUS\ with\ holes}/C_{w,g}$		1.04	1.03	1.01	0.99	1.11	1.04	1.06	1.02	1.04	0.04
	$C_{w,ABAQUS\ with\ holes}/C_{w,net}$		1.07	1.06	1.10	1.04	1.18	1.13	1.17	1.13	1.11	0.05

[a] $J_{,g}$ and $C_{w,g}$ are calculated for the gross cross-section with the CUFSM section property calculator

A.4.2.3 Verification of torsional property approximations – Method 3

Table A.4.5 demonstrates that the weighted average approach for method 3 greatly under predicts St. Venants torsional constant. Assuming the mid-hole properties, the weighted average approach is also shown to under predict St. Venants torsional constant by a maximum of 25% compared to that predicted by the semi-analytical approach (compare $J_{ABAQUS\ with\ holes}$ to J_{avg} in Table A.4.5). The weighted average approach also under predicts the deeper member's torsional constant by a maximum of 15% more than the smaller members as in the first two methods.

The net section warping torsion constant, $C_{w,net}$, under predicts C_w by a maximum of 19% for the 6000-33 member when compared to the semi-analytical approach (compare $C_{w\ ABAQUS\ with\ holes}$ to $C_{w,net}$ in Table A.4.5).

Table A.4.5 Influence of edge-stiffened holes on torsion properties – Method 3

Buckling Mode	Comparison		Steelform Section								ABAQUS-to-predicted statistics	
			3625x1625-33 L=80 in	3625x1625-43 L=80 in	3625x1625-54 L=80 in	3625x1625-68 L=80 in	6000x1625-33 L=80 in	6000x1625-43 L=80 in	6000x1625-54 L=80 in	6000x1625-68 L=80 in	Mean	COV
St Venant's torsion constant, J	$J_{,g}$ [a]	($in.^4$)	0.000120	0.000259	0.000516	0.001018	0.000156	0.000347	0.000682	0.001361		
	$J_{,ABAQUS\ no\ holes}$	($in.^4$)	0.000119	0.000262	0.000516	0.001024	0.000156	0.000346	0.000680	0.001354		
	$J_{,ABAQUS\ with\ holes}$	($in.^4$)	0.000124	0.000268	0.000518	0.001003	0.000170	0.000361	0.000718	0.001361		
	$J_{,avg}$	($in.^4$)	0.000113	0.000247	0.000486	0.000963	0.000136	0.000299	0.000585	0.001154		
	$J_{,ABAQUS\ no\ holes}/J_{,g}$		1.00	1.01	1.00	1.01	1.00	1.00	1.00	1.00	1.00	0.01
	$J_{,ABAQUS\ with\ holes}/J_{,g}$		1.04	1.03	1.00	0.99	1.09	1.04	1.05	1.00	1.03	0.03
	$J_{,ABAQUS}/J_{,avg}$		1.10	1.08	1.07	1.04	1.25	1.21	1.23	1.18	1.14	0.07
Warping torsion constant, C_w	$C_{w,g}$ [a]	($in.^6$)	0.29	0.37	0.45	0.54	0.85	1.08	1.31	1.58		
	$C_{w,ABAQUS\ no\ holes}$	($in.^6$)	0.30	0.38	0.45	0.55	0.86	1.08	1.32	1.61		
	$C_{w,ABAQUS\ with\ holes}$	($in.^6$)	0.31	0.38	0.45	0.54	0.94	1.13	1.39	1.61		
	$C_{w,net}$	($in.^6$)	0.30	0.37	0.45	0.57	0.79	1.00	1.20	1.49		
	$C_{w,ABAQUS\ no\ holes}/C_{w,g}$		1.01	1.01	1.01	1.01	1.02	1.00	1.01	1.02	1.01	0.01
	$C_{w,ABAQUS\ with\ holes}/C_{w,g}$		1.04	1.03	1.01	0.99	1.11	1.04	1.06	1.02	1.04	0.04
	$C_{w,ABAQUS\ with\ holes}/C_{w,net}$		1.04	1.03	1.01	0.94	1.19	1.12	1.16	1.08	1.07	0.08

[a] $J_{,g}$ and $C_{w,g}$ are calculated for the gross cross-section with the CUFSM section property calculator

A.4.2.4 Verification of torsional property approximations – Alternate Method 4

In an effort to find the best viable predictor of the torsion and warping constants, an alternate method is suggested where the gross section properties are used instead of the net section. Since the finite element analysis has predicted a St. Venants torsional constant for a member with holes to be higher than a member without holes, this method should produce the most accurate results. Table A.4.6 demonstrates that the gross section property approach for method 4 still under predicts St. Venants torsional constant, however, at a much less percentage by a maximum of 9% compared to that predicted by the semi-analytical approach (compare $J_{ABAQUS\ with\ holes}$ to J_g in Table A.4.6). For the 3625-68 member, the gross section property actually over-predicts J by 1%. The gross property approach also under predicts the deeper member's torsional constant by a maximum of 10% more than the smaller members as in the first two methods. The gross section approach predicts the most accurate torsional constant compared to the other three methods.

Using the gross section warping torsion constant, $C_{w,g}$, under predicts C_w by a maximum of 11% for the 6000-33 member when compared to the semi-analytical approach (compare $C_{w\ ABAQUS\ with\ holes}$ to $C_{w,g}$ in Table A.4.6). Just as with the St. Venants torsional constant, method 4 proves to be the most accurate when compared to methods 1,2 and 3.

Table A.4.6 Influence of edge-stiffened holes on torsion properties – Method 4

Buckling Mode	Comparison		Steelform Section								ABAQUS-to-predicted statistics	
			3625-33	3625-43	3625-54	3625-68	6000-33	6000-43	6000-54	6000-68		
			L=80 in	L=80 in	L=80 in	L=80 in	L=80 in	L=80 in	L=80 in	L=80 in	Mean	COV
St Venant's torsion constant, J	$J_{,g}$ [a]	($in.^4$)	0.000120	0.000259	0.000516	0.001018	0.000156	0.000347	0.000682	0.001361		
	$J_{,ABAQUS\ no\ holes}$	($in.^4$)	0.000119	0.000262	0.000516	0.001024	0.000156	0.000346	0.000680	0.001354		
	$J_{,ABAQUS\ with\ holes}$	($in.^4$)	0.000124	0.000268	0.000518	0.001003	0.000170	0.000361	0.000718	0.001361		
	$J_{,ABAQUS\ no\ holes}/J_{,g}$		1.00	1.01	1.00	1.01	1.00	1.00	1.00	1.00	1.00	0.01
	$J_{,ABAQUS\ with\ holes}/J_{,g}$		1.04	1.03	1.00	0.99	1.09	1.04	1.05	1.00	1.03	0.03
Warping torsion constant, C_w	$C_{w,g}$ [a]	($in.^6$)	0.29	0.37	0.45	0.54	0.85	1.08	1.31	1.58		
	$C_{w,ABAQUS\ no\ holes}$	($in.^6$)	0.30	0.38	0.45	0.55	0.86	1.08	1.32	1.61		
	$C_{w,ABAQUS\ with\ holes}$	($in.^6$)	0.31	0.38	0.45	0.54	0.94	1.13	1.39	1.61		
	$C_{w,ABAQUS\ no\ holes}/C_{w,g}$		1.01	1.01	1.01	1.01	1.02	1.00	1.01	1.02	1.01	0.01
	$C_{w,ABAQUS\ with\ holes}/C_{w,g}$		1.04	1.03	1.01	0.99	1.11	1.04	1.06	1.02	1.04	0.04

[a] $J_{,g}$ and $C_{w,g}$ are calculated for the gross cross-section with the CUFSM section property calculator

A.4.3 Verification for flexural-torsional buckling of members with edge-stiffened holes

A.4.3.1 Verification for flexural-torsional buckling of a column with edge-stiffened holes - Method 1

The second elastic global mode of all Steelform columns analyzed is flexural-torsional buckling. Table A.4.1 shows that the flexural-torsional mode is not as sensitive to hole size than the weak-axis flexural mode (compare $P_{cre,ABAQUS\ with\ holes}/P_{cre,ABAQUS\ no\ holes}$). The flexure-torsional buckling loads of the Steelform columns with edge-stiffened holes from ABAQUS are within an on average conservative 5% of the flexural buckling loads predicted by the weighted average approach using Method 1 (compare $P_{cre,ABAQUS\ \ with\ \ holes}/P_{cre,avg}$ in Table A.4.1). This conservatively is partially due to the under prediction of St. Venant torsional constant, J_{avg}, and warping torsion constant, $C_{w,net}$. It should be noted that even though the torsion and warping constants are under predicted by a large percentage, that the flexural torsional buckling load using weighted average is only conservative by a maximum of 11%. It should also be noted that ABAQUS results are systematically 5-7% lower than the weighted average approximations as they assume a rigid cross-section rotation that might not exist in thin complex members.

A.4.3.2 Verification for flexural-torsional buckling of a column with edge-stiffened holes - Method 2

The flexure-torsional buckling loads of the Steelform columns with edge-stiffened holes from ABAQUS are within an on average conservative 4% of the flexural buckling loads predicted by the weighted average approach using method 2 (compare $P_{cre,ABAQUS\ with\ holes}/P_{cre,avg}$ in Table A.4.2). St. Venant torsional constant, J_{avg}, and warping torsion constant, $C_{w,net}$ do not change compared to method 1 therefore, the resulting difference is due to the moment of inertia properties. In Method 2, the 3.625" members weak axis moment of inertia is greater than in Method 1, whereas the 6.000" members strong axis moment of inertia is greater than in Method 1 (See Table 5.2 where I_{yy} and I_{xx} change between Methods 1 and 2). It should be noted that even though the torsion and warping constants are under predicted by a large percentage, that the flexural torsional buckling load using weighted average is only conservative by a maximum of 9% which is less than in Method 1. Method 2 demonstrates that using the minimum cross section properties (Method 1) is too conservative for the flexural torsional buckling analysis.

A.4.3.3 Verification for flexural-torsional buckling of a column with edge-stiffened holes - Method 3

The flexure-torsional buckling loads of the Steelform columns with edge-stiffened holes from ABAQUS are within an on average unconservative 3% of the flexural buckling loads predicted by the weighted average approach using method 2 (compare $P_{cre,ABAQUS\ with\ holes}/P_{cre,avg}$ in Table A.4.2). St. Venant torsional constant, J_{avg}, and warping torsion constant, $C_{w,net}$ do change compared to Methods 1 and 2 therefore, the resulting difference is due to the moment of inertia properties as well as the torsion and warping constants. Ixx is greatly increased at the mid-hole section which what causes the buckling values to be unconservative. Method 3 demonstrates that

using the mid-hole cross section properties alone is too unconservative for the flexural torsional buckling analysis.

A.4.4 Verification for lateral-torsional buckling of members with edge-stiffened holes

A.4.4.1 Verification for lateral-torsional bucking of a beam with edge-stiffened holes – Method 1

The cold-formed steel Steelform members evaluated in the previous sections as columns are now evaluated as beams with uniform moments with the same methods as columns. The beam ends are modeled as pinned warping-free and the cross-section at the longitudinal midline is warping-fixed. The critial elastic lateral-torsional buckling moment, M_{cre}, decreases with the presence of edge-stiffened holes by a maximum of 18% as shown in Table A.4.7. The "weighted average" prediction method is demonstrated to be an accurate predictor of M_{cre} within 6% on average when compared to the ABAQUS eigen-buckling results (see $M_{cre,ABAQUS\ with\ holes}/M_{cre,avg}$ in Table A.4.7). The unconservative prediction is a function of thickness, the thicker members buckling load is predicted much closer to the eigen-buckling results. Since the buckling predictions are a function of thickness, it can be concluded there is increased transverse bending in the cross section that cannot be accounted for in the classical buckling equation. This method is the best of all three methods looked at in this study.

Table A.4.7 Influence of edge-stiffened holes on beam global buckling – Method 1

Buckling Mode	Comparison		Steelform Section								ABAQUS-to-predicted statistics	
			3625-33 L=80 in	3625-43 L=80 in	3625-54 L=80 in	3625-68 L=80 in	6000-33 L=80 in	6000-43 L=80 in	6000-54 L=80 in	6000-68 L=80 in	Mean	COV
Beam lateral-torsional buckling	$M_{cre,CLASSICAL\ no\ holes}$ [a]	(kip in.)	8.47	11.12	14.11	18.29	14.91	19.38	24.12	30.45		
	$M_{cre,ABAQUS\ no\ holes}$	(kip in.)	8.27	10.93	13.96	18.11	14.87	19.29	23.94	30.29		
	$M_{cre,ABAQUS\ with\ holes}$	(kip in.)	6.94	9.13	11.58	14.99	12.42	16.68	20.22	24.86		
	$M_{cre,avg}$	(kip in.)	7.35	9.59	11.74	15.13	12.80	16.34	19.94	24.86		
	$M_{cre,ABAQUS\ no\ holes}/M_{cre,CLASSICAL\ no\ holes}$ [a]		0.98	0.98	0.99	0.99	1.00	1.00	0.99	0.99	0.99	0.01
	$M_{cre,ABAQUS\ with\ holes}/M_{cre,ABAQUS\ no\ holes}$		0.84	0.84	0.83	0.83	0.84	0.86	0.84	0.82	0.84	0.02
	$M_{cre,ABAQUS\ with\ holes}/M_{cre,avg}$		0.94	0.95	0.99	0.99	0.97	1.02	1.01	1.00	0.98	0.03

[a] The critical lateral-torsional buckling moment for a beam without holes is denoted as $M_{cre,CLASSICAL\ no\ holes}$

A.4.4.2 Verification for lateral-torsional bucking of a beam with edge-stiffened holes – Method 2

Method 2 using the worst section properties is demonstrated to be an a slightly inaccurate predictor of M_{cre} within a maximum of 8% when compared to the ABAQUS eigen-buckling results (see $M_{cre,ABAQUS\ with\ holes}/M_{cre,avg}$ in Table A.4.8). The unconservative prediction is a function of thickness as in Method 1 where the thicker members buckling load is predicted much closer to the eigen-buckling results. This method predicts a much more unconservative buckling load due to the section being chosen. The moment of inertia in the weak axis is higher for the 3.625" members whereas for the 6.000" members it stayed the same (Refer to Table 5.2 for clarification). Therefore, the 3.625" members buckling load is driven up which causes discrepancy when looking at the mean. Compare $M_{cre,ABAQUS\ with\ holes}/M_{cre,avg}$ in Table A.4.8 to the same row in Table A.4.7.

Table A.4.8 Influence of edge-stiffened holes on beam global buckling – Method 2

Buckling Mode	Comparison		Steelform Section								ABAQUS-to-predicted statistics	
			3625-33	3625-43	3625-54	3625-68	6000-33	6000-43	6000-54	6000-68		
			L=80 in	L=80 in	L=80 in	L=80 in	L=80 in	L=80 in	L=80 in	L=80 in	Mean	COV
Beam lateral-torsional buckling	$M_{cre,CLASSICAL\ no\ holes}$ [a]	(kip in.)	8.47	11.12	14.11	18.29	14.91	19.38	24.12	30.45		
	$M_{cre,ABAQUS\ no\ holes}$	(kip in.)	8.27	10.93	13.96	18.11	14.87	19.29	23.94	30.29		
	$M_{cre,ABAQUS\ with\ holes}$	(kip in.)	6.94	9.13	11.58	14.99	12.42	16.68	20.22	24.86		
	$M_{cre,avg}$	(kip in.)	7.52	9.82	11.96	15.52	12.80	16.34	19.94	24.86		
	$M_{cre,ABAQUS\ no\ holes}/M_{cre,CLASSICAL\ no\ holes}$ [a]		0.98	0.98	0.99	0.99	1.00	1.00	0.99	0.99	0.99	0.01
	$M_{cre,ABAQUS\ with\ holes}/M_{cre,ABAQUS\ no\ holes}$		0.84	0.84	0.83	0.83	0.84	0.86	0.84	0.82	0.84	0.02
	$M_{cre,ABAQUS\ with\ holes}/M_{cre,avg}$		0.92	0.93	0.97	0.97	0.97	1.02	1.01	1.00	0.97	0.04

[a] The critical lateral-torsional buckling moment for a beam without holes is denoted as $M_{cre,CLASSICAL\ no\ holes}$

A.4.4.3 Verification for lateral-torsional bucking of a beam with edge-stiffened holes – Method 3

Method 3 using the mid-hole properties is demonstrated to be an a highly inaccurate predictor of M_{cre} within a maximum of 13% when compared to the ABAQUS eigen-buckling results (see $M_{cre,ABAQUS\ with\ holes}/M_{cre,avg}$ in Table A.4.9). The unconservative prediction does not seem to be function of thickness as it was in Methods 1 and 2. This method predicts a much more unconservative buckling load due to the cross section properties being chosen. As mentioned in previous sections, the weak-axis moment of inertia in the is higher at mid-hole than in other sections taken.

Table A.4.9 Influence of edge-stiffened holes on beam global buckling – Method 3

Buckling Mode	Comparison		Steelform Section								ABAQUS-to-predicted statistics	
			3625-33	3625-43	3625-54	3625-68	6000-33	6000-43	6000-54	6000-68		
			L=80 in	L=80 in	L=80 in	L=80 in	L=80 in	L=80 in	L=80 in	L=80 in	Mean	COV
Beam lateral-torsional buckling	$M_{cre,CLASSICAL\ no\ holes}$ [a]	(kip in.)	8.47	11.12	14.11	18.29	14.91	19.38	24.12	30.45		
	$M_{cre,ABAQUS\ no\ holes}$	(kip in.)	8.27	10.93	13.96	18.11	14.87	19.29	23.94	30.29		
	$M_{cre,ABAQUS\ with\ holes}$	(kip in.)	6.94	9.13	11.58	14.99	12.42	16.68	20.22	24.86		
	$M_{cre,avg}$	(kip in.)	7.92	10.36	13.09	17.23	13.08	16.92	20.75	26.54		
	$M_{cre,ABAQUS\ no\ holes}/M_{cre,CLASSICAL\ no\ holes}$ [a]		0.98	0.98	0.99	0.99	1.00	1.00	0.99	0.99	0.99	0.01
	$M_{cre,ABAQUS\ with\ holes}/M_{cre,ABAQUS\ no\ holes}$		0.84	0.84	0.83	0.83	0.84	0.86	0.84	0.82	0.84	0.02
	$M_{cre,ABAQUS\ with\ holes}/M_{cre,avg}$		0.88	0.88	0.88	0.87	0.95	0.99	0.97	0.94	0.92	0.05

[a] The critical lateral-torsional buckling moment for a beam without holes is denoted as $M_{cre,CLASSICAL\ no\ holes}$

A.4.5.Verification for distortional buckling of members with edge-stiffened holes

A.4.5.1 Verification for distortional bucking of members with edge-stiffened holes – Method 1

The first method assumes the most conservative edge-stiffener length, Q_{hole1} , which only exists around the vertical sections of holes. This method also uses the hole length as specified in Figure 5.2b(L_{hole1}) which is the longest hole horizontal leg dimension.

The finite strip simplified equations using Method 1 for predicting P_{crdh} and M_{crdh} using the modified web thickness in Eq. 4.11 and n=1, m=3 for columns, n=1, m=1 for beams, is an accurate predictor of P_{crdh} (ABAQUS-to-predicted mean of 1.26 for columns in Table A.4.10, 1.03 for beams in Table A.4.11), however the coefficient of variation (COV) of the ABAQUS-to-predicted buckling loads is high, especially for columns (0.25 for columns, 0.05 for beams). The overall distortional buckling prediction, $P_{crd,simp}$ is in good agreement with $P_{crd,ABAQUS.}$ In some cases the finite strip distortional buckling prediction is lower than the ABAQUS results ($P_{crd,\ ABAQUS}/P_{crd,simp}$=0.92 and 0.93 for the 3625-68 and 3625-43 columns in Table A.4.10) but is good agreement with $M_{crd,ABAQUS}$ for all beams considered(See $M_{crd,\ ABAQUS}/M_{crd,simp}$ in Table A.4.11).

The simplified methods predict buckling loads very close to the defined end distortional buckling mode as shown in Figure 5.5c. As there is no defined gross section long enough to accept a distortional half-wavelength by itself, concluding that there only exists a hole mode in the Steelform members considered: the end mode which engages holes and a higher order typical looking distortional buckling mode. ABAQUS eigen-buckling results show that with the full edge-stiffener accounted for, the hole provides enough rotational restraint to boost distortional

buckling loads (Except for the 3625-68 and 6000-68 members which distortional buckling decreases). However, the simplified methods are conservative and suggest that the hole stiffener $Q=Q_{hole1}$ does not provide enough rotational restraint to the compressed flanges to compensate for the loss in web material at the hole, resulting in distortional buckling occurring at holes lower than that of members without holes. This is true for all columns analyzed, however, all the 6.000" beams considered except for 6000-68 beam, the edge stiffeners do provide enough restraint and the hole mode is higher than the no hole mode by a maximum of 20%. Although, the simplified methods take the minimum of $M_{crdh,simp}$ and $M_{crdnh,simp}$, looking at Table A.4.11, if $M_{crd,simp}$ is taken as the hole mode is taken as $M_{crdh,simp,}$ there is good agreement between ABAQUS eigen-buckling analysis and the simplified values with a mean less than $M_{crdh,ABAQUS}/M_{crdh,simp}$ at 1.03 compared to 1.09. This means that when subjected to flexure, the edge stiffeners provide adequate rotational restraint and actually boost the distortional buckling load.

Table A.4.10 Influence of edge-stiffened holes on column distortional buckling – Method 1

Steelform Section	$P_{crdnh,simp}$ (kip)	$L_{crd,nh}$ (in.)	t_r/Q	$P_{crdh,simp}$ (kip)	$P_{crd,simp}$ (kip)	$P_{crdend,ABAQUS}$ (kip)	$L_{crdend,ABAQUS}$ (in.)	$P_{crdh,ABAQUS}$ (kip)	$L_{crd,ABAQUS}$ (in.)	$P_{crd,ABAQUS}$ (kip)	$P_{crdend,ABAQUS}/P_{crdh,simp}$	$P_{crdh,ABAQUS}/P_{crdh,simp}$	$P_{crd,ABAQUS}/P_{crd,simp}$
Columns													
3625-33	9.56	20.00	0.13	8.92	8.92	10.10	15.00	14.20	20.00	10.10	1.13	1.59	1.13
3625-43	16.70	17.00	0.17	15.38	15.38	14.30	12.30	24.76	16.00	14.30	0.93	1.61	0.93
3625-54	27.00	15.00	0.21	24.80	24.80	27.60	12.10	38.41	16.00	27.60	1.11	1.55	1.11
3625-68	44.60	13.00	0.26	40.31	40.31	37.00	10.90	61.88	13.33	37.00	0.92	1.54	0.92
6000-33	6.02	19.50	0.10	4.72	4.72	7.10	16.50	13.34	20.00	7.10	1.51	2.83	1.51
6000-43	9.74	16.50	0.12	8.08	8.08	14.85	15.50	21.86	20.00	14.85	1.84	2.71	1.84
6000-54	15.50	15.30	0.15	12.89	12.89	17.70	15.40	34.90	20.00	17.70	1.37	2.71	1.37
6000-68	26.00	13.50	0.19	20.73	20.73	25.80	11.60	55.98	20.00	25.80	1.24	2.70	1.24
							ABAQUS-to-predicted statistics			Mean	1.26	2.15	1.26
										COV	0.25	0.29	0.25

Table A.4.11 Influence of edge-stiffened holes on beam distortional buckling – Method 1

Steelform Section	$M_{crdnh,simp}$ (kip-in.)	$L_{crd,nh}$ (in.)	t_r/Q	$M_{crdh,simp}$ (kip)	$M_{crd,simp}$ (kip)	$M_{crdend,ABAQUS}$ (kip-in.)	$L_{crdend,ABAQUS}$ (in.)	$M_{crdh,ABAQUS}$ (kip-in.)	$L_{crd,ABAQUS}$ (in.)	$M_{crd,ABAQUS}$ (kip-in.)	$M_{crdend,ABAQUS}/M_{crdh,simp}$	$M_{crdh,ABAQUS}/M_{crdh,simp}$	$M_{crd,ABAQUS}/M_{crd,simp}$
Beams													
3625-33	19.62	17.90	0.14	20.02	19.62	N/A		21.45	16.00	21.45	N/A	1.07	1.09
3625-43	33.90	15.40	0.18	33.83	33.83	N/A		36.15	16.00	36.15	N/A	1.07	1.07
3625-54	54.66	13.60	0.22	53.57	53.57	N/A		56.43	13.33	56.43	N/A	1.05	1.05
3625-68	88.95	11.90	0.27	85.60	85.60	N/A		88.30	11.91	88.30	N/A	1.03	1.03
6000-33	28.13	19.30	0.12	34.85	28.13	N/A		32.18	20.00	32.18	N/A	0.92	1.14
6000-43	49.39	16.70	0.15	56.12	49.39	N/A		56.58	16.00	56.58	N/A	1.01	1.15
6000-54	80.72	14.80	0.18	85.42	80.72	N/A		90.21	16.00	90.21	N/A	1.06	1.12
6000-68	133.24	13.00	0.22	131.59	131.59	N/A		140.48	13.30	140.48	N/A	1.07	1.07
							ABAQUS-to-predicted statistics			Mean	N/A	1.03	1.09
										COV	N/A	0.05	0.04

A.4.5.2 Verification for distortional bucking of members with edge-stiffened holes – Method 2

Since ABAQUS is predicting that distortional buckling loads are increased and not decreased in most members due to the presence of edge-stiffened holes, Method 2 uses a weighted average stiffener length (Q_{avg}) based on the stiffener heights and their lengths around the hole. This is done because equation 4.11 assumes that only the vertical stiffener parts are contributing to the stiffness of the web with an edge-stiffened hole. The vertical stiffener is also varying to a point around the edges(See Steelform details).To make sure that is a reasonable assumption, using the weighted average will take into account the large stiffener at the top and bottom of the holes. The length of the holes remains the same as Method 1. Table 5.4 shows the differences between the two methods.

The finite strip simplified equations using Method 2 for predicting P_{crdh} using the modified web thickness in Eq. 4.11 and n=1, m=3 for columns, is on average a better predictor of P_{crdh} (ABAQUS-to-predicted mean of 1.11 for columns in Table A.4.12). The coefficient of variation (COV) of the ABAQUS-to-predicted buckling loads decreases slightly compared to Method 1, especially for columns (0.17 for columns, compare that to .25 in Method 1). In some cases the finite strip distortional buckling prediction is lower than the ABAQUS results ($P_{crd,ABAQUS}/P_{crd,simp}$=0.91 for the 3625-68 and 0.93 for the 3625-43 columns in Table A.4.12 and 0.93 for the 6000-68 beam in Table A.4.13). The COV drops to 0.28 for beams (Compare to .05 for Method 1) because the simplified methods over predict the hole distortional loads by a large margin.

Just as in Method 1, when subjected to compression, the simplified methods predict buckling loads very close to the defined end distortional buckling mode as shown in Figure 5.5c. However, the simplified methods are still predicting that hole stiffeners with $Q = Q_{avg}$ do not provide enough rotational restraint to the compressed flanges to compensate for the loss in web material at the hole, resulting in distortional buckling occurring at holes even though ABAQUS predicts otherwise. Looking at Table A.4.13, It should be noted that the prediction equations are very unconservative in all cases for members subjected to flexure up to a maximum of 9% for the 3.625" members and 51% for the 6.000% when comparing $M_{crdh,simp}$ to $M_{crdh,ABAQUS}$. However, because the prediction methods call for the minimum of $M_{crdh,simp}$ and $M_{crdnh,simp}$ the agreement is ok since the no hole distortional buckling loads are not too far off from the hole loads. Method 2 shows that even a slight overestimation in the contribution of the edge stiffeners can cause unconservative results.

Table A.4.12 Influence of edge-stiffened holes on column distortional buckling – Method 2

Steelform Section	$P_{crdnh,simp}$ (kip)	$L_{crd,nh}$ (in.)	t_r/Q	$P_{crdh,simp}$ (kip)	$P_{crd,simp}$ (kip)	$P_{crdend,ABAQUS}$ (kip)	$L_{crdend,ABAQUS}$ (in.)	$P_{crdh,ABAQUS}$ (kip)	$L_{crd,ABAQUS}$ (in.)	$P_{crd,ABAQUS}$ (kip)	$P_{crdend,ABAQUS}/P_{crdh,simp}$	$P_{crdh,ABAQUS}/P_{crdh,simp}$	$P_{crd,ABAQUS}/P_{crd,simp}$
Columns													
3625-33	9.56	20.00	0.08	8.95	8.95	10.10	15.00	14.20	20.00	10.10	1.13	1.59	1.13
3625-43	16.70	17.00	0.11	15.45	15.45	14.30	12.30	24.76	16.00	14.30	0.93	1.60	0.93
3625-54	27.00	15.00	0.13	24.91	24.91	27.60	12.10	38.41	16.00	27.60	1.11	1.54	1.11
3625-68	44.60	13.00	0.17	40.51	40.51	37.00	10.90	61.88	13.33	37.00	0.91	1.53	0.91
6000-33	6.02	19.50	0.06	6.06	6.02	7.10	16.50	13.34	20.00	7.10	1.17	2.20	1.18
6000-43	9.74	16.50	0.08	10.79	9.74	14.85	15.50	21.86	20.00	14.85	1.38	2.03	1.52
6000-54	15.50	15.30	0.10	16.94	15.50	17.70	15.40	34.90	20.00	17.70	1.04	2.06	1.14
6000-68	26.00	13.50	0.13	28.01	26.00	25.80	11.60	55.98	20.00	25.80	0.92	2.00	0.99
							ABAQUS-to-predicted statistics			Mean	1.07	1.82	1.11
										COV	0.15	0.15	0.17

Table A.4.13 Influence of edge-stiffened holes on beam distortional buckling – Method 2

Steelform Section	$M_{crdnh,simp}$ (kip-in.)	$L_{crd,nh}$ (in.)	t_r/Q	$M_{crdh,simp}$ (kip)	$M_{crd,simp}$ (kip)	$M_{crdend,ABAQUS}$ (kip-in.)	$L_{crdend,ABAQUS}$ (in.)	$M_{crdh,ABAQUS}$ (kip-in.)	$L_{crd,ABAQUS}$ (in.)	$M_{crd,ABAQUS}$ (kip-in.)	$M_{crdend,ABAQUS}/M_{crdh,simp}$	$M_{crdh,ABAQUS}/M_{crdh,simp}$	$M_{crd,ABAQUS}/M_{crd,simp}$
Beams													
3625-33	19.62	17.90	0.10	23.35	19.62	N/A		21.45	16.00	21.45	N/A	0.92	1.09
3625-43	33.90	15.40	0.13	38.57	33.90	N/A		36.15	16.00	36.15	N/A	0.94	1.07
3625-54	54.66	13.60	0.15	60.09	54.66	N/A		56.43	13.33	56.43	N/A	0.94	1.03
3625-68	88.95	11.90	0.19	97.26	88.95	N/A		88.30	11.91	88.30	N/A	0.91	0.99
6000-33	28.13	19.30	0.11	66.23	28.13	N/A		32.18	20.00	32.18	N/A	0.49	1.14
6000-43	49.39	16.70	0.13	104.55	49.39	N/A		56.58	16.00	56.58	N/A	0.54	1.15
6000-54	80.72	14.80	0.15	156.38	80.72	N/A		90.21	16.00	90.21	N/A	0.58	1.12
6000-68	133.24	13.00	0.18	236.57	133.24	N/A		140.48	13.30	140.48	N/A	0.59	1.05
							ABAQUS-to-predicted statistics			Mean	N/A	0.74	1.08
										COV	N/A	0.28	0.05

A.4.5.3 Verification for distortional bucking of members with edge-stiffened holes – Method 3

The simplified prediction equations are based on an input of a hole length, and varying the hole length can drastically change the equation as it appears in the prediction equation multiple times. As the hole length increases relative to the distortional half-wavelength, the stiffeners are assumed to be less effective at restraining the compression flanges. Therefore, Method 3 sets the hole length equal to L_{hole3} in Figure 5.1 to see the effects on the predicted distortional buckling loads. The edge stiffeners will be assumed equal to Q_{hole1} as in Method 1 since that stiffener length was more accurate overall when compared to Method 2 results.

The finite strip simplified equations using Method 3 for predicting P_{crdh} and M_{crdh} using the modified web thickness in Eq. 4.11 and n=1, m=3 for columns, n=1, m=1 for beams, is a more conservative predictor of P_{crdh} compared to Methods 1 and 2(ABAQUS-to-predicted mean of 1.28 for columns in Table A.4.14, 1.03 for beams in Table A.4.15), with the coefficient of variation (COV) of the ABAQUS-to-predicted buckling loads decreasing slightly compared to Method 1, especially for columns (0.22 for columns, compare that to .25 in Method 1). The COV increases to 0.06 for beams (Compare to .05 for Method 1). In some cases the finite strip distortional buckling prediction is still lower than the ABAQUS results ($P_{crd,\ ABAQUS}/P_{crd,simp}$=0.97 for the 3625-43 and 3625-68 columns in Table A.4.14). For beams, is less conservative than Method 1 with a maximum unconservative estimation of a 12% maximum for the 6000-33 beam in Table A.4.15). Since, the prediction methods call for the minimum of $M_{crdh,simp}$ and $M_{crdnh,simp}$ the agreement is satisfactory since the no hole distortional buckling loads are not too far off from the hole loads (See $P_{crd,ABAQUS}/P_{crd,simp}$ and $M_{crd,ABAQUS}/M_{crd,simp}$).

Table A.4.14 Influence of edge-stiffened holes on column distortional buckling – Method 3

Steelform Section	$P_{crdnh,simp}$ (kip)	$L_{crd,nh}$ (in.)	t_r /Q	$P_{crdh,simp}$ (kip)	$P_{crd,simp}$ (kip)	$P_{crdend,ABAQUS}$ (kip)	$L_{crdend,ABAQUS}$ (in.)	$P_{crdh,ABAQUS}$ (kip)	$L_{crd,ABAQUS}$ (in.)	$P_{crd,ABAQUS}$ (kip)	$P_{crdend,ABAQUS}$ /$P_{crdh,simp}$	$P_{crdh,ABAQUS}$ /$P_{crdh,simp}$	$P_{crd,ABAQUS}$ /$P_{crd,simp}$
Columns													
3625-33	9.56	20.00	0.13	8.64	8.64	10.10	15.00	14.20	20.00	10.10	1.17	1.64	1.17
3625-43	16.70	17.00	0.16	14.81	14.81	14.30	12.30	24.76	16.00	14.30	0.97	1.67	0.97
3625-54	27.00	15.00	0.20	23.74	23.74	27.60	12.10	38.41	16.00	27.60	1.16	1.62	1.16
3625-68	44.60	13.00	0.25	38.33	38.33	37.00	10.90	61.88	13.33	37.00	0.97	1.61	0.97
6000-33	6.02	19.50	0.10	4.75	4.75	7.10	16.50	13.34	20.00	7.10	1.50	2.81	1.50
6000-43	9.74	16.50	0.13	8.15	8.15	14.85	15.50	21.86	20.00	14.85	1.82	2.68	1.82
6000-54	15.50	15.30	0.15	12.79	12.79	17.70	15.40	34.90	20.00	17.70	1.38	2.73	1.38
6000-68	26.00	13.50	0.18	20.43	20.43	25.80	11.60	55.98	20.00	25.80	1.26	2.74	1.26
							ABAQUS-to-predicted statistics			Mean	1.28	2.19	1.28
										COV	0.22	0.27	0.22

Table A.4.15 Influence of edge-stiffened holes on beam distortional buckling – Method 3

Steelform Section	$M_{crdnh,simp}$ (kip-in.)	$L_{crd,nh}$ (in.)	t_r /Q	$M_{crdh,simp}$ (kip)	$M_{crd,simp}$ (kip)	$M_{crdend,ABAQUS}$ (kip-in.)	$L_{crdend,ABAQUS}$ (in.)	$M_{crdh,ABAQUS}$ (kip-in.)	$L_{crd,ABAQUS}$ (in.)	$M_{crd,ABAQUS}$ (kip-in.)	$M_{crdend,ABAQUS}$ /$M_{crdh,simp}$	$M_{crdh,ABAQUS}$ /$M_{crdh,simp}$	$M_{crd,ABAQUS}$ /$M_{crd,simp}$
Beams													
3625-33	19.62	17.90	0.14	20.22	19.62	N/A		21.45	16.00	21.45	N/A	1.06	1.09
3625-43	33.90	15.40	0.18	33.80	33.80	N/A		36.15	16.00	36.15	N/A	1.07	1.07
3625-54	54.66	13.60	0.22	52.99	52.99	N/A		56.43	13.33	56.43	N/A	1.06	1.06
3625-68	88.95	11.90	0.26	83.83	83.83	N/A		88.30	11.91	88.30	N/A	1.05	1.05
6000-33	28.13	19.30	0.13	36.44	28.13	N/A		32.18	20.00	32.18	N/A	0.88	1.14
6000-43	49.39	16.70	0.16	57.91	49.39	N/A		56.58	16.00	56.58	N/A	0.98	1.15
6000-54	80.72	14.80	0.18	86.77	80.72	N/A		90.21	16.00	90.21	N/A	1.04	1.12
6000-68	133.24	13.00	0.22	131.35	131.35	N/A		140.48	13.30	140.48	N/A	1.07	1.07
							ABAQUS-to-predicted statistics			Mean	N/A	1.03	1.09
										COV	N/A	0.06	0.03

A.4.5.4 Verification for distortional bucking of members with edge-stiffened holes – Method 4

Method 4 looks at averaging only the vertical stiffener lengths. Since there is such a large horizontal stiffener on both sides of the holes, and the prediction equations only take into account the additional stiffness from the vertical stiffeners, this method will eliminate the effects of the other stiffeners. The edge stiffeners will be assumed equal to 2/3 the height of $Q_{hole2.}$ The hole length will be the same as Method 1 as that seemed the most accurate.

The finite strip simplified equations using Method 4 for predicting P_{crdh} and M_{crdh} using the modified web thickness in Eq. 4.11 and n=1, m=3 for columns, n=1, m=1 for beams, accurately predicts P_{crdh} compared to Methods 1 and 2 and 3(ABAQUS-to-predicted mean of 1.22 for columns in Table A.4.16, 0.93 for beams in Table A.4.17), with the coefficient of variation (COV) of the ABAQUS-to-predicted buckling loads decreasing slightly compared to Method 1, especially for columns (0.23 for columns, compare that to .25 in Method 1). The COV

increases to 0.09 for beams (Compare to .05 for Method 1). In some cases the finite strip distortional buckling prediction is still lower than the ABAQUS results ($P_{crd,\ ABAQUS}/P_{crd,simp}$=0.92 for the 3625-43 and 0.93 for the 3625-68 columns in Table A.4.16). This method predicts very accurately the distortional buckling load at a hole within 2%, ($M_{crdh,ABAQUS}/M_{crdh,simp}$ in Table A.4.17), however, it fails to predict the 6.000" beams accurately with a maximum error of 22% in the thinnest 6000-33 beam. Since, the prediction methods call for the minimum of $M_{crdh,simp}$ and $M_{crdnh,simp}$ the agreement is satisfactory since the no hole distortional buckling loads are not too far off from the hole loads (See $P_{crd,ABAQUS}/P_{crd,simp}$ and $M_{crd,ABAQUS}/M_{crd,simp}$.

Table A.4.16 Influence of edge-stiffened holes on column distortional buckling – Method 4

Steelform Section	$P_{crdnh,simp}$ (kip)	$L_{crd,nh}$ (in.)	t_r /Q	$P_{crdh,simp}$ (kip)	$P_{crd,simp}$ (kip)	$P_{crdend,ABAQUS}$ (kip)	$L_{crdend,ABAQUS}$ (in.)	$P_{crdh,ABAQUS}$ (kip)	$L_{crd,ABAQUS}$ (in.)	$P_{crd,ABAQUS}$ (kip)	$P_{crdend,ABAQUS}$ /$P_{crdh,simp}$	$P_{crdh,ABAQUS}$ /$P_{crdh,simp}$	$P_{crd,ABAQUS}$ /$P_{crd,simp}$
Columns													
3625-33	9.56	20.00	0.10	8.93	8.93	10.10	15.00	14.20	20.00	10.10	1.13	1.59	1.13
3625-43	16.70	17.00	0.13	15.41	15.41	14.30	12.30	24.76	16.00	14.30	0.93	1.61	0.93
3625-54	27.00	15.00	0.16	24.84	24.84	27.60	12.10	38.41	16.00	27.60	1.11	1.55	1.11
3625-68	44.60	13.00	0.20	40.40	40.40	37.00	10.90	61.88	13.33	37.00	0.92	1.53	0.92
6000-33	6.02	19.50	0.08	4.89	4.89	7.10	16.50	13.34	20.00	7.10	1.45	2.73	1.45
6000-43	9.74	16.50	0.11	8.46	8.46	14.85	15.50	21.86	20.00	14.85	1.75	2.58	1.75
6000-54	15.50	15.30	0.13	13.46	13.46	17.70	15.40	34.90	20.00	17.70	1.31	2.59	1.31
6000-68	26.00	13.50	0.16	21.79	21.79	25.80	11.60	55.98	20.00	25.80	1.18	2.57	1.18
						ABAQUS-to-predicted statistics				Mean	1.22	2.09	1.22
										COV	0.23	0.27	0.23

Table A.4.17 Influence of edge-stiffened holes on beam distortional buckling – Method 4

Steelform Section	$M_{crdnh,simp}$ (kip-in.)	$L_{crd,nh}$ (in.)	t_r /Q	$M_{crdh,simp}$ (kip)	$M_{crd,simp}$ (kip)	$M_{crdend,ABAQUS}$ (kip-in.)	$L_{crdend,ABAQUS}$ (in.)	$M_{crdh,ABAQUS}$ (kip-in.)	$L_{crd,ABAQUS}$ (in.)	$M_{crd,ABAQUS}$ (kip-in.)	$M_{crdend,ABAQUS}$ /$M_{crdh,simp}$	$M_{crdh,ABAQUS}$ /$M_{crdh,simp}$	$M_{crd,ABAQUS}$ /$M_{crd,simp}$
Beams													
3625-33	19.62	17.90	0.11	21.58	19.62	N/A		21.45	16.00	21.45	N/A	0.99	1.09
3625-43	33.90	15.40	0.14	36.02	33.90	N/A		36.15	16.00	36.15	N/A	1.00	1.07
3625-54	54.66	13.60	0.18	56.55	54.66	N/A		56.43	13.33	56.43	N/A	1.00	1.03
3625-68	88.95	11.90	0.22	89.69	88.95	N/A		88.30	11.91	88.30	N/A	0.98	0.99
6000-33	28.13	19.30	0.12	41.25	28.13	N/A		32.18	20.00	32.18	N/A	0.78	1.14
6000-43	49.39	16.70	0.14	65.68	49.39	N/A		56.58	16.00	56.58	N/A	0.86	1.15
6000-54	80.72	14.80	0.17	98.87	80.72	N/A		90.21	16.00	90.21	N/A	0.91	1.12
6000-68	133.24	13.00	0.20	150.64	133.24	N/A		140.48	13.30	140.48	N/A	0.93	1.05
						ABAQUS-to-predicted statistics				Mean	N/A	0.93	1.08
										COV	N/A	0.09	0.05

APPENDIX B - MBMA DISTORTIONAL STUDY

APPENDIX B.1 Miscellaneous Test Details

APPENDIX B.2 Pressure Box Experiment Results

APPENDIX B.1 Miscellaneous Test Details

Presented are miscellaneous details related to MBMA testing performed in Chapter 6.

Roofing Panel Provided by VP Buildings

VP ROOF SYSTEMS

STYLE	FEATURES
PANEL RIB ROOF	THE MOST ECONOMICAL CHOICE FOR A GOOD LOOKING, HIGH-QUALITY AND LOW MAINTENANCE METAL ROOF

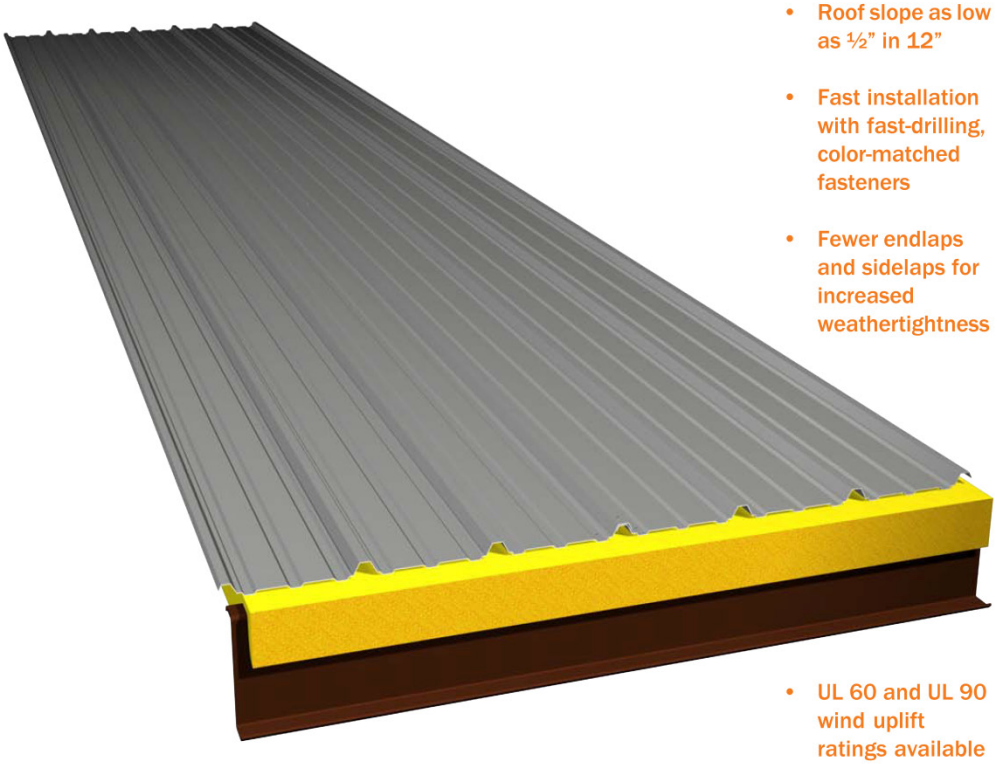

- Roof slope as low as ½" in 12"
- Fast installation with fast-drilling, color-matched fasteners
- Fewer endlaps and sidelaps for increased weathertightness
- UL 60 and UL 90 wind uplift ratings available

Panel Rib Roof has a reputation as an economical, quality roof. Built-up and single ply membrane roofs cannot match the economy and integrity of this VP roof system.

VP BUILDINGS
VARCO PRUDEN

Roofing Panel Provided by VP Buildings (continued)

PANEL RIB ROOF PANELS OFFER ENHANCED ROOF INTEGRITY AND QUICKER INSTALLATION

PANEL RIB ROOF

If you are on a tight budget, but still need an attractive, high-quality, low-maintenance roof, VP's Panel Rib Roof offers the best combination of economy and durability.

Panel Rib Roof panels are standard in 26 gauge with 24 gauge and 22 gauge options. The steel panel is 36" wide with 1 ¼"-high ribs and is available in lengths up to 41'. The panel includes a purlin bearing edge (PBE) for superior strength and rigidity. Additionally, a narrow ridge (anti-capillary bead) runs the length of each sidelap for increased weathertightness.

The panels are attached with self-drilling, color-matched fasteners. Installation is fast since no field seaming is required. In addition, the panel's wide module and long length minimizes sidelaps and endlaps which increases both installation speed and improves weathertightness. Sealant is applied to every metal-to-metal contact point, resulting in a weather-resistant roof. Roof slope can be as low as ½:12.

Panel Rib Roof can accommodate up to 6 inches of fiberglass blanket insulation for high levels of energy efficiency.

All gauges of Panel Rib Roof are available with standard Galvalume finish. All gauges of Panel Rib are available in thirteen (13) standard colors with KXL finishes or four (4) color choices with SP finishes as well as a variety of custom colors. The KXL paint system is a PVDF finish applied to the Galvalume surface to give a long-life color that resists fading and chalking. KXL is a 1 mil nom. PVDF finish with a 70% Kynar 500 or Hylar 5000 standard.

Panel Rib Roof will meet the requirements for UL Class 60 or UL Class 90 wind uplift. VP meets the highest standards and certifications in the industry, including AISC and Miami-Dade County, Florida Product Approved:

NOA #02-0123.08 expires 03/07/2007
NOA #02-0417.01 expires 07/01/2007

For information about this or any other VP product or service, contact your local authorized VP Builder.

FEATURES

- Economical
- Roof slopes as low as ½" in 12"
- 36" coverage
- Lengths up to 41'-0"
- UL 60 and UL 90 wind uplift ratings available
- Dade County Product Approval
- Purlin bearings edge improves erectability

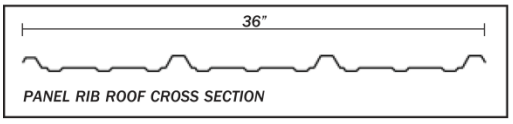

PANEL RIB ROOF CROSS SECTION

NOTE: ALL PANELS FORMED FROM LIGHT GAUGE METAL MAY EXHIBIT WAVINESS, ALSO KNOWN AS "OIL CANNING," COMMONLY OCCURRING IN, BUT NOT RESTRICTED TO, FLAT PORTIONS OF A PANEL. THIS INHERENT CHARACTERISTIC IS NOT A DEFECT OF MATERIAL OR MANUFACTURING AND IS NOT CAUSE FOR REJECTION.

VP BUILDINGS VARCO PRUDEN

The Ultimate Building Solution
VP Buildings
3200 Players Club Circle
Memphis, TN 38125
1-800-238-3246 • www.vp.com
2062 Revised 1/06

IAS

FM APPROVED ROOF ASSEMBLIES

AISC QUALITY CERTIFICATION METAL BUILDINGS

Cross Section Provided by Blue Scope Buildings

BLUESCOPE BUILDINGS

DP 20.1.1

SECTION PROPERTIES — Page 2 of 5

Zee Sections — Revision & Date 1 (06/10)

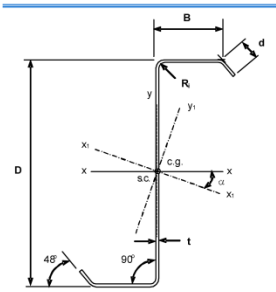

8 ½" Zee Section

D = 8 ½"
B = 2 ½"
R_i =0.3125"
F_y = 60 ksi
F_u = 70 ksi

j = 0.0"
m = 0.0"
x_o = 0.0"

Section Properties have been derived in accordance with AISI Standard "North American Specification for the Design of Cold-Formed Steel Structural Members", 2007 Edition
See DP 20.1 for definition of terms.

Full Properties											
Dimensions					Axis x-x			Axis y-y			α_1
Thick in.	Blank in.	Area in^2	Lip, d in.	Weight plf	I_x in^4	S_x in^3	r_x in.	I_y in^4	S_y in^3	r_y in.	deg.
0.060	14.500	0.870	0.766	2.99	9.30	2.19	3.266	1.24	0.42	1.195	-15.76
0.068	14.500	0.986	0.782	3.38	10.52	2.48	3.263	1.42	0.47	1.198	-15.83
0.073	14.750	1.077	0.916	3.69	11.52	2.71	3.267	1.69	0.55	1.253	-16.60
0.079	14.750	1.165	0.928	3.99	12.45	2.93	3.264	1.84	0.60	1.255	-16.65
0.088	14.750	1.298	0.945	4.44	13.84	3.26	3.260	2.06	0.67	1.259	-16.72
0.098	14.750	1.446	0.964	4.94	15.37	3.62	3.256	2.31	0.75	1.263	-16.81
0.113	14.750	1.667	0.993	5.70	17.67	4.16	3.250	2.69	0.87	1.269	-16.93

						Distortional Buckling				
	Full Properties					Critical Stress			Critical Unbraced Length	
Thick in.	J in^4	C_w in^6	r_o in.	I_{yc} in^4	I_{xy} in^4	$F_{db(0.0)}$ ksi	$F_{db(2.4)}$ ksi	$F_{da(0.0)}$ ksi	$L_{crd\text{-}bend}$ in.	$L_{crd\text{-}axial}$ in.
0.060	0.00105	15.749	3.478	0.622	2.470	31.22	180.14	14.36	21.19	23.43
0.068	0.00152	17.931	3.476	0.709	2.806	36.71	154.57	16.82	20.09	22.21
0.073	0.00192	21.538	3.499	0.847	3.214	42.66	155.67	20.52	21.48	23.75
0.079	0.00243	23.382	3.497	0.920	3.484	47.19	144.56	22.65	20.76	22.95
0.088	0.00336	26.172	3.495	1.031	3.889	54.26	133.81	25.96	19.83	21.92
0.098	0.00464	29.299	3.492	1.156	4.342	62.52	127.60	29.82	18.96	20.95
0.113	0.00712	34.050	3.489	1.347	5.024	75.68	125.69	35.95	17.89	19.76

	Effective Properties Evaluated at f = 60 ksi							Deflection Properties at f = 36 ksi	
	Axis x-x			Axis y-y					
Thick in.	I_{ex} in^4	S_{ex} in^3	M_{nxo} k-in.	I_{ey} in^4	S_{ey} in^3	M_{nyo} k-in.	$A_{e\ col}$ in^2	I_{dx} in^4	I_{dy} in^4
0.060	8.26	1.803	108.18	1.00	0.322	19.29	0.447	9.07	1.24
0.068	9.66	2.164	129.84	1.21	0.396	23.75	0.538	10.48	1.42
0.073	10.92	2.486	149.16	1.67	0.543	32.59	0.639	11.52	1.69
0.079	12.07	2.786	167.16	1.84	0.597	35.81	0.741	12.45	1.84
0.088	13.77	3.251	195.08	2.06	0.668	40.07	0.902	13.84	2.06
0.098	15.37	3.618	217.05	2.31	0.747	44.81	1.055	15.37	2.31
0.113	17.67	4.157	249.40	2.69	0.867	51.99	1.273	17.67	2.69

Author: Bob Hodges

Test Setup Details

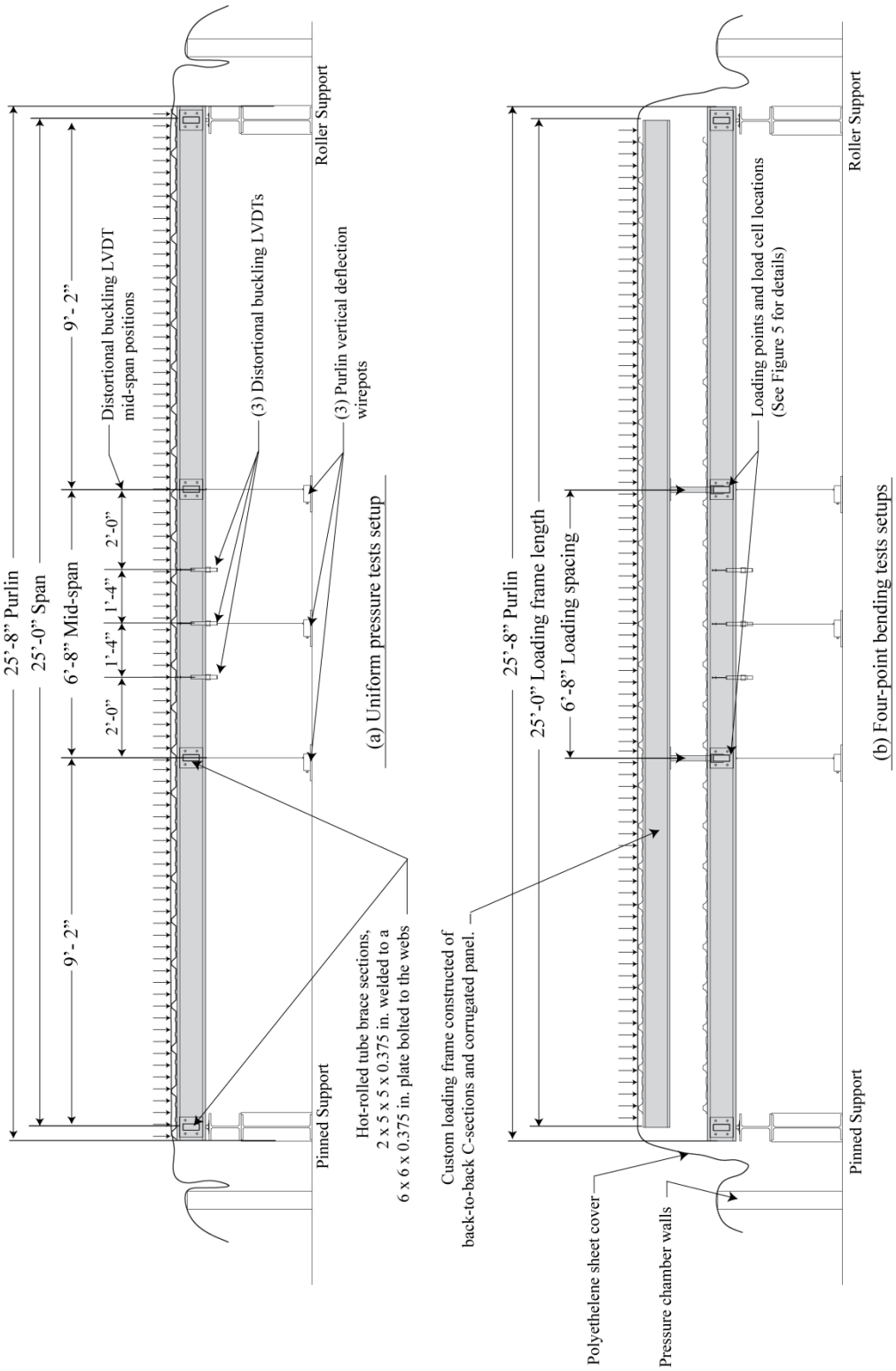

Instrumentation Details

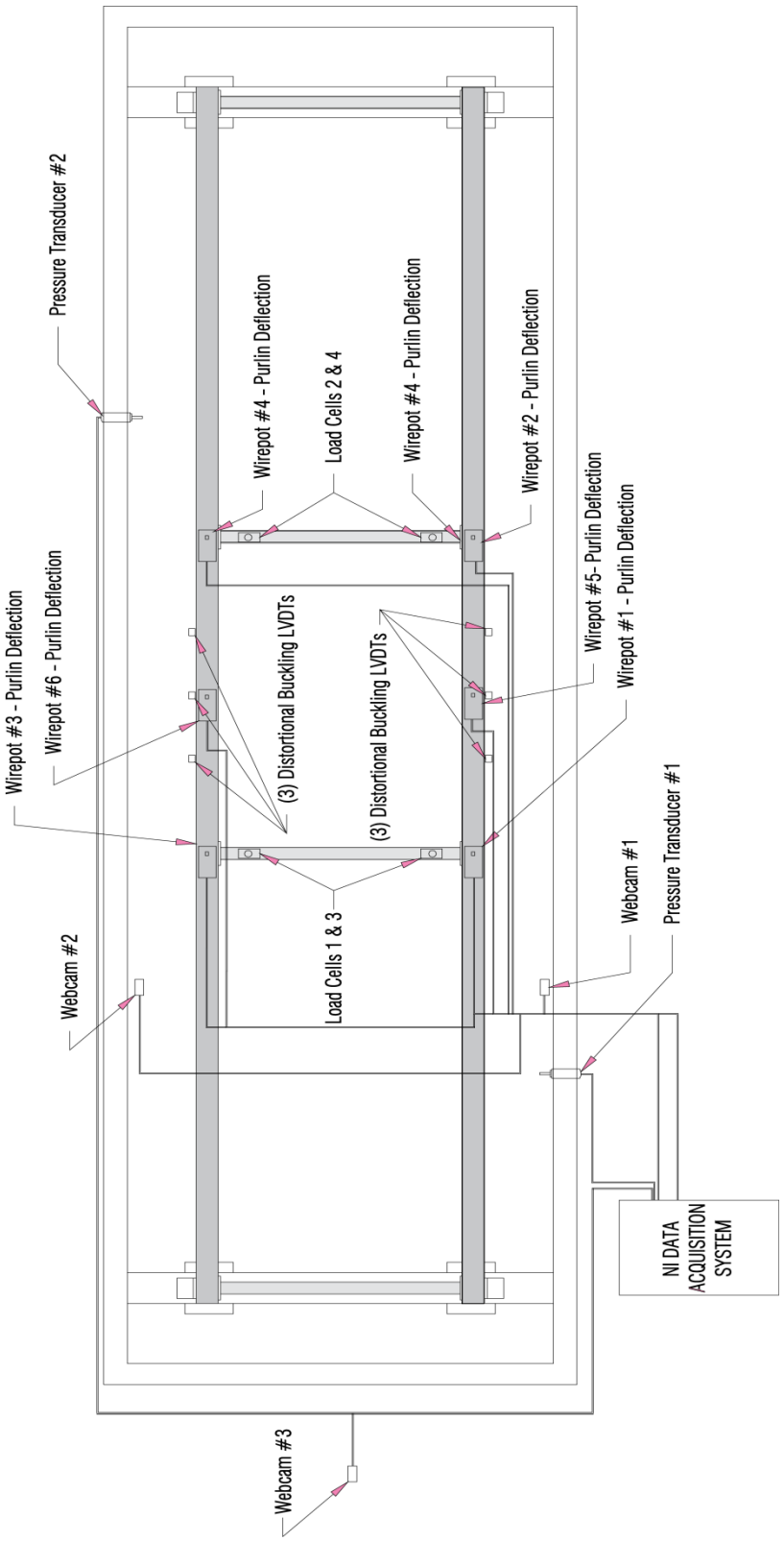

Distortional Buckling LVDT Locations

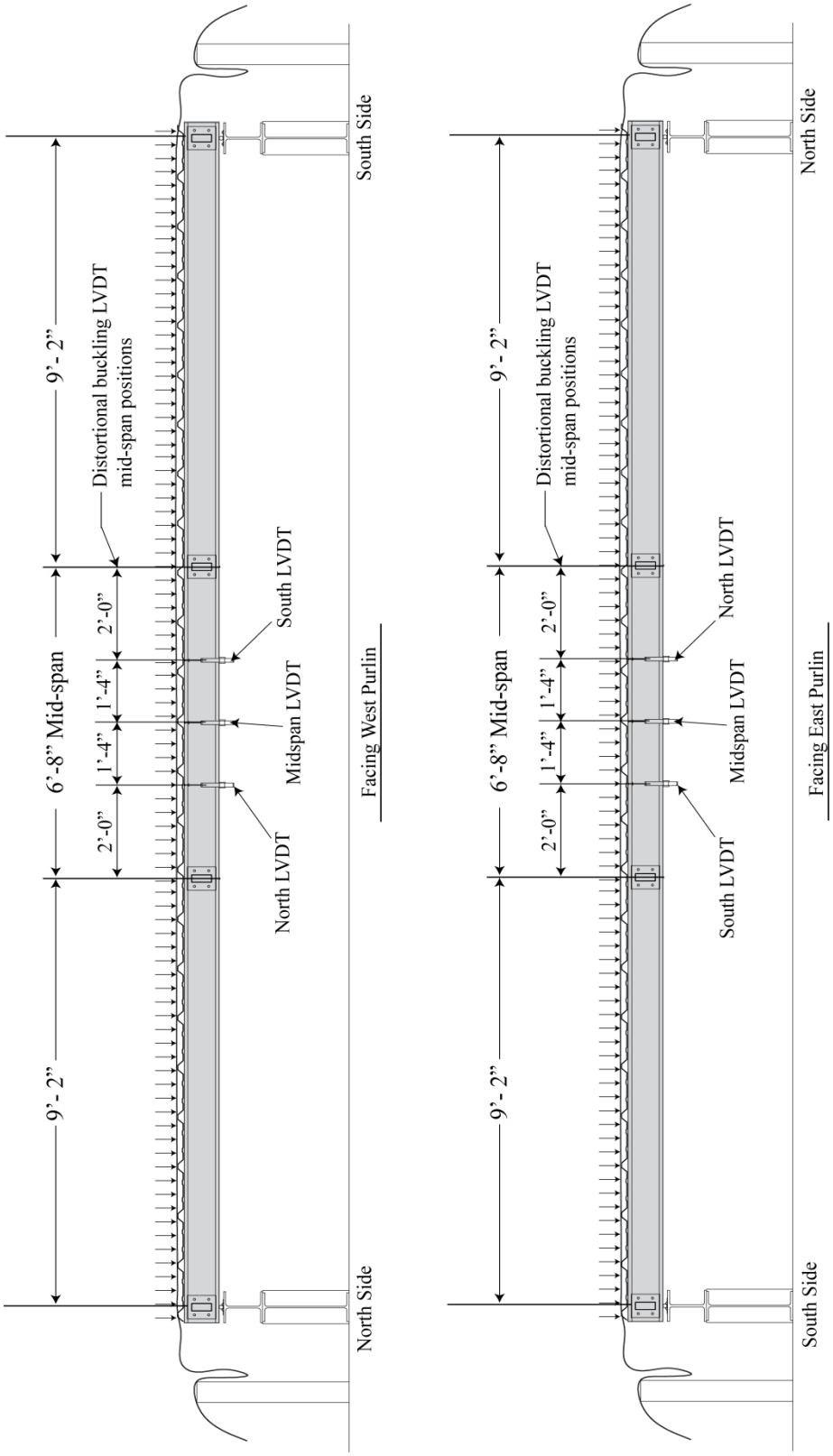

APPENDIX B.2 Pressure Box Experiment Results

PURLIN TEST SUMMARY

Test Identification: UB-P-1-24E25W
Test Date: 12/1/2010

Test Parameters:

Loading	Uniform Pressure w/ Panel
Panel	Through-fastened (26 ga) 3'-0" width x 7'-0" length
Screw Spacing	12" o.c.
Span	25'- 0"
Purlin Length	25'- 8"
Purlin Spacing	5'- 0" o.c. with 1' deck overhang
Lateral Bracing	Provided 9'-2" from each support
Purlin Orientation	Opposing directions
East Purlin Designation	24
West Purlin Designation	25
Purlin Thickness	0.079"

Failure Details

Failure Mode	Combination local flange and web buckling.
Failure Location	34" from North Brace in Center Span – West Purlin
Failure Pressure	40.92 psf
Failure Moment	125.62 kip-in.

DSM Theoretical Predicted Failure Load:

East Purlin - 24

Yield Stress	72.56 ksi
Yield Moment	211.79 kip-in.
Local Buckling	228.22 kip-in.
Distortional Buckling	167.60 kip-in.
Global Buckling	168.83 kip-in.
Nominal Theoretical Moment Capacity	148.15 kip-in.

West Purlin -25

Yield Stress	72.61 ksi
Yield Moment	211.70 kip-in.
Local Buckling	230.29 kip-in.
Distortional Buckling	156.08 kip-in.
Global Buckling	170.50 kip-in.
Nominal Theoretical Moment Capacity	147.44 kip-in.

PURLIN TEST SUMMARY

Test Identification: UB-P-2-22E23W
Test Date: 1/13/2011

Test Parameters:

Loading	Uniform Pressure w/ Panel
Panel	Through-fastened (26 ga) 3'-0" width x 7'-0" length
Screw Spacing	12" o.c.
Span	25'- 0"
Purlin Length	25'- 8"
Purlin Spacing	5'- 0" o.c. with 1' deck overhang
Lateral Bracing	Provided 9'-2" from each support
Purlin Orientation	Opposing directions
East Purlin Designation	22
West Purlin Designation	23
Purlin Thickness	0.079"

Failure Details

Failure Mode	Combination local flange and web buckling.
Failure Location	56" from North Brace in Center Span – East Purlin
Failure Pressure	41.21 psf
Failure Moment	124.71 kip-in.

DSM Theoretical Predicted Failure Load:

East Purlin - 22

Yield Stress	72.25 ksi
Yield Moment	206.93 kip-in.
Local Buckling	238.37 kip-in.
Distortional Buckling	160.86 kip-in.
Global Buckling	205.96 kip-in.
Nominal Theoretical Moment Capacity	147.77 kip-in.

West Purlin -23

Yield Stress	72.13 ksi
Yield Moment	215.80 kip-in.
Local Buckling	232.40 kip-in.
Distortional Buckling	146.99 kip-in.
Global Buckling	184.13 kip-in.
Nominal Theoretical Moment Capacity	145.77 kip-in.

PURLIN TEST SUMMARY

Test Identification: UB-P-3-12E13W
Test Date: 1/17/2011

Test Parameters:

Loading	Uniform Pressure w/ Panel
Panel	Through-fastened (26 ga) 3'-0" width x 7'-0" length
Screw Spacing	12" o.c.
Span	25'- 0"
Purlin Length	25'- 8"
Purlin Spacing	5'- 0" o.c. with 1' deck overhang
Lateral Bracing	Provided 9'-2" from each support
Purlin Orientation	Opposing directions
East Purlin Designation	12
West Purlin Designation	13
Purlin Thickness	0.079"

Failure Details

Failure Mode	Combination local flange and web buckling.
Failure Location	67" from North Brace in Center Span – East Purlin
Failure Pressure	43.72 psf
Failure Moment	129.72 kip-in.

DSM Theoretical Predicted Failure Load:

East Purlin - 12

Yield Stress	71.83 ksi
Yield Moment	203.25 kip-in.
Local Buckling	102.56 kip-in.
Distortional Buckling	229.31 kip-in.
Global Buckling	146.37 kip-in.
Nominal Theoretical Moment Capacity	138.98 kip-in.

West Purlin -13

Yield Stress	71.68 ksi
Yield Moment	200.72 kip-in.
Local Buckling	228.60 kip-in.
Distortional Buckling	156.60 kip-in.
Global Buckling	192.31 kip-in.
Nominal Theoretical Moment Capacity	142.84 kip-in.

TEST DATA PLOTS

Distortional Buckling Plots

Test Identification: UB-P-1-24E25W **Test Date:** 12/1/2010

--- NO DISTORTIONAL INFORMATION ---

Test Identification: UB-P-2-22E23W **Test Date:** 1/13/2011

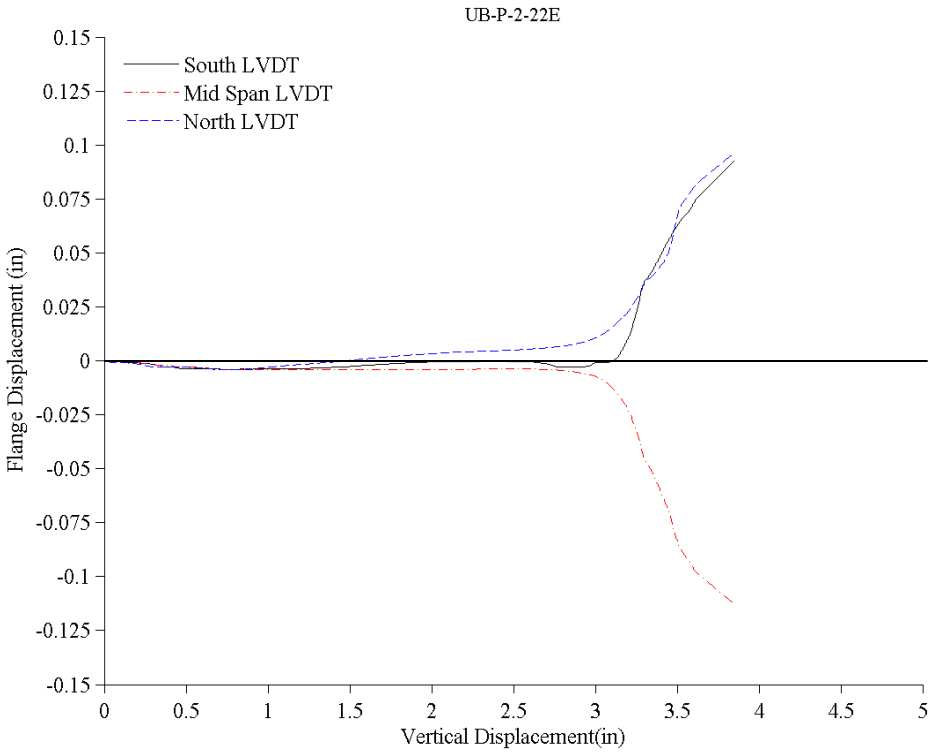

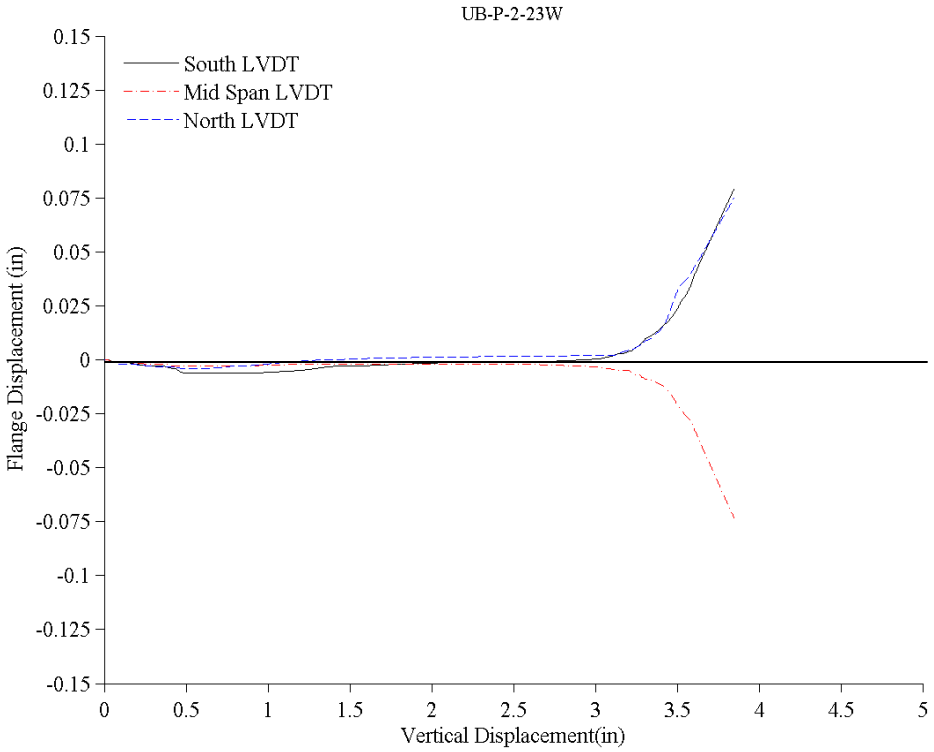

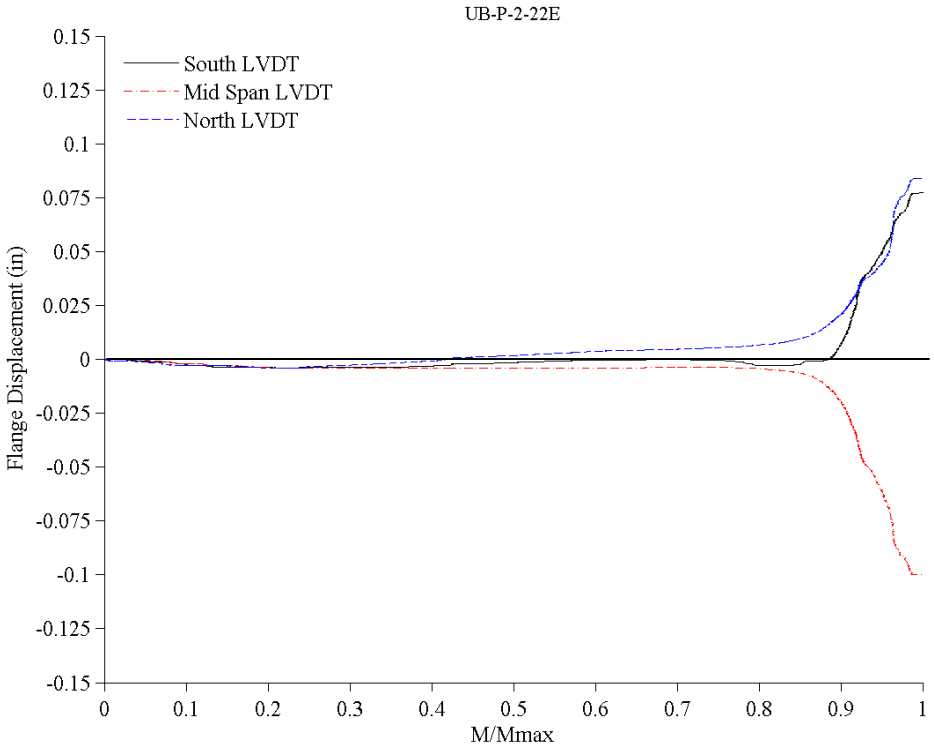
UB-P-2-22E
South LVDT
Mid Span LVDT
North LVDT
Flange Displacement (in)
M/Mmax
0.15
0.125
0.1
0.075
0.05
0.025
0
-0.025
-0.05
-0.075
-0.1
-0.125
-0.15
0
0.1
0.2
0.3
0.4
0.5
0.6
0.7
0.8
0.9
1

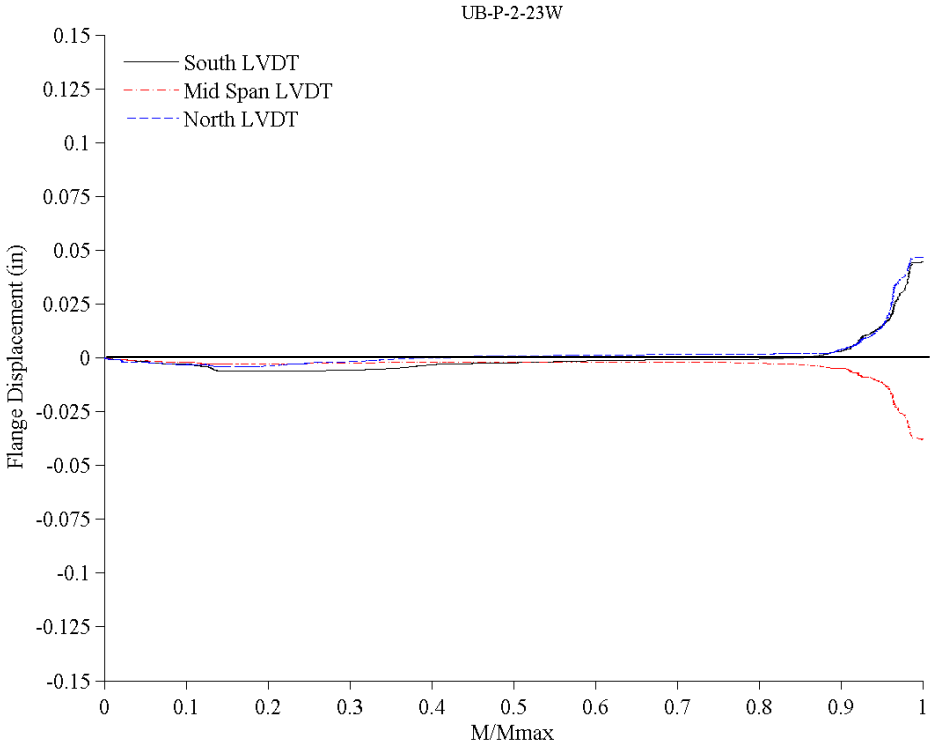
UB-P-2-23W
South LVDT
Mid Span LVDT
North LVDT
Flange Displacement (in)
M/Mmax
0.15
0.125
0.1
0.075
0.05
0.025
0
-0.025
-0.05
-0.075
-0.1
-0.125
-0.15
0
0.1
0.2
0.3
0.4
0.5
0.6
0.7
0.8
0.9
1

Test Identification: UB-P-3-12E13W **Test Date:** 1/17/2011

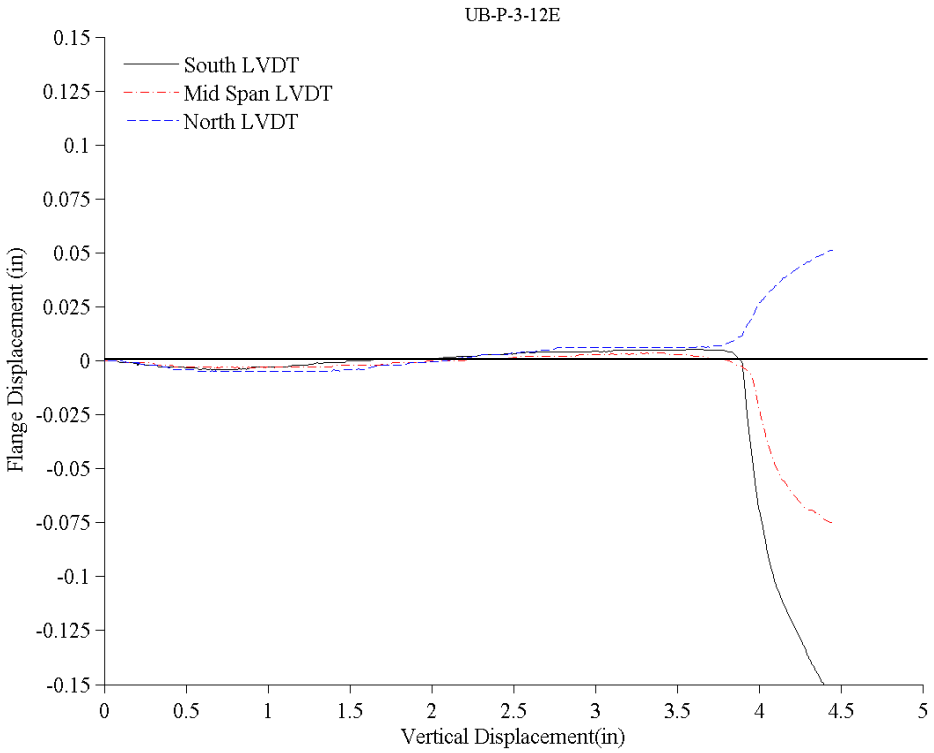

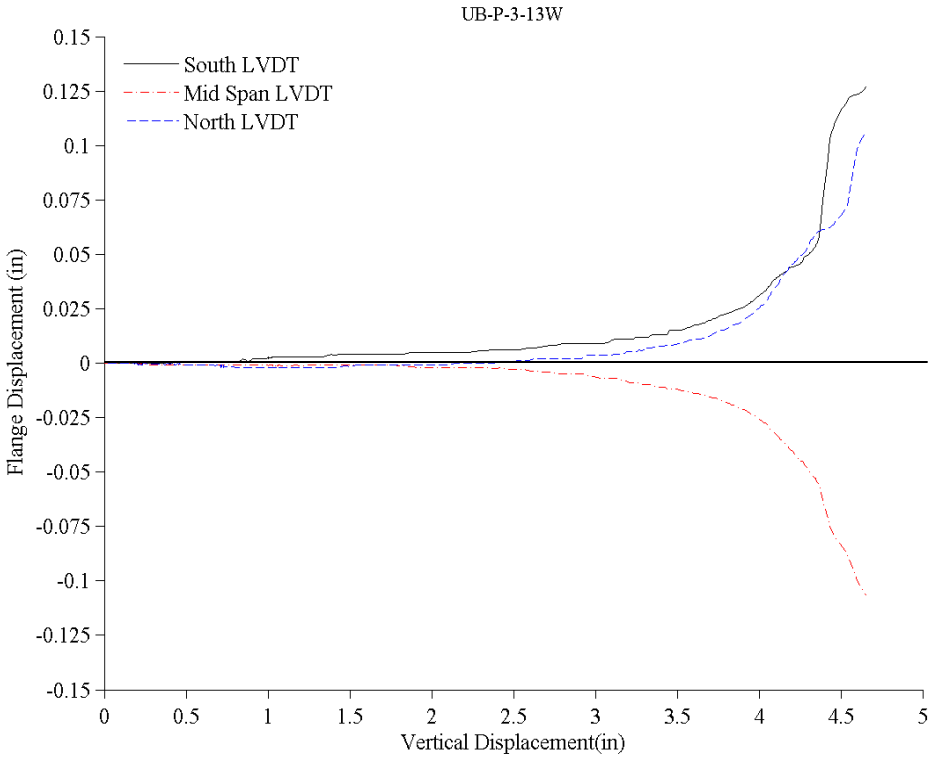

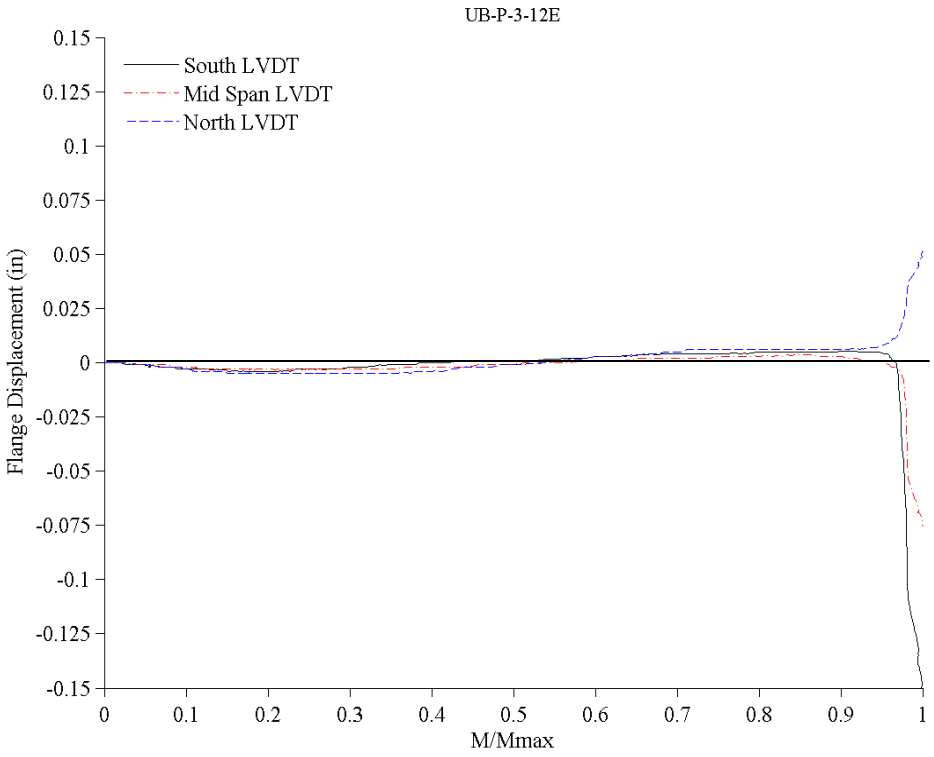
UB-P-3-12E
South LVDT
Mid Span LVDT
North LVDT
Flange Displacement (in)
0.15
0.125
0.1
0.075
0.05
0.025
0
-0.025
-0.05
-0.075
-0.1
-0.125
-0.15
0
0.1
0.2
0.3
0.4
0.5
0.6
0.7
0.8
0.9
1
M/Mmax

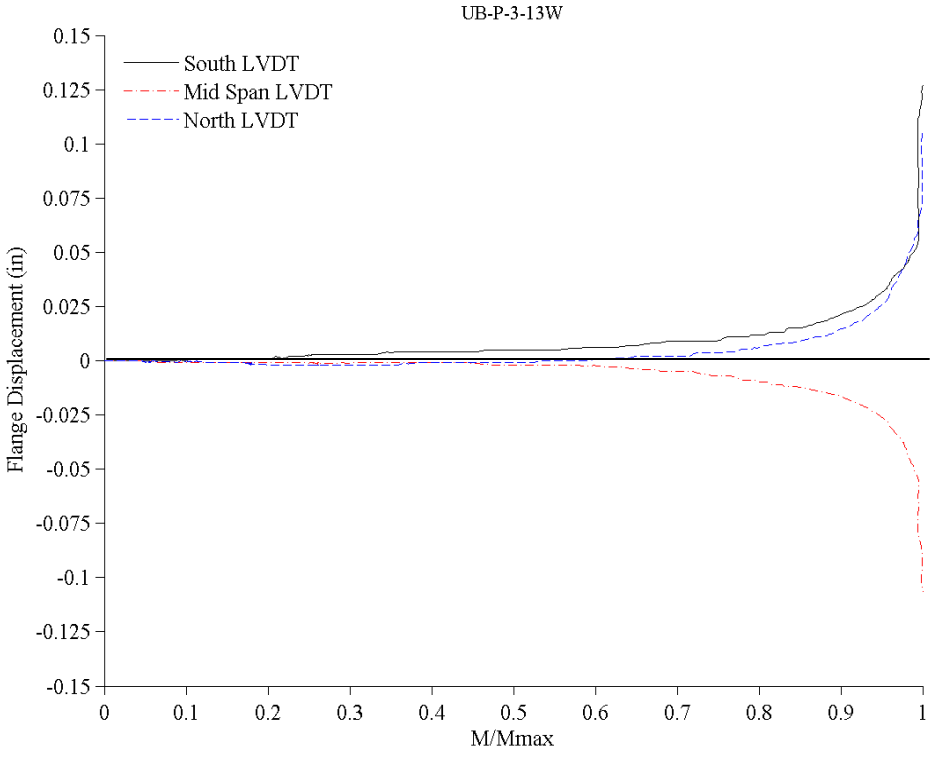
UB-P-3-13W
South LVDT
Mid Span LVDT
North LVDT
Flange Displacement (in)
0.15
0.125
0.1
0.075
0.05
0.025
0
-0.025
-0.05
-0.075
-0.1
-0.125
-0.15
0
0.1
0.2
0.3
0.4
0.5
0.6
0.7
0.8
0.9
1
M/Mmax

PURLIN TEST SUMMARY

Test Identification: 4PB-P-1-16E14W
Test Date: 2/2/2011

Test Parameters:

Loading	Four-point Bending via Pressure Box w/ Panel
Panel	Through-fastened (26 ga) 3'-0" width x 7'-0" length
Screw Spacing	12" o.c.
Span	25'- 0"
Purlin Length	25'- 8"
Purlin Spacing	5'- 0" o.c. with 1' deck overhang
Lateral Bracing	Provided 9'-2" from each support
Purlin Orientation	Opposing directions
East Purlin Designation	16
West Purlin Designation	14
Purlin Thickness	0.079"

Failure Details

Failure Mode	Combination local flange and web buckling.
Failure Location	7" from North Brace in Center Span – East Purlin
Failure Pressure	24.81 psf
Failure Moment	148.70 kip-in.

DSM Theoretical Predicted Failure Load:

East Purlin - 16

Yield Stress	72.21 ksi
Yield Moment	204.70 kip-in.
Local Buckling	224.50 kip-in.
Distortional Buckling	143.48 kip-in.
Global Buckling	168.44 kip-in.
Nominal Theoretical Moment Capacity	139.81 kip-in.

West Purlin -14

Yield Stress	71.97 ksi
Yield Moment	203.66 kip-in.
Local Buckling	226.51 kip-in.
Distortional Buckling	161.63 kip-in.
Global Buckling	168.03 kip-in.
Nominal Theoretical Moment Capacity	145.67 kip-in.

PURLIN TEST SUMMARY

Test Identification: 4PB-P-2-19E11W
Test Date: 2/7/2011

Test Parameters:

Loading	Four-point Bending via Pressure Box w/ Panel
Panel	Through-fastened (26 ga) 3'-0" width x 7'-0" length
Screw Spacing	12" o.c.
Span	25'- 0"
Purlin Length	25'- 8"
Purlin Spacing	5'- 0" o.c. with 1' deck overhang
Lateral Bracing	Provided 9'-2" from each support
Purlin Orientation	Opposing directions
East Purlin Designation	19
West Purlin Designation	11
Purlin Thickness	0.079"

Failure Details

Failure Mode	Combination local flange and web buckling.
Failure Location	46.5" from North Brace in Center Span – East Purlin
Failure Pressure	25.95 psf
Failure Moment	150.02 kip-in.

DSM Theoretical Predicted Failure Load:

East Purlin - 19

Yield Stress	71.61 ksi
Yield Moment	199.06 kip-in.
Local Buckling	254.29 kip-in.
Distortional Buckling	163.23 kip-in.
Global Buckling	216.01 kip-in.
Nominal Theoretical Moment Capacity	144.35 kip-in.

West Purlin -11

Yield Stress	72.25 ksi
Yield Moment	206.29 kip-in.
Local Buckling	236.90 kip-in.
Distortional Buckling	164.30 kip-in.
Global Buckling	199.98 kip-in.
Nominal Theoretical Moment Capacity	147.95 kip-in.

PURLIN TEST SUMMARY

Test Identification: 4PB-P-3-21E7W
Test Date: 2/12/2011

Test Parameters:

Loading	Four-point Bending via Pressure Box w/ Panel
Panel	Through-fastened (26 ga) 3'-0" width x 7'-0" length
Screw Spacing	12" o.c.
Span	25'- 0"
Purlin Length	25'- 8"
Purlin Spacing	5'- 0" o.c. with 1' deck overhang
Lateral Bracing	Provided 9'-2" from each support
Purlin Orientation	Opposing directions
East Purlin Designation	21
West Purlin Designation	7
Purlin Thickness	0.079"

Failure Details

Failure Mode	Combination local flange and web buckling.
Failure Location	40" from North Brace in Center Span – East Purlin
Failure Pressure	27.19 psf
Failure Moment	146.12 kip-in.

DSM Theoretical Predicted Failure Load:

East Purlin - 21

Yield Stress	72.40 ksi
Yield Moment	213.09 kip-in.
Local Buckling	246.23 kip-in.
Distortional Buckling	154.93 kip-in.
Global Buckling	212.36 kip-in.
Nominal Theoretical Moment Capacity	147.61 kip-in.

West Purlin -7

Yield Stress	72.38 ksi
Yield Moment	210.48 kip-in.
Local Buckling	243.46 kip-in.
Distortional Buckling	165.49 kip-in.
Global Buckling	198.52 kip-in.
Nominal Theoretical Moment Capacity	150.22 kip-in.

TEST DATA PLOTS

Four-Point Bending w/Panel - Distortional Buckling Plots

Test Identification: 4PB-P-1-16E14W **Test Date:** 2/2/2011

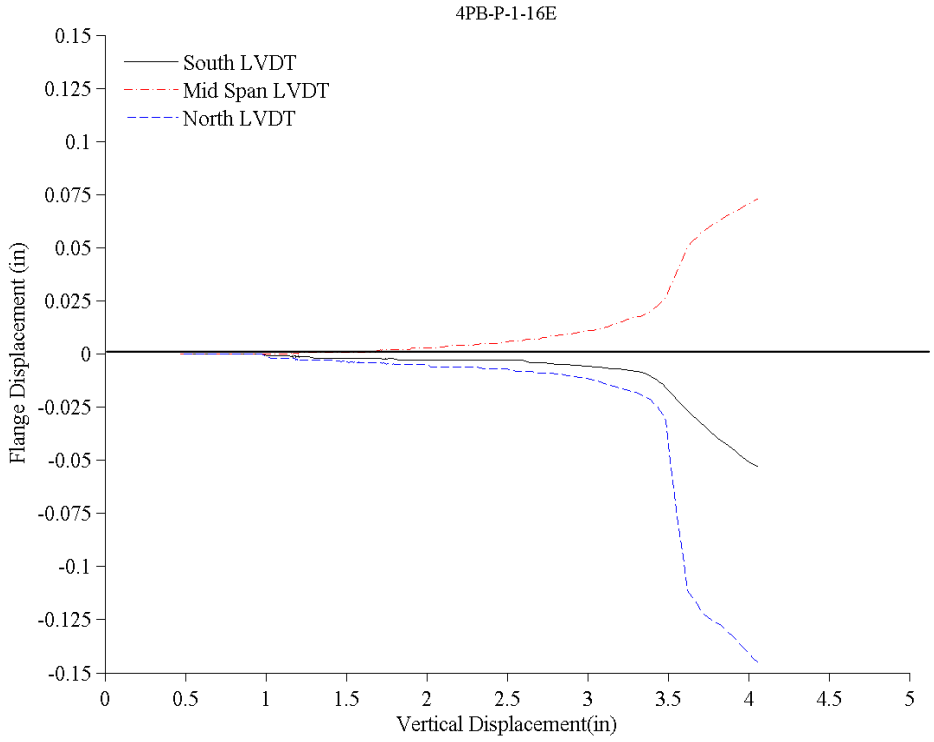

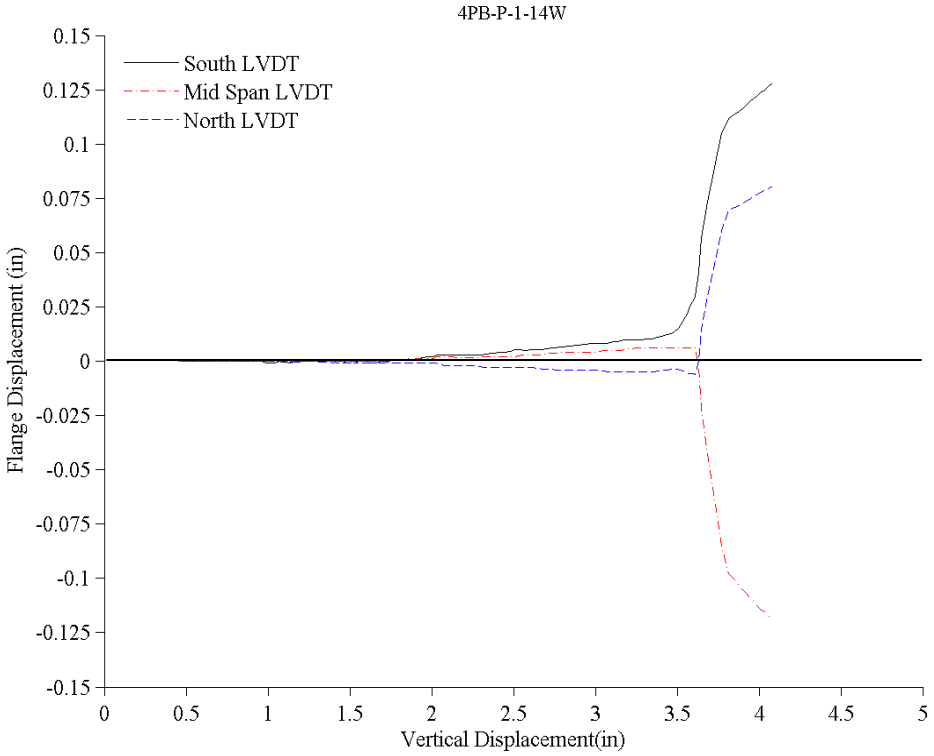

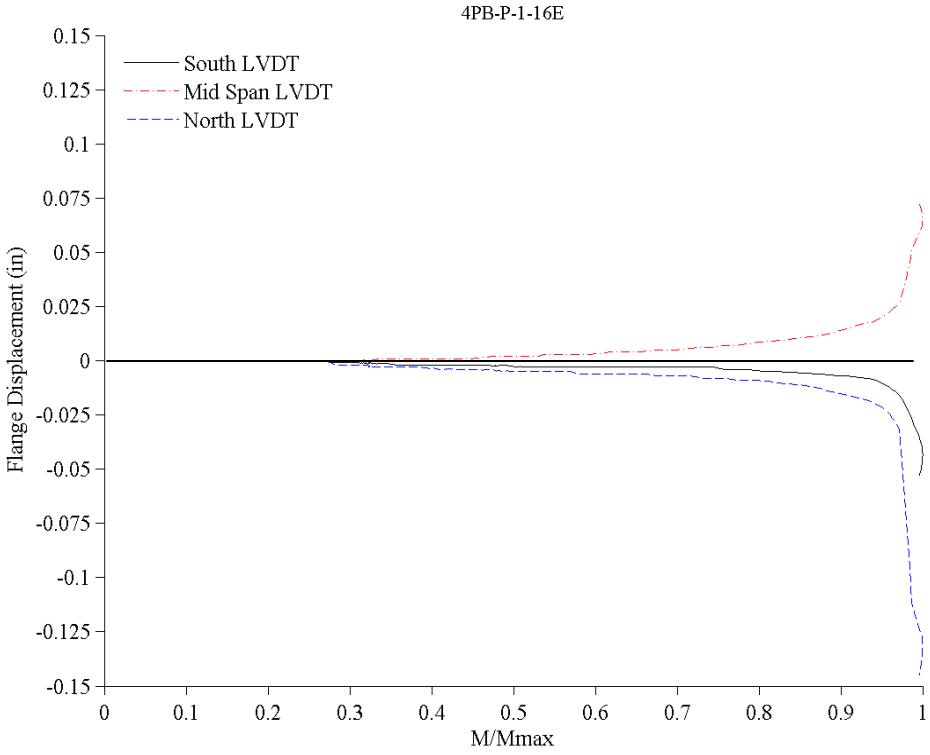
4PB-P-1-16E
South LVDT
Mid Span LVDT
North LVDT
Flange Displacement (in)
M/Mmax
0.15
0.125
0.1
0.075
0.05
0.025
0
-0.025
-0.05
-0.075
-0.1
-0.125
-0.15
0
0.1
0.2
0.3
0.4
0.5
0.6
0.7
0.8
0.9
1

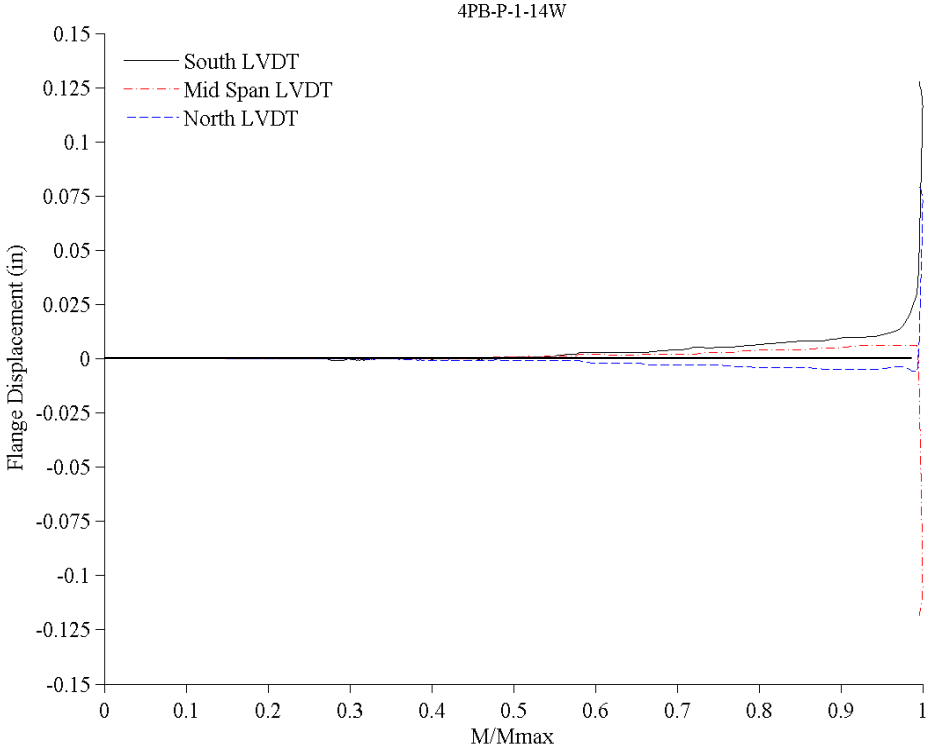
4PB-P-1-14W
South LVDT
Mid Span LVDT
North LVDT
Flange Displacement (in)
M/Mmax
0.15
0.125
0.1
0.075
0.05
0.025
0
-0.025
-0.05
-0.075
-0.1
-0.125
-0.15
0
0.1
0.2
0.3
0.4
0.5
0.6
0.7
0.8
0.9
1

Test Identification: 4PB-P-2-19E11W **Test Date:** 2/7/2011

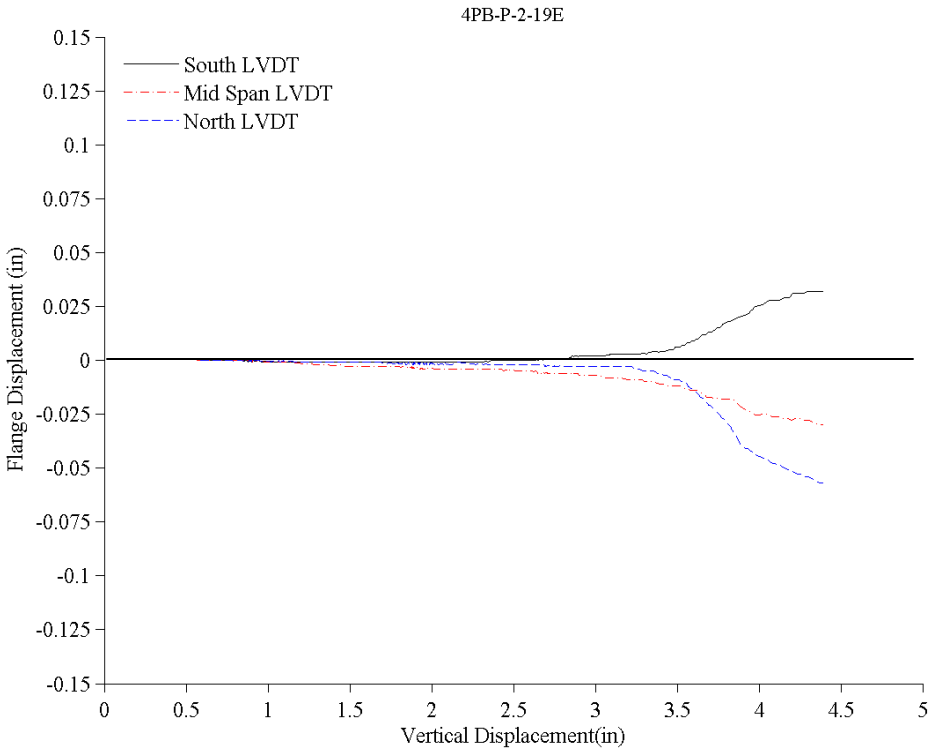

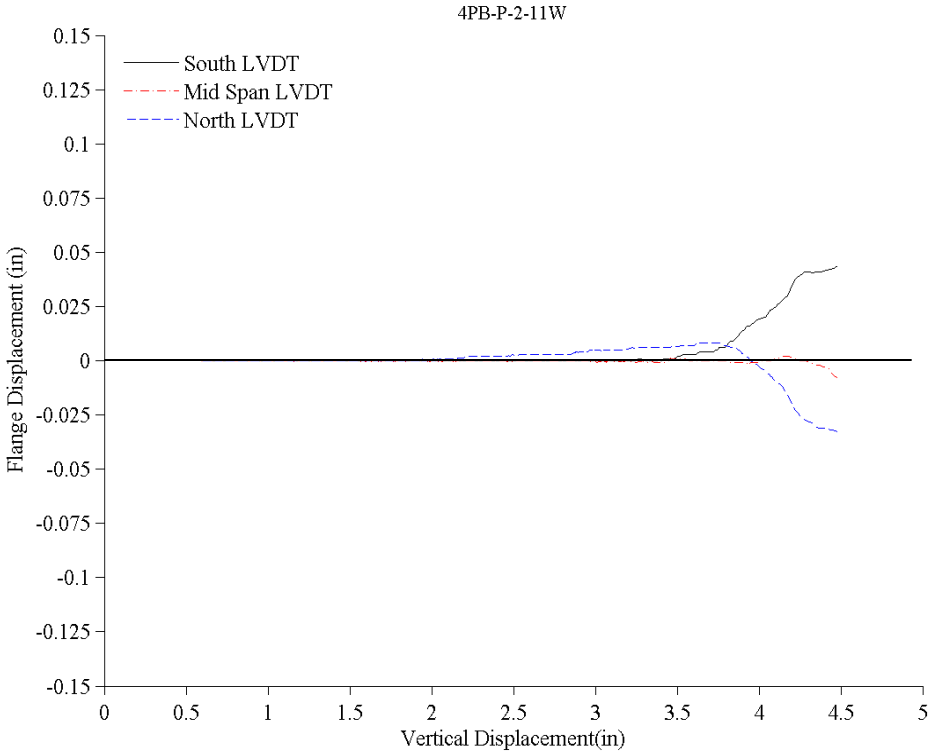

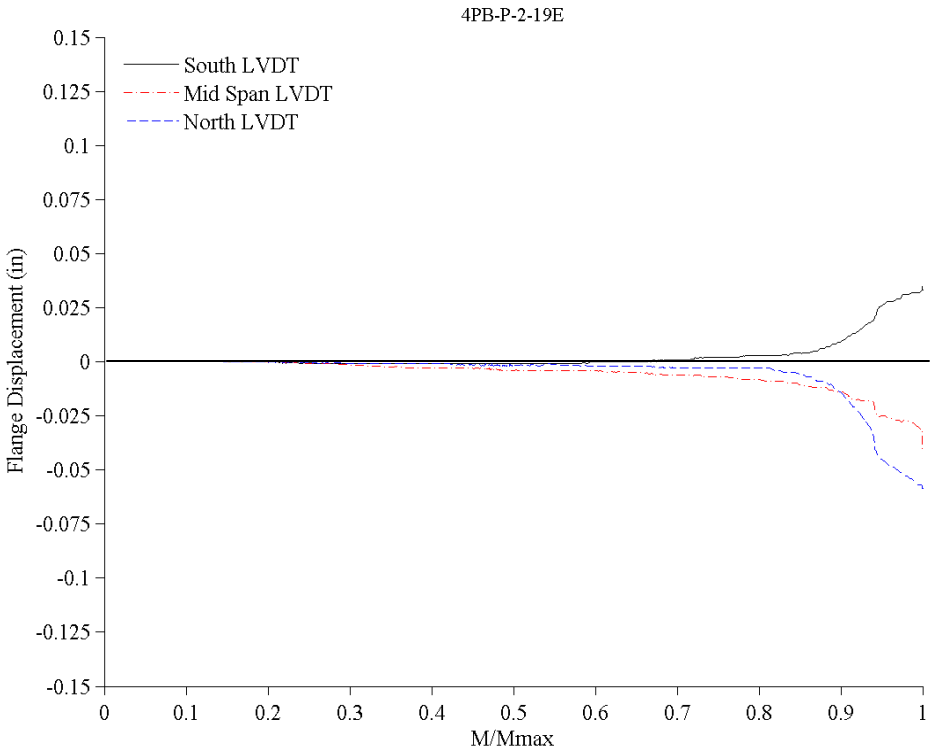
4PB-P-2-19E
South LVDT
Mid Span LVDT
North LVDT
Flange Displacement (in)
0.15
0.125
0.1
0.075
0.05
0.025
0
-0.025
-0.05
-0.075
-0.1
-0.125
-0.15
0
0.1
0.2
0.3
0.4
0.5
0.6
0.7
0.8
0.9
1
M/Mmax

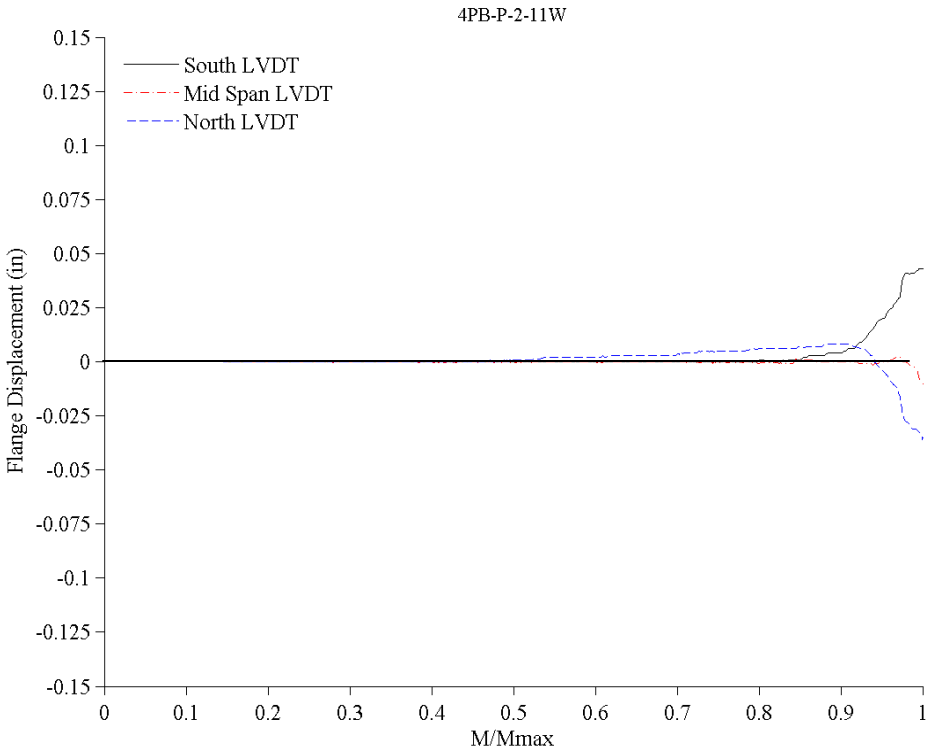
4PB-P-2-11W
South LVDT
Mid Span LVDT
North LVDT
Flange Displacement (in)
0.15
0.125
0.1
0.075
0.05
0.025
0
-0.025
-0.05
-0.075
-0.1
-0.125
-0.15
0
0.1
0.2
0.3
0.4
0.5
0.6
0.7
0.8
0.9
1
M/Mmax

Test Identification: 4PB-P-3-21E7W **Test Date:** 2/12/2011

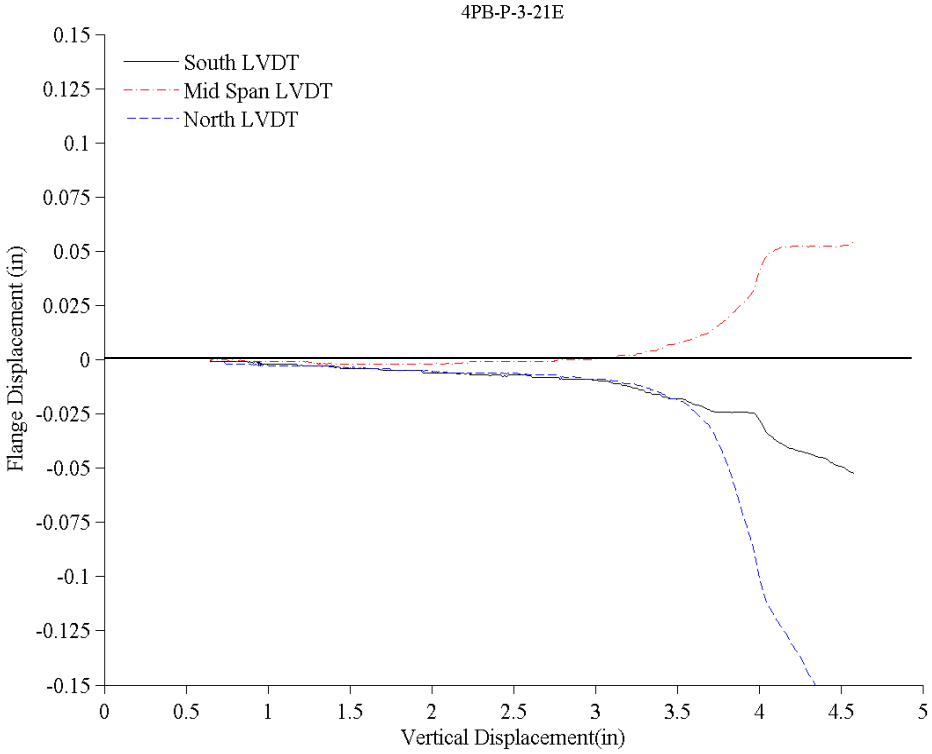

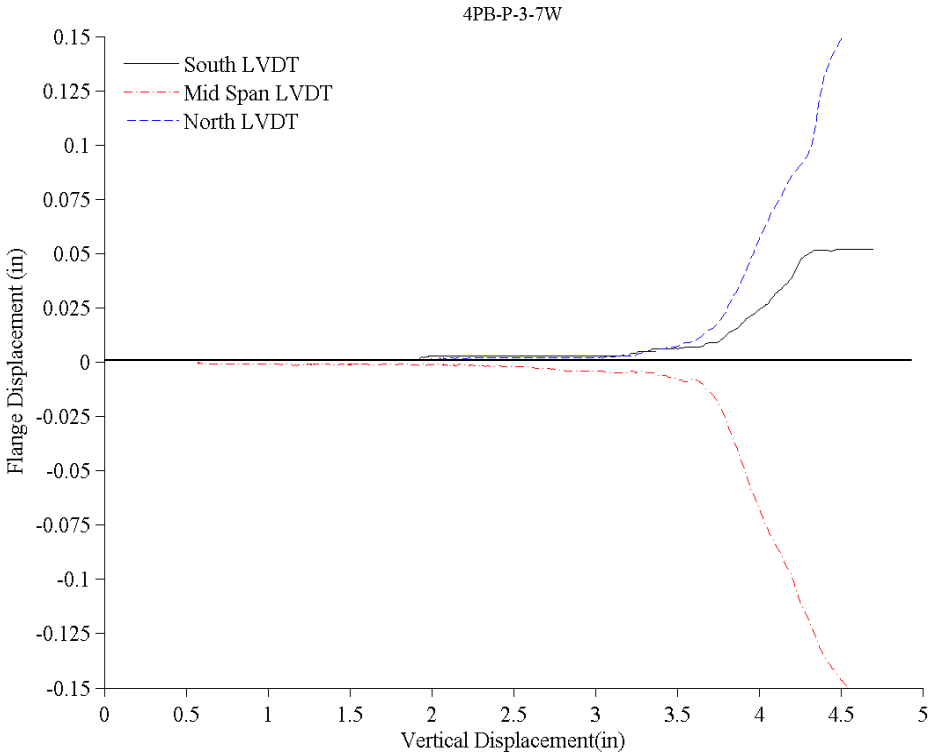

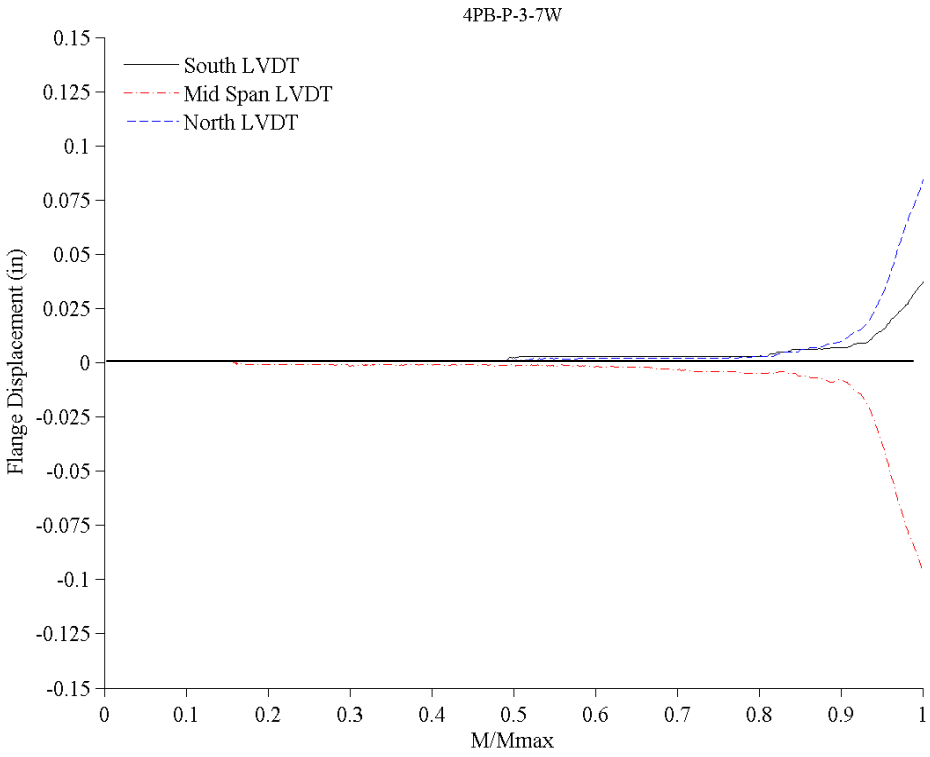
4PB-P-3-7W
South LVDT
Mid Span LVDT
North LVDT
Flange Displacement (in)
M/Mmax
0.15
0.125
0.1
0.075
0.05
0.025
0
-0.025
-0.05
-0.075
-0.1
-0.125
-0.15
0
0.1
0.2
0.3
0.4
0.5
0.6
0.7
0.8
0.9
1

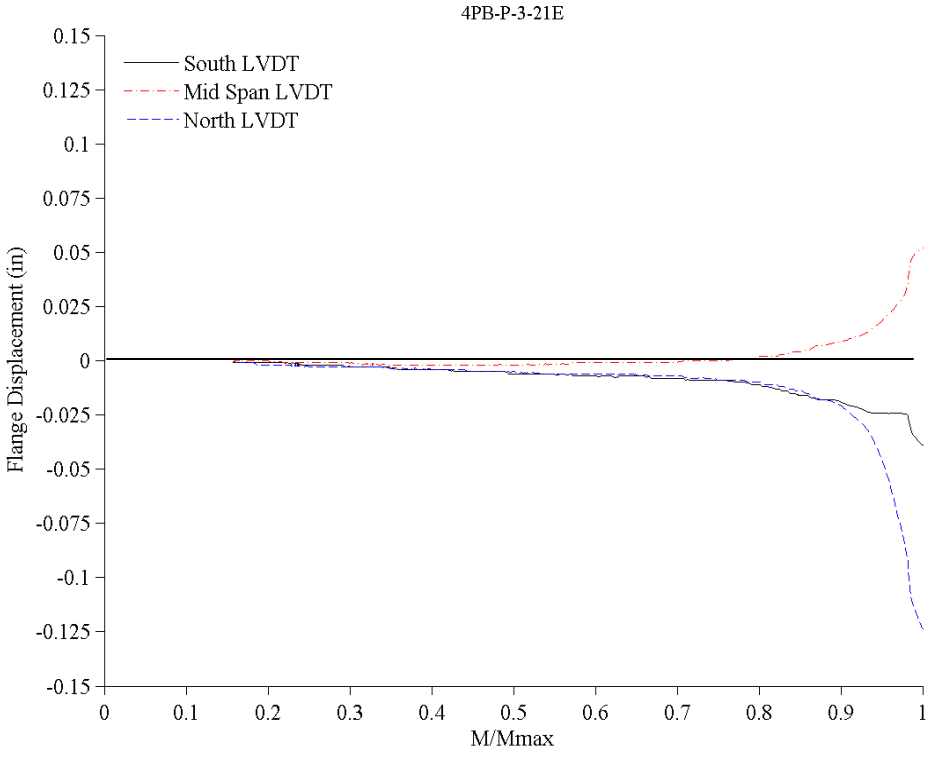
4PB-P-3-21E
South LVDT
Mid Span LVDT
North LVDT
Flange Displacement (in)
M/Mmax
0.15
0.125
0.1
0.075
0.05
0.025
0
-0.025
-0.05
-0.075
-0.1
-0.125
-0.15
0
0.1
0.2
0.3
0.4
0.5
0.6
0.7
0.8
0.9
1

PURLIN TEST SUMMARY

Test Identification:	4PB-NP-1-15E8W
Test Date:	2/4/2011

Test Parameters:

Loading	Four-point Bending via Pressure Box w/o Panel
Panel	None
Screw Spacing	12” o.c.
Span	25’- 0”
Purlin Length	25’- 8”
Purlin Spacing	5’- 0” o.c.
Lateral Bracing	Provided 9’-2” from each support
Purlin Orientation	Opposing directions
East Purlin Designation	15
West Purlin Designation	8
Purlin Thickness	0.079”

Failure Details

Failure Mode	Distortional buckling failure.
Failure Location	38” from North Brace in Center Span – East Purlin
Failure Pressure	16.66 psf
Failure Moment	94.59 kip-in.

DSM Theoretical Predicted Failure Load:

East Purlin - 15

Yield Stress	71.83 ksi
Yield Moment	101.25 kip-in.
Local Buckling	114.47 kip-in.
Distortional Buckling	114.47 kip-in.
Global Buckling	166.10 kip-in.
Nominal Theoretical Moment Capacity	82.47 kip-in.

West Purlin -8

Yield Stress	73.00 ksi
Yield Moment	105.89 kip-in.
Local Buckling	110.60 kip-in.
Distortional Buckling	110.60 kip-in.
Global Buckling	205.21 kip-in.
Nominal Theoretical Moment Capacity	83.89 kip-in.

PURLIN TEST SUMMARY

Test Identification: 4PB-NP-2-10E9W
Test Date: 2/5/2011

Test Parameters:

Loading	Four-point Bending via Pressure Box w/o Panel
Panel	None
Screw Spacing	12” o.c.
Span	25’- 0”
Purlin Length	25’- 8”
Purlin Spacing	5’- 0” o.c.
Lateral Bracing	Provided 9’-2” from each support
Purlin Orientation	Opposing directions
East Purlin Designation	10
West Purlin Designation	9
Purlin Thickness	0.079”

Failure Details

Failure Mode	Distortional buckling failure.
Failure Location	17” from North Brace in Center Span – East Purlin
Failure Pressure	16.92 psf
Failure Moment	95.42 kip-in.

DSM Theoretical Predicted Failure Load:

East Purlin - 10

Yield Stress	71.67 ksi
Yield Moment	99.53 kip-in.
Local Buckling	113.82 kip-in.
Distortional Buckling	113.82 kip-in.
Global Buckling	159.13 kip-in.
Nominal Theoretical Moment Capacity	81.40 kip-in.

West Purlin -9

Yield Stress	72.18 ksi
Yield Moment	102.14 kip-in.
Local Buckling	107.81 kip-in.
Distortional Buckling	107.81 kip-in.
Global Buckling	217.68 kip-in.
Nominal Theoretical Moment Capacity	81.22 kip-in.

PURLIN TEST SUMMARY

Test Identification: 4PB-NP-3-17E18W
Test Date: 2/8/2011

Test Parameters:

Loading	Four-point Bending via Pressure Box w/o Panel
Panel	None
Screw Spacing	12” o.c.
Span	25’- 0”
Purlin Length	25’- 8”
Purlin Spacing	5’- 0” o.c.
Lateral Bracing	Provided 9’-2” from each support
Purlin Orientation	Opposing directions
East Purlin Designation	17
West Purlin Designation	18
Purlin Thickness	0.079”

Failure Details

Failure Mode	Distortional buckling failure.
Failure Location	15” from North Brace in Center Span – East Purlin
Failure Pressure	23.33 psf
Failure Moment	119.77 kip-in.

DSM Theoretical Predicted Failure Load:

East Purlin - 17

Yield Stress	74.46 ksi
Yield Moment	115.27 kip-in.
Local Buckling	152.75 kip-in.
Distortional Buckling	152.75 kip-in.
Global Buckling	177.34 kip-in.
Nominal Theoretical Moment Capacity	99.09 kip-in.

West Purlin -18

Yield Stress	73.60 ksi
Yield Moment	114.17 kip-in.
Local Buckling	145.17 kip-in.
Distortional Buckling	145.17 kip-in.
Global Buckling	229.51 kip-in.
Nominal Theoretical Moment Capacity	96.80 kip-in.

PURLIN TEST SUMMARY

Test Identification:	4PB-NP-4-32E20W
Test Date:	2/22/2011

Test Parameters:

Loading	Four-point Bending via Pressure Box w/o Panel
Panel	None
Screw Spacing	12” o.c.
Span	25’- 0”
Purlin Length	25’- 8”
Purlin Spacing	5’- 0” o.c.
Lateral Bracing	Provided 9’-2” from each support
Purlin Orientation	Opposing directions
East Purlin Designation	32
West Purlin Designation	20
Purlin Thickness	0.079”

Failure Details

Failure Mode	Distortional buckling failure.
Failure Location	18” from North Brace in Center Span – East Purlin
Failure Pressure	18.40 psf
Failure Moment	109.17 kip-in.

DSM Theoretical Predicted Failure Load:

East Purlin - 10

Yield Stress	75.89 ksi
Yield Moment	109.26 kip-in.
Local Buckling	110.99 kip-in.
Distortional Buckling	110.99 kip-in.
Global Buckling	222.88 kip-in.
Nominal Theoretical Moment Capacity	85.70 kip-in.

West Purlin -9

Yield Stress	71.54 ksi
Yield Moment	101.31 kip-in.
Local Buckling	107.45 kip-in.
Distortional Buckling	107.45 kip-in.
Global Buckling	226.15 kip-in.
Nominal Theoretical Moment Capacity	80.70 kip-in.

TEST DATA PLOTS

Four-Point Bending No Panel - Distortional Buckling Plots

Test Identification: 4PB-NP-1-15E8W **Test Date:** 2/4/2011

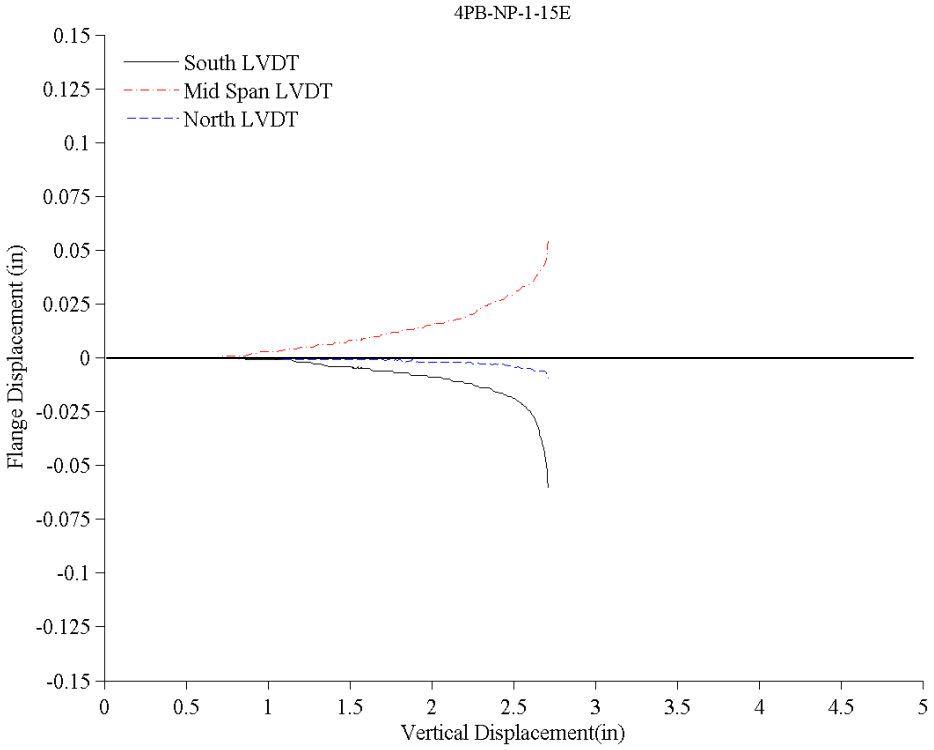

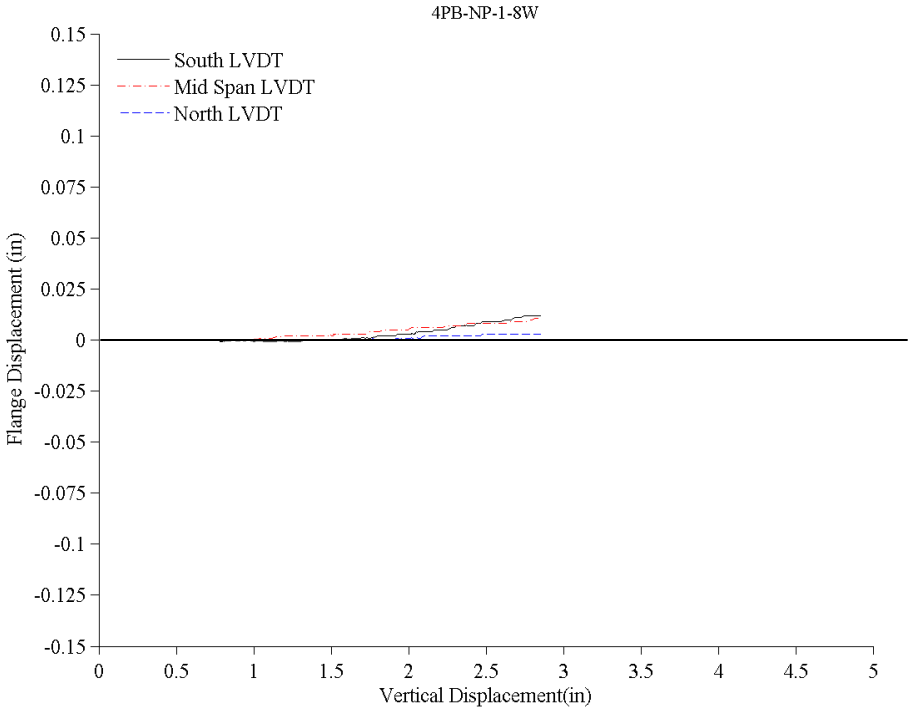

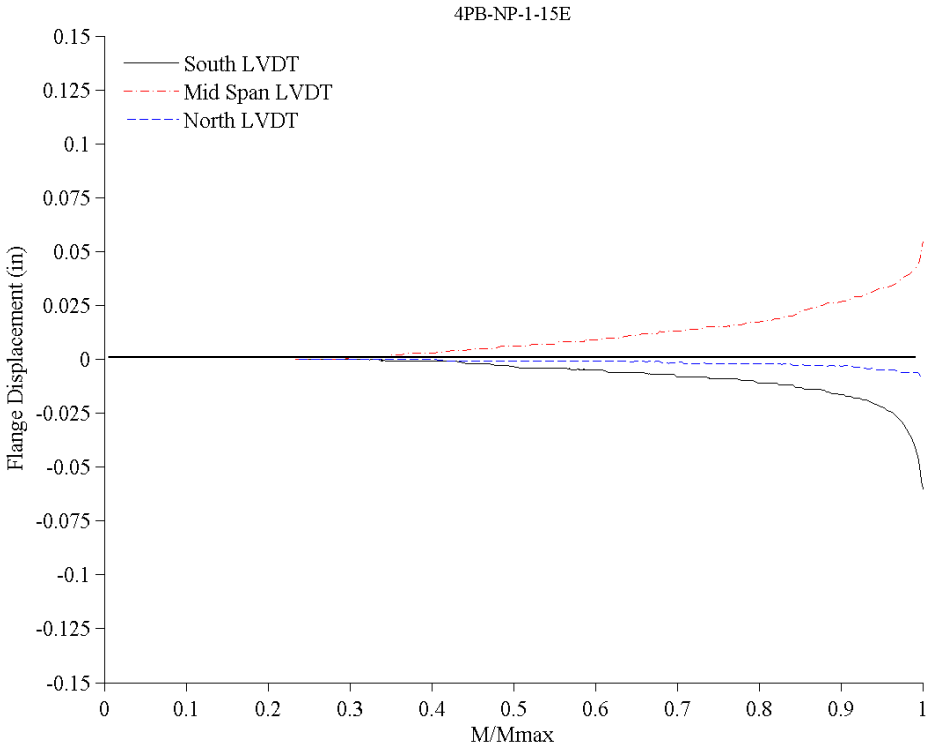
4PB-NP-1-15E
South LVDT
Mid Span LVDT
North LVDT
Flange Displacement (in)
0.15
0.125
0.1
0.075
0.05
0.025
0
-0.025
-0.05
-0.075
-0.1
-0.125
-0.15
0
0.1
0.2
0.3
0.4
0.5
0.6
0.7
0.8
0.9
1
M/Mmax

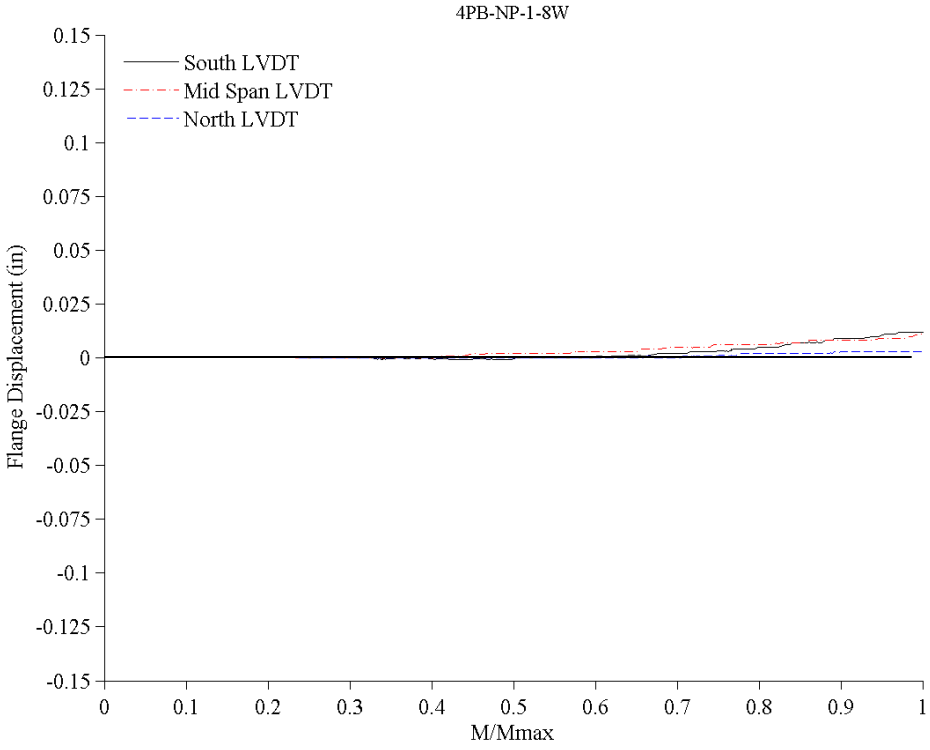
4PB-NP-1-8W
South LVDT
Mid Span LVDT
North LVDT
Flange Displacement (in)
0.15
0.125
0.1
0.075
0.05
0.025
0
-0.025
-0.05
-0.075
-0.1
-0.125
-0.15
0
0.1
0.2
0.3
0.4
0.5
0.6
0.7
0.8
0.9
1
M/Mmax

Test Identification: 4PB-NP-2-10E9W **Test Date:** 2/5/2011

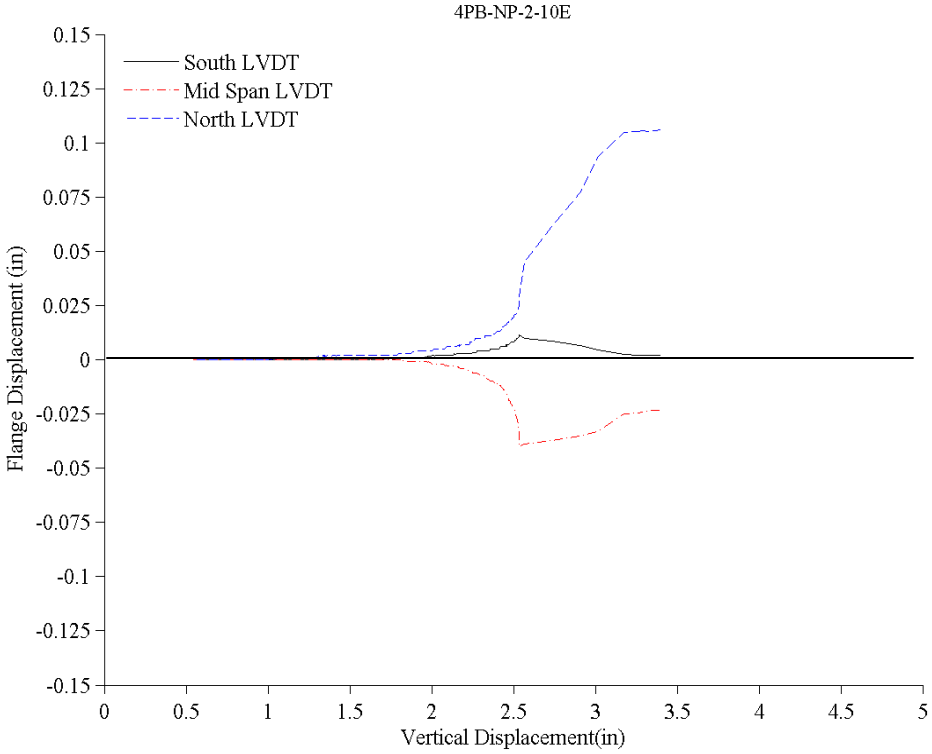

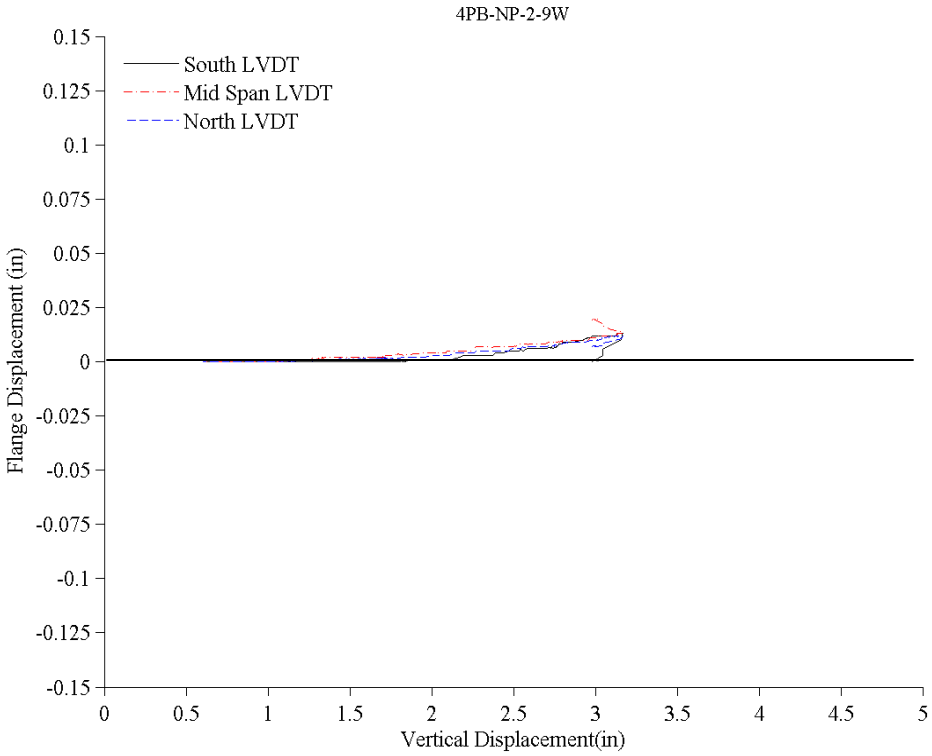

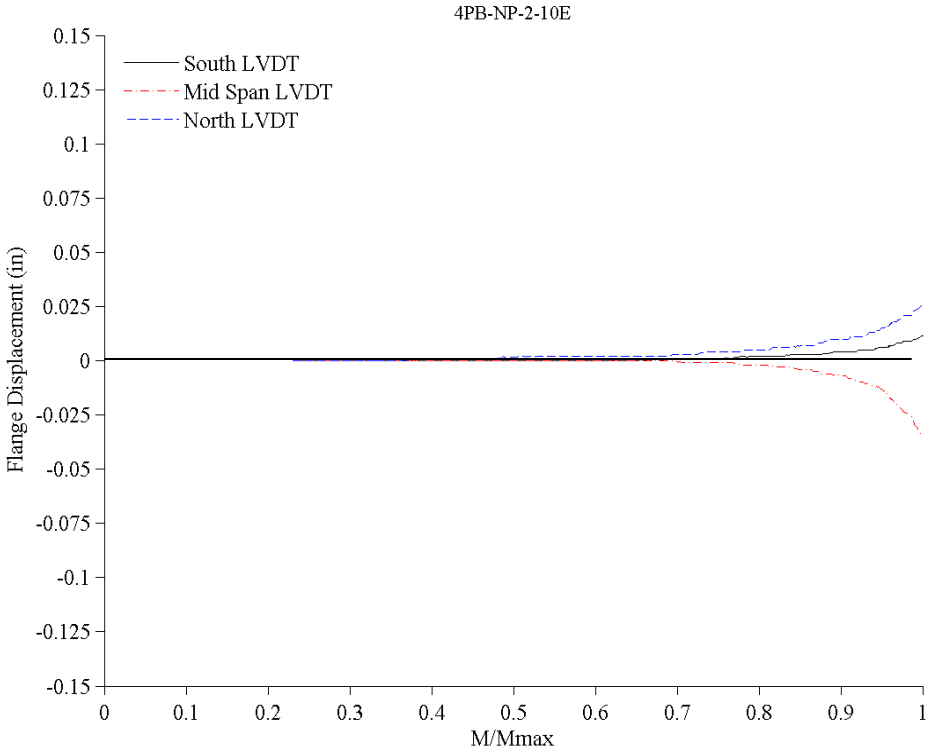
4PB-NP-2-10E
South LVDT
Mid Span LVDT
North LVDT
Flange Displacement (in)
0.15
0.125
0.1
0.075
0.05
0.025
0
-0.025
-0.05
-0.075
-0.1
-0.125
-0.15
0
0.1
0.2
0.3
0.4
0.5
0.6
0.7
0.8
0.9
1
M/Mmax

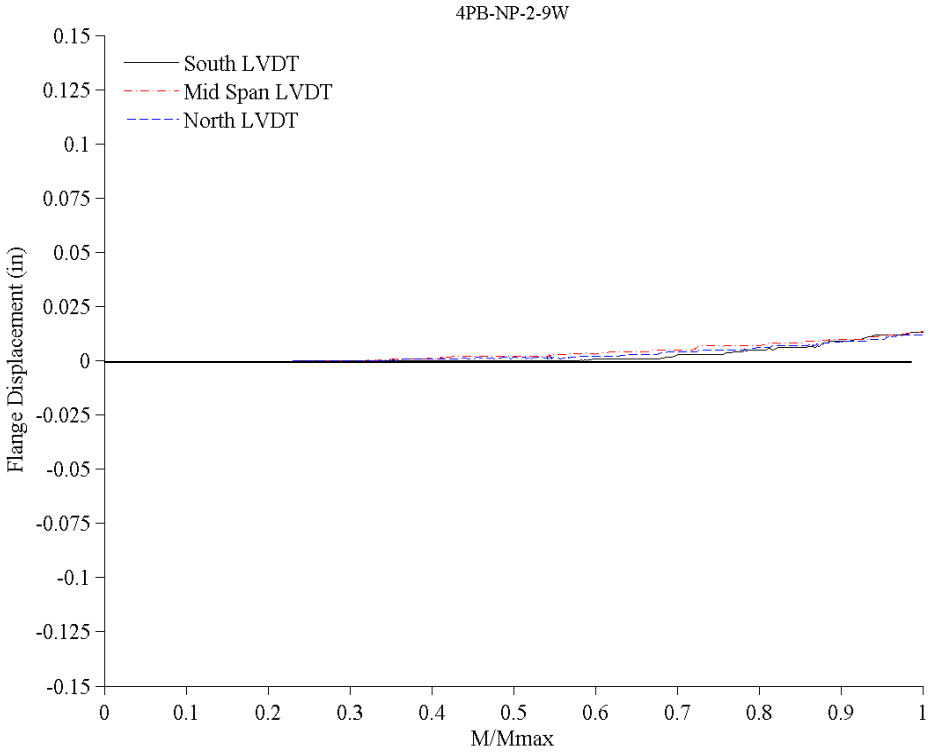
4PB-NP-2-9W
South LVDT
Mid Span LVDT
North LVDT
Flange Displacement (in)
0.15
0.125
0.1
0.075
0.05
0.025
0
-0.025
-0.05
-0.075
-0.1
-0.125
-0.15
0
0.1
0.2
0.3
0.4
0.5
0.6
0.7
0.8
0.9
1
M/Mmax

Test Identification: 4PB-NP-3-17E18W **Test Date:** 2/8/2011

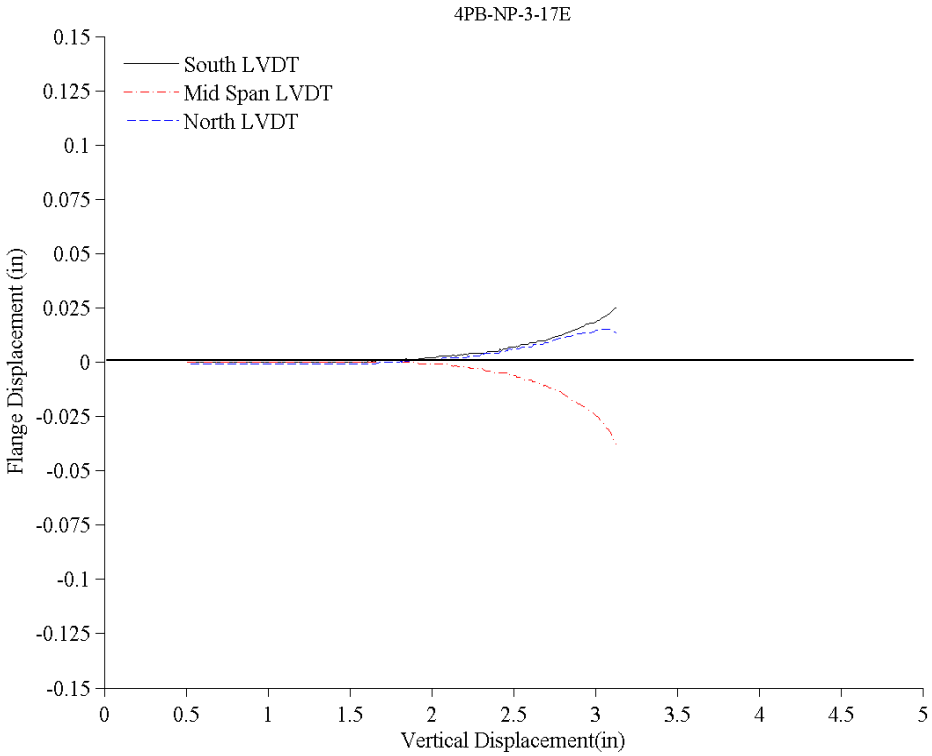

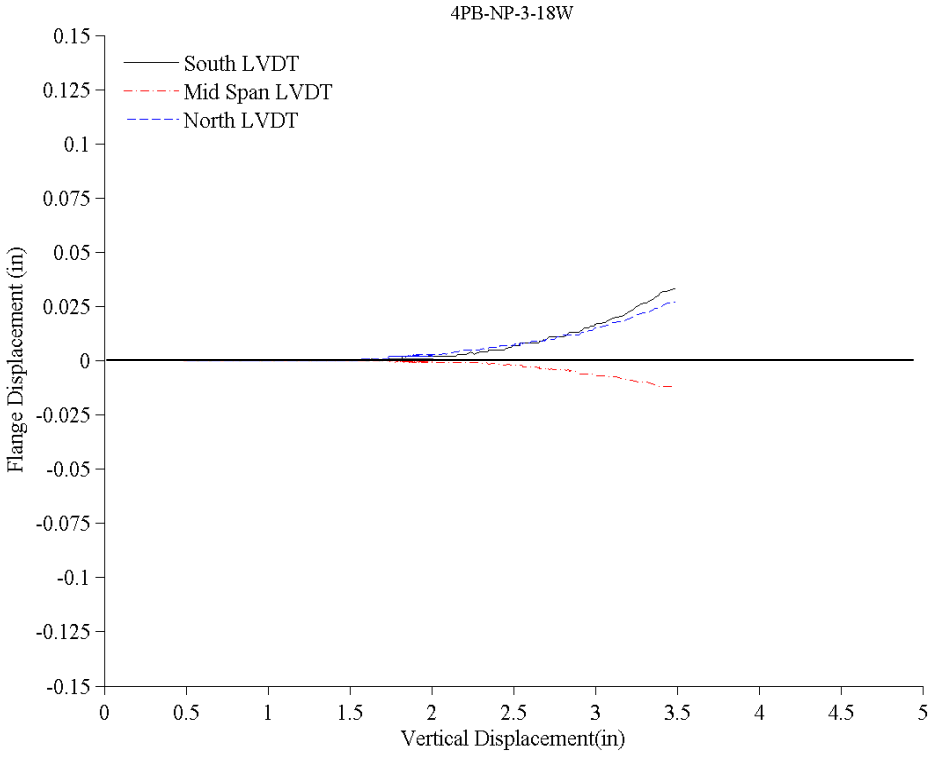

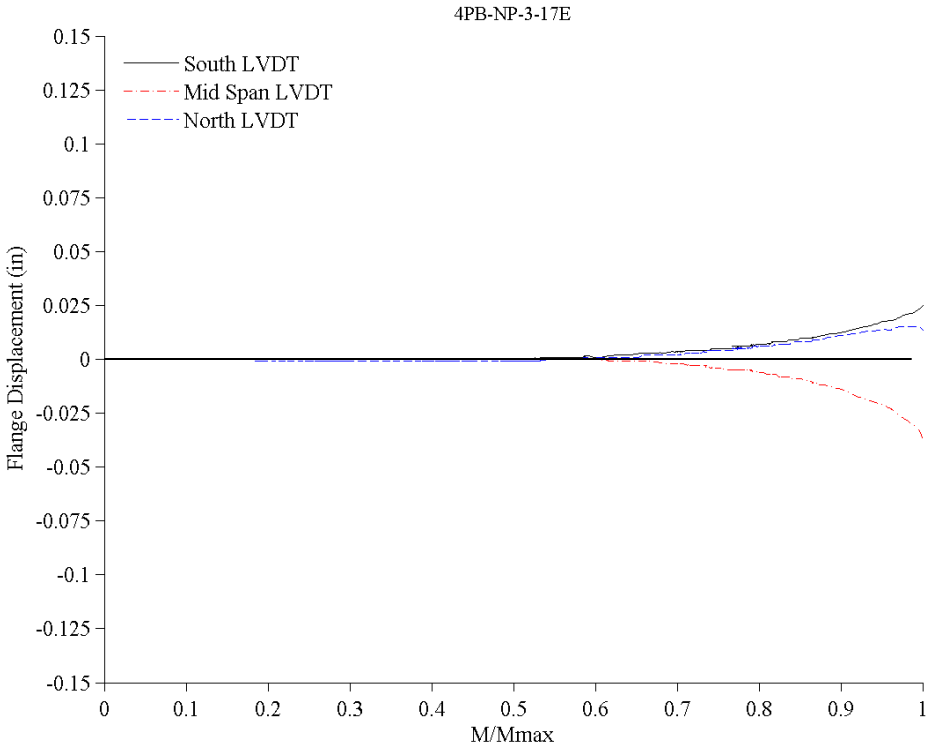
4PB-NP-3-17E
South LVDT
Mid Span LVDT
North LVDT
Flange Displacement (in)
0.15
0.125
0.1
0.075
0.05
0.025
0
-0.025
-0.05
-0.075
-0.1
-0.125
-0.15
0
0.1
0.2
0.3
0.4
0.5
0.6
0.7
0.8
0.9
1
M/Mmax

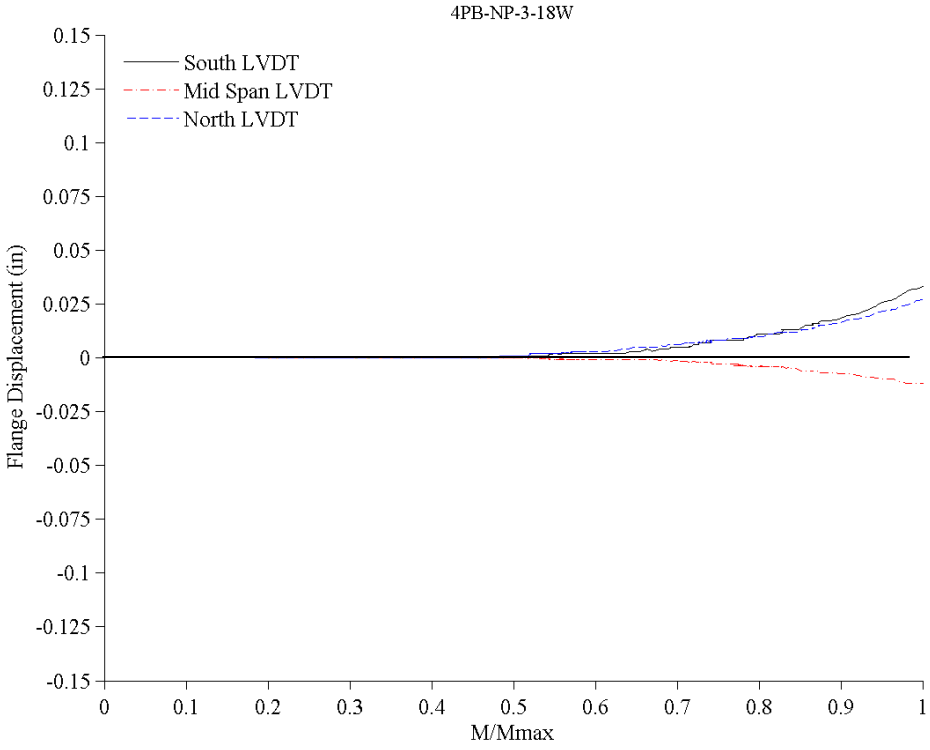
4PB-NP-3-18W
South LVDT
Mid Span LVDT
North LVDT
Flange Displacement (in)
0.15
0.125
0.1
0.075
0.05
0.025
0
-0.025
-0.05
-0.075
-0.1
-0.125
-0.15
0
0.1
0.2
0.3
0.4
0.5
0.6
0.7
0.8
0.9
1
M/Mmax

Test Identification: 4PB-NP-4-32E20W **Test Date:** 2/22/2011

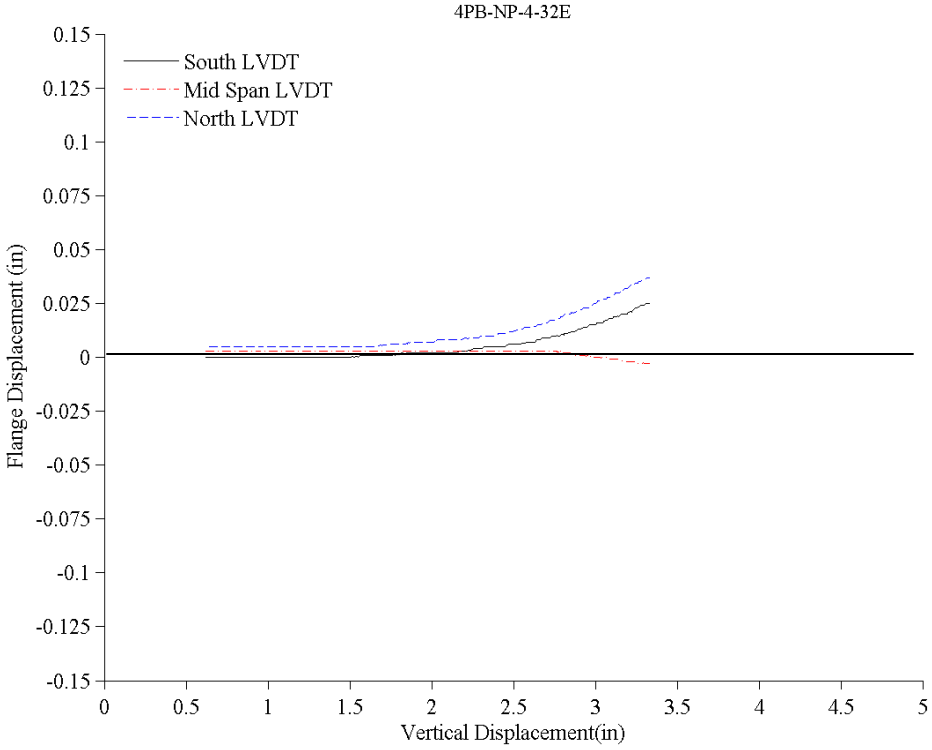

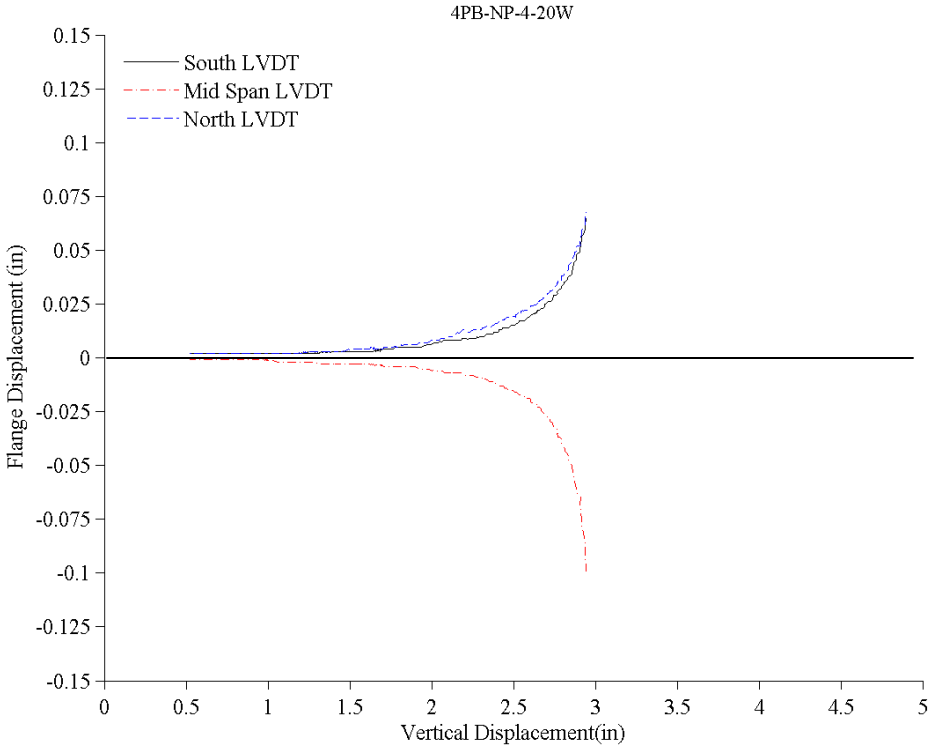

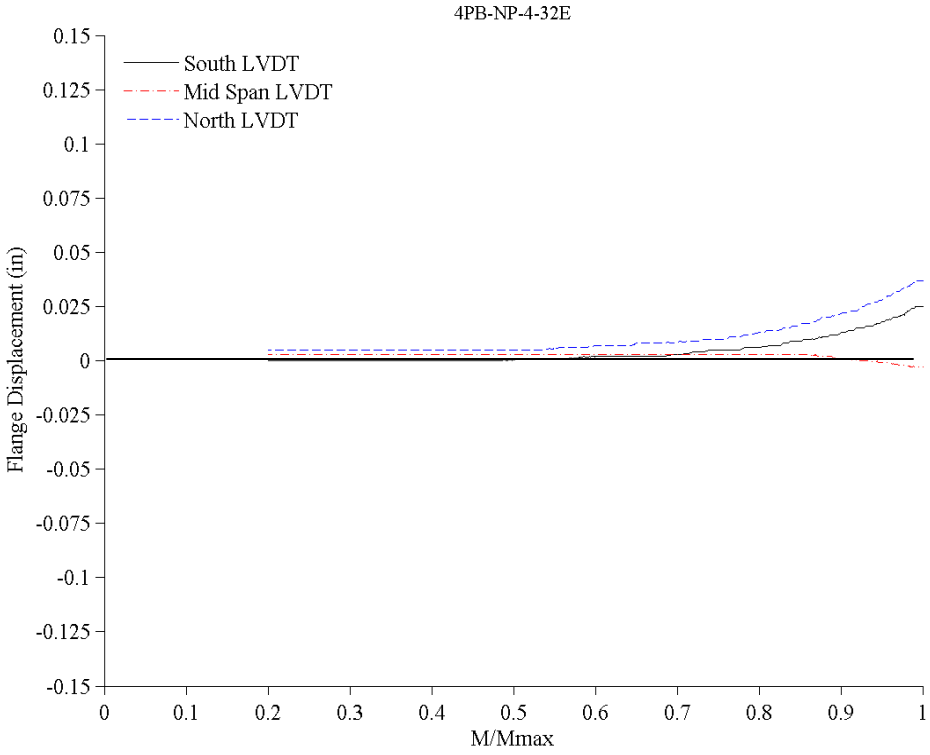
4PB-NP-4-32E
South LVDT
Mid Span LVDT
North LVDT
Flange Displacement (in)
M/Mmax
0.15
0.125
0.1
0.075
0.05
0.025
0
-0.025
-0.05
-0.075
-0.1
-0.125
-0.15
0
0.1
0.2
0.3
0.4
0.5
0.6
0.7
0.8
0.9
1

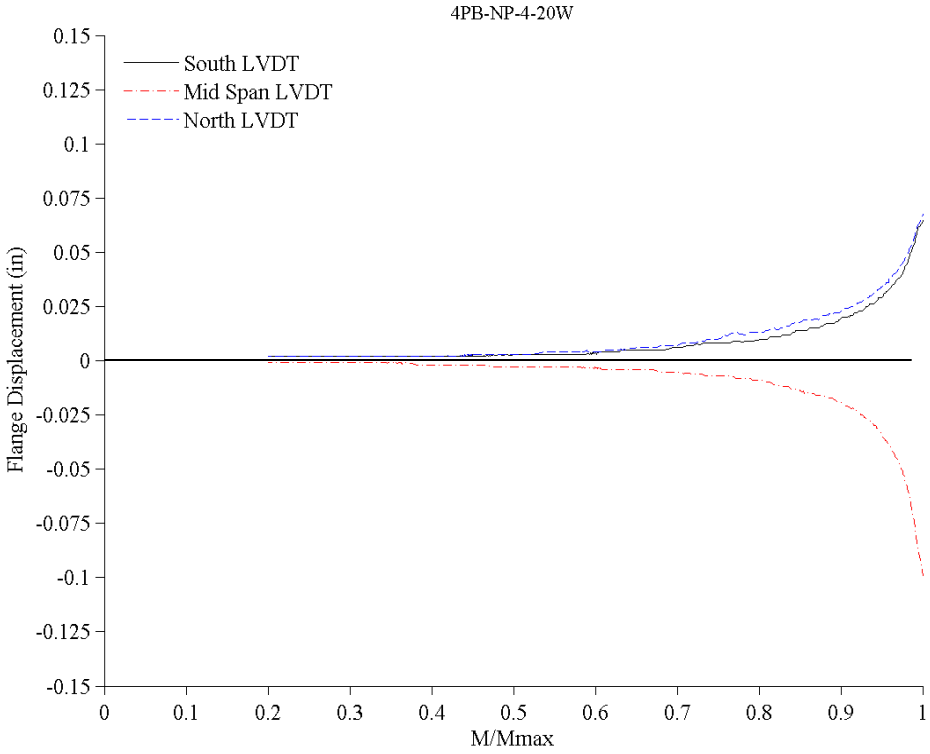
4PB-NP-4-20W
South LVDT
Mid Span LVDT
North LVDT
Flange Displacement (in)
M/Mmax
0.15
0.125
0.1
0.075
0.05
0.025
0
-0.025
-0.05
-0.075
-0.1
-0.125
-0.15
0
0.1
0.2
0.3
0.4
0.5
0.6
0.7
0.8
0.9
1

TEST DATA PLOTS

Uniform Bending - Load Displacement Plots

Test Identification:	UB-P-1-24E25W	**Test Date:**	12/1/2010
	UB-P-2-22E23W		1/13/2011
	UB-P-3-12E13W		1/17/2011

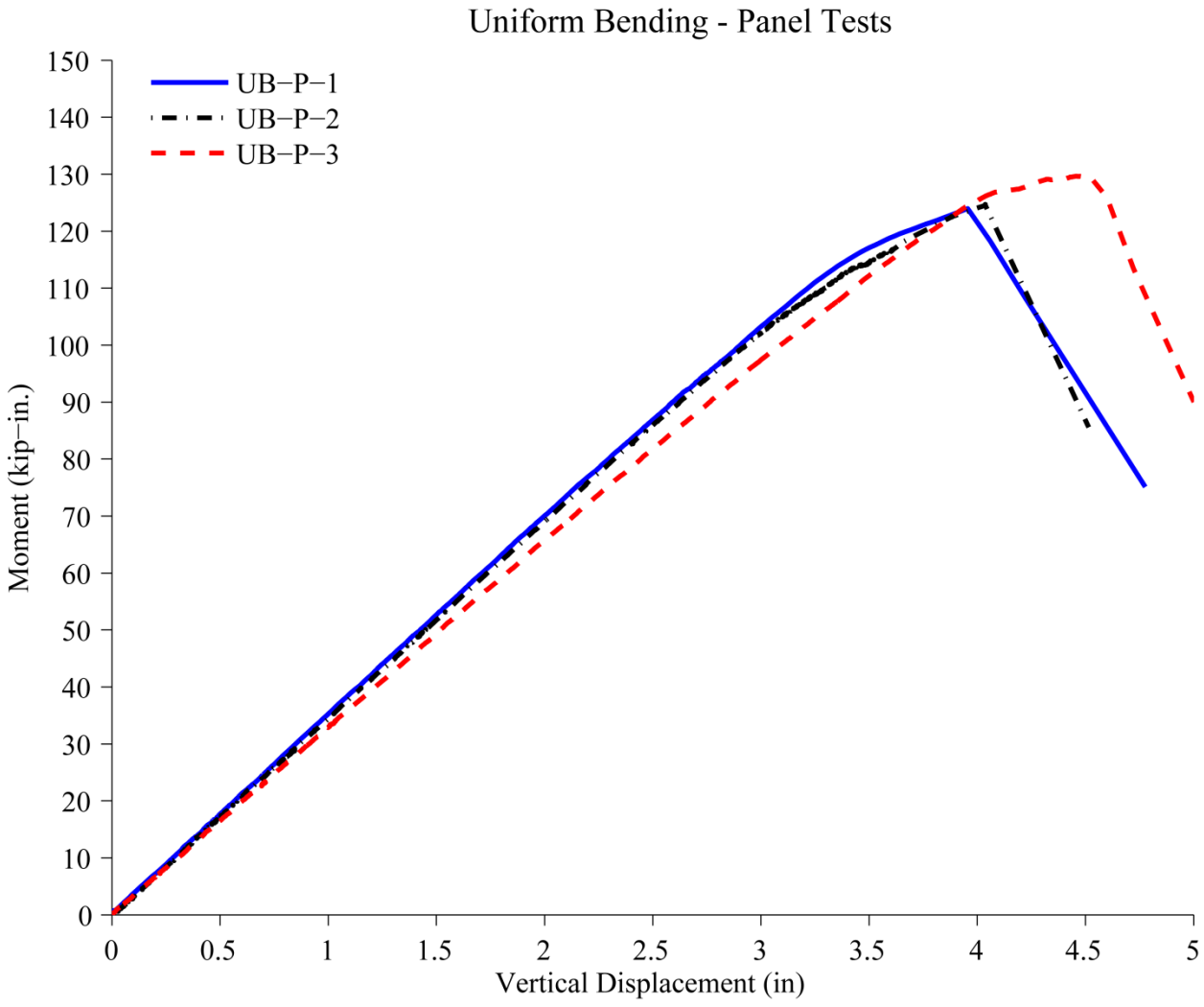

TEST DATA PLOTS

Four-Point Bending w/Panel - Load Displacement Plots

Test Identification:	4PB-P-1-16E14W	**Test Date:**	2/2/2011
	4PB-P-2-19E11W		2/7/2011
	4PB-P-3-21E7W		2/12/2011

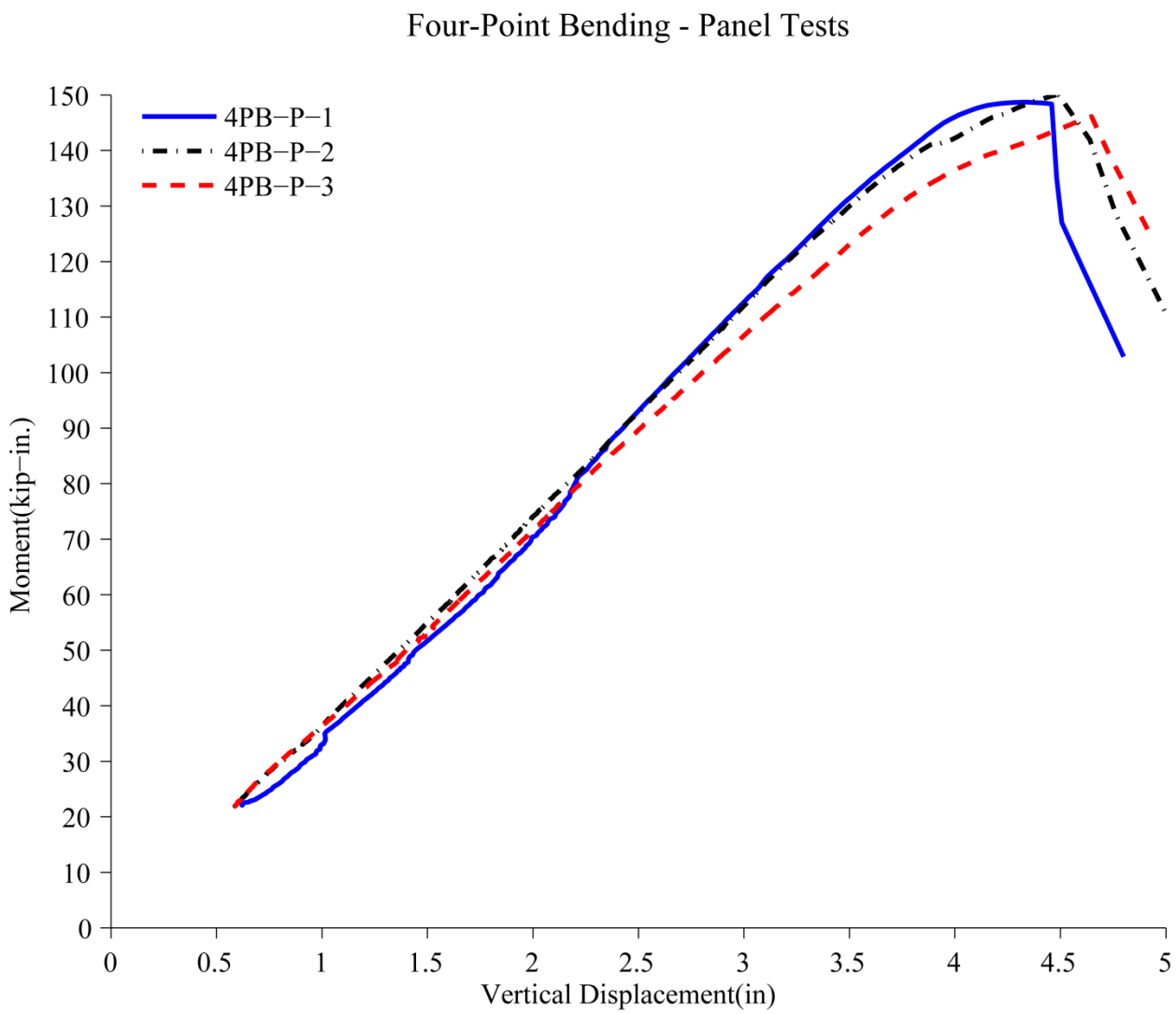

TEST DATA PLOTS

Four-Point Bending No Panel - Load Displacement Plots

Test Identification:		**Test Date:**	
	4PB-NP-1-15E8W		2/4/2011
	4PB-NP-2-10E9W		2/5/2011
	4PB-NP-3-17E18W		2/8/2011
	4PB-NP-4-32E20W		2/22/2011

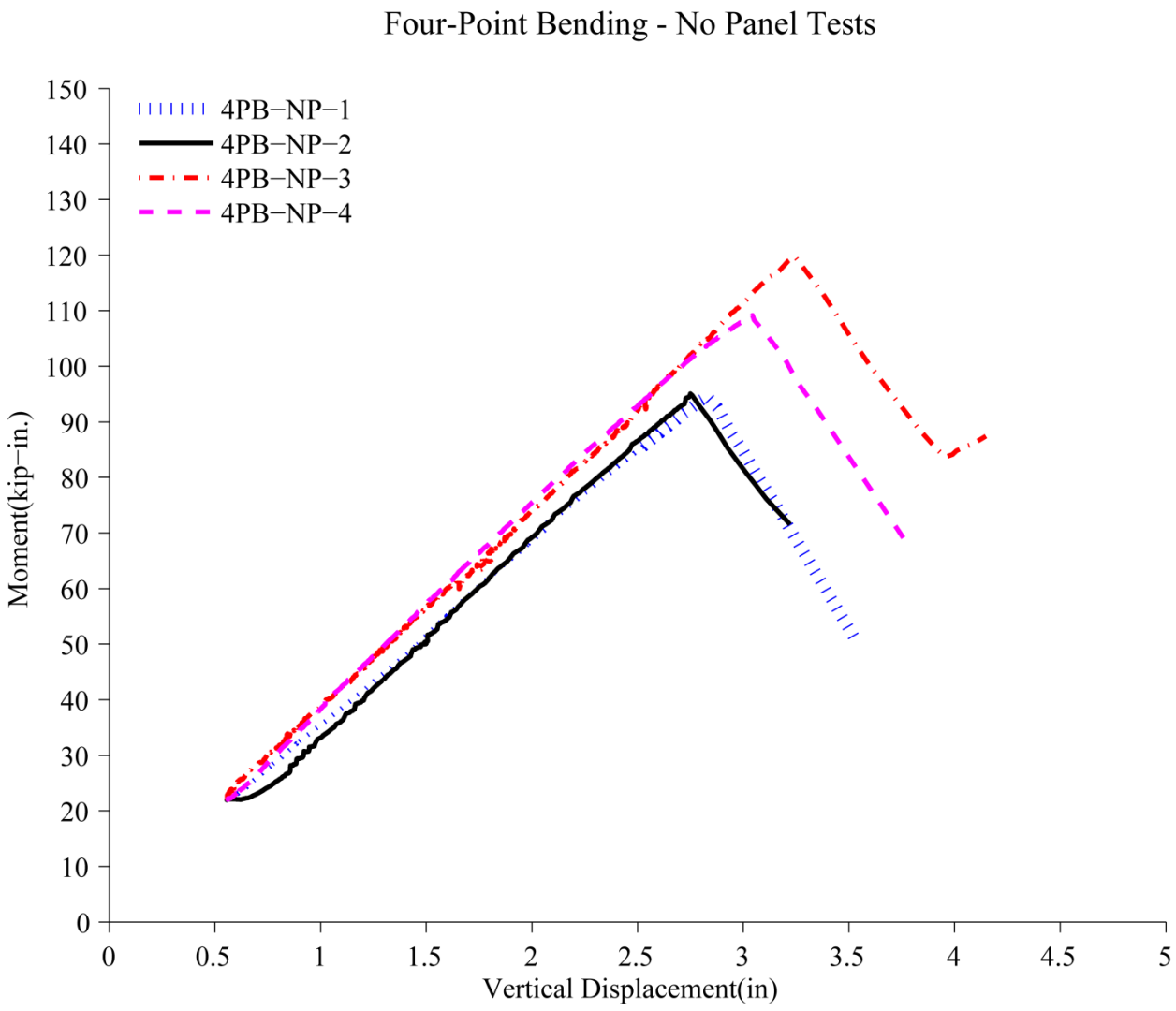

ABAQUS (2010). ABAQUS/Standard Version 6.9-2. Providence (RI), Dessault Systèmes**:** ABAQUS V.6.9-2 Finite Element Program.

AISI-S100 (2007). North American Specification for the Design of Cold-Formed Steel Structural Members. Washington, D.C., American Iron and Steel Institute.

Autodesk (2010). INVENTOR. San Rafael (CA), Autodesk, Inc.

Moen, C. D. and B. W. Schafer (2009). Elastic buckling of cold-formed steel columns and beams with holes. Engineering Structures. **31(12),2812-2824**.

Moen, C. D. and C. Yu (2010). Elastic Buckling of Thin-Walled Structural Components with Edge-Stiffened Holes. Proceedings of the 51st AIAA/ASME/ASCE/AHS/ASC Structures, Structural Dynamics, and Materials Conference. Orlando, FL.

Sarawit, A. (2006). CUTWP Thin-walled section properties. update <www.ce.jhu.edu/bschafer/cutwp>.

Schafer, B. W. (2008). Computational modeling of cold-formed steel. CIMS 2008, Fifth International Conference on Coupled Instabilities in Metal Structures. Sydney, Australia 53-60.

Schafer, B. W. and S. Ádány (2006). Buckling analysis of cold-formed steel members using CUFSM: conventional and constrained finite strip methods. Eighteenth International Specialty Conference on Cold-Formed Steel Structures. Orlando (FL).

SSMA (2001). Product Technical Information, ICBO ER-4943P, Steel Stud Manufacturers Association.